Immunoregulatory functions of granzyme M: behind enemy lines

Stefanie Adriana Hendrika de Poot

ISBN: **978-90-393-6041-5**

Printed by: Proefschriftmaken.nl, Uitgeverij BOXPress, 's-Hertogenbosch

Cover: Two toy-soldiers are shown as paratroopers landing in the hostile environment of an enemy cell (a biohazardous nucleus in pink, endoplasmic reticulum in green, mitochondria in yellow and the Golgi system in blue) – behind enemy lines. This reflects the entry of GrM into a virus-infected or transformed cell, where it can exert its anti-tumor and anti-viral functions. Designed and created by Stefanie de Poot. Special thanks to Ron Schackmann for critical input.

The research described in this thesis was performed at the Department of Pathology of the University Medical Center Utrecht, the Netherlands, and was financially supported by the Dutch Cancer Society (Grant UU-2009-4302).

Printing of this thesis was financially supported by the Department of Pathology of the University Medical Center Utrecht, the Dutch Cancer Society, ChipSoft BV, tebu-bio, and the Infection & Immunity Center Utrecht.

Immunoregulatory functions of granzyme M: behind enemy lines

Immunoregulatoire functies van granzym M: achter de vijandelijke linies
(met een samenvatting in het Nederlands)

Proefschrift

ter verkrijging van de graad van doctor aan de Universiteit Utrecht op gezag van rector magnificus, prof. dr. G.J. van der Zwaan, ingevolge het besluit van het college voor promoties in het openbaar te verdedigen

op donderdag 12 december 2013 des ochtends te 10.30 uur

door

Stefanie Adriana Hendrika de Poot

geboren op 23 augustus 1986
te ’s-Hertogenbosch

Promotor:	Prof. dr. P.J. van Diest
Co-promotor:	Dr. N. Bovenschen

Contents

Chapter 1

Granzyme M: Behind Enemy Lines

de Poot SAH and Bovenschen N.

Department of Pathology, University Medical Center Utrecht, Utrecht, the Netherlands

Submitted to Cell Death Differ.

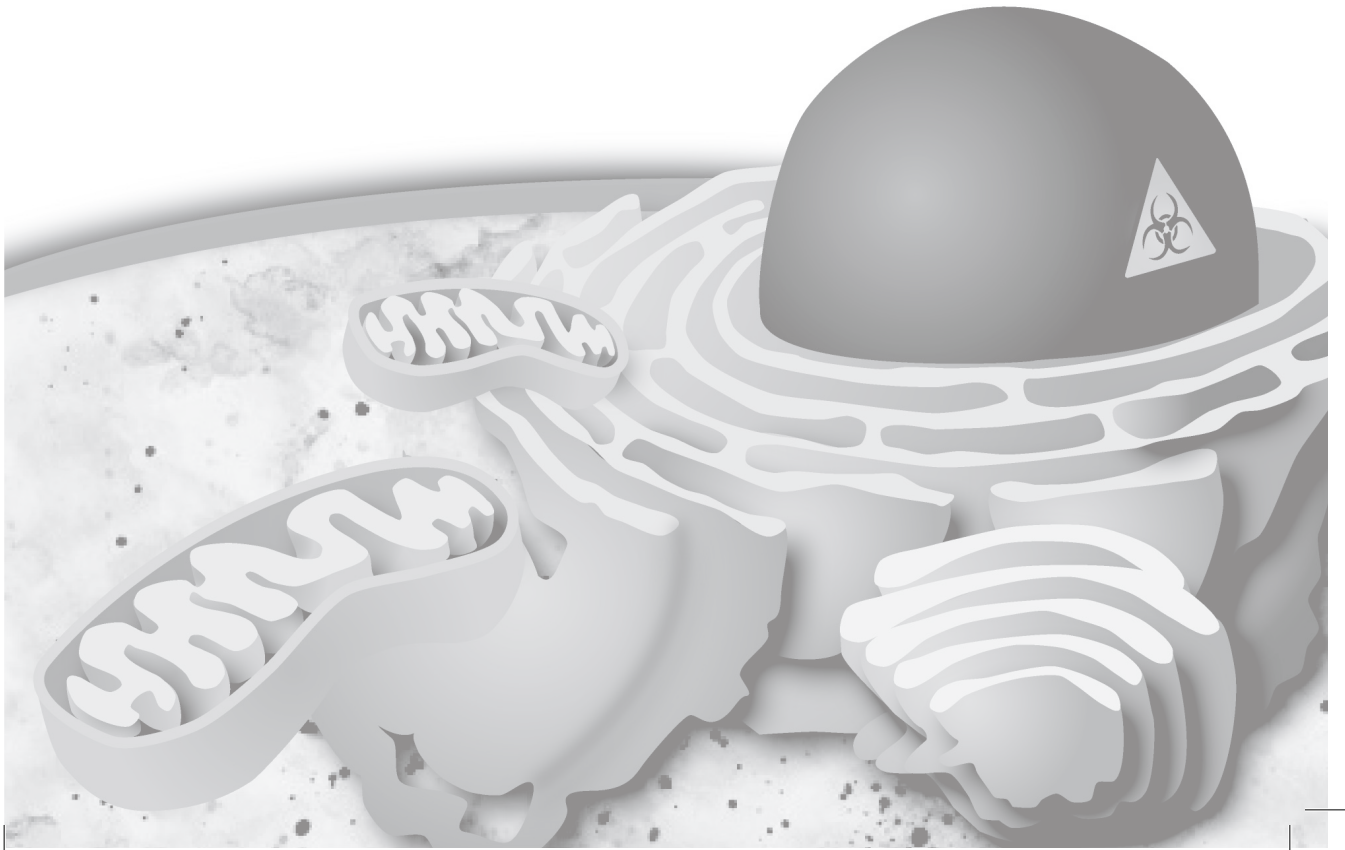

Abstract

The granule-exocytosis pathway is the major mechanism via which cytotoxic lymphocytes eliminate virus-infected and tumor cells. In this pathway, cytotoxic lymphocytes release granules containing the pore-forming protein perforin and a family of structurally homologous serine proteases known as granzymes into the immunological synapse. Pore-formation by perforin facilitates entry of granzymes into the target cell, where they can activate various signaling pathways to induce apoptosis or to cripple viral replication. Humans express five different granzymes, of which granzymes A and B have been most extensively characterized. Much less, however, is known about granzyme M. Recently, novel proteomics approaches have determined the primary and extended specificity of granzyme M. In addition, the crystal structure of granzyme M has been resolved, giving new insight into the structural determinants of granzyme M specificity. The list of granzyme M functions has expanded over the past few years: not only can granzyme M efficiently induce cell death in tumor cells, it can also inhibit cytomegaloviral replication in a non-cytotoxic manner. Finally, a role for granzyme M in the LPS-induced inflammatory response has been proposed. In this review, we recapitulate the current status of granzyme M expression, substrate specificity, functionality, and inhibitors.

Introduction

To counteract virus-infected cells and tumor tissue, the immune system utilizes a variety of specialized cytotoxic lymphocytes, including natural killer (NK) cells and cytotoxic T lymphocytes. These cells constitute the effector arm of the cellular immune response and can exert their protective function by either killing potentially harmful cells or by crippling viral replication within the host cell. Upon recognition of a target cell, effector cells engage with the target cell and form an immunological synapse. Target cells are executed via two mechanisms: (I) by ligation of death receptor ligands on the surface of the effector cell with death receptors on the membrane of the target cell [1], or (II) by secretion of cytolytic granules from the effector cells into the immunological synapse [2-4](Figure 1). The latter mechanism is generally believed to be the principal mechanism of killing. The released cytolytic granules contain a family of structurally homologous serine proteases known as granzymes, and the pore-forming protein perforin. Perforin enables granzyme entry into the target cell [5], allowing granzymes to cleave intracellular substrates and in that way induce cell death [2, 3].

There are five human granzymes: granzyme A (GrA), GrB, GrH, GrK and GrM. This non-sequential nomenclature in humans results from the more extensive granzyme family in mice, which express GrA-GrG and GrK-GrN [6]. The five human granzymes share an amino acid sequence homology of approximately 40% [7], and are structurally related to the trypsin family of serine proteases. They all share the same catalytic triad, consisting of a His, Ser, and Asp residue. GrA and GrB are most extensively studied, but less is known about the other granzymes, which are often

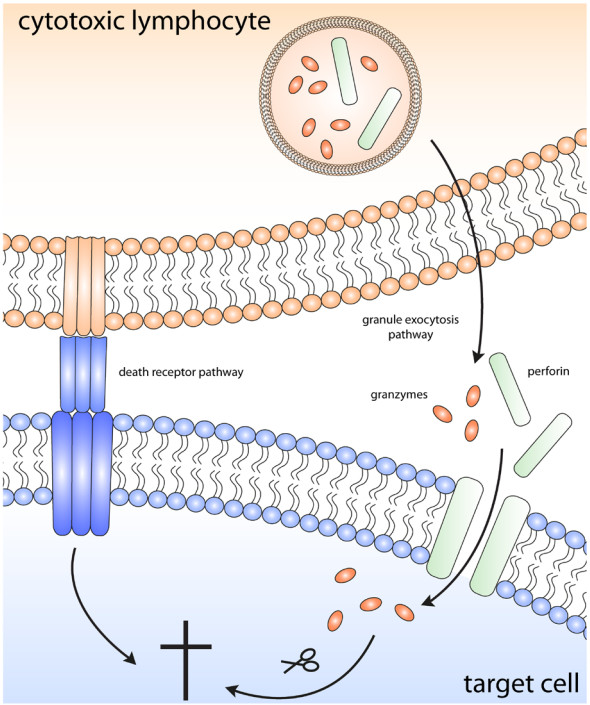

Figure 1. Cytotoxic lymphocyte-mediated killing. Cytotoxic lymphocytes can eliminate target cells via two main mechanisms: the death receptor pathway and the granule exocytosis pathway. The death receptor pathway involves the docking of a ligand on the membrane of the effector cell to a death receptor on the membrane of the target cell. This results in the initiation of an intracellular cell death signalling cascade. The granule exocytosis pathway is the major mechanism via which cytotoxic lymphocytes exert their cytotoxic function. In this pathway, the effector cell releases preformed granules into the immunological synapse. These granules contain the protein perforin, which forms pores in the membrane of the target cell, and a set of serine proteases known as granzymes. Pore-formation by perforin facilitates the entry of granzymes into the target cell, where they can cleave intracellular substrates and induce cell death.

referred to as 'orphan' granzymes [8]. In this review, we will summarize and discuss the current insights into the substrate specificity, structure, cellular expression, functions, and inhibitors of GrM [9].

Gene characteristics

GrM (also known as Met-ase or Met-1) was first identified in a rat NK leukemia cell line as a granular protease that displayed Met-ase activity, *i.e.* hydrolyzed peptide substrates after a methionine or leucine residue [10]. Soon after this initial discovery, the human [11] and mouse [12] orthologs of GrM were cloned. Interestingly, the genes encoding human GrM (hGrM) and mouse GrM (mGrM) are situated on human chromosome 19p13.3 [13, 14] and a syntenic region of mouse chromosome 10C [14, 15], respectively, which closely localize to a cluster of neutrophil elastase-like proteases [16]. Moreover, the organization of the hGrM gene – which is approximately 7.5 kb long and consists of 4 introns and 5 exons – also resembles that of neutrophil elastase-like genes. Together, these findings suggest that GrM and the neutrophil elastase-like proteases may have arisen by duplication and divergence of a common ancestor gene [17].

Protein synthesis and structure

All granzymes are synthesized as inactive precursors, or pre-pro-proteases. The pre-sequence, also known as the leader-sequence, is cleaved off by signal peptidases at the endoplasmic reticulum. Removal of the propeptide sequence is subsequently catalyzed inside the secretory granules by the lysosomal cathepsin C (also known as dipeptidyl peptidase I) [18]. Whereas most granzymes contain a propeptide of two amino acids, the propeptide of GrM is not a dipeptide, but instead consists of six amino acids [11, 19, 20]. Removal of the pre-pro-peptide reveals the N-terminal tail of GrM, containing the highly conserved Ile-Ile-Gly-Gly motif [18, 21, 22], and leads to a conformational change of the granzyme resulting in exposure of the active site. Whilst at this point GrM is fully processed (232 amino acids, ~28 kDa), it is not yet enzymatically active, since granzymes are stored in granules at low pH [23]. Mature GrM is maximally active at a pH between 7.5-9 [24]. Granzymes are highly basic (with an iso-electric point above 10) and bind to proteoglycans within the secretory granules. This is also likely to keep the granzymes proteolytically inactive.

The crystal structures of active hGrM and an inactive hGrM-mutant complexed with a synthetic substrate have recently been solved at <2.7Å by the group of Fan [24], and are accessible at the Protein Data Bank (http://www.rscb.org) under accession codes 2ZGC and 2ZGJ, respectively. The non-conserved L3 loop (residues 199-212), which is in close proximity to the catalytic triad, is most likely an important determinant of hGrM substrate specificity, since this loop changes in conformation upon binding of a substrate [24]. Whilst granzymes generally have three conserved disulfide bridges, GrM has four. In addition, several potential *N*-glycosylation sites have been identified: Asn21, Asn152, Asn158 [25] and other possible *N*- and *O*-glycosylation sites [26], phosphorylation sites, and myristoylation sites [7] have been proposed.

Substrate specificity

In protease biology, nomenclature proposed by Schechter and Berger is used to define the position of amino acids in the substrate and protease [27]. Amino acids surrounding the scissile bond are denoted as P*n*-P2-P1↓P1'-P2'-P*n*', with amine bond hydrolysis occurring after P1, and the corresponding binding sites in the protease are numbered S*n*-S2-S1-S1'-S2'-S*n*'. Although all granzymes share the His-Asp-Ser catalytic triad, their substrate specificities only partially overlap. GrM was initially thought to have a unique primary (P1) specificity for which it was first named Met-ase or Met-1: it was found to preferentially cleave substrates after a Met residue [11, 12, 20]. Later, using a positional scanning synthetic combinatorial library of tetrapeptides, hGrM was found to indeed hydrolyze substrates after a Met, but its preferred P1 residue is actually Leu, another long hydrophobic amino acid [28] (Figure 2). This is in agreement with the crystal structure of hGrM, which shows that the S1 pocket (Pro177-Cys178-Gly180-Ser182-Ser199) can only accommodate long, narrow hydrophobic amino acids due to its size and its hydrophobic properties [24].

The P4-P1 specificity of hGrM has been further defined using a similar approach, which reveals that hGrM has a strong preference for a Lys at the P4, no clear preference for the P3, and a preference for a small amino acid such as a Pro or Ala at the P2 position [29] (Figure 2). This is again corroborated by the hGrM structure data: the size of the S2 pocket, which is formed by His41, Val80, Leu83 and Phe200, is constricted and can only fit small residues [24]. Furthermore, the S4 pocket – which is formed by Pro81, Ala82, Glu84, Ser160, and supported by Leu83 and Phe200 – constitutes a groove with a calculated negative electrostatic potential

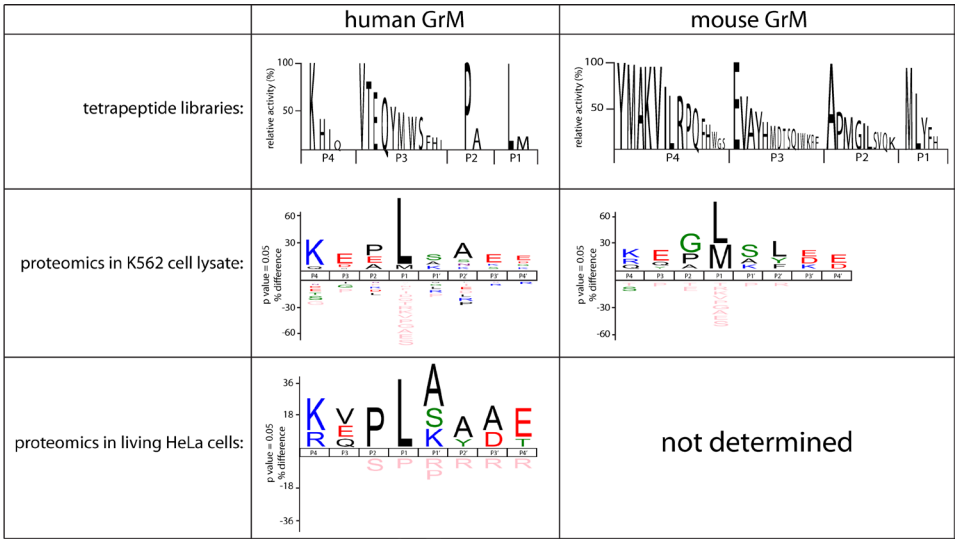

Figure 2. The primary and extended specificities of human and mouse GrM. A positional scanning synthetic combinatorial library of tetrapeptides has been used to determine the P4-P1 specificity of human [29] and mouse [30] GrM. In addition, complementary positional proteomics have been used to determine the consensus cleavage sites of human and mouse GrM in K562 tumor cell lysates [30]. Finally, complementary positional proteomics have been used on living HeLa tumor cells treated with the pore-forming perforin-analogue streptolysin O and GrM (Chapter 5).

due to the presence of Glu84. This groove can therefore only accommodate residues with a hydrophobic neck and a basic head, such as Lys, His, or Arg [24]. Contrary to the S4-S1 pockets, the S' pocket, which determines binding to the P' residues, could not be clearly defined [24]. Together, these data suggest that the optimal P4–P1 tetrapeptide specificity of hGrM would be Lys-Val-Pro-Leu (KVPL) [29]. Indeed, this tetrapeptide is highly specific for hGrM, as it cannot be hydrolyzed by other granzymes, neutrophil elastase, cathepsin G, and chymotrypsin [29]. To determine the consensus cleavage site of hGrM in macromolecular substrates, we have used combined fractional diagonal chromatography (COFRADIC)-based complementary positional proteomics in human K-562 tumor cell lysates treated with recombinant hGrM [30] (Figure 2). These data largely confirm the results obtained with tetrapeptide libraries: hGrM clearly prefers a Leu over a Met at the P1, a Pro or Ala at the P2, and a Lys at the P4 position [30]. In addition, for the first time, these data confirm the contribution of prime residues to GrM substrate recognition [30]. To determine GrM substrate specificity in a more physiological setting, we have recently used COFRADIC-based N-terminal positional proteomics coupled with a triple L-Arg SILAC labeling strategy to determine GrM substrates in living human HeLa tumor cells (Chapter 5). Only 25 substrates with a Met or a Leu at the P1 are identified, and the consensus cleavage site in these substrates displays an almost perfect correlation with the previously identified substrate specificities of GrM (Figure 2). Together, these data confirm that hGrM is a highly specific serine protease with a specificity that extends beyond its preferences for P4-P1.

The substrate specificities of hGrM and mGrM have been shown to only partially overlap [30]. While these two orthologs share a sequence homology of approximately 69% [12], their primary and extended specificities are distinct. In combinatorial positional scanning tetrapeptide libraries, mGrM prefers a Met over a Leu at the P1, in comparison to the strong Leu-preference of hGrM. In addition, mGrM displays a broader tolerance for various amino acids at the P2 and P4 positions [30]. The macromolecular substrate specificities of both orthologs are also distinct: using a fluorescence 2D-DIGE proteomic approach, hGrM and mGrM specificities have been compared in lysates of human HeLa and mouse C2C12 tumor cells. The macromolecular substrate specificities of hGrM and mGrM overlap for ~42% in the human tumor cell lysate, and for ~34% in the mouse tumor cell lysate [30]. A similar, partial overlap in hGrM and mGrM macromolecular specificities has been found using COFRADIC-based complementary positional proteomics, revealing that the orthologs share ~67% of the cleavage events in human K562 tumor lysate [30]. The species-specific differences between hGrM and mGrM extend beyond the granzymes' substrate preferences: the substrates themselves can also differ between species. This is for instance the case for known GrM substrate nucleophosmin (NPM) [31]. Whereas human NPM is efficiently cleaved by both hGrM and mGrM, mouse NPM cannot be cleaved by either ortholog [30]. Replacement of the putative P1'–P2' residues in mouse NPM with the corresponding residues of human NPM restores cleavage by both granzymes. This further underlines the importance of

the prime residues for GrM-mediated substrate recognition. For hGrM substrate Fas Associated protein with Death Domain (FADD) [32], a similar species-specific difference in the cleavage site has been reported [33]. Replacement of the putative P1 and P1' residues in mouse FADD with the corresponding amino acids of human FADD restores cleavage of mouse FADD by both human and mouse GrM [33]. Collectively, these data show that hGrM and mGrM display narrow macromolecular substrate specificities that only partially overlap, and that caution is essential when extrapolating data from mouse models.

Cellular expression

Granzymes make up ~90% of the total amount of granule proteins in cytotoxic T lymphocytes and NK cells [13]. Initially, expression of GrM was believed to be restricted to NK cells [10-12]. Based on northern blots for GrM, high mRNA expression has been identified in two NK leukemia cell lines as well as in purified $CD3^-CD56^+$ large granular NK cells. In contrast, very low levels to no expression of GrM mRNA is detected in other leukemia/lymphoma cell lines – including Jurkat, Daudi and K-562 cells – purified $CD3^+CD56^-$ peripheral blood mononuclear T cells and $CD3^-CD56^+$ small high density NK cells [11, 34]. Further evidence for NK-cell specific GrM expression is based on a reporter construct consisting of the rat or mouse 5' flanking region of GrM coupled to a chloramphenicol acetyltransferase reporter gene. Transfection of this construct into a number of mouse and rat cell lines allows transcription of chloramphenicol acetyltransferase in NK but not in T cell lines [12, 17]. Another means that has been used to determine the cellular expression of GrM is based on the proteolytic Met-ase activity of GrM. While sorted NK cells/NK cell lines have high Met-ase activity [11, 17], no activity is detected in a variety of leukemia/lymphoma cell lines [11]. Using western blot and immunohistochemistry on FACS-purified cell populations, Sayers *et al*. have also found that GrM expression is restricted to $CD3^-CD56^+$ NK cells, $CD3^+CD56^+$ NKT cells, and γδ T lymphocytes, and absent in $CD4^+$ and $CD8^+$ T-cells, neutrophils and monocytes [35]. This highly specific expression of GrM by NK, NKT and γδ T cells suggests a role for GrM in innate immunity.

In recent years, however, GrM expression has also been detected in cells of the adaptive immune system. Murine lymphokine activated killer (LAK) cells and murine cytotoxic T lymphocyte clones, for instance, contain similar levels of mGrM mRNA, and both display Met-ase activity [36]. Bade *et al.* have characterized GrM protein levels in human peripheral blood mononuclear cells (PBMCs) using flow cytometry, and show GrM expression in NK cells (both $CD16^+CD56^+$ and $CD3^-CD56^{bright}$), NKT cells, γδ T cells and in ~35% of the $CD3^+CD8^+$ T-cell population [37]. In contrast, no GrM expression is detected in B-cells, and only a small subset of the T helper cells express GrM [37]. These data are confirmed by de Koning *et al.*, who – by means of real-time quantitative PCR and flow cytometry – also demonstrate high expression of GrM in human NK cells, NKT cells, γδ T cells, and in differentiated effector $CD8^+$ $CD27^-$ $CD45RO^-$ T cells [38]. GrM expression correlates with the expression of

perforin, and GrM levels gradually increase during T cell differentiation from naïve T-cells, via effector-memory cells, to effector cells [38]. Interestingly, elevated GrM levels have recently also been detected in human cytomegalovirus (hCMV)-specific $CD8^+$ T lymphocytes as compared with naïve $CD8^+$ T cells [39]. These findings show that GrM is expressed by effector cells of both innate and adaptive immunity.

Transcription of certain granzymes, such as GrA, GrB and GrK, can be up-regulated in response to a variety of stimuli, such as interleukin (IL)-2, IL-12, IL-15, or interferon (IFN)α [40]. None of these factors, however, have an effect on the GrM mRNA levels in the human NK92 NK cell line, suggesting that GrM transcription is regulated differently [40]. This has later been confirmed at the protein level using flow cytometry: GrM expression is not up-regulated in response to IL-2, IL-6, IL-7, IL-12, IL-15, IL-21, IL-27, IFNα, or LPS [38].

Functions of GrM

Over the years, the role of GrM has been studied in a variety of processes, ranging from cell death induction to inflammation. Although its mechanism of action and its cellular substrates are not fully understood, it has become increasingly clear that GrM is a key player in immune processes (Figure 3).

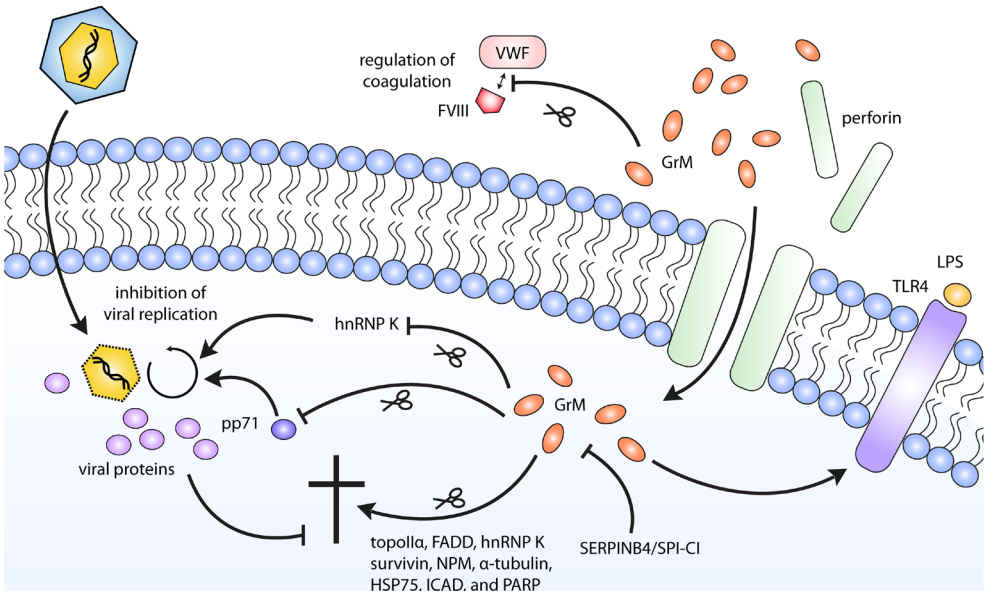

Figure 3. The functions of GrM. After entry into a target cell via perforin-mediated pore formation in the target cell membrane, GrM can activate various signalling pathways. GrM can induce apoptosis via cleavage of a number of death substrates, amongst which topoIIα (Chapter 5), FADD [94], hnRNP K [47], survivin [42], NPM [31], α-tubulin [45], Hsp75 [43], ICAD and PARP [44]. GrM can also function in a noncytotoxic manner to inhibit hCMV replication by either cleaving the host protein hnRNP K [39] or the viral protein pp71 [70]. In addition, GrM can stimulate LPS/TLR-4 mediated signalling via yet to be identified mechanisms [87]. GrM intracellular functioning can be inhibited tumor cells by human SERPINB4 [89] and mouse SPI-CI [36]. Next to these intracellular effects, GrM has also been found to cleave VWF, and may in that way regulate FVIII levels and coagulation [88].

Induction of target cell death

Granzymes are best known for their pro-apoptotic role in the cellular immune response against virus-infected and tumor cells. The role of GrM in cell death induction has therefore been studied most extensively. Even so, much remains unclear and it is difficult to find a consensus between the contradicting findings that have been published. Here, we will briefly summarize the different aspects of GrM cell death.

The first study describing GrM-mediated cytotoxicity was published in 2004 and shows efficient tumor cell death induction with low concentrations of GrM and sublytic concentrations of perforin [41]. GrM-treated cells contain condensed chromatin, large vacuoles and rounded mitochondria, but lacked classical apoptosis markers such as phosphatidylserine exposure in the absence of membrane permeabilization, caspase-3 activation, DNA fragmentation, and mitochondrial damage [41]. Similar results are found in a later study: GrM-treated cells die in the absence of caspase activation and phosphatidylserine exposure [31]. In contrast, several other studies have shown that GrM treatment can lead to phosphatidylserine exposure, DNA fragmentation, targeting of the mitochondria and caspase activation [32, 42-44](Chapter 5). Some classical hallmarks of apoptosis (such as phosphatidylserine exposure, DNA fragmentation and mitochondrial damage) can be the result of caspase activation, so whether or not caspases are activated in response to GrM may determine whether or not these apoptotic hallmarks are observed. Differences between studies may be due to the method used to produce recombinant GrM (in *E. coli* or *P. pastoris*), the applied GrM concentrations, or the means used for intracellular delivery of GrM (purified perforin, Pro-Ject protein transfection reagent, adenovirus, or the pore-forming protein streptolysin O [SLO]).

Using different methods, including proteomic techniques such as gel-based 2D-DIGE [45] and MS-based COFRADIC [30](Chapter 5), a number of GrM substrates have been identified that may induce cell death in tumor cells. GrM cleaves and activates the inhibitor of caspase-activated DNase (ICAD) and Poly (ADP-ribose) polymerase (PARP) [44]. Both of these proteins are also caspase-substrates during apoptosis [46]. In addition, GrM hydrolyzes cytoskeleton components ezrin and α-tubulin [45]. Cleavage of the latter results in increased tubulin polymerization and in the destabilization of the microtubule network [45]. The contribution of these substrates to GrM-mediated cell death, however, remains unclear. A few other GrM substrates have been studied in more detail, using siRNA-mediated knockdown or overexpression (of uncleavable mutants) to determine their physiological relevance. One such substrate is the chaperone protein TRAP1 (HSP75), cleavage of which leads to increased reactive oxygen species [43]. While RNAi-mediated depletion of TRAP1 does not induce spontaneous cell death, it does sensitize tumor cells to GrM [43], suggesting that TRAP1 cleavage by GrM contributes to cell death, but does not directly induce it. The nucleolar phosphoprotein nucleophosmin (NPM) is also efficiently hydrolyzed by GrM and knockdown of this protein leads to apoptosis [31]. Overexpression of an uncleavable NPM mutant, however, failes to protect tumor

cells from GrM-induced cell death [31]. Similarly, knockdown of heterogeneous nuclear ribonucleoprotein K (hnRNP K) – the first substrate known to be cleaved by all five human granzymes – sensitizes tumor cells to LAK-cell mediated cytotoxicity [47], and knockdown of survivin, another GrM substrate, sensitizes tumor cells to GrM-induced cell death by lowering the threshold for caspase activation [42]. All of these pathways are likely to contribute to GrM-induced cell death, but none of these appear to be absolutely essential for apoptosis induction. In contrast, GrM-mediated cleavage of FADD seems to be an important event in cell death induction. FADD-deficient Jurkat cells are significantly less sensitive to GrM, and cells expressing an uncleavable FADD-mutant are also more resistant to GrM-induced apoptosis [32]. GrM-mediated cleavage of FADD leads to increased self-association of the protein, resulting in the recruitment and activation of procaspase-8 and subsequent activation of the other members of the caspase cascade [32]. Whilst FADD-deficient cells are less sensitive to GrM, cell death is not completely impaired, suggesting that other mechanisms are still at play in these cells. Indeed, we have recently identified DNA topology enzyme topoisomerase II alpha (topoIIα) as a highly efficient GrM substrate (Chapter 5). Cleavage of topoIIα by GrM leads to a dissection of the protein's catalytic domains from the C-terminal regulatory domain, resulting in nuclear exit of the functional domains. Knockdown of topoIIα induces G2/M cell cycle arrest and subsequently leads to apoptosis. This pathway is therefore also of importance in GrM-mediated cytotoxicity. In agreement with the substrate specificity profiles determined for GrM, most of the identified cleavage sites within these substrates have either a Leu (NPM, survivin, topoIIα, α-tubulin) or a Met (FADD) at the P1. Proteomics approaches have revealed more potential GrM substrates [30, 45](Chapter 5) which may also contribute to GrM-induced cytotoxicity. Thus, GrM targets multiple intracellular proteins that cooperate in the induction of target cell death.

Another potential interesting pro-apoptotic function of GrM is its role as a synergistic effector that aids GrB-mediated apoptosis. GrB, which can directly cleave (and activate) both Bid and procaspase-3 [48, 49], is a potent inducer of cell death. Tumor cells, however, can evade GrB-mediated cytotoxicity by overexpressing the serine protease inhibitor (serpin) PI-9, expression of which is associated with poor clinical outcome [50-53]. Upon cleavage by GrB in its reactive center loop (RCL), PI-9 undergoes a conformational change after which it covalently binds GrB, rendering GrB kinetically inactive. Interestingly, GrM can also cleave PI-9, but cannot be trapped by the serpin [28]. Instead, cleavage of PI-9 by GrM renders the serpin inactive, and GrM may therefore bypass GrB inhibition [28]. A similar synergistic mechanism has been reported for GrB and GrH: GrH can inactivate an adenovirus-encoded GrB inhibitor [54]. The physiological relevance of the GrB-GrM interplay deserves further study, since inhibition of GrB by PI-9 occurs at faster kinetics than GrM-mediated inactivation of PI-9 [28].

The physiological relevance of GrM in tumor clearance *in vivo* is still unclear. There is convincing evidence, however, that underlines the importance of the

granule-exocytosis pathway in tumor rejection. Perforin-deficient mice are severely immunodeficient, and are significantly compromised in their ability to eradicate transplanted and injected tumor cells and viruses [55, 56]. In addition, these mice spontaneously develop highly aggressive disseminated B-cell lymphomas [57], implying a role for the granule-exocytosis pathway in immune surveillance of tumors. The importance of the granule-exocytosis pathway in tumor rejection is further supported by humans with mutations in the perforin gene *PRF1*. These mutations are extremely rare, but recent studies suggest that carriers of *PRF1* alleles with temperature-sensitive missense mutations may be more than 100 times more susceptible to the development of hematological cancers [58, 59]. On the contrary, knockout mice of single or multiple granzymes rarely display a clear phenotype: knockout of GrA and GrB-F, for instance, has no effect on tumor clearance, and mice lacking these granzymes can still handle most infections [60, 61]. Two studies have looked specifically at the role of mGrM in tumor clearance *in vivo*. In the first study, GrM knockout mice develop normally, and NK cells isolated from these mice display efficient cytotoxicity towards tumor cells *ex vivo* [62]. GrM knockout mice can still successfully clear several mouse lymphoma cell lines, whereas perforin-deficient mice die within 50 days [62]. In addition, upon i.v. inoculation of melanoma cells, no effect on the number of metastases can be observed [62]. In a later study, adoptively transferred NK cells from GrM knockout mice display impaired tumor cell killing *in vivo* towards a chemically (MCA) induced tumor cell line, but not *in vitro* [63]. The absence of clear phenotypes in granzyme knockout mice is likely due to the redundancy of the granzyme system. It is of importance to note that absence of a clear role for mGrM in tumor rejection in mice may not reflect its function in humans: as mentioned previously, mGrM and hGrM display species-specific substrate specificities. mGrM is not cytotoxic towards a panel of mouse tumor cell lines and the GrM death substrates NPM and FADD cannot be cleaved in mice [30, 33]. Ideally, GrM function would therefore be studied in a humanized cancer mouse model.

Noncytotoxic inhibition of viral replication

A longstanding dogma in granzyme biology is that granzymes exert their functions by inducing target cell death. Recently, however, evidence is emerging that granzymes also have noncytotoxic functions. This may be particularly true for virus-infected cells, as viruses have evolved multiple mechanisms to block cell death pathways [64]. Indeed, GrB can inhibit HSV-1 reactivation from neuronal latency in an apoptosis independent manner [65], GrK can inhibit influenza A viral replication via cleavage of the host cell nuclear transport complex importin α1/β [66], and GrH cleaves host cell protein La, which is important for viral RNA metabolism [67], and the HBx protein which is required for replication of hepatitis B virus [68].

Interestingly, GrM knockout mice are more sensitive to murine cytomegalovirus (mCMV) infection [62], but not to HSV-1 or influenza A infection [69]. This cell death-independent antiviral activity towards CMV has been validated in human cells

with human cytomegalovirus (hCMV) *in vitro* [70]. GrM inhibits hCMV replication in at least two ways: via cleavage of the viral phosphoprotein pp71 [70] and via cleavage of the host cell protein hnRNP K [39]. GrM-mediated cleavage of hCMV protein pp71 - which is indispensible for efficient hCMV replication [71] - disturbs its nuclear localization and abrogates its transcriptional activity towards the hCMV major immediate-early promoter [70]. GrM can also cleave host protein hnRNP K, which is essential for the translation of hCMV immediate early 2 protein and hCMV replication [39]. Lending credibility to this antiviral activity of GrM is the fact that hGrM protein levels are elevated in hCMV-specific CD8+ T cells, supporting an active antiviral role for GrM in hCMV infection and in the prevention of hCMV reactivation [39]. Interestingly, a number of other known hGrM substrates have been implicated in viral replication: α-tubulin [45], for instance, plays a crucial role in viral intracellular transport [72], the shuttling capacity of NPM can be used by viral proteins to enter the nucleus [73, 74], and topoIIα is thought to be involved in the replication of HIV-1 [75, 76], HSV-1 [77], vaccinia virus [78], and Epstein-Barr virus [79]. It is therefore tempting to speculate that GrM-mediated cleavage of these host proteins may also contribute to its antiviral functions.

Regulation of inflammation

Although granzymes are best known for their intracellular roles – and mainly for their role in target cell killing –, extracellular functions for granzymes have recently been suggested [80, 81]. Granzymes have been linked to extracellular matrix degradation [82, 83], immune regulation, and inflammation [84-86].

Using the GrM knockout mouse model, a role for GrM in inflammation has been established. In comparison to wild-type mice, GrM knockout mice and perforin knockout mice are significantly more resistant to toll-like receptor (TLR)4-dependent lipopolysaccharide (LPS)-induced endotoxicosis [87]. GrM-deficient mice have decreased serum levels of proinflammatory cytokines such as IL-1α, IL-1β, TNF, and IFNγ following LPS challenge. It has been proposed that GrM likely acts intracellular and downstream of caspase-1 in this LPS-induced model of sepsis. Interestingly, elevated plasma levels of GrM have been detected in meningococcal sepsis patients [88], pointing to a role of GrM in the inflammatory response to bacteria.

Other functions

In addition to its role in inflammation, GrM may also have an extracellular function in the regulation of blood coagulation: GrM can cleave the pro-hemostatic multimer plasma protein Von Willebrand Factor (VWF) *in vitro* [88]. VWF normally promotes platelet aggregation and stabilizes coagulation factor VIII, but VWF cleaved by GrM can no longer bind factor VIII *in vitro* [88]. In this manner, GrM may play a role in the regulation of factor VIII plasma levels and blood coagulation.

Inhibitors of GrM

Over the years, several inhibitors of GrM have been identified. The synthetic

compounds z-Met^{P}-(OPh-4-Cl)$_2$ [28] and Ac-KVPL-CMK [24] specifically inhibit GrM. The CMK-group of Ac-KVPL-CMK ensures that a covalent bond is formed between the inhibitor and the catalytic Ser182 and His41 residues, and therefore irreversibly inhibits GrM proteolytic activity [24]. Pre-treatment of human Jurkat tumor cells with this inhibitor significantly inhibited GrM-mediated cell death [24], and pre-treatment of LAK cells prior to co-culture with human HeLa tumor cells led to a significant decrease in LAK-cell mediated cytotoxicity [32]. These inhibitors are valuable tools in elucidating GrM function.

Next to these synthetic inhibitors of GrM, a number of proteinaceous inhibitors have also been identified. One of these is the bacterially-expressed serine protease inhibitor ecotin, but this protein is a broad-spectrum serine protease inhibitor, and therefore not specific for GrM [28]. Two extracellular human serpins in plasma, SerpinA1 (α1-antitrypsin) and SerpinA3 (α1-antichymotrypsin), inhibit hGrM activity and form SDS-stable complexes with hGrM [28]. GrM – which is undetectable in the serum of healthy controls – has been detected in the serum of sepsis patients [88]. Whether or not SerpinA1 and/or SerpinA3 inhibit GrM activity *in vivo* remains an open question.

Recently, two intracellular GrM-inhibiting serpins have been identified: the murine serine protease inhibitor involved in cytotoxic inhibition (SPI-CI, also known as R86) [36] and human SerpinB4 (also known as squamous cell carcinoma antigen-2 or leupin) [89]. SPI-CI has been initially identified in mouse cytotoxic T lymphocytes [90] and has later been found to inhibit purified rat GrM [36] and – to a lesser extent – hGrM [91]. SPI-CI forms the classical SDS-stable serpin-protease complex with rat GrM, and is expressed by purified murine CD8^{+} T cells and even more by murine LAK cells [36]. Transfection of SPI-CI prevents both rat GrM and – with reduced efficiency – hGrM mediated cell death in tumor cells [36, 91]. No human ortholog of SPI-CI has been identified yet.

SerpinB4 is the only human intracellular B-clade serpin that contains a Leu residue at the putative P1 position in its RCL, and was therefore predicted to inhibit GrM [89]. Indeed, SerpinB4 directly inhibits hGrM proteolytic activity, and its overexpression in human HeLa tumor cells protects against both GrM-induced and NK cell-induced cell death [89]. Inhibition of hGrM by SerpinB4 occurrs with kinetics that resembled SerpinB4-mediated inhibition of CathepsinG and chymase [92]. More serpins that target hGrM might exist. Interestingly, SerpinB1, which also inhibits neutrophil elastase and harbors a Cys at the putative P1 and a Met at P1' [93], has recently been identified as a human GrH inhibitor [94], but also forms an SDS-stable complex with hGrM [94]. It is therefore tempting to speculate that this complex is formed by GrM-mediated hydrolysis of SerpinB1 at the P1' Met. Further investigation is required to determine the physiological relevance of this interaction.

Originally, granzyme-inhibiting serpins were mainly believed to act as a fail-safe mechanism for cytotoxic lymphocytes, to avoid self-injury during granule-exocytosis [95]. Lately, however, it is thought that tumor cells often misuse these serpins to avoid eradication by the immune system. It has been well established that some

tumors evade cytotoxic lymphocyte-mediated killing by blocking the activity of GrB through expression of the intracellular serpin PI-9. Expression of PI-9 by tumors not only correlates with decreased susceptibility to GrB-mediated apoptosis, but also positively associates with unfavorable clinical outcome [50-53]. Expression of the GrM inhibitor SerpinB4 may therefore constitute an analogous mechanism via which tumor cells could evade cell death. Interestingly, SerpinB4 expression has been found in numerous squamous cell carcinoma's: in the squamous cell carcinomas of the cervix [96], head and neck, and lung [97]. Moreover, elevated SerpinB4 mRNA levels correlate with the progression from normal, to dysplastic, to cancerous tissue [98], and to be a predictor of head and neck squamous cell carcinoma prognosis [99]. Furthermore, SPI-CI is also expressed by mouse colon carcinoma cell lines, suggesting it may serve a protective role in these cells as well [91].

Conclusion

Over the last five years, the arsenal of GrM functions has expanded enormously. While it was initially believed to function only in the induction of apoptosis in target cells, evidence is emerging that GrM functions in many other biological processes, amongst which noncytotoxic inhibition of viral replication and the regulation of inflammation. With the discovery of new GrM substrates, the mechanisms via which GrM exerts its function will become increasingly clear. Proteomics-based profiling of protease substrates (degradomics) will prove to be a valuable tool in this process [100].

A common theme in GrM functioning seems to be its substrate redundancy. In the induction of apoptosis, GrM targets multiple death substrates that all contribute to the execution of cell death. To inhibit CMV replication, GrM not only targets important viral proteins, but also essential host cell proteins. This high level of redundancy has likely evolved in an arms-race with viruses and tumor cells, which have also developed multiple strategies to counteract granzyme attacks. Tipping the balance in favor of GrM could lead to novel treatment modalities.

Acknowledgements

Authors are supported by the Dutch Cancer Society (KWF) [grant number UU-2009–4302 (to N. B.)] and the Netherlands Organization for Scientific Research (NWO) [grant number 916.66.044 (to N. B.)].

Outline of the thesis

The aim of this thesis is to provide novel insights into the anti-viral and anti-cancer functions of GrM. **Chapter 2** discusses state-of-the-art proteomic techniques that can be used to profile GrM specificity and to identify new GrM substrates. In **Chapters 3 and 4**, we identify several species-specific differences between human GrM and its mouse orthologue, which has implications for the use of GrM-knockout mouse models. In **Chapter 5**, we comprehensively characterize GrM-induced cell death in tumor cells. Furthermore, we show that GrM triggers cell cycle arrest and caspase-dependent apoptosis by cleaving the nuclear enzyme DNA topoisomerase II alpha. **Chapter 6** identifies SerpinB4 as an intracellular inhibitor of GrM that can inhibit its pro-apoptotic function in tumor cells. **Chapter 7** describes that GrM exerts an anti-viral function in CMV-infected cells by targeting the host cell protein heterogeneous nuclear ribonucleoprotein K. In **Chapter 8**, we describe the development of a novel biosensor for intracellular GrM activity, which can be used to investigate the physiological role of GrM *in vitro* and *in vivo*. Finally, the implications of our findings will be discussed in **Chapter 9**.

Chapter 2

Proteomic profiling of proteases: tools for granzyme degradomics

de Poot SAH[1], Van Domselaar R[1], and Bovenschen N.

Department of Pathology, University Medical Center Utrecht, Utrecht, The Netherlands.

[1]These authors contributed equally to this work.

Expert Rev Proteomics. 2010;7(3):347-59.

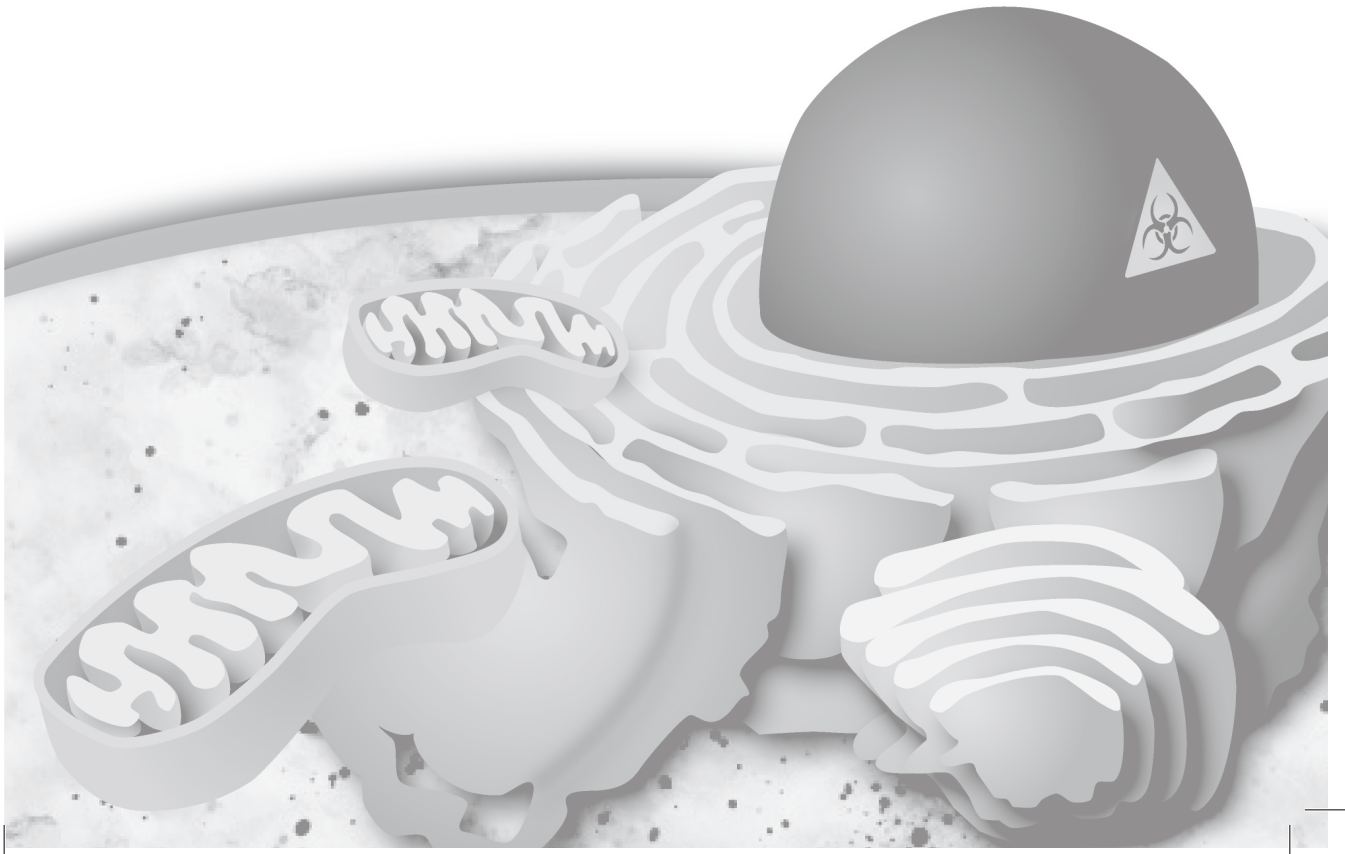

Abstract

Proteases are a family of proteolytically active enzymes whose dysfunction is implicated in a wide variety of human diseases. Although an estimated 2% of the human genome encodes for proteases, only a small fraction of these enzymes have well-characterized functions. Identification of the specificity and natural substrates of proteases in complex biological samples is challenging, but proteomic screens for proteases are currently experiencing impressive progress. Such proteomic screens include peptide-based libraries, fluorescent 2D difference gel electrophoresis with mass spectrometry, differential isotope labeling in combination with mass spectrometry, quantitative degradomics analysis of proteolytically generated neo-N-termini, and activity-based protein profiling. In the present article, we summarize and discuss the current status of proteomic techniques to identify protease specificity, cleavage sites and natural substrates with a particular focus on the cytotoxic lymphocyte granule serine proteases granzymes.

Keywords: 2D-DIGE • activity-based probes • granzyme • isotopic labeling • peptide libraries • protease • proteomics • substrate

Introduction

Proteases are enzymes that catalyze the hydrolysis of peptide bonds (also termed scissile bonds), and might thereby activate or inactivate proteins, or affect protein localization. In many organisms, including humans, approximately 2% of all genes encode for proteases and homologs [101, 102]. They are, therefore, likely to play an important role in many cellular processes in all living organisms. The complete set of proteases and protease inhibitors has been defined as the degradome [101]. The human degradome comprises 668 known and putative proteases, including membrane-bound proteases, and 400 nonpeptidase homologues [103]. Human proteases are divided into five classes according to their domains and their catalytic mechanism; aspartic, cysteine, metallo, serine and threonine proteases. Whereas aspartic and threonine protease classes have approximately 20 and 30 members, respectively, cysteine, metallo, and serine proteases are more numerous with approximately 160, 220 and 240 members, respectively. Aspartic and metalloproteases both use an activated water molecule as a nucleophile to attack the scissile bond. Aspartic proteases bind the water molecule through two aspartic residues, whereas metalloproteases use a zinc ion to bind the water molecule. Cysteine, serine and threonine proteases, on the other hand, attack the scissile bond through a nucleophile created by a catalytic triad.

Since proteases are involved in many cellular processes and since proteolysis is irreversible, the activity of proteases is tightly regulated. Like transcription, which is modulated by numerous stimulatory and inhibitory signals, post-translational regulation includes zymogen activation, allosteric regulation, inactivation through internal cleavage and endogenous inhibitors [104]. All proteases are synthesized as inactive pro-proteases, called zymogens, and activation of these precursors is often mediated by hydrolysis, resulting in exposure of the protease active site. Activation can also occur through environmental changes. Some proteins of the pepsin family, for instance, are activated in the lysosomal system by acidification, in which a change in pH results in a conformational change and the subsequent activation of the proteases. Once activated, protease activity is mainly controlled by endogenous inhibitors.

Aberrant protease activity is implicated in a wide variety of human diseases [102]. For example, gain-of-function mutations in aspartic protease genes of presenilins 1 and 2 cause early-onset familial Alzheimer's disease [105]. In the coagulation cascade, mutations in serine protease factor IX or its cofactor VIII cause hemophilia [106]. Furthermore, Papillon–Lefevre syndrome and pycnodysostosis are associated with loss-of-function mutations of cathepsin C and K, respectively [107, 108], and loss-of-function mutations in caspase-10 result in type II autoimmune lymphoproliferative syndrome [109]. Polymorphisms in the metalloprotease gene *ADAM33* are associated with asthma, and polymorphisms in the cysteine protease gene calpain-10 with Type-2 diabetes mellitus [110, 111]. Finally, a role for proteases in cancer is emerging since they are implicated as important mediators in angiogenesis, cell survival, cell growth, inflammation and metastasis [101, 112].

Proteases play crucial roles in both the adaptive and innate immune system. The complement system, for instance, comprises a cascade of proteases that, when triggered, can lead to the opsonization, phagocytosis and killing of microbes. In addition, effector cells of both the adaptive and innate immune system secrete proteases in order to eliminate pathogens, viral-infected cells and transformed cells. Cytotoxic T lymphocytes and natural killer cells, for instance, are key effector cells in eliminating viral-infected and transformed cells [113], and can induce cell death either via a cell death receptor signaling pathway, or, more importantly, via the release of cytotoxic granules directed towards the target cell[9, 114]. These cytotoxic granules contain several components, including perforin and a family of highly homologous serine proteases called granzymes. Perforin facilitates the entry of granzymes into the target cell, where the granzymes can exert their antiviral and antitumoral effects by the proteolysis of substrates. In humans, five granzymes have been identified (GrA, GrB, GrH, GrK and GrM) that differ on the basis of their primary substrate specificity. GrA and GrK cleave after Arg or Lys, GrB cleaves after Asp or Glu, GrM cleaves after Leu or Met, and GrH cleaves after Tyr or Phe [29]. In addition to their intracellular functions, granzymes have also been identified as extracellular proteases in several inflammatory responses [115, 116]. Moreover, activation of the complement system and secretion of proteases by effector cells might contribute to the pathogenesis, inflammation and tissue damage in several clinical conditions, including allograft rejection, Alzheimer's disease, ischemic-reperfusion injury, cardiovascular diseases, allergies and autoimmune diseases [115-118].

Proteases can not only be used as diagnostic tools in a broad variety of diseases but are also promising targets for therapy [119]. This implies that it is critical to fully understand the role of proteases in health and disease. So far, only a small fraction of all proteases has been well characterized. Therefore, novel proteomic techniques have been developed in the last decade to identify protease specificity, to screen for natural protease substrates and to monitor protease activity. In the present article, we summarize and discuss the current status of these proteomic developments, with a particular focus on the cytotoxic family of granzymes as model serine proteases.

Profiling protease primary & extended substrate specificity using peptide libraries

Primary protease substrate specificity has been defined as the amino acid residue (also referred to as P1) after which a protease prefers to cleave. The residues that are C-terminal to the cleavage site are designated as the nonprime-side sequence (P2, P3 and P4), whereas N-terminal residues are known as the prime-side sequence (e.g., P1´, P2´ and P3´) [27]. These residues flank the P1 amino acid and constitute the extended substrate binding site, which contributes to protease specificity to a large extent. Peptide-based approaches have been valuable biochemical tools to characterize the primary and extended protease specificity.

One method that is commonly used to screen for protease specificity is substrate phage display [120]. Variable substrate peptide sequences are displayed

on phages that are immobilized by affinity tags. Cleavage of its variable peptide sequence separates a phage from its affinity tag, resulting in its release. These protease-sensitive phages are then collected and propagated in bacteria, followed by the sequencing of the variable peptide sequence of each clone. Substrate phage display has been used to compare substrate specificities from P4 to P3´ between human and mouse GrB [121]. Two libraries were constructed, one of which comprised randomized peptide sequences and one with randomized peptides that each contained an aspartate residue near the center of their sequence. While their primary P1 specificity is shared, human and mouse GrB show distinct extended substrate specificities [121, 122]. The observations that human GrB cleaves both human and mouse Bid, but mouse GrB cleaves neither mouse nor human Bid, suggest that GrB has species-specific functions [121, 122].

In an alternative method using cellular libraries of peptide substrates (CLIPS), a variable substrate peptide acts as a linker between a cell surface protein and a fluorescent-probe peptide ligand on the surface of *Escherichia coli* [123]. Cleavage of the variable substrate peptide results in reduced fluorescent labeling and nonfluorescent cells are sorted by flow cytometry. Although both substrate phage display and CLIPS are powerful tools to identify protease specificity, multiple rounds of selection are required for enrichment, followed by extensive sequencing, which often includes the analysis of identical clones. Furthermore, these methods require knowledge of the primary P1 substrate specificity of the protease in order to predict the cleavage site within the variable peptide sequence. Follow-up experiments are typically required to validate the predicted cleavage site.

To avoid time-consuming rounds of selection and enrichment, a PepChip Protease array is available to screen for extended substrate specificity in a similar fashion [124]. This array contains 1000 random 15-mer peptides, each with a biotin-labeled C-terminus and an N-terminus coupled to the microarray surface. Intact 15-mer peptides can be visualized by fluorescein-labeled streptavidin, while cleavage of peptides by incubation with a protease results in the release of the biotin label and reduced fluorescent labeling. However, prior knowledge of primary P1 substrate specificity is also a prerequisite for this technique. We have previously used this method to compare the extended specificity of GrA and GrK [124]. Our data show that both GrK and GrA prefer P1 Arg over P1 Lys and display partially overlapping extended substrate specificities. However, no clear amino acid preference at subsites near the cleavage site has been identified, which is consistent with known cleavage sites in macromolecular substrates [124-126].

In order to determine protease specificity without prior knowledge of primary substrate specificity, peptide libraries of the human proteome have been developed and can be used for the proteomic identification of protease cleavage sites (PICS) [127]. Proteins from human cell lysates are digested into oligopeptides, using, for instance, trypsin or chymotrypsin. Next, cysteines are reduced with iodacetamide to prevent cross-linking and chemical cross-reactivity of the cysteine sulfhydryls and the primary amino termini are blocked by reductive methylation. These proteome-

derived peptide libraries can be incubated with a protease of interest. Subsequently, newly generated amino termini are labeled with biotin and isolated by immobilized streptavidin. Eluted peptides are subjected to mass spectrometry (MS) to identify the prime-side sequences (P1´–P6´). The nonprime-side sequences (P6–P1) are reconstructed by automated database searches of the human proteome. This method is very powerful since cleavage sites spanning from P6 to P6´ can be identified in the same experiment, whereas the previously described methods only predict the nonprime-side residues and require follow-up experiments to determine the primary substrate specificity. Thus, PICS directly determines the P1 scissile bond and is uniquely suited for studying subsite cooperativity. There are some drawbacks to using PICS. First, in cases where the prime-side sequence occurs in more than one protein, the nonprime-side sequence cannot be reconstructed. Second, cleavage sites that match the specificity of the digestion enzyme used to create the library are excluded because these could be the result of incomplete inactivation of primary amines. Furthermore, when the protease cleavage site overlaps with the cleavage site of the digestion enzyme, cleavage does not occur. However, proteome-derived peptide libraries can be created using different digestion enzymes in order to overcome these limitations. This method has been used to identify protease specificity for several proteases, including matrix metalloprotease (MMP)2, thrombin, neutrophil elastase, cathepsin G and K, and caspase-3 and -7 [127].

The most powerful screening tool for peptide substrate specificity makes use of positional scanning substrate libraries (PSLs), which were developed in the early 1990s [128, 129]. In order to map which residues of the substrate interact with the active site of the protease, small peptides are used that represent possible P4–P3–P2–P1 combinations with a quenched fluorophore linked to the P1 residue. This fluorophore is released upon peptide cleavage and then elicits fluorescence. Peptide libraries comprising 20 P1-diverse sublibraries with a fixed P1 and randomized P4–P3–P2 have been developed. At the moment, these peptide libraries provide the fastest method to map protease specificity, although they are limited to P1–P4 characterization and cysteines are excluded from the libraries. PSLs have been used for numerous proteases, including granzymes. Harris *et al.* have combined PSLs with substrate phage display to define the extended substrate specificity of GrB spanning from P4 to P2´ [130]. In addition, PSLs have been used to determine the P4–P1 specificity for all five human granzymes [28, 29, 125, 131]. Fairly distinct substrate specificities were found for each granzyme, suggesting that they may exert their antitumoral and antiviral activities via different mechanisms.

Defining the primary and extended protease specificity by peptide-based approaches is perfectly suited for the design of tailored small-molecule inhibitors towards proteases. However, in order to understand the role of a protease in biological and pathological processes, it is important to identify its natural substrates. Since protease substrates are not peptides, peptide cleavage motifs rarely reflect cleavage sites within macromolecular substrates. Peptide cleavage motifs may for instance be buried within the 3D fold of a particular substrate. Furthermore,

protease exosites can also contribute to the recognition and cleavage of substrates [132, 133]. Finally, a single protease often has several substrates and may, therefore, be implicated in more than one biological process. Hence, for functional protease profiling, the focus has shifted towards the identification of natural substrates in complex biological samples.

Proteomic identification of natural protease substrates

2D difference gel electrophoresis

To screen for natural protease substrates, 2D gel electrophoresis (2-DE) can be used [134]. Protein samples are first separated by isoelectric focusing on acrylamide strips on which a pH gradient is generated. When an electric potential is applied to the strip, proteins will migrate to the position within the strip where the pH is equal to their isoelectric point. Then the strips are subjected to SDS-PAGE gels, where proteins are separated according to their molecular weight. Previously, proteins were visualized by common protein stainings, such as silver staining, where every spot represents a protein with unique coordinates within the gel. This 2D gel-based proteomics approach was successful in studying natural substrates of GrM [45] and GrB in the presence or absence of effector caspase-3 or -7 [135]. These studies have shown that GrM targets the microtubule network and that GrB facilitates cellular demolition mainly through activation of caspase-3, with the identification of 17 GrB-substrates after analysis of a subset of altered protein spots. However, by using this classical 2-DE, quantification of protein spots between multiple samples is difficult since every sample has to be applied to a different gel and inter-gel variability is high. With the development of fluorescent dyes, this method has been improved for the relative quantification of protein spots between two samples and is called 2D difference gel electrophoresis (2D-DIGE) [136, 137]. In 2D-DIGE, protein samples are labeled with different fluorescent dyes, for example, CyDye fluor-2, -3 or -5, which bind lysine residues through their *N*-hydroxysuccinimide (NHS)-ester reactive group. Since these dyes are chemically similar in both charge and molecular weight, they have very limited effects on the migration pattern of proteins. The fluorescently labeled protein samples are pooled and subjected to 2D electrophoresis. For each sample, proteins are then visualized according to the specific excitation and emission wavelengths of each dye within the same gel. To further improve relative quantification of two samples, an internal control is created by labeling a mixture of equal amounts of both protein samples with Cy-2 [136]. This also allows relative quantification between multiple gels. Protein spots of interest can be excised and analyzed by MS for protein identification. Both 2-DE and 2D-DIGE have limited use for low-abundance proteins, membrane-bound proteins, very-low-molecular-weight proteins and proteins with an isoelectric point outside the pH range of 3–10.

Bredemeyer *et al.* have evaluated this method for protease substrate discovery by testing whether known GrB targets could be identified using 2D-DIGE [138]. Mouse lymphoma cell lysates were prepared in the presence of caspase inhibitors

and treated with either purified murine GrB followed by red fluorescent Cy-5 labeling, or no protease followed by green fluorescent Cy-3 labeling as a control sample. Both samples were pooled and subjected to 2D-DIGE, and the gel was sequentially scanned for both fluorescent dyes. An overlay of both fluorescent images showed a map of protein spots, with yellow spots representing proteins that were unaffected by GrB, green spots representing intact GrB substrates, and red spots representing GrB-induced cleavage products. Spots that showed high reproducibility and more than twofold changes in abundance were excised and identified by MS. In this study, 13 spots could be identified that corresponded to eight different proteins. Cleavage of the well-established GrB substrate procaspase-3 has been confirmed with this method, but novel GrB substrates have also been identified. Furthermore, 2D-DIGE proved to be successful in studying the kinetics of GrB-induced cleavage of substrates [138].

GrA and GrB have been studied extensively and their cell death pathways are well characterized [114]. In addition, GrA has been implicated in inflammation by inducing a proinflammatory cytokine response [84]. By contrast, not much is known regarding GrK besides its shared primary trypsin-like substrate specificity with GrA. Therefore, it is believed that GrK may provide a backup and failsafe mechanism for GrA with redundant specificity. Recently, we have employed 2D-DIGE to compare the macromolecular substrate specificities of human GrA and GrK (Figure 1) [124]. Out of approximately 1500 proteins, 14 spots disappeared (~0.9%) (intact substrates), and 22 spots appeared (cleavage products) following the incubation of tumor cell lysate with GrK (Figure 1C). For GrA, 30 spots disappeared (~2%) and 55 spots appeared following the incubation of tumor cell lysate with GrA (Figure 1C). The relatively low number of disappearing spots for GrK (~0.9%) and GrA (~2%) indicates that macromolecular substrate specificities of both granzymes are highly restricted and that GrK has an approximately twofold more restricted substrate specificity compared with GrA. Six proteins were cleaved and shared by both granzymes, indicating that the macromolecular substrate specificities of both granzymes partially overlap in approximately 16%. Of the cleavage products that appear during granzyme incubation, 14 spots are shared by both granzymes, strongly suggesting that GrA and GrK cleave these proteins at the same P1 cleavage sites. However, N-termini have to be identified in order to validate that GrA and GrK share these P1 cleavage sites. Although the identified macromolecular substrates need to be validated *in vivo*, this 2D-DIGE approach suggests that GrK not only functions as a redundant granzyme that assists GrA-mediated responses, but also displays unique functions [124].

Protein topography & migration analysis platform

Recently, a new method has been developed to screen for natural protease substrates using 1D SDS-PAGE coupled to liquid chromatography (LC)-tandem mass spectrometry (MS/MS), called protein topography and migration analysis platform (PROTOMAP) [139]. Previously, Thiede *et al.* described a proteomic approach

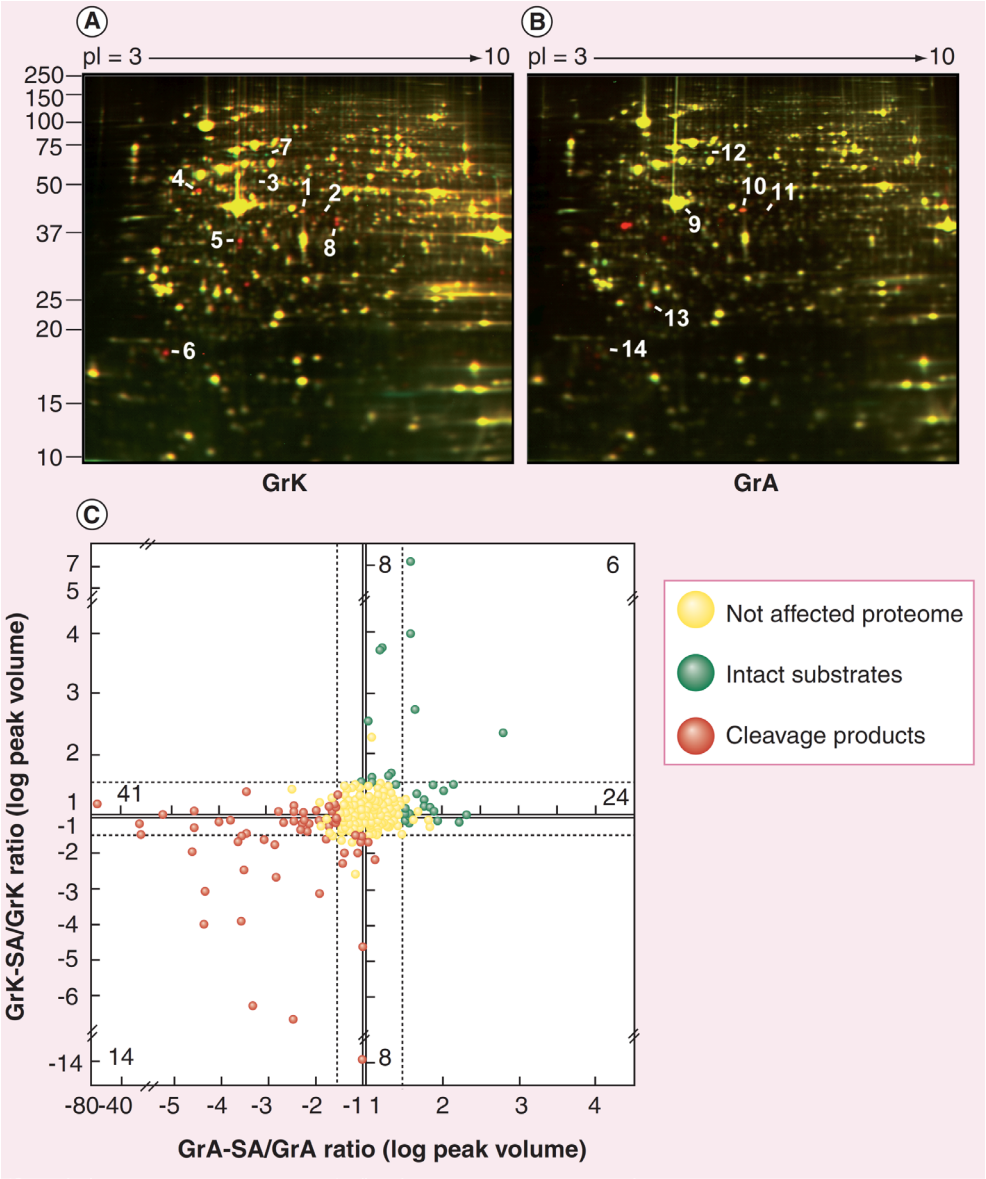

Figure 1. Proteomic profiling of GrA and GrK by 2D-DIGE. (A) Jurkat cell lysates were incubated with GrK (1 μM) or catalytically inactive GrK-SA mutant (1 μM) for 60 min at 37°C followed by red fluorescent Cy-5 and green fluorescent Cy-3 labeling, respectively. Samples were pooled and subjected to 2D-DIGE. **(B)** Jurkat cell lysates were incubated with GrA (1 μM) or catalytically inactive GrA-SA mutant (1 μM) for 60 min at 37°C followed by red fluorescent Cy-5 and green fluorescent Cy-3 labeling, respectively. Samples were pooled and subjected to 2D-DIGE. Both experiments were repeated four times. Yellow spots represent unaffected proteins, green spots represent intact protease substrates and red spots represent cleavage products. Numbers indicate protein spots that were excised and identified by mass spectrometry. **(C)** Gels were matched and protein spots were quantified. GrK/GrK-SA log peak volume ratios of protein spots (y-axis) were plotted against GrA/GrA-SA log peak volume ratios of the same protein spots (x-axis). Spots are depicted in yellow (unaffected proteome), green (intact substrates) or red (cleavage products) according to peak volume ratios (>1.5-fold, dotted line; $p < 0.05$). 2D-DIGE: 2D difference in gel electrophoresis; GrA: Granzyme A; GrK: Granzyme K. Redrawn with permission from [124] © 2009 The American Society for Biochemistry and Molecular Biology.

in which biological samples are first fractionated by SDS-PAGE to reduce sample complexity. After electrophoresis, proteins from gel slices are digested with trypsin before protein abundance is measured by LC-MS/MS [140]. PROTOMAP, however, integrates the information of SDS-PAGE protein migration rates with LC-MS/MS analysis. In PROTOMAP, a control and experimental sample are subjected to SDS-PAGE and then gel bands are excised from each sample lane at fixed intervals. Bands are digested with trypsin to release peptides that are subsequently analyzed by 1D reverse-phase LC-MS/MS. For each protein, information on SDS-PAGE migration rates, sequence coverage and spectral counts – that is the relative abundance of intact proteins and cleavage products – are integrated into graphs, termed peptographs. In addition to the identification of natural protease substrates in complex biological samples, PROTOMAP provides semiquantitative information on cleavage efficiency and stability of cleavage products, that indicates whether proteins are completely degraded or whether new forms of cleaved proteins are generated. It is possible to identify macromolecular cleavage sites when half-tryptic peptides are detected and one terminus matches the substrate specificity of the protease, although this method was not originally designed for this purpose.

To test this method, proteolytic events induced by the intrinsic apoptotic pathway were analyzed. Jurkat cells were treated with staurosporine to induce the intrinsic apoptotic pathway and cell lysates of apoptotic and control cells were analyzed by PROTOMAP [139]. More than 250 cleaved proteins were identified, including well-established caspase substrates as well as 170 proteins that were not previously known to be proteolyzed during apoptosis. Cleavage of those proteins was partly validated by Western blotting and many cleavage sites that matched caspase substrate specificity were identified. Strikingly, proteins that were not previously reported to be cleaved during apoptosis were identified with lower spectral counts compared with proteins known to be cleaved during apoptosis, indicating that PROTOMAP is sensitive in detecting low-abundance peptides. However, this technique is limited in its detection of cleavage events that cause very small changes in mass owing to its reliance on SDS-PAGE.

Quantitative degradomics

In addition to gel-based techniques, such as 2D-DIGE, a wide variety of gel-free techniques can be employed to identify novel macromolecular protease substrates. These gel-free techniques are coupled to MS and can provide quantitative information regarding proteolytic processing. With quantitative gel-free techniques, peptide ratios describing the relative abundance of specific peptides in two or more samples can be obtained. In order to establish peptide ratios, the differential labeling of proteomes is required. This is often realized by isotopic labeling, which can be done either chemically or metabolically. The isotopic labeling of proteomes creates a small mass difference between the peptides that originate from one proteome and the peptides originating from another proteome. When two or more samples are mixed and analyzed by MS, the mass difference between the peptides

then allows them to be traced back to their sample of origin. The peak intensities of the peptides can be used to establish peptide ratios. Numerous labeling techniques have been developed over the years, and the most commonly used techniques are described here.

With isotope-coded affinity tags (ICAT), developed in the late 1990s, differential labeling of proteomes is achieved by the chemical modification of cysteine residues with isotopically coded biotin-tagged reagents [141]. These biotin-tagged reagents consist of three moieties: a thiol-reactive group that mediates cysteine modification, a linker and a biotin tag. The linker, which is necessary for the quantitative comparison of proteomes, can be either light or heavy, depending on its isotopic contents. After cysteine labeling, the two samples are combined and digested with trypsin. Peptides that contain a biotin-labeled cysteine residue are captured using affinity chromatography with an avidin column, and can subsequently be analyzed by LC-MS/MS. The MS analysis results in the identification of peptides, and the mass difference between the ICAT labels imparts to which sample each peptide peak belongs, allowing relative quantification of proteins or peptides.

Originally, the heavy ICAT probes contained the heavy isotope deuterium. Peptides labeled with either the deuterated or the nondeuterated ICAT probes, however, were found to separate into different fractions in LC, complicating reliable quantitative analysis [142]. In order to eliminate these and additional problems of deuterated ICAT probes, new probes containing the ^{12}C or ^{13}C isotopes were developed. It has been shown that these isotope labels do coelute in LC for reactive tags similar to ICAT probes [143]. While these second-generation probes were a large improvement on the deuterated probes, some problems – such as false positives caused by fragmentation of the relatively large ICAT tags – remained, which is why variants of the classical ICAT method have been designed. For instance, in the solid ICAT method [144], and in methods using cleavable ICAT, the biotin element of the ICAT label is removed, resulting in smaller labels and, therefore, fewer false positives. One of the main advantages of ICAT is its avidin-mediated selection step for peptides that contain biotin-labeled cysteine residues, which results in a substantial reduction of sample complexity. Conversely, this selection for cysteines also forms one of the technique's largest drawbacks: by only analyzing peptides with cysteine residues, just a small fraction of the proteome can be analyzed.

Whereas ICAT specifically labels cysteine residues, isobaric tag for relative and absolute quantitation (iTRAQ) labels both N-termini and the side chains of lysine residues [145]. In iTRAQ, samples are digested with trypsin, after which the N-termini and lysine side chains of peptides are reduced and alkylated. These can then be modified chemically by the amine-reactive NHS group of an iTRAQ tag. The samples are labeled with different iTRAQ probes, mixed, and subjected to LC-MS/MS. Aside from a NHS group, an iTRAQ tag also contains a reporter group and a balance group. Currently, eight different iTRAQ reporter groups exist, with masses varying from 113.1 to 121.1 Da. The mass of the entire iTRAQ tag is stabilized by the balance group, which ensures that all iTRAQ probes have an identical mass of 305

Da. This greatly simplifies initial sample analysis and peptide identification, since peptides that are differently tagged behave similarly in chromatography and appear as a single precursor ion in MS [145]. After collision induced dissociation (CID) in tandem MS/MS, the reporter ions fragment from the peptides and can be detected as low-mass fragment ions, enabling relative quantification of peptide abundance in two or more samples.

While iTRAQ and ICAT label proteins chemically, labeling is achieved metabolically in stable isotope labeling with amino acids in cell culture (SILAC) [146]. In SILAC, cells are grown in a medium deficient for a certain amino acid, but supplemented with an isotopically labeled form of that amino acid (e.g., ^{12}C- or ^{13}C-labeled arginine). This ensures the full incorporation of the isotopic label, whereas chemical labeling often fails to label all of the targeted amino acids. While chemical labeling techniques may fail to label all targeted amino acids, the effect on relative quantification should be minimal, as the quantification is relative. Since the incorporation of SILAC labels depends on protein synthesis, however, SILAC labeling can only be performed on living cells.

N-terminal enrichment

Labeling techniques such as ICAT, iTRAQ and SILAC, are especially useful for proteomic analysis of cell-surface proteolysis, in which proteins that are normally immobilized are released into the extracellular environment by proteolysis. ICAT has, for instance, been employed by Butler *et al.* to study proteolytic processing of membrane proteins from human breast cancer cells transfected with matrix metalloproteinase (MMP)-14 treated with or without an MMP inhibitor [147]. In addition, Tam *et al.* used ICAT to examine changes in protein abundance in medium from a human breast carcinoma cell line transfected with membrane type 1 MMP [148]. In the latter study, over 100 proteins showed increased abundance in the medium of MT1-MMP transfected cells, probably due to shedding from the cell surface. In addition, both ICAT and iTRAQ have been employed to determine the levels of cleaved and intact proteins from culture medium of fibroblasts expressing low levels of MMP-2 [149]. The iTRAQ approach allowed the high confidence identification of nine-fold more proteins than ICAT, showing its improved potential as a high-content proteomics technique. For proteomic analysis of intracellular proteolysis, however, it remains difficult to identify protease substrates owing to high sample complexity. Isotopic labeling techniques do enable peptide quantification but become much more powerful for protease substrate identification and cleavage site analysis when they are coupled to specific N-terminal enrichment approaches.

All current forms of N-terminal enrichment make use of the fact that N-termini – such as lysine side chains – display reactive nitrogen atoms. While N-termini have α-amines, lysine residues have side chains with ε-amines, which behave differently in certain reactions. N-terminal enrichment can be achieved via either negative or positive selection of N-termini. In negative selection, the N-termini and lysine side chains of proteins in both a protease-treated and an untreated sample are chemically modified in such a way that they are blocked from further modification.

Subsequently, the samples are enzymatically digested and newly formed N-termini are chemically modified, selected and discarded. The peptides that remain are those with the original and protease-generated N-termini. In negative selection, the preservation of peptides with original N-termini positionally anchors most of the peptides to precise locations within parent proteins, enabling higher confidence of protein identification [150]. The removal of peptides with labeled neo-N-termini, however, is not always very efficient, and even small inefficiencies in their removal can create significant background levels and false positives. In N-terminal enrichment approaches that positively select for N-termini, the N-termini of protease-treated and untreated samples are modified, after which the proteins are enzymatically digested (Figure 2). The peptides that contain a modified N-terminus are captured and analyzed. One aspect of this technique is the loss of endogenously *N*-acetylated N-termini, which account for approximately 80% of all N-termini [151]. This significantly reduces sample complexity and, therefore, increases the sensitivity of the technique for proteolytic cleavage products.

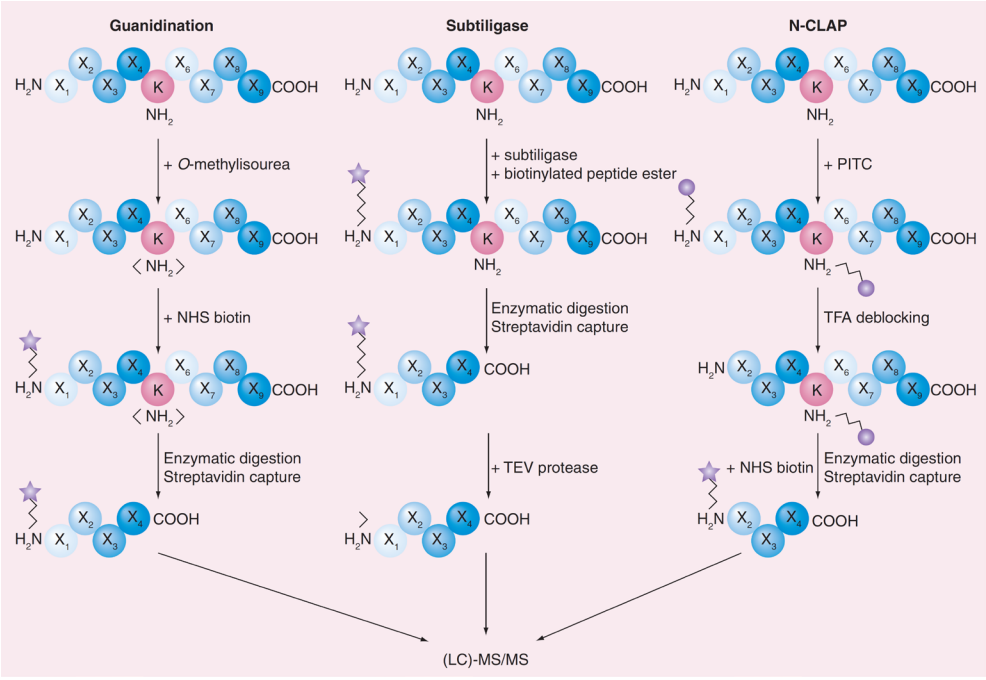

Figure 2. Positive selection of N-termini. In guanidination-mediated selection of N-termini, lysine residues (K; pink circles) are specifically blocked by *O*-methylisourea to protect them from further modification. The subtiligase approach, on the other hand, specifically labels N-termini by transferring part of a biotinylated peptide ester onto the a-amine of an N-terminus. In N-CLAP, both N-termini and lysines are initially blocked with PITC. Addition of TFA then results in the intramolecular cyclization of PITC-modified (N-terminal) a-amines and the cleavage of the peptide bond between X1 and X2. The newly formed N-terminus at X2, which is unblocked, can then be modified with an amine-reactive reagent, such as NHS-biotin. After specific labeling of the N-termini in all three approaches, proteins can be digested enzymatically, and N-terminal peptides can be isolated and analyzed by (LC)-MS/MS. K: Lysine residue; LC: Liquid chromatography; MS: Mass spectrometry; N-CLAP: N-terminalomics by chemical labeling of the a-amines; NHS: *N*-hydroxysuccinimide; PITC: Phenyl isothiocyanate; TEV: Tobacco etch virus; TFA: Trifluoroacetic acid; X1: N-terminal amino acid; X2: Second amino acid.

Negative selection of N-termini

Combined fractional diagonal chromatography (COFRADIC) facilitates protease substrate identification via negative N-termini selection [152]. In COFRADIC, the N-termini and lysine side chains of proteins are acetylated with NHS acetate, effectively blocking them from further modifications. The protein samples are then digested with trypsin, after which they are fractionated using reverse-phase high-performance liquid chromatography (HPLC). The newly formed, unblocked N-termini of the tryptic peptides are subsequently modified with 2,4,6-trinitrobenzenesulfonic acid (TNBS), creating highly hydrophobic trinitrophenyl derivatives. The separate fractions are then subjected to reverse-phase HPLC once more. As a result of TNBS-modification, peptides with newly formed, modified N-termini will elute in later fractions than the fractions they originally eluted in, while peptides with blocked N-termini will elute in the same fraction as before. The peptides that elute in their original fraction in the second reverse-phase HPLC run are collected and identified with MS/MS. The addition of a strong cation exchange (SCX) step prior to fractionation may enrich even further for original N-termini, yielding over 90% of pure N-terminal peptides [153, 154]. While this method allows for significant N-terminal enrichment, it does not permit relative quantification of identified peptides. When COFRADIC is combined with differential labeling techniques, however, quantitative analysis of COFRADIC peptides becomes possible. A slightly modified COFRADIC approach, for instance, in which the C-termini of peptides are labelled with stable ^{16}O or ^{18}O isotopes during trypsin digestion [155], has been used to relatively quantify peptide levels [156]. In addition, other forms of isotopic labeling may also be used to allow peptide quantification, such as SILAC labeling [154, 157]. While COFRADIC is a powerful technique for the quantification and identification of protease substrates, it is also very laborious and time consuming.

Recently, Van Damme and colleagues have used a combination of SILAC labeling and COFRADIC N-terminal enrichment to identify the substrates of mouse and human GrB orthologs [154]. Human K-562 or mouse YAC-1 cells were metabolically labeled with $^{12}C_6$-, $^{13}C_6$-, or $^{13}C_6\ ^{15}N_4$-labeled L-arginine. This triple SILAC labeling allows direct comparison of untreated cells with cells exposed to human GrB and cells exposed to mouse GrB. Furthermore, the triple SILAC labeling enables the determination of the relative cleavage efficiencies of human and mouse GrB. As a result, Van Damme *et al.* have identified 322 human and 282 mouse substrates of human and mouse GrB, respectively, and over 100 orthologous substrates that were cleaved by both granzymes. The identification of known GrB substrates, such as caspase-7, lupus La protein and fibrillarin, confirmed the validity of the technique. Moreover, the GrB cleavage sites in these substrates could also be determined. In another study, Kaiserman *et al.* have successfully used a similar COFRADIC approach to identify substrates of the rodent GrC in YAC-1 cell lysates [157]. GrC, which normally suffers from autoinhibition as a result of an unusual conformation of its active site, can be unlocked by mutation of Glu-192 and Glu-193 to the corresponding residues in mouse GrB. By comparing the cleavage specificities and efficiencies of wild-type

GrC with the E192R/E193G unlocked GrC mutant, Kaiserman and colleagues have been able to demonstrate that the granzyme variants share six substrates, that were significantly more efficiently processed by the unlocked GrC mutant. In addition, proteolytic processing occurred at the same positions in the substrates for both granzymes, suggesting that substrate specificities were similar for the wild-type and mutant GrC.

In addition to COFRADIC, numerous other approaches exist that enrich for N-termini via negative selection. In one approach, original N-termini are first blocked via acetylation, after which the proteins are enzymatically digested. The newly formed N-termini are modified with an amino-reactive NHS-ester derivative of biotin and the resulting biotinylated peptides are selectively removed by streptavidin beads [150]. In a slightly modified version of this protocol, amino-reactive NHS-activated sepharose is used instead of biotin [158]. This enables the direct removal of peptides with novel N-termini, decreasing the number of steps required for N-terminal peptide isolation and, therefore, also decreasing sample loss. If this technique were to be used in combination with isotopic labeling of samples, identification and quantification of protease substrates would become possible. In a second approach known as terminal amine isotopic labeling of substrates (TAILS), recently developed by Kleifeld *et al.*, samples are reduced, alkylated and labeled with amino-reactive isotopically labeled reagents, such as iTRAQ [159, 160]. After being labeled, proteins are enzymatically digested with trypsin, and peptides containing new, unblocked N-termini are extracted by an amine-scavenging dendritic polyglycerol aldehyde polymer. The peptides that remain are then analyzed by LC-MS/MS, allowing the quantitative analysis of protease substrates and the identification of cleavage sites.

Positive selection of N-termini

Techniques that enrich for N-terminal peptides via positive selection have to distinguish between the α-amines of N-termini and the ε-amines of lysine side chains (Figure 2). In one strategy, proteins are first denatured, reduced and alkylated, after which all lysine side chains are blocked from further modification via lysine-specific guanidination with *O*-methylisourea [161, 162]. After enzymatic digestion, this then allows the specific labeling of N-terminal amines with NHS-biotin, which can subsequently be captured by streptavidin in affinity chromatography and analyzed with LC-MS/MS. While the positive selection of N-termini in this technique reduces sample complexity by excluding endogenously acetylated N-termini, the biotinylation of serine, threonine or histidine side chains could introduce false positives, and should, therefore, be highly efficient and specific for the amine groups of N-termini. *O*-biotinylation, however, can be converted chemically and database searching of MS/MS spectra should identify such false positives.

Another approach that selectively labels the α-amines of N-termini exploits the ability of subtiligase, an engineered variant of the bacterial serine protease subtilisin (BPN´) [163], to specifically recognize α-amines [164]. Subtiligase can transfer the N-terminal portion of a biotinylated peptide ester onto the free α-amines of

N-termini. After enzymatic digestion of the proteins, N-terminal peptides can be isolated using streptavidin beads, after which they are released by TEV protease-mediated cleavage of the biotin tag. Following TEV cleavage, a dipeptide tag remains on the N-terminal peptides, which can be measured in MS/MS analysis to verify the peptides as true N-terminal peptides. Unfortunately, subtiligase labeling is not very efficient and, therefore, necessitates large quantities of complex material.

A third method that has recently been developed to label N-termini is known as N-terminalomics by chemical labeling of the α-amine of proteins, or N-CLAP [165]. In N-CLAP, N-termini and lysine side chains are blocked by the amine-reactive reagent phenyl isothiocyanate (PITC). Trifluoroacetic acid can then cause the intramolecular cyclization of PITC-modified α-amines, but cannot cyclize PITC-modified ε-amines. The intramolecular cyclization of the α-amines results in the cleavage of the peptide bond between the first (N-terminal) amino acid and the second, generating proteins that are one amino acid shorter, with unblocked amines at their newly formed N-termini. These can then be labeled (e.g., with biotin) using amine-reactive reagents, after which the proteins can be digested, purified and analyzed by MS. Since initial experiments with this method seemed to identify fewer cleavage sites than other studies did with N-terminal labeling approaches, the technique and instrumentation might still require some optimization to yield more results.

Activity-based proteomics

In order to understand whether an activated protease is involved in biological processes and whether aberrant protease activity is associated with disease, it is crucial to determine protease activity in biological samples *in vivo*. To this end, activity-based probes (ABPs) have been developed that irreversibly bind to the activated form of the protease. These probes consist of a reactive group that covalently binds the active site, a linker and a tag that either allows the visualization or the isolation of the active protease. Most often, fluorophores or radioactive molecules are used for visualization, while common affinity tags, such as biotin and streptavidin, are used for isolation. ABPs have been successfully developed for serine [166-170], cysteine [171-176] and threonine proteases [177, 178], with a reactive group that targets the conserved active site nucleophiles of these specific protease classes. It proved more challenging to design ABPs for metalloproteases and aspartic acid proteases, since these proteases use an activated water molecule to exert hydrolysis, and chemical reactive groups often lack the ability to covalently bind these active sites. To overcome this difficulty, ABPs for metalloproteases were designed that consist of a hydroxamate group that binds the zinc-molecule non-covalently but with high affinity, a photolabile group that can be activated by light to form covalent bonds between the probe and the target protease, and an affinity tag [179, 180]. ABPs with affinity tags allow proteomic profiling of activated proteases in biological samples and the characterization of protease function in biological processes [181]. It is challenging to design ABPs with complete selectivity towards all members of a specific protease class, which makes activity-based protein

profiling difficult. ABPs that bind one specific protease, however, can be achieved by introducing a peptide moiety into the ABP with a peptide sequence that matches the protease substrate specificity.

To demonstrate the use of ABPs, Winssinger *et al.* have investigated cytotoxic lymphocyte-mediated cell death by incubating cell lysates with GrB, and examined activity of several cysteine proteases using ABPs [182]. Incubation of ABPs with crude Jurkat cell lysates pretreated with GrB showed increased labeling of active caspase-3, a protein known to be cleaved and activated by GrB. In another study, Mahrus *et al.* have constructed chemical functional probes for GrA and GrB to elucidate their role in natural killer cell-mediated killing of target cells. These biotinylated and substrate specificity-based diphenyl phosphonates allowed facile evaluation of selectivity through activity-based profiling in cell lysates and intact cells. Both inhibitors are extremely selective *in vitro* and in cells. Use of these inhibitors in cell-based assays has revealed GrA to be a minor effector and GrB to be a major effector of target cell killing by natural killer cells [29].

Recent developments made it possible to image protease activity *in vivo*. Stable fluorescently labeled ABPs have been developed that covalently bind active cysteine cathepsins [183] and caspases [184]. The latter study demonstrates the potential of these novel fluorescent ABPs by monitoring caspase activity in two distinct mouse models. In the first model, apoptosis in the thymus was induced by dexamethasone treatment, whereas in the second model, apoptosis was induced in cells of human colorectal tumors that had been xenografted onto mice. In contrast to the control probes, intravenous injection of the active fluorescent probes followed by noninvasive optical imaging led to the detection of specifically labeled activated caspases in apoptotic thymocytes *ex vivo* and human colorectal tumor cells *in vivo*. The activation of caspases was confirmed by SDS-PAGE analysis and tissue histology. Although control probes failed to bind active caspases, they accumulated as free probes in apoptotic tissue and showed low tumor-specific fluorescence. These developments allow new methods to assess the specificity of therapeutic agents *in vivo* and provide valuable information on the role of proteases in clinical conditions.

Expert commentary

During the past few decades, peptide-based proteomics has allowed us to profile and define the primary and extended specificity of proteases (Table 1). This peptide-centric profiling does not contribute significantly to our understanding of protease function *in vivo*, since protease specificity profiles rarely reflect cleavage sites in macromolecular substrates. Importantly, however, information on P1 and subsite substrate specificity enables the design of specific tailored small peptide-based protease inhibitors and the development of new tools to characterize protease function *in vivo*, such as activity-based probes. The development and improvement of protein-centric methods to identify natural substrates of proteases, on the other hand, has led to a better understanding of the role of several proteases in biological processes (Table 1). This means that, while they may sometimes provide overlapping

Table 1. Proteomic screens that characterize protease function

Proteomic screen	Primary P1 specificity	Extended specificity	Natural substrates	Macromolecular cleavage sites	Kinetics of cleavage
Phage display	-	+	-	-	-
CLIPS	-	+	-	-	-
PepChip protease array	-	+	-	-	-
PICS	+	+	-	-	-
PSL	+	+	-	-	-
2D-DIGE	+/-*	+/-*	+	+	+
Protomap	-	-	+	+/-*	+
Isotopic labeling coupled to N-terminal enrichment **	+	+	+	+	+

* It is possible to characterize these features of protease function using these proteomic screens, but they are not commonly used for this purpose.
** Although isotopic labeling alone is enough to characterize all of these features of protease function, it is highly recommended to combine it with N-terminal enrichment to reduce sample complexity.

CLIPS: cellular libraries of peptide substrates; PICS: proteomic identification of protease cleavage sites; PSL: positional scanning libraries; 2D-DIGE: two-dimensional difference gel electrophoresis; PROTOMAP: protein topography and migration analysis platform.

information, peptide- and protein-centric approaches may also complement one another and offer unique information regarding a protease of interest. In addition, data obtained from a peptide-centric approach may facilitate protein-centric approaches, for instance, by enabling the faster identification of proteolytically processed peptides in MS/MS-based proteomics.

Five-year view

Proteomic screens are powerful tools to study protease function in a proteomic setting and naturally generate large datasets. As the number of proteomic screens within protease biology expands, the amount of data generated by these screens also increases dramatically. Complete datasets are often provided as supplementary data and important information can easily be overlooked. Hence, it is crucial to gather these datasets in an easily accessible central database in the near future. The field of bioinformatics is emerging and will be essential in this context.

Owing to their high sensitivity for substrates, MS-based techniques often pick up physiologically irrelevant bystander substrates and might miss real, but less abundant substrates. A novel technique known as selective reaction monitoring (SRM) might allow higher selectivity for true protease substrates [185]. SRM, which employs a triple quadrupole MS, offers higher selectivity than conventional MS techniques as a result of two mass filtering steps, and also enables the detection of low-abundance peptides in highly complex mixtures. In SRM, samples can be spiked with internal standard peptides, allowing absolute quantification of a

predetermined set of target peptides. Moreover, the absolute quantitative data that is obtained in SRM allows the reliable comparison of defined sets of proteins across multiple samples.

The focus of future studies will move towards the analysis of protease activity in physiological and clinical conditions, which will provide a better understanding of the role of proteases in health and disease. Studies that address protease function in physiological conditions are emerging and several research groups are now pioneering on this issue [156, 159, 162, 183, 184, 186-188].With the recent development of ABPs, the activity of proteases in clinical conditions can be assessed in a physiological context. These probes can be used in mouse models to study protease function within its microenvironment, which increases the physiological relevance of new results. Although the design of ABPs for *in vivo* imaging remains challenging, great effort is being made to overcome limitations in stability, toxicity, specificity and cell permeability. With these novel ABPs, we will gain insight into the role of proteases in many clinical conditions. Since proteases are promising targets for clinical therapy and substrate specificity can now be easily assessed, drug design will improve significantly. Peptide-based small-molecule inhibitors can be designed with high affinity towards one specific protease, thereby setting the stage for specific therapeutic interventions.

Financial & competing interests disclosure

Niels Bovenschen is supported by the Dutch Cancer Society (UU-2009-4302) and the Netherlands Organization for Scientific Research (916.66.044). The authors have no other relevant affiliations or financial involvement with any organization or entity with a financial interest in or financial conflict with the subject matter or materials discussed in the manuscript apart from those disclosed. No writing assistance was utilized in the production of this manuscript.

Key issues

- Aberrant protease function is implicated in a wide variety of clinical conditions.
- Peptide libraries are powerful tools to screen for protease substrate specificity.
- Identification of natural protease substrates increases our understanding of protease function in biological processes.
- In 2D difference in gel electrophoresis, fluorescent labeling of protein mixtures is used to allow relative quantification of proteins from multiple samples within one or more gels.
- Differential isotopic labeling of protein samples in combination with N-terminal enrichment approaches can be used to identify protease substrates and cleavage sites within these substrates, and to determine cleavage efficiencies.
- Activity-based probes provide novel methods to monitor protease activity *in vivo.*
- Proteases are promising targets for therapeutic intervention, since tailored peptide-based inhibitors can be designed that are directed towards the active site of the protease.
- Characterization of protease function will provide valuable information for clinical applications.

Chapter 3

Human and mouse granzyme M display divergent and species-specific substrate specificities

Stefanie A.H. de Poot*[1], Marijn Westgeest*[1], Daniel R. Hostetter†, Petra van Damme‡§, Kim Plasman‡§, Kimberly Demeyer‡§, Roel Broekhuizen*, Kris Gevaert‡§, Charles S. Craik† and Niels Bovenschen*

*Department of Pathology, University Medical Center Utrecht, Utrecht, The Netherlands
†Department of Pharmaceutical Chemistry, University of California, San Francisco, U.S.A
‡Department of Medical Protein Research, VIB, B-9000 Ghent, Belgium
§Department of Biochemistry, Ghent University, B-9000, Ghent, Belgium
[1]These authors contributed equally to this work.

Biochem J. 2011;437(3):431-42.

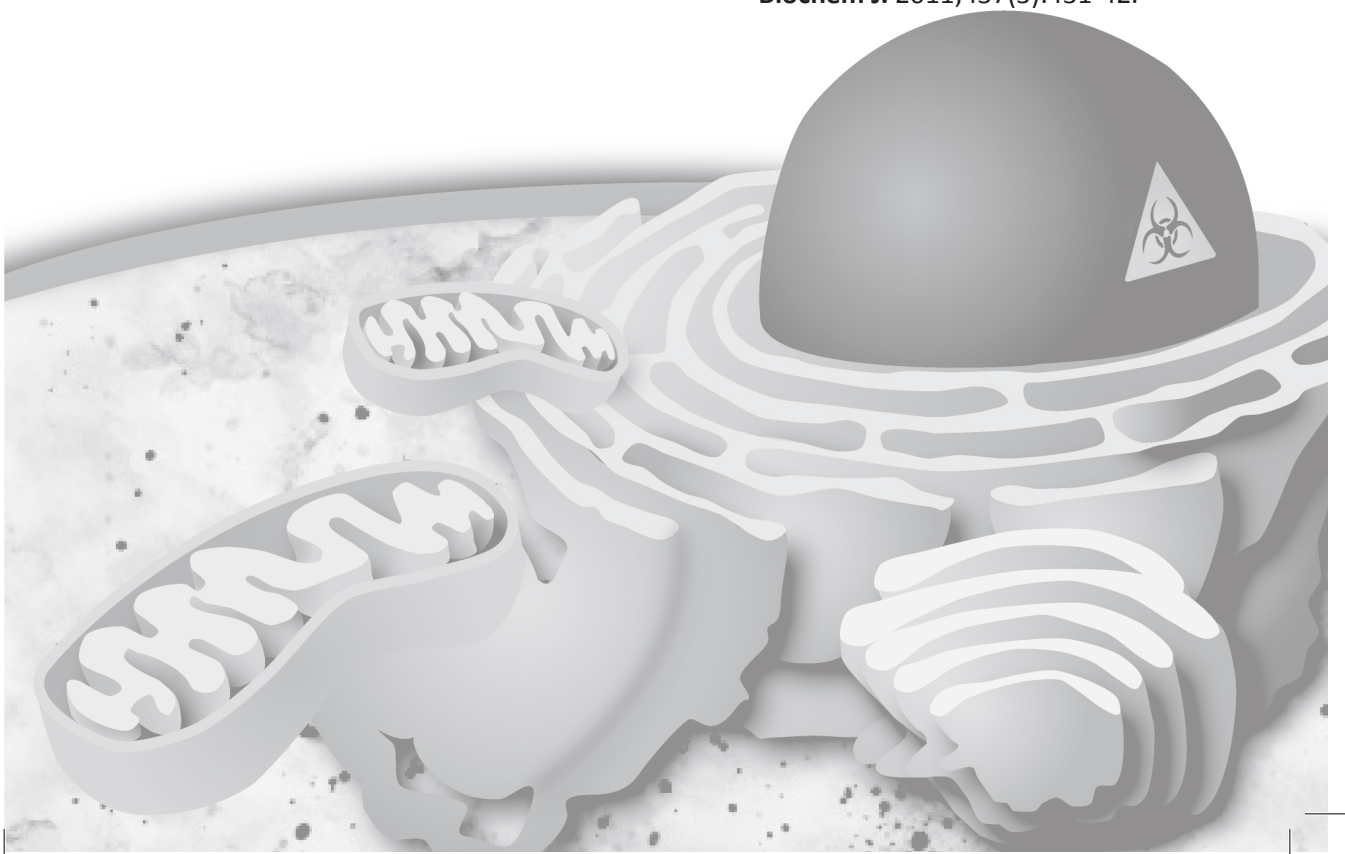

Abstract

Cytotoxic lymphocyte protease GrM (granzyme M) is a potent inducer of tumour cell death and a key regulator of inflammation. Although hGrM (human GrM) and mGrM (mouse GrM) display extensive sequence homology, the substrate specificity of mGrM remains unknown. In the present study, we show that hGrM and mGrM have diverged during evolution. Positional scanning libraries of tetrapeptide substrates revealed that mGrM preferred to cleave after a methionine residue, whereas hGrM clearly favours a leucine residue at the P1 position. The kinetic optimal non-prime subsites of both granzymes were also distinct. Gel-based and complementary positional proteomics showed that hGrM and mGrM have a partially overlapping set of natural substrates and a diverged prime and non-prime consensus cleavage motif with leucine and methionine residues being major P1 determinants. Consistent with positional scanning libraries of tetrapeptide substrates, P1 methionine was more frequently used by mGrM as compared with hGrM. Both hGrM and mGrM cleaved α-tubulin with similar kinetics. Strikingly, neither hGrM nor mGrM hydrolysed mouse NPM (nucleophosmin), whereas human NPM was hydrolysed efficiently by GrM from both species. Replacement of the putative P1′–P2′ residues in mouse NPM with the corresponding residues of human NPM restored cleavage of mouse NPM by both granzymes. This further demonstrates the importance of prime sites as structural determinants for GrM substrate specificity. GrM from both species efficiently triggered apoptosis in human but not in mouse tumour cells. These results indicate that hGrM and mGrM not only exhibit divergent specificities but also trigger species-specific functions.

Key words: apoptosis, degradomics, granzyme M (GrM), N- and C-terminal combined fractional diagonal chromatography (COFRADIC), nucleophosmin (NPM), α-tubulin.

Abbreviations used: ACC, amino-4-carbamoylmethylcoumarin; COFRADIC, combined fractional diagonal chromatography; 2D-DIGE, two-dimensional difference gel electrophoresis; DMEM, Dulbecco's modified Eagle's medium; GrA, granzyme A; GrB, granzyme B; GrM, granzyme M; GrM-SA, GrM with S195A mutation in catalytic centre; hGrM, human GrM; HSP, heat-shock protein; iCAD, inhibitor of caspase-activated DNase; mGrM, mouse GrM; mGrM-SA, mGrM with S195A mutation in catalytic centre; MS/MS, tandem MS; NK cell, natural killer cell; NPM, nucleophosmin; PARP, poly(ADP-ribose) polymerase; PI, propidium iodide; pNA, *p*-nitroanalide; PS-SCL, positional scanning synthetic combinatorial library; ROS, reactive oxygen species; SILAC, stable isotope labelling by amino acids in cell culture; SLO, streptolysin O.

Identified tandem MS (MS/MS) spectra are made publicly available in the Proteomics Identifications Database (PRIDE) [189] under the accession code 15475.

Introduction

The first line of defence against tumour and virus-infected cells is formed by cytotoxic T-lymphocytes and NK cells (natural killer cells) [3, 4]. Upon recognition of a target cell, these cytotoxic lymphocytes can initiate target cell death via either the death receptor [1] or the granule exocytosis pathway [2]. In the granule exocytosis pathway, cytotoxic lymphocytes secrete a family of granule-associated serine proteases known as granzymes and the pore-forming protein perforin [190]. Perforin facilitates the entry of granzymes into the target cell, enabling granzymes to induce cell death by cleaving intracellular substrates. In humans, five granzymes have been identified [GrA (granzyme A), GrB (granzyme B), GrH (granzyme H), GrK (granzyme K) and GrM (granzyme M)] [6, 69, 191]. The mechanisms via which GrA and GrB induce cytotoxicity have been studied extensively, whereas far less is known about the other human granzymes [8]. Granzymes have also been postulated to play key roles in regulating inflammation [84, 87].

hGrM (human GrM) [9] is unique in that it preferably cleaves after a leucine residue [28, 29] and is highly expressed in NK cells and to a lesser extent in CD8+ T-cells [11, 38]. hGrM is a potent and efficient inducer of tumour cell death*in vitro* and *in vivo* [41, 63]. This cell death is characterized by rapid cell swelling, formation of large cytoplasmic vacuoles, chromatin condensation with only slight segmentation of the nuclei, and finally lysis of the cells [41]. The molecular mechanisms by which hGrM initiates cell death remain controversial in the literature. hGrM has been demonstrated to trigger cell death in a caspase-independent fashion, with no fragmentation of DNA, no formation of ROS (reactive oxygen species) and no perturbation of mitochondria [31, 41, 45]. In these studies, hGrM has been demonstrated to cleave the microtubule network component α-tubulin, leading to disorganization of the microtubule network [45], and NPM (nucleophosmin)/B23, a multifunctional phosphoprotein essential for cell survival [31]. In contrast, Fan and co-workers have reported that hGrM promotes cell death in a manner similar to GrB, including caspase 3 activation, DNA fragmentation, generation of ROS and cytochrome *c* release from the mitochondria, through cleavage of HSP-75 (heat-shock protein-75), iCAD (inhibitor of caspase-activated DNase), PARP [poly(ADP-ribose) polymerase] and survivin [42-44].

While there are five granzymes in humans, mice express at least ten granzymes (A, B, C, D, E, F, G, K, M and N) [6]. hGrM has an orthologue in mice and mGrM (mouse GrM) functions *in vivo* have been studied in an mGrM knockout mouse model [62, 63, 87]. Like hGrM, mGrM has been implicated to participate in tumour clearance [63]. More recently mGrM has also been proposed to play a key role in the regulation of inflammation *in vivo* via yet to be established mechanisms [87]. Although hGrM and mGrM display extensive sequence homology, very little is known about the specificity of the mGrM protease. In the present study, we show that hGrM and mGrM exhibit divergent and species-specific substrate specificities. hGrM and mGrM display distinct P1 and subsite preferences, have narrow macromolecular substrate specificities that overlap only partially, cleave human but

not mouse NPM, and trigger apoptosis in certain human but not mouse tumour cell lines. This stresses that caution is needed when using mouse models to elucidate GrM functions in humans.

Experimental

Cell lines, antibodies and reagents

Human HeLa and murine C2C12 cells were grown in DMEM (Dulbecco's modified Eagle's medium), supplemented with 10% fetal bovine serum, 100 units/ml penicillin and 100 µg/ml streptomycin (Invitrogen). For the N- and C-terminal COFRADIC (combined fractional diagonal chromatography) analyses, human K-562 cells were grown in RPMI 1640 glutamax medium, supplemented with 10% dialysed fetal bovine serum, 100 units/ml penicillin and 100 µg/ml streptomycin containing 57.5 µM natural, $^{13}C_6$ or $^{13}C_6{}^{15}N_4$ L-arginine (Cambridge Isotope Laboratories). Cells were passaged for at least six population doublings for complete incorporation of the labelled arginine. Cell-free protein extracts were generated from exponentially growing HeLa, C2C12 and K-562 cells. Cells (10^8 cells/ml) were washed two times in a buffer containing either 50 mM Tris (pH 7.4) and 150 mM NaCl (HeLa and C2C12 cells) or 50 mM Tris (pH 8.0) and 100 mM NaCl (K-562 cells), and lysed in the same buffer by three cycles of freeze–thawing. Samples were centrifuged for 10 min at 20000 ***g*** at 4 °C, and cell-free protein extracts were stored at −80 °C. The protein concentration was quantified using the Bradford method. Antibodies used were anti-α-tubulin clone B-5-1-2 (Sigma), anti-β-tubulin clone TUB 2.1 (Sigma) and anti-NPM clone FC-61991 (Invitrogen). SLO (streptolysin O) was purchased from Aalto Bio Reagents. Homology modelling was performed using SWISS-MODEL [192].

Recombinant proteins

The cDNA encoding mature mGrM (residues Ile^{27}-Val^{264}) was amplified from mouse thymus cDNA (MD-702, Zyagen) using the oligonucleotides 5′-CCGCTCGAGAAACGTATCATTGGGGGTCGAG-3′ and 5′-TAAAGCGGCCGCCTTAGAC-CAAAGATTGGGG-3′, and cloned into yeast expression vector pPIC9 (Invitrogen). Catalytically inactive mGrM-SA (mGrM with S195A mutation in catalytic centre), in which the Ser^{195} residue in the catalytic centre is replaced by alanine, was generated by site-directed mutagenesis (Stratagene). Plasmids were transformed into the GS115 (his4) strain of *Pichia pastoris*. hGrB, hGrM and mGrM and the catalytically inactive GrM-SA (GrM with S195A mutation in catalytic centre) mutants were produced in *P. pastoris* and purified using cation-exchange chromatography as described previously [45]. GrM fractions were dialysed against 50 mM Tris (pH 7.4) and 150 mM NaCl and stored at −80 °C. GrM activity was determined using the synthetic chromogenic substrates Suc-Ala-Ala-Pro-Leu-pNA (*p*-nitroanalide) (Bachem) and Suc-Lys-Val-Pro-Leu-pNA (GL Biochem). To directly compare hGrM and mGrM substrate specificity, both enzymes were titrated using the synthetic chromogenic substrate Suc-Ala-Ala-Pro-Leu-pNA. hGrM was twice as efficient as

its mouse counterpart in cleaving this substrate. The catalytically inactive GrM-SA mutants of both hGrM and mGrM did not show any activity (results not shown). Human and mouse granzyme concentrations in all experiments were matched based on Suc-Ala-Ala-Pro-Leu-pNA hydrolysis. Human α-tubulin, mouse α-tubulin, human NPM and mouse NPM cDNAs were amplified from IMAGE clones 3871729, 6306481, 5575414 and 30438901 respectively, and cloned into the bacterial expression vector pQE80L. N-terminally His-tagged α-tubulin and His-tagged NPM were expressed in *Escherichia coli* strain BL21 as recommended by the manufacturer (Roche). The NPM P1′, P2′ and P1′/P2′ mutants were generated by site-directed mutagenesis (Stratagene). Recombinant α-tubulin and NPM proteins were purified by metal-chelate chromatography (Clontech), dialysed against PBS, and stored at −80 °C.

Granzyme killing assays

HeLa and C2C12 cells were grown to confluence in a 96-well tissue-culture plate. Cells were washed twice in serum-free DMEM, after which they were incubated at 37 °C with a sublytic dose of SLO (Jurkat, 0.25 μg/ml SLO; HeLa and PC3, 0.5 μg/ml SLO; LR7, C26 and C2C12, 1 μg/ml SLO) and indicated concentrations of granzyme in a buffer containing 20 mM Tris and 150 mM NaCl for 30 min. The cells were washed twice with supplemented DMEM, after which the cells were incubated for another 20 h at 37 °C. Cell viability was assessed using flow cytometry. Cells were stained with Annexin V-fluos (Invitrogen) and PI (propidium iodide) for 15 min in a buffer containing 140 mM NaCl, 4 mM KCl, 0.75 mM $MgCl_2$, 1.5 mM $CaCl_2$ and 10 mM Hepes (pH 7.4). Flow cytometry was performed on a FACSCalibur™ instrument (BD Biosciences) and results were analysed using CellQuest Pro software (BD Biosciences). Cells that were negative for both Annexin V and PI were regarded as living cells. The percentage of viable cells after treatment with SLO only was set at 100% and the percentage of viable cells in other conditions were calculated accordingly.

Single substrate kinetics

Granzyme activity was monitored by the synthetic chromogenic substrates Suc-Ala-Ala-Pro-Leu-pNA (Bachem) and Suc-Lys-Val-Pro-Leu-pNA (GL Biochem Ltd) in 100 mM Hepes (pH 7.4) and 200 mM NaCl at 37 °C. The GrM concentration was 100 nM and the substrate concentration ranged from 0.5 to 3 mM. Hydrolysis of pNA substrates was monitored spectrophotometrically at 405 nm on an Anthos Zenyth 340 rt microtitre plate reader (Anthos). Kinetic parameters (k_{cat}/K_M) were determined using standard Michaelis–Menten kinetic equations.

Positional scanning synthetic combinatorial libraries

The preparation and characterization of the P1-diverse and P1-Met libraries of 7-ACC (amino-4-carbamoylmethylcoumarin) substrates used in the present study are described elsewhere [193, 194]. Then 10^{-10} mol of each well of the P1-diverse stock

library was added to 20 wells of a 96-well microfluor plate. The final concentration of each substrate in the assay was 250 µM. Assays were initiated by the addition of 5.9 µM GrM and were conducted at 25 °C in buffer containing 50 mM Tris (pH 7.4) and 150 mM NaCl for 2 h. Hydrolysis of substrates was monitored fluorimetrically with an λ_{ex} of 380 nm and an λ_{em} of 460 nm on a Spectramax Gemini microtitre plate reader (Molecular Devices).

Fluorescent 2D-DIGE (two-dimensional difference gel electrophoresis)
For 2D-DIGE, 100 µg of HeLa or C2C12 cell-free protein extract was incubated for 1 h at 37 °C with 1 µM hGrM or mGrM or their catalytically inactive mutants. Samples were precipitated, solubilized, labelled, rehydrated and isoelectrically focused as we have described previously [124]. The strips were reduced and overlaid on an SDS/12% PAGE gel. The images were acquired on a Typhoon 9410 scanner (GE Healthcare). Each condition was performed at least five times, and a dye swap was included to exclude preferentially labelled proteins from the analysis. The relative quantification of matched gel features was performed using Decyder DIA and BVA software (GE Healthcare). For inter-gel analyses, the internal standard method was used as described previously [195]. Statistical analysis was performed using the Student's *t* test. $P<0.05$ was regarded as statistically significant.

N- and C-terminal COFRADIC: isolation of terminal peptides
For N- and C-terminal COFRADIC, 1250 µg of a K-562 cell-free protein extract was either left untreated ($^{13}C_6{}^{15}N_4$ L-arginine-labelled sample) or treated with 200 nM recombinant hGrM ($^{12}C_6$ L-arginine-labelled sample) or recombinant mGrM ($^{13}C_6$ L-arginine-labelled sample) for 1 h at 37 °C. Following protease incubation, guanidinium hydrochloride was added to the cell lysates to a final concentration of 4 M in order to denature and inactivate the proteases. The protein samples were reduced and S-alkylated, followed by trideutero-acetylation of primary amines and trypsin digestion as described previously [153, 156]. N- and C- terminal COFRADIC analyses were performed as described in [196]. In this setup, $^{12}C_4$-butyrylation was used for the hGrM-treated sample, $^{13}C_4$-butyrylation for the mGrM-treated sample and $^{13}C_2$-butyrylation for the control sample.

LC (liquid chromatography)–MS/MS (tandem MS) analysis
LC–MS/MS analysis was performed using an Ultimate 3000 HPLC system (Dionex) in-line connected to an LTQ Orbitrap XL mass spectrometer (Thermo Electron) and, per LC–MS/MS analysis, 5 µl of sample (one-quarter of the total sample) was consumed. LC–MS/MS analysis and generation of MS/MS peak lists were performed as described in [197]. These MS/MS peak lists were then searched with Mascot using the Mascot Daemon interface (version 2.2.0, Matrix Science). Searches were performed in the Swiss-Prot database with taxonomy set to human (UniProtKB/Swiss-Prot database version 2010_10 containing 20258 human protein sequences). Trideutero-acetylation at lysine residues, carbamidomethylation of cysteine residues

and methionine oxidation to methionine-sulfoxide were set as fixed modifications. Variable modifications were trideutero-acetylation and acetylation of protein N-termini. Semi-ArgC was set as the used protease (no missed cleavages were allowed) and the mass tolerance on the precursor ion was set to 10 p.p.m. and on fragment ions to 0.5 Da. In addition, Mascot's C13 setting was set to 1. Only MS/MS spectra that exceeded the corresponding Mascot threshold score of identity (at 95% confidence level) were withheld. The estimated false discovery rate by searching decoy databases was typically found to lie between 2 and 4% on the spectrum level [153]. All quantifications [SILAC (stable isotope labelling by amino acids in cell culture); $^{12}C_6$ L-arginine compared with $^{13}C_6$ L-arginine, $^{12}C_6$ L-arginine compared with $^{13}C_6\,^{15}N_4$ L-arginine and $^{13}C_6$ L-arginine compared with $^{13}C_6\,^{15}N_4$ L-arginine) and butyrylation ($^{12}C_4$-butyrylated compared with $^{13}C_4$-butyrylated, $^{12}C_4$-butyrylated compared with $^{13}C_2$-butyrylated and $^{13}C_2$-butyrylated compared with $^{13}C_4$-butyrylated)] were carried out using the Mascot Distiller Quantitation Tool (version 2.2.1). The quantification method details were as follows: constrain search, yes; protein ratio type, average; report detail, yes; minimum peptides, 1; protocol, precursor; allow mass time match, yes; allow elution shift, no; all charge states, yes; fixed modifications, mass values. Ratios for the proteins were calculated by comparing the XIC (extracted ion chromatogram) peak areas of all matched light compared with medium, light compared with heavy and medium compared with heavy peptides. The calculated ratios that were reported as FALSE were all verified by visual inspection of all highest scoring MS spectra.

Results

The primary and extended specificities of hGrM and mGrM are distinct

hGrM and its mouse orthologue display a considerable sequence homology of 69% (Figure 1A), whereas the serine, histidine and aspartic acid residues of the catalytic triad are completely conserved between hGrM and mGrM, several residues that are predicted to play key roles in the substrate recognition of hGrM [24] differ between both granzymes (Figure 1A). These differences result in an altered substrate-binding pocket in mGrM as can be visualized in a homology model of mGrM based on the known crystal structure of hGrM (Figure 1B) [24]. hGrM prefers to cleave after a leucine residue at the P1 position (nomenclature for amino acid positions in substrates is P*n*-P2-P1-P1′-P2′-P*n*′, with amide bond hydrolysis occurring after P1, and the corresponding enzyme-binding sites denoted as S*n*-S2-S1-S1′-S2′-S*n*′) [27]. The optimal P4–P1 tetrapeptide specificity of hGrM has previously been identified as Lys-Val-Pro-Leu [28, 29]. To test whether the tetrapeptide specificity of mGrM is similar to that of hGrM, mGrM was incubated with the chromogenic optimal human tetrapeptide substrate Suc-Lys-Val-Pro-Leu -pNA (Figure 1C). While hGrM efficiently hydrolysed this substrate (k_{cat}/K_m=6.6×10^3 M^{-1}·s^{-1}), mGrM was approx. 4.5-fold less efficient (k_{cat}/K_m=1.5×10^3 M^{-1}·s^{-1}). This suggests that hGrM and mGrM are indeed structurally distinct proteases with distinct substrate-binding pockets. The primary

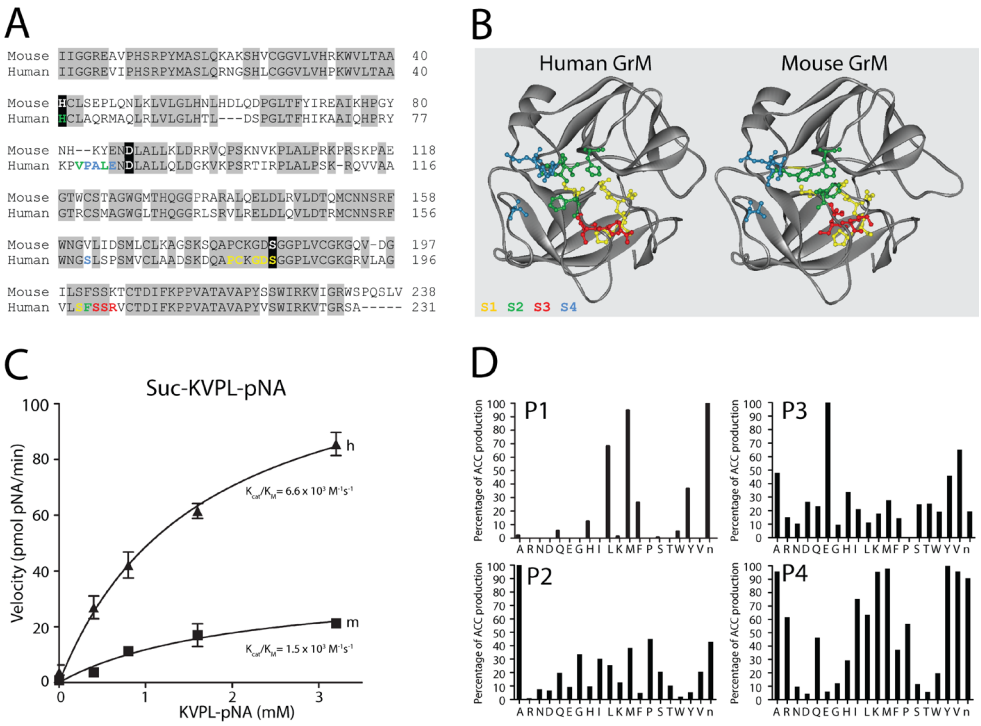

FIG. 1. The primary and extended specificities of human and mouse GrM are distinct.
(A) Alignment of hGrM and mGrM primary sequence. Residues boxed in grey are shared amino acids between hGrM and mGrM, those boxed in black are residues that form the catalytic triad. The S1-S2-S3-S4 amino acids are highlighted in yellow, green, red and blue, respectively. (B) Crystal structure of hGrM [24]. Based on the structure of hGrM, a homology model for mGrM was generated (Swiss-Prot). S1-S4 amino acids are indicated. (C) Michaelis plots of peptide substrate KVPL-pNA hydrolysis by different concentrations of human (h) and mouse (m) GrM. Calculated k_{cat}/K_m values are indicated. Results are representative of two independent triplicate experiments. (D) The primary specificity of mGrM was determined using a P1-ACC diverse tetrapeptide library. The extended specificity of mGrM was determined using a P1 fixed Met-ACC tetrapeptide library. The *y* axis represents the rate of ACC production as a percentage of the maximum rate observed in each experiment. The *x* axis shows the positioned P1 amino acids as represented by the one-letter code. Data is representative of three separate experiments.

specificity of mGrM was profiled using a PS-SCL (positional scanning synthetic combinatorial library) of tetrapeptide coumarin substrates known as the P1-diverse library [28, 194]. For hGrM, this method has previously demonstrated a strong P1 preference for leucine (100%) over methionine (~16%) and non-physiological Nle (~46%), and no tolerance for other residues at this position [28, 29]. In contrast with hGrM, mGrM displayed a preference for Nle (100%) and methionine (~95%) over leucine (~68%) (Figure 1D). The residues alanine, glutamine, histidine, lysine, phenylalanine, serinine, tryptophan and tyrosine were also tolerated at the P1 position, although to a lesser extent. The P4–P2 extended substrate specificity of mGrM was determined using a P1-fixed methionine PS-SCL library (Figure 1D). Strikingly, whereas hGrM shows an almost absolute requirement for proline at the P2 with some tolerance for alanine [29], mGrM clearly preferred alanine over proline and displayed a broad tolerance for other amino acids at P2. Although the preferred P3 residues of mGrM differed slightly from those of hGrM, both granzymes seemed

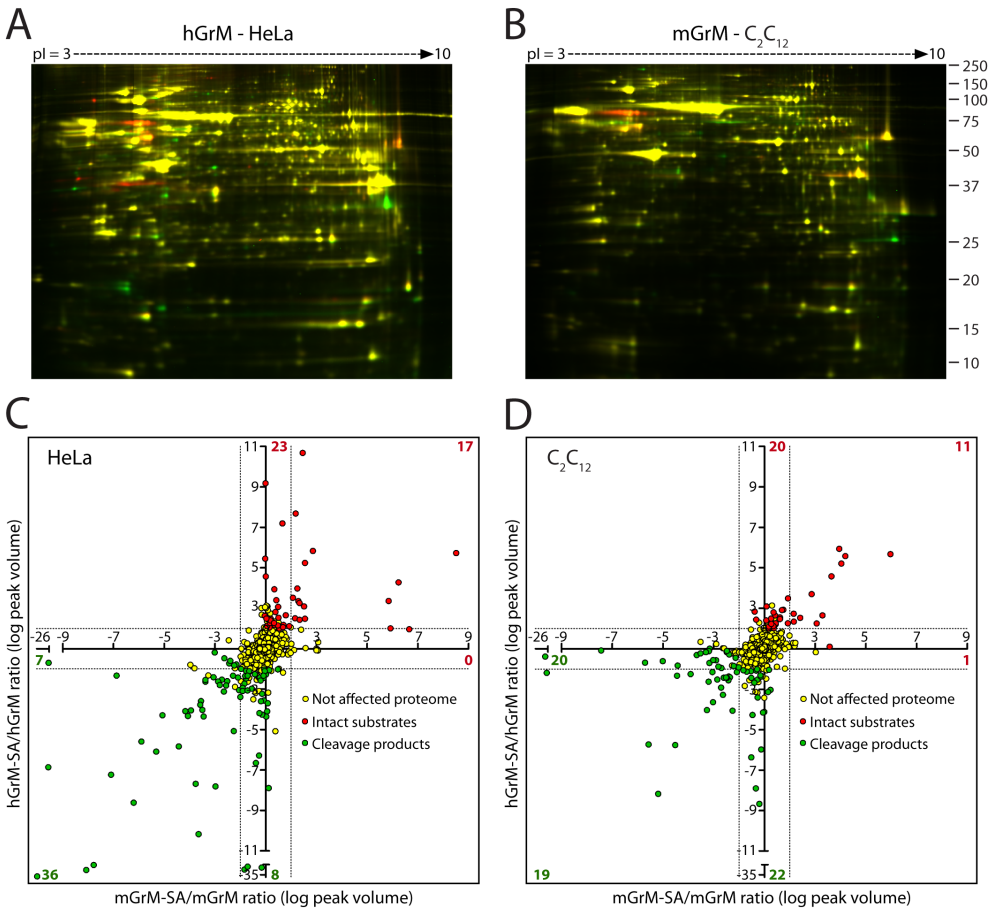

FIG. 2. Human and mouse GrM display highly restricted macromolecular substrate specificities that only partially overlap. (A) HeLa cell freeze/thaw lysates (100 µg) were incubated with 1 µM hGrM (*green*) or 1 µM human GrM-SA (hGrM-SA) (*red*) for 1 h at 37°C. The samples were then subjected to 2D-DIGE. Protein spots shared between the two samples appear *yellow*. Protein spots with decreased abundance after protease digestion (GrM substrates) are *red*, while new spots (cleavage products) that appear after protease digestion are *green*. (B) C_2C_{12} cell freeze/thaw lysates (100 µg) were incubated with 1 µM mGrM (*green*) or 1 µM mouse GrM-SA (mGrM-SA) (*red*) for 1 h at 37°C and subjected to 2D-DIGE. These results are representative for five independent experiments. (C) Human GrM/GrM-SA and mouse GrM/GrM-SA gels from HeLa lysate were matched, and human GrM-SA/GrM log peak volume ratios (*y* axis) were plotted against mouse GrM-SA/GrM log peak volume ratios (*x* axis). Protein spots are labeled *red* (intact substrates), *green* (cleavage fragments), or *yellow* (not affected proteome). Protein spot intensity was considered to be changed when peak volume ratios were 2-fold (*dotted lines*) and $p < 0.05$. (D) Human GrM/GrM-SA and mouse GrM/GrM-SA gels from C_2C_{12} lysate were matched, and human GrM-SA/GrM log peak volume ratios (*y* axis) were plotted against mouse GrM-SA/GrM log peak volume ratios (*x* axis).

to favour glutamine or valine at P3. At the P4 position, mGrM was highly tolerant to a large number of amino acids, whereas hGrM showed a distinct preference for a lysine, Nle or a histidine residue at P4 [29]. Taken together, these results indicate that hGrM and mGrM differ in their primary and P4–P2 substrate specificity.

hGrM and mGrM display restricted macromolecular substrate specificities that overlap only partially

To compare the macromolecular substrate specificities of hGrM and mGrM, two

different proteomics-based strategies were applied. First, a fluorescence 2D-DIGE proteomic approach was employed that scans the native proteome of tumour cells for macromolecular substrates of both granzymes and directly determines the efficiency of substrate cleavage (Figure 2). Cell lysates of human cervix carcinoma (HeLa) and mouse myoblast (C2C12) cells were incubated with hGrM, hGrM-SA, mGrM or mGrM-SA and were subsequently labelled with either a red fluorescent dye [Cy5 (indodicarbocyanine)] or a green fluorescent dye [Cy3 (indocarbocyanine)]. Two representative 2D-DIGE gels of cell lysates after hGrM (Figure 2A) or mGrM (Figure 2B) treatment are shown. GrM-treated lysates in these gels were labelled green, whereas the lysates that had been treated with GrM-SA were labelled red. Spots present in greater abundance in the control sample appear red and indicate possible intact GrM substrates, whereas spots present in greater abundance in the granzyme-treated sample appear green and reflect the appearance of specific cleavage products (the unaffected proteome appears yellow). Approx. 3000 protein spots were resolved from the human HeLa cell lysate, of which 44 spots clearly appeared (cleavage products) and 40 (~1.3%) decreased in intensity with different efficiencies (intact substrates) after hGrM treatment (Figure 2A) (log peak volume change >2-fold, $P<0.05$). For mouse C2C12 cell lysates, approx. 2300 proteins spots were resolved. After mGrM treatment, 39 protein spots clearly appeared (cleavage products) and 12 (~0.5%) decreased in intensity with different efficiencies (intact substrates) (Figure 2B) (log peak volume change >2-fold, $P<0.05$). This relatively low number of recognized substrates for hGrM and mGrM suggests that the macromolecular substrate specificities of both granzymes are highly restricted. Interestingly, 17 out of the 40 macromolecular substrates that could be detected were cleaved and shared by both granzymes in HeLa lysates (log peak volume change >2-fold, $P<0.05$), indicating a ~42% overlap in macromolecular substrate specificity (Figure 2C). For the cleavage fragments, 36 out of 51 spots with at least a 2-fold log peak volume change were shared, strongly suggesting that part of the detected cleavage events occurred at the same P1 cleavage sites, whereas, for the selection criteria applied, other events were considered unique for mGrM or hGrM. In the C2C12 lysate, 11 out of 32 proteins were cleaved by both granzymes, indicative of an ~34% overlap in macromolecular substrate specificity, while 19 out of 61 cleavage fragments overlapped (~31%) (Figure 2D).

To further probe the macromolecular differences in substrate selection among the human and mGrM orthologues, we made use of the COFRADIC-based complementary positional proteomics approach to study GrM-specific proteolysis in human K-562 cell lysates. This approach allows us to identify and to compare the (consensus) cleavage sites of hGrM and mGrM, but does not directly determine efficiencies of cleavage events. Analogous to previous GrB setups analysed [154, 196], a SILAC [146] $^{12}C_6$-L-Arg- and $^{13}C_6$-L-Arg-labelled cell lysate served as a hGrM and mGrM substrate pool respectively, whereas a $^{13}C_6{}^{15}N_4$-L-Arg-labelled proteome served as a control. This allowed quantification of (neo-)N-terminal peptides since all samples were subject to tryptic digestion and therefore end with an arginine

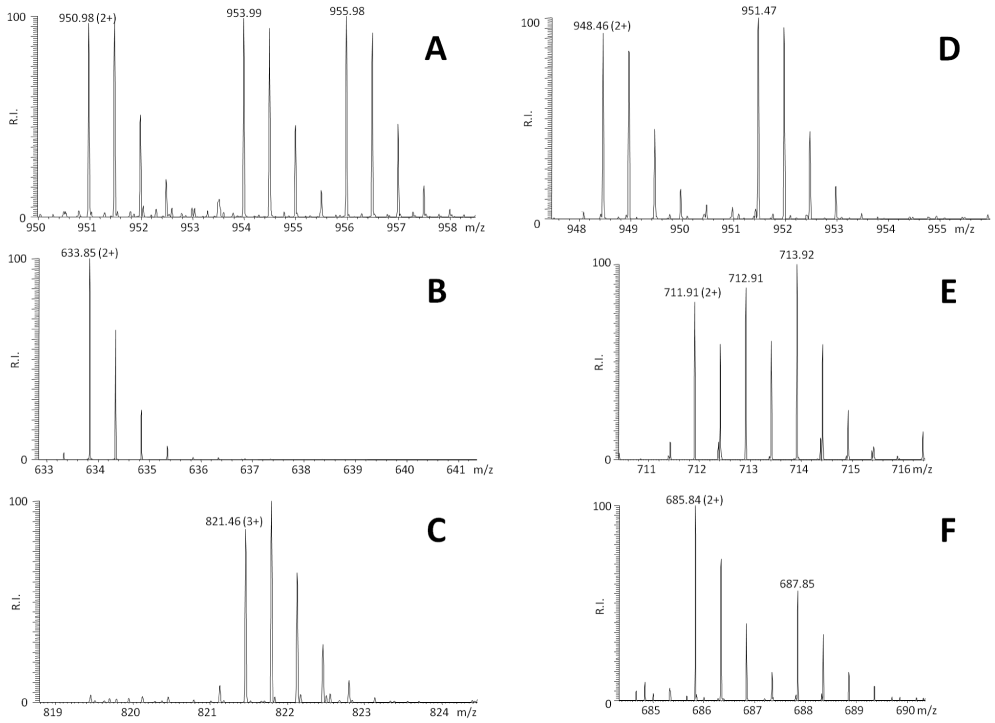

FIG. 3. Illustration of the different categories of isolated terminal peptides found in K-562 lysates. SILAC-labeled K-562 freeze-thaw lysates were treated with hGrM ($^{12}C_6$), mGrM ($^{13}C_6$) or left untreated ($^{13}C_6\,^{15}N_4$). (A) Unaltered database annotated protein-N-termini: these peptides were identified as Ac-^{2}TSKGPEEEHPSVTLFR^{17} (Ac denotes α-acetylated amino group) from aminoacylase-1 and the ion intensities of their three different forms are about equal, indicating that this peptide was not affected by GrM. (B) Unique neo-N-terminus (QEAL↓AcD3-^{349}AKLKEEEER^{357}, AcD3 denotes a trideutero-acetylated α-amino group), generated only by hGrM in the eukaryotic translation initiation factor 5B. (C) Unique neo-N-terminus (RNGL↓AcD3-^{61}LAALKKALAAGGYDVEKNNSR^{82}) generated exclusively through the action of mGrM in histone H1.5. (D) Neo-N-termini of the serine/arginine repetitive matrix protein 2 (LAAL↓AcD3-^{2310}SLTGSGTPPTAANYPSSSR^{2328}) generated with similar efficiency by hGrM and mGrM. (E) Unaffected protein C-termini were identified as differentially butyrylated-^{72}LAKADGIVSKNF^{83} peptides of which the ion intensities are about equal (L/M, L/H, and M/H ratios of 1.1, 1, and 1.1 respectively). (F) A neo-C terminus But$^{12/13}C_4$-^{416}KNLDVMKEAM^{425}↓VQAE (But$^{12/13}C_4$ denotes an α-amino group modified by 4 carbon-12 or 4 carbon-13 butyric acid) originating from the Nucleolar protein 56 was identified, according to the ion intensities, approx. 2.5 times more efficiently cleaved by hGrM than by mGrM. In a separate peptide fraction, the neo-N-terminus generated after cleavage at KEAM^{425}↓ was also identified following GrM treatment with a similar hGrM/mGrM ratio of 2.4 (See also Suppl.Table 1).

residue. We further differentially tagged protein C-terminal peptides using NHS-esters of $^{12}C_4$ (hGrM), $^{13}C_2$ (control) or $^{13}C_4$ butyric acid (mGrM). Following LC-MS/MS analysis, we here identified 720 unique hGrM- and/or mGrM-specific cleavage sites in 488 protein substrates based on their corresponding 577 neo-N and/or 155 neo-C-terminal peptide(s) (see Supplementary Table S1 at http://www.BiochemJ.org/bj/437/bj4370431add.htm). Of these, 411 hGrM- and/or mGrM-specific cleavage sites were generated by processing at leucine (57%), 75 by cleavage after methionine (10%) and the remaining 234 cleavage sites (33%) were, consistent with the positional scanning results, raised upon processing at alternative P1-specificities, including alanine, cysteine and glutamine. Besides monitoring of (neo-)

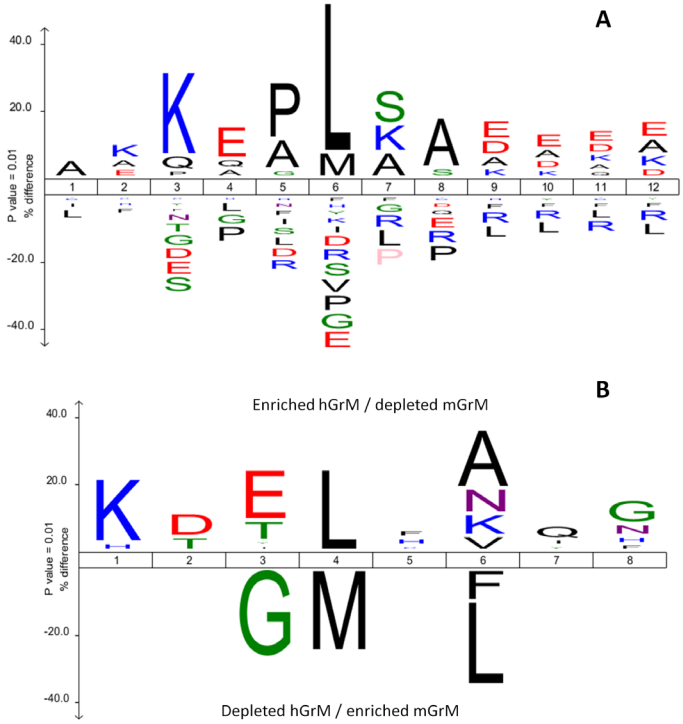

FIG. 4. IceLogo representations of the cleavage sites identified by proteome-wide screening for GrM substrates. IceLogo representations were created using the respectively 220 (A) and 72 (B) Leu/Met P1-containing cleavage motifs of identified neo-termini exhibiting hGrM/mGrM cleavage ratios deviating at least 50% of the mean (i.e. preferred/unique hGrM (A) or preferred/unique mGrM cleavages (B)). Multiple sequence alignments [198] of peptide substrate motifs are given as 1, 2, 3 to 8 corresponding to cleavage site residues P4, P3, P2 to P4' with the P1 cleavage site indicated as position 4. Statistically significant residues with a p-value threshold of 0.05 are plotted. The amino acids heights are indicative for their degree of conservation at the indicated position. The frequency of the amino acid occurrence at each position in the sequence set was compared with the human Swissprot 56.0 database. Residues with a statistically significant lower frequency of occurrence as compared to SwissProt are indicated at the negative site of the *x* axis. Residues with a 0% occurrence are colored in the lightest greyscale. (C) A differential iceLogo representation was created using the P1 Leu (248) and P1 Met (44) containing cleavage motifs of identified neo-termini with corresponding hGrM and/or mGrM cleavage ratios deviating at least 50% of the mean. Statistically significant residues with a p-value threshold of 0.01 around the P1 Leu or P1 Met are plotted with the size of the amino acids proportional to the difference observed in cleavage efficiency between hGrM and mGrM on their respective substrates. On the *y* axis the height of the symbol is proportional to the difference in occurrence of amino acid usage in more efficient hGrM versus more efficient mGrM cleavage site motifs.

termini generated by GrM, the differential labelling strategies applied allow for a direct comparison of differences in substrate specificity profiles for both granzymes. As such, single $^{12}C_6$ L-Arg neo-N- or $^{12}C_4$-butyrylated neo-C-termini and $^{13}C_6$ L-Arg neo-N- or $^{13}C_4$-butyrylated neo-C-termini indicate respectively unique hGrM and mGrM substrates, whereas couples spaced by six or four mass units respectively indicate neo-N- or neo-C-termini raised by both orthologues (Figure 3). The ratio of ion signal intensities of such couples is further indicative of the difference in substrate cleavage efficiency between hGrM and mGrM. Of all sites identified, 481 sites (67%) in 359 substrates were found to be cleaved by both proteases, whereas

230 (196 proteins) and nine cleavages (nine proteins) were uniquely introduced by the action of hGrM and mGrM respectively (see Supplementary Table S1). As deduced from the neo-termini-specific hGrM/mGrM ratios, on average, hGrM seemed to be 4- to 5-fold more efficient in cleaving its substrates as compared with mGrM.

The COFRADIC-based complementary positional proteomics approach allows us to directly compare consensus cleavage sites of hGrM and mGrM. The general amino acid conservation in the set of GrM substrates with a leucine or methionine residue at P1 that were more efficiently cleaved by hGrM than by mGrM is shown in Figure 4A. The general amino acid conservation in the set of more efficiently cleaved mGrM substrates with P1 leucine or methionine is shown in Figure 4B. Overall, the identified P1–P4 specificity of mGrM is consistent with our PS-SCL data (Figure 1D). To further distinguish between differentially accommodated amino acids from P4 to P4′ in their respective subsites of hGrM and mGrM, a differential iceLogo [198] was created using the human and mouse leucine and methionine P1-specific data subsets for which the hGrM or mGrM cleavage efficiency (as deduced from the proteomics data) was at least 50% more efficient as compared with the mean hGrM compared with the mGrM cleavage ratio observed (Figure 4C). Statistically significant residues ($P \leq 0.01$) are plotted with the size of the amino acid proportional to the difference observed in cleavage efficiency between hGrM and mGrM on their respective substrates (Figure 4C). In line with the PS-SCL data, a P1 methionine residue seems to be better accommodated by mGrM as compared with hGrM. Other differentially accommodated residues include glycine or glutamine residues at P2, a P2 glycine residue being generally inhibitory for hGrM-specific cleavage (the increased prevalence of a glycine residue at P2 is also apparent when comparing the P2 hGrM and mGrM PS-SCL preferences), and a glutamine residue being inhibitory for mGrM-specific cleavage (see also representative examples Figures 3A–3F). In general, the presence of a positively charged P4 lysine or histidine residue is more stimulatory for hGrM-specific cleavage as compared with mGrM-specific cleavage (an arginine residue at P4). Beyond the P4–P1 motif, the amino acid occupancy of P2′ is also clearly discriminative with leucine, phenylalanine, tyrosine and aspartic acid residues being better accommodated by the mGrM S2′ pocket, whereas alanine, asparagine, lysine, serine, glycine and valine residues represent better accommodated hGrM P2′ residues. In addition, Supplementary Figure S1 plots the different amino acid occurrences in percentages at the most discriminative P and P′-positions in more efficient hGrM compared with more efficient mGrM cleavage site motifs as histograms.

Collectively, these results indicate that hGrM and mGrM display narrow macromolecular substrate specificities that overlap only partially. Interestingly, the hGrM and mGrM substrates that were identified by this complementary positional proteomics approach include the already known hGrM substrates α-tubulin [45] and NPM [31](Supplementary Table S1).

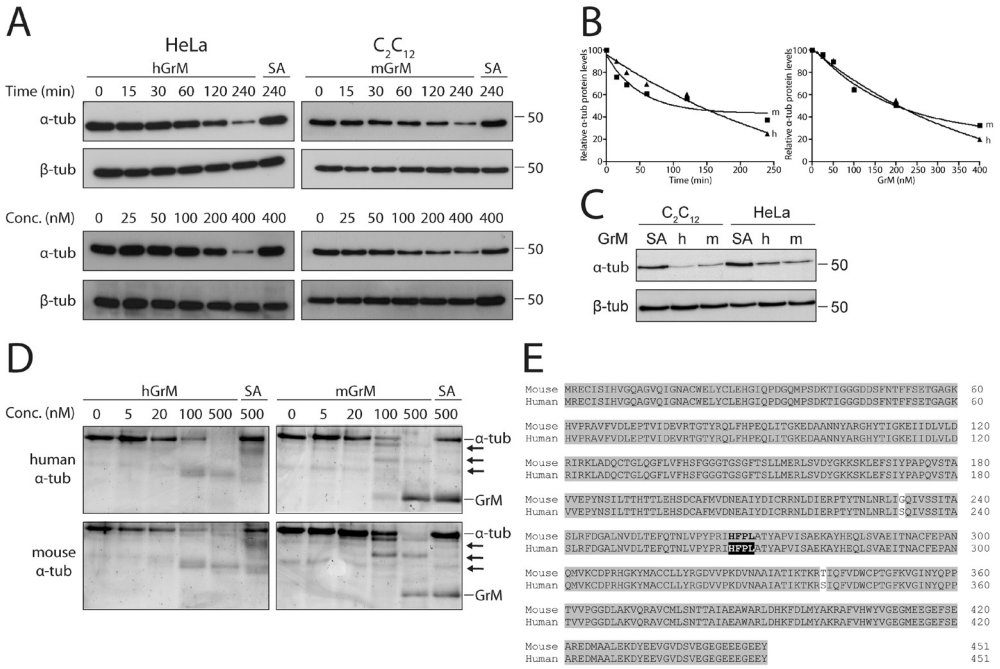

FIG. 5. Human and mouse GrM cleave α-tubulin with similar efficiency. (A) Cell lysates derived from HeLa (human) or C_2C_{12} (mouse) cells were treated with hGrM or mGrM (400 nM) for indicated lengths of time or with different concentrations of hGrM or mGrM (0-400 nM). Catalytically inactive GrM-SA served as a negative control. Reactions were separated by SDS-PAGE and analyzed by immunoblotting, using an antibody against α-tubulin or β-tubulin (which served as a loading control, since no significant cleavage could be observed at the conditions assayed). (B) Signal intensities of protein bands were quantified by densitometry, α-tubulin/β-tubulin ratios were calculated, and plotted against time or GrM concentration. (C) Both HeLa and C_2C_{12} lysates were incubated for 4 h at 37°C with either human (h) or mouse (m) GrM (400 nM). Samples were immunoblotted using an antibody against α-tubulin or β-tubulin (loading control). Results are representative of three independent experiments. (D) Purified recombinant human and mouse His-α-tubulin were incubated for 2 h at 37°C with indicated concentrations of hGrM or mGrM. Reactions were separated on SDS-PAGE and visualized by Simply Blue protein staining. His-α-tubulin and GrM are indicated, arrows indicate cleavage products. Results are representative of three independent experiments. (E) Alignment of human and mouse α-tubulin. Residues boxed in grey are the shared amino acids between human and mouse α-tubulin. Boxed in black is one known hGrM cleavage site [45].

hGrM and mGrM cleave human and mouse α-tubulin with similar efficiency

We have previously demonstrated that hGrM cleaves the microtubule component α-tubulin, leading to a disorganization of the microtubule network that may contribute to cell death [45]. The proteolysis of α-tubulin was further biochemically analysed in human (HeLa) and mouse (C2C12) cell lysates. Mouse α-tubulin was cleaved by mGrM in a time- and concentration-dependent manner similar to the cleavage of human α-tubulin by hGrM (Figure 5A). Semi-quantitative analysis of the protein bands indeed showed similar kinetics of α-tubulin cleavage by both hGrM and mGrM (Figure 5B). mGrM also cleaved human α-tubulin and vice versa with similar efficiency (Figure 5C). To exclude the possibility that GrM-induced cleavage of α-tubulin is indirect and to visualize GrM-induced cleavage products, these experiments were repeated using purified recombinant human and mouse His-tagged α-tubulin. Consistent with Figures 5(A)–5(C), both human and mouse

His-tagged α-tubulin were cleaved by both hGrM and mGrM (Figure 5D). Despite the fact that α-tubulin is extremely well conserved between human and mouse (99.6% sequence homology) (Figure 5E), the cleavage fragments that appeared after GrM treatment of purified His-tagged α-tubulin differed between hGrM and mGrM (Figure 5D). These results indicate that although both hGrM and mGrM cleave α-tubulin with similar efficiency, distinct cleavage sites are preferred (see also Supplementary Table S1).

Species-specific substrate proteolysis: hGrM and mGrM cleave human but not mouse NPM

The nucleolar phosphoprotein NPM is a multifunctional tumour-suppressor protein that has been directly implicated in cancer pathogenesis [199] and apoptosis [31]. Cleavage of NPM by GrM has been proposed to contribute to the mechanism by which GrM triggers tumour cell death [31]. The proteolysis of NPM by hGrM and mGrM was tested in HeLa and C2C12 cell lysates (Figure 6A). As expected [31], cleavage of human NPM by hGrM was highly efficient and time- and concentration-dependent, with proteolysis almost going to completion at 15 min after the addition of 400 nM hGrM or at 1 h after the addition of 50 nM hGrM (Figure 6B). Cleavage of mouse NPM, however, was far less efficient, with virtually no reduction of the full-length protein band after 2 h incubation with 400 nM mGrM. Kinetic analysis revealed that mGrM was ~40-fold less efficient in cleaving its species-matched NPM as compared with hGrM (Figure 6B). To determine whether this marked variation in NPM cleavage was due to differences between hGrM and mGrM or due to differences between human and mouse NPM, NPM from both human and mouse cell lysates was exposed to both granzymes (Figure 6C). Interestingly, while human NPM was hydrolysed with similar efficiency by both hGrM and mGrM, mouse NPM was a poor substrate of both mGrM and hGrM. Similar results were obtained when the granzymes were incubated with purified recombinant human and mouse His-tagged NPM (Figure 6D), suggesting that differences in NPM between species rather than differences in GrM explain these findings. Human and mouse NPM share a sequence similarity of 93.9% and the known hGrM cleavage site [31](at least P9–P1) in NPM is conserved between human and mouse. Cleavage of NPM at this site was also detected in a human K-562 lysate using complementary positional proteomics (observed hGrM/mGrM ratio of 1.6, see Supplementary Tables S1A and S1B). Notably, there are two alanine residues at the P1′ and P2′ positions of human NPM that are not present in mouse NPM. Instead, mouse NPM harbours the non-preferred (Figure 4A) negatively charged Asp^{159} and Glu^{160} residues at these positions (Figure 6E) respectively. To determine whether this difference is responsible for the impaired cleavage of mouse NPM by both mGrM and hGrM, the Asp^{159} and Glu^{160}residues of mouse NPM were ‘humanized’ using site-directed mutagenesis (Figure 6F). The efficiency of both hGrM and mGrM-mediated cleavage of mouse NPM slightly increased when the P1′ residue of mouse NPM was mutated into the corresponding residue of human NPM, and the efficiency was completely restored

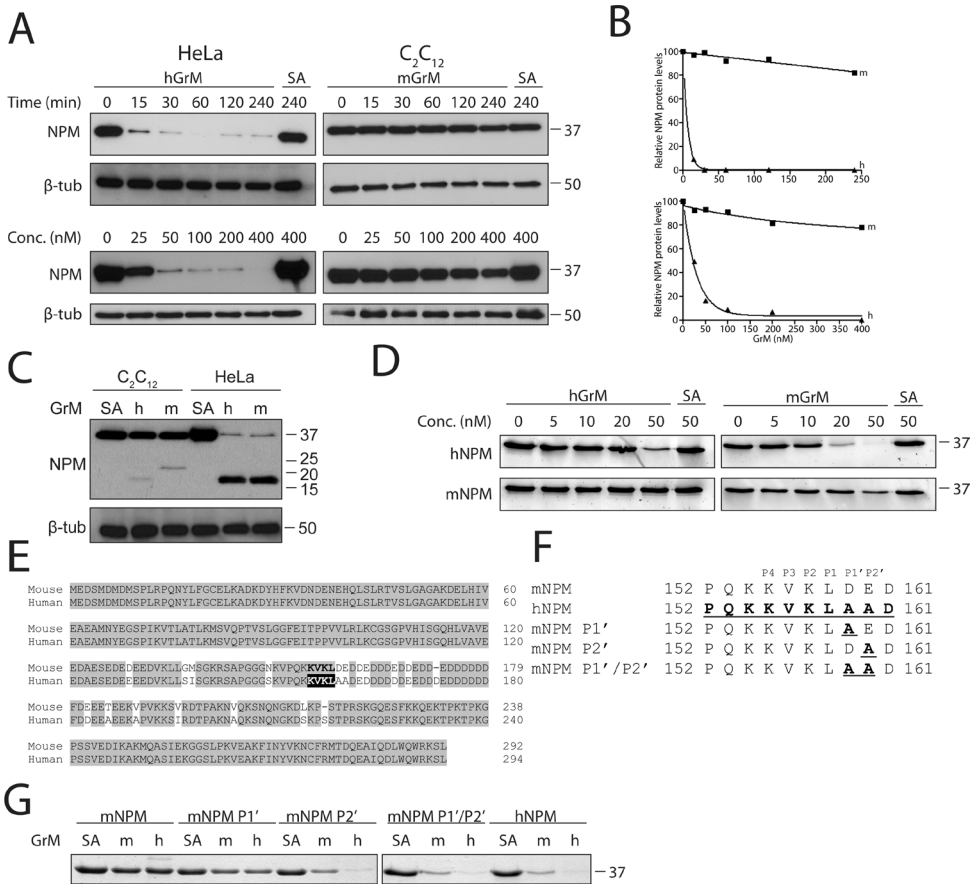

FIG. 6. Human and mouse GrM cleave human but not mouse nucleophosmin. (A) Cell lysates derived from HeLa (human) or C_2C_{12} (mouse) cells were treated with hGrM or mGrM (400 nM) for indicated lengths of time or with different concentrations of hGrM or mGrM (0-400 nM). Reactions were separated by SDS-PAGE and analyzed by immunoblotting, using an antibody against NPM or β-tubulin (which served as a loading control, since no significant cleavage could be observed at the conditions assayed). (B) Signal intensities of protein bands were quantified by densitometry, NPM/β-tubulin ratios were calculated, and plotted against time or GrM concentration. (C) Both HeLa and C_2C_{12} lysates were incubated for 4 h at 37°C with either human (h) or mouse (m) GrM (400 nM). Samples were immunoblotted using an antibody against NPM or β-tubulin (loading control). Results are representative of three independent experiments. (D) Recombinant human and mouse NPM were incubated for 2 h at 37°C with the indicated concentrations of hGrM or mGrM. Reactions were separated on SDS-PAGE and visualized by Simply Blue staining. Results are representative of three independent experiments. (E) Alignment of human and mouse NPM. Residues boxed in grey are the shared amino acids between human and mouse NPM. Boxed in dark grey is the known hGrM cleavage site [31]. (F) Alignment of the GrM cleavage site in human and mouse NPM. The P1-P4 are completely conserved between mouse and human, but the P1' and P2' residues differ. Different mutants of mouse NPM generated are depicted. (G) Purified recombinant wild type (wt) human NPM (hNPM), wt mouse NPM (mNPM) and different NPM mutants were incubated for 2 h at 37°C with the indicated concentrations of human (h) or mouse (m) GrM. Products were separated by SDS-PAGE and visualized by Simply Blue staining. Results are representative of four independent experiments.

when only the P2' residue was replaced with an alanine or when both residues were replaced simultaneously (Figure 6G). These results show that mouse NPM cannot be cleaved by both hGrM and mGrM because of species-specific differences in the prime site residues P1' and predominantly P2'. Consistent with our positional

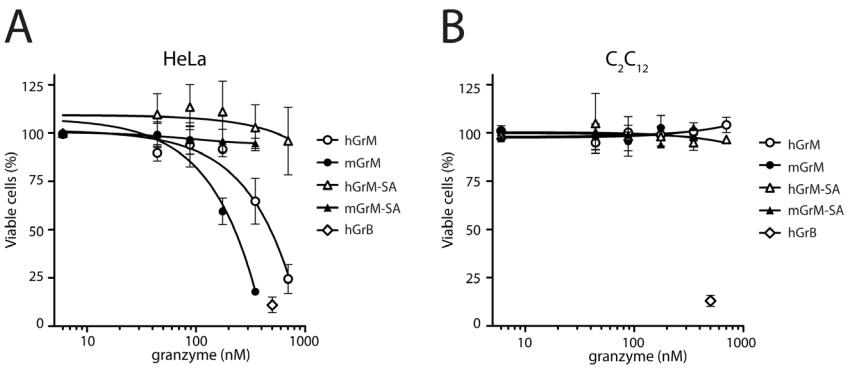

FIG. 7. Human and mouse GrM trigger cell death in human HeLa but not mouse C2C12 tumor cells. Human HeLa cells (A) or mouse C_2C_{12} cells (B) were treated with sublytic concentrations of SLO and various concentrations of hGrM, mGrM or their catalytically inactive mutants (GrM-SA), for 30 min. Cells were treated with hGrB as a positive control. After washing, cells were incubated for another 20 h at 37°C. Cell viability was determined using flow cytometry, with AnnexinV and PI negative cells considered viable.

proteomics analysis, this further stresses that prime sites in macromolecular substrates are important structural determinants for GrM substrate specificity.

GrM-induced cell death is species-dependent

The functional and structural species-dependent differences identified in the present study between hGrM and mGrM prompted us to investigate the tumour cell death potential of both granzymes. Human (HeLa) and mouse (C2C12) cells were incubated with purified GrM in the presence or absence of the pore-forming protein SLO, a perforin analogue. The cells were subsequently stained with apoptosis markers Annexin V and PI, and cell viability was assessed by means of flow cytometry. Both hGrM and mGrM efficiently induced cell death in human HeLa cells, with mGrM being slightly more potent than hGrM (Figure 7A). Additionally, hGrM and mGrM displayed clear cytotoxic potential towards the human prostate cancer PC3 and leukaemic Jurkat cell lines (see Supplementary Figure S2). Under the same conditions, however, neither hGrM nor mGrM was able to induce apoptosis in mouse C2C12 cells (Figure 7B). GrM from both species also failed to trigger apoptosis in several other mouse cell lines, including the colon carcinoma C26 cell line and the fibroblast LR7 cell line (Supplementary Figure S2). The catalytically inactive GrM-SA mutants and SLO alone displayed no cytotoxicity in these experiments, whereas human GrB efficiently induced apoptosis in all above-mentioned cell lines (Figure 7 and Supplementary Figure S2). These results indicate that, at least in the cell lines tested, both mGrM and hGrM have cytotoxic potential in human cells, but not in mouse cells.

Discussion

Granzymes are key players in the effector arm of the immune response against tumour and virus-infected cells [2, 3]. Previously, it has been demonstrated that hGrB and mGrB are structurally and functionally different in that GrB from both

species cleaves pro-caspase 3, whereas only hGrB is able to cleave BID [121, 122, 154, 200]. In the present study, we have employed three distinct (proteomic) approaches to show that hGrM and mGrM also exhibit divergent and species-specific substrate specificities. mGrM and hGrM displayed distinct, but to some extent overlapping, tetrapeptide and macromolecular substrate specificities that were partially species-specific (Figures 1–4), whereas α-tubulin was a shared GrM substrate between species (Figure 5), only human but not mouse NPM was cleaved by both granzymes (Figure 6). Both hGrM and mGrM efficiently triggered apoptosis in human HeLa cells, but not in several mouse (tumour) cell lines (Figure 7). These results show that hGrM and mGrM are structurally and functionally divergent and cannot be used interchangeably.

Using a PS-SCL and a complementary positional proteomics approach, we showed that the P1 and extended specificities of hGrM and mGrM differ substantially. The PS-SCL results showed that, whereas hGrM prefers a leucine residue at P1 [28, 29], mGrM favoured a methionine (or Nle) leucine residue at this position (Figure 1D). The results of the PS-SCL were confirmed by positional proteomics, which also revealed that leucine and methionine residues are major P1 determinants for hGrM and mGrM (Figure 4). Upon differential comparison between both granzymes (Figure 4C), mGrM was better able to accommodate a methionine residue at P1, whereas hGrM clearly preferred a leucine residue. These results are in agreement with the facts that leucine and methionine are large hydrophobic residues and that the S1 pocket of hGrM – which can only accommodate long, narrow hydrophobic amino acids [20, 24] – is conserved in mGrM (Figure 1). The substrate specificity of hGrM and mGrM diverges further at the P2 position. PS-SCL and positional proteomics showed preferences for alanine and proline residues at P2 for hGrM [28, 29] and mGrM (Figures 1D, 4A and 4B). Major differences between hGrM and mGrM at the P2 position include a better tolerance to glutamic acid, threonine and valine by hGrM and to glycine by mGrM (Figure 4C). Both hGrM and mGrM displayed a clear preference for a glutamic acid residue at the P3 position, which was demonstrated by both PS-SCL (Figure 1D) and positional proteomics (Figure 4). The PS-SCL results showed that mGrM had a broad preference at the P4 position (Figure 1D), whereas in natural substrates mGrM favoured a lysine or arginine residue at this position, the latter being discriminative for mGrM as compared with hGrM (Figure 4). In PS-SCL, hGrM shows a clear preference for the positively charged lysine and histidine residues at P4 [28], which can also be deduced from positional proteomics (Figure 4).

Apart from the non-prime subsite preferences, we show for the first time that prime site residues are also important structural determinants for GrM-substrate recognition. In our positional proteomics approach, the amino acid occupancy of the P2′ position was found to be clearly discriminative between hGrM and mGrM, with hGrM accommodating alanine, asparagine, lysine, serine, glycine and valine residues, and mGrM accommodating leucine, phenylalanine and tyrosine residues to a better extent at this position (Figure 4C). Furthermore, replacement of the

putative P1′–P2′ residues in mouse NPM with the corresponding residues of human NPM fully restored cleavage of mouse NPM by both hGrM and mGrM (Figure 6). It seems unlikely that major structural differences around the GrM cleavage site between human and mouse NPM affect GrM proteolysis, since secondary structures and solvent accessibility of the GrM cleavage site regions in human and mouse NPM are predicted to be similar. The importance of prime site residues for GrM cleavage is compatible with the notion that relatively high concentrations of GrM were required for robust activity in PS-SCL (Figure 1D).

We employed two proteomic approaches to dissect the macromolecular substrate specificities of hGrM and mGrM (Figures 2–4 and Supplementary Table S1). Some substrates were shared, whereas others were specific for either hGrM or mGrM. Using the 2D-DIGE gel-based approach, only limited sets of hGrM (40, ~1.3% of total spots) and mGrM (12, ~0.5% of total spots) substrates were resolved in their species-matched cell lysates, indicating that both granzymes are highly specific. In the human HeLa cell lysate, 40 GrM substrates were identified, of which 17 (~42%) were shared by hGrM and mGrM. Using the gel-free complementary positional proteomics approach, we identified a total of 488 GrM substrates in the human K-562 cell lysate, of which 359 substrates (~74%) were shared between hGrM and mGrM. This indicates that the macromolecular substrate specificities of hGrM and mGrM only partially overlap. The discrepancy in the number of identified GrM substrates between the gel-free positional proteomics approach as compared with the gel-based 2D-DIGE approach is most likely due to the selection criteria and to the intrinsic higher sensitivity of gel-free proteomics [201]. Both the 2D-DIGE and the COFRADIC approach showed that while hGrM and mGrM share some cleavage sites in macromolecular substrates, they also make use of unique sites, which is in agreement with the partially overlapping primary and extended substrate specificity data as determined by both the PS-SCL and the positional proteomics approach (Figures 1D and 4, and Supplementary Table S1). Interestingly, both approaches revealed only few unique mGrM substrates.

The ability of GrM to cleave specific macromolecular substrates partially depends on the substrate conservation between human and mouse, suggesting that GrM has species-specific functions (Figures 5 and 6). The multifunctional phosphoprotein NPM is essential for cell viability and plays a role in viral replication [31, 74, 202]. Recently, it has been demonstrated that cleavage of human NPM by hGrM abolishes NPM function, which has been suggested to contribute to GrM-induced cell death [31]. NPM is a species-specific substrate of GrM: murine NPM was cleaved by neither mGrM nor hGrM, whereas human NPM was cleaved by both granzymes (Figure 6). Interestingly, hGRB and mGrB can also efficiently cleave human NPM [203], but fail to cleave mouse NPM [122]. These results indicate that the cleavage and inactivation of NPM does not contribute to GrM and GrB function in mice. In contrast, the microtubule network component α-tubulin of both human and mouse origin was cleaved by GrM of both species (Figure 5). Although α-tubulin is highly conserved between human and mouse (>99%), it is cleaved by hGrM and

mGrM at different sites and/or with different efficiencies at specific sites (Figure 5D and Supplementary Table S1). Apparently, targeting of α-tubulin by GrM and subsequent disorganization of the microtubule network are conserved between human and mouse and probably contributes to cytotoxic lymphocyte-induced cell death [45].

Although hGrM has previously been shown to efficiently induce cell death in multiple human cell lines [24, 31, 41, 43, 45], both hGrM and mGrM did not trigger cell death in several (tumour) cell lines of mouse origin (Figure 5). Whether or not GrM induces cell death in mice remains unclear and its lack of cytotoxicity in mouse cell lines may be due to several reasons. First, the cell death potential of GrM may depend on the type of target cell line that is used. mGrM efficiently induced cell death in human HeLa cells, indicating the apoptotic potential of this granzyme (Figure 5). Strikingly, mGrM did not trigger apoptosis in several mouse cell lines (i.e. C2C12, C26 and LR7) (Figure 5). In agreement with this, Pao et al. [62] have shown that GrM is not essential for NK cell-mediated cytotoxicity against tumour targets in mice. However, a more recent mouse study has demonstrated that adoptively transferred NK cells from wild-type mice, but not from GrM-deficient mice, effectively inhibit the growth of a subcutaneous tumour [63]. Secondly, the ability of GrM to trigger apoptosis in mouse cell lines may be hampered by the presence of specific inhibitors of GrM-mediated apoptosis such as the murine serine protease inhibitor SPI-CI, which has previously been shown to directly inhibit GrM activity [36]. Currently, no natural intracellular inhibitor of hGrM has been described. Finally, apart from α-tubulin and NPM, it remains unknown whether murine orthologues of other known hGrM death substrates such as HSP-75, iCAD, PARP and survivin [42-44] are cleaved by GrM in mice.

Mouse models are often employed to study the role of granzymes *in vivo*. GrM-knockout mice have demonstrated a role for GrM in the host response against tumours [63] and cytomegalovirus infection [62]. Recently, GrM-deficient mice have allowed the identification of GrM as being a key regulator of inflammation, possibly by enhancing the inflammatory cascade downstream of LPS (lipopolysaccharide)-TLR4 (Toll-like receptor 4) signalling [87]. Whether or not these *in vivo* data can be directly extrapolated to elucidate the functions of GrM in humans remains uncertain, since the species-specific substrate specificities of GrM signify that caution is essential when interpreting data from mouse studies.

Author Contribution

Stefanie de Poot and Marijn Westgeest participated in the design of the study, performed experiments, analysed and interpreted the data, and wrote the paper. Daniel Hostetter and Petra Van Damme participated in the design of the study, performed experiments, analysed and interpreted the data. Kim Plasman, Kimberly Demeyer and Roel Broekhuizen performed experiments. Kris Gevaert and Charles Craik participated in the design of the study, and analysed and interpreted the data. Niels Bovenschen participated in the design of the study, analysed and interpreted

the data, and wrote the paper.

Acknowledgements
We thank Dr C.E. Hack for critical reading of this manuscript before submission and Dr E.L. Schneider for helpful discussions. The recombinant granzymes used in the N- and C-terminal COFRADIC analyses were kindly provided by Dr P.I. Bird (Department of Biochemistry and Molecular Biology, Monash University, Melbourne, Victoria, Australia).

Funding
P. V. D. is a Postdoctoral Fellow of the Research Foundation-Flanders (FWO-Vlaanderen). K. P. is supported by a Ph.D. grant of the Institute for the Promotion of Innovation through Science and Technology in Flanders (IWT-Vlaanderen). This work was supported by the Fund for Scientific Research-Flanders (Belgium) [grant numbersG.0077.06 and G.0042.07 (to K.G.)], the Concerted Research Actions [grant number BOF07/GOA/012 (to K. G.)] fromGhent University and the Interuniversity Attraction Poles [grant number IUAP06], the Dutch Cancer Society (KWF) [grant number UU-2009–4302 (to N. B.)] and the Netherlands Organization for Scientific Research (NWO) [grant number 916.66.044 (to N. B.)].

Supplemental Data

SUPPLEMENTAL TABLE 1. Lists of neo-N-termini (tri-deuteroacetylated, internal peptides) or neo-C-termini (list of butyrylated, internal peptides) that are only present in the digested proteome of mGrM and/or hGrM treated human K-562 lysates. Swissprot database primary accession number, Swissprot entry name, protein description, start/end, cleavage site (P4-P1 and P1), N-terminal modification identified, sequence, for neo-N-termini: C-terminal arginine variant(s) identified in MS/MS, cleavage type, mean hGrM/mGrM-cleavage ratio identified, isoforms, number of identified spectra (spectra #), highest Mascot ion score, Mascot identitythreshold and Δ threshold of the identified spectra with highest Mascot ion score are given. (A) Neo-N-termini are classified according to the cleavage site location in their protein and alphabetically ranked according to their protein description. (B) Neo-N-termini are classified according to their P1-cleavage site preference and subsequently ranked according to the cleavage site location in their protein and alphabetically ranked according to their protein description. (C) Neo-C-termini are classified according to the cleavage site location in their protein and alphabetically ranked according to their protein description. (D) Neo-C-termini are classified according to their P1-cleavage site preference and subsequently ranked according to the cleavage site location in their protein and alphabetically ranked according to their protein description. Furthermore, whenever the corresponding protein N- and/or C-terminus was identified the corresponding sequence and hGrM/mGrM ratio calculated is indicated. **Suppl. Table 1** can be viewed at: https://docs.google.com/file/d/0B17lRh8XPFn6Q2psSkVOMm9rQWc/edit?usp=sharing.

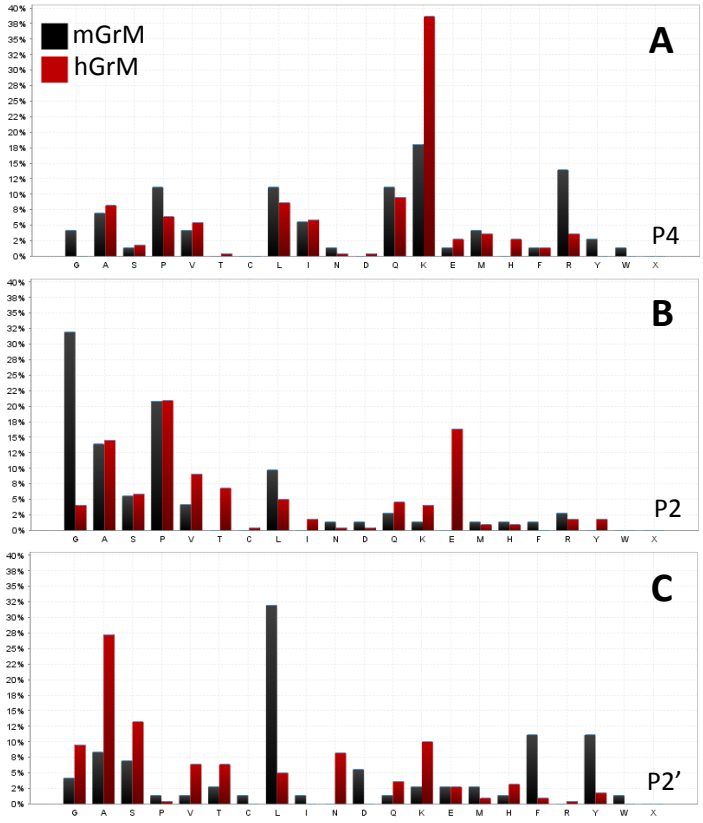

SUPPLEMENTAL FIG. 1. (A-C). Bar charts of the different amino acid occurrences at discriminating P and P'-positions (P4, P2 and P2') in more efficient hGrM versus more efficient mGrM cleavage site motifs.

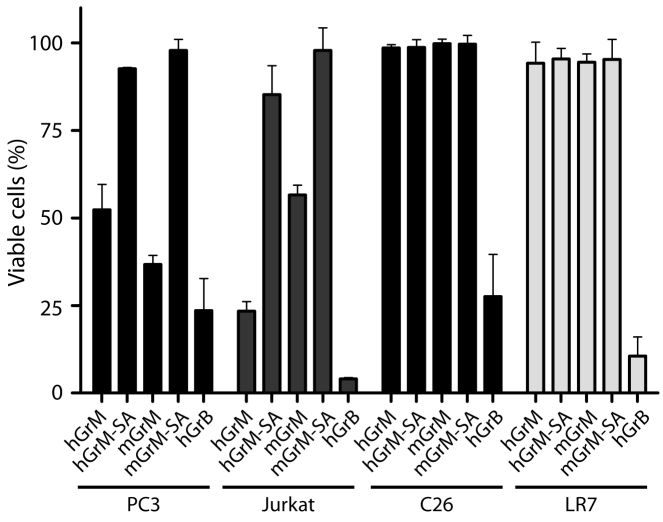

SUPPLEMENTAL FIG. 2. Human and mouse GrM trigger cell death in human but not mouse cell lines. Human PC3 and Jurkat cells or mouse C26 and LR7 cells were treated with sublytic concentrations of SLO and 500 nM of hGrM, mGrM or their catalytically inactive mutants (GrM-SA) for 30 min. Cells were treated with hGrB as a positive control. After washing, cells were incubated for another 20 h at 37°C. Cell viability was determined using flow cytometry, with AnnexinV and PI negative cells considered viable.

Chapter 4

Granzyme M cannot induce cell death via cleavage of mouse FADD

Stefanie A. H. de Poot, Ka Wai Lai, Elise S. Hovingh and Niels Bovenschen

Department of Pathology, University Medical Center Utrecht, Utrecht, the Netherlands

Apoptosis. 2013;18(4):533-4.

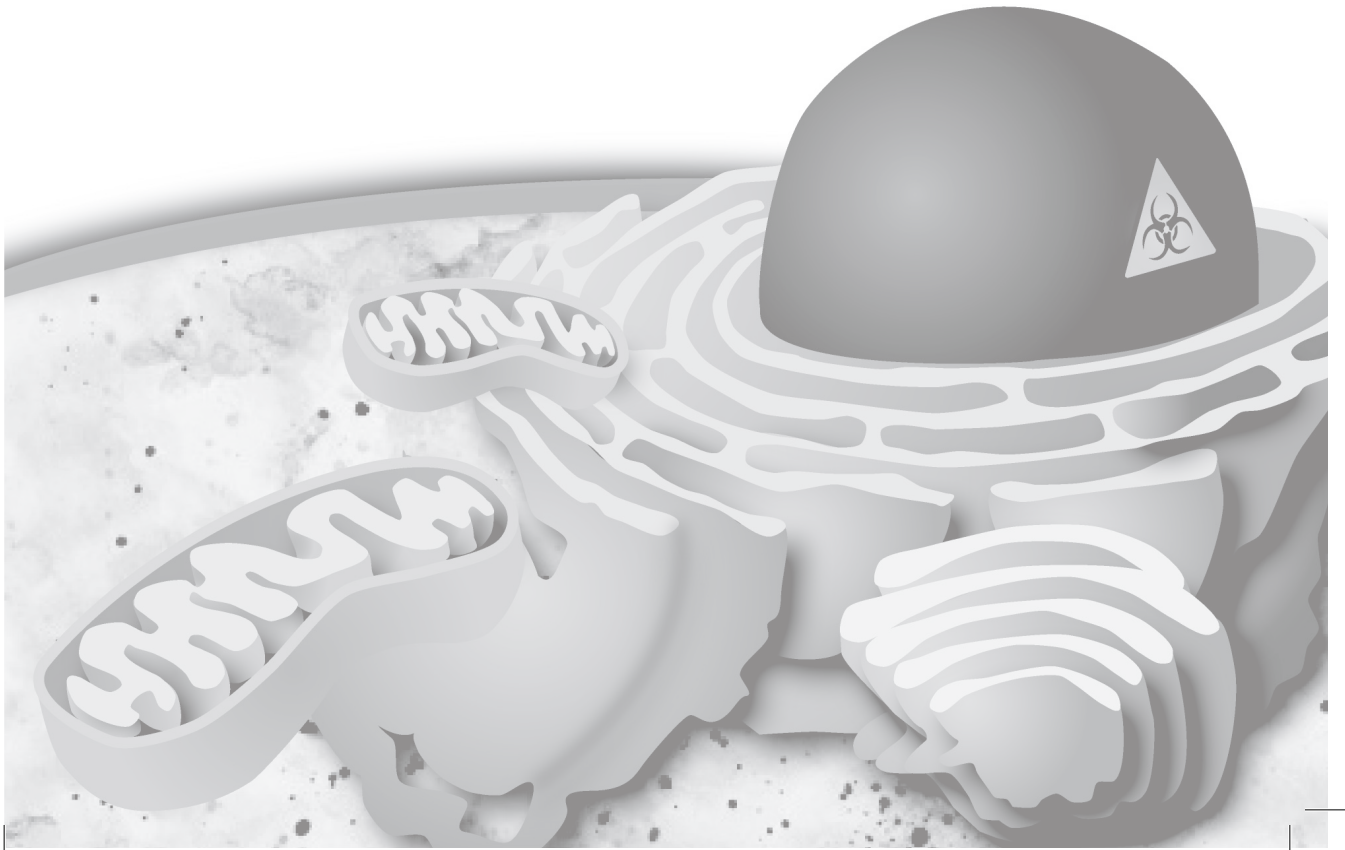

To the Editor,

Cytotoxic lymphocytes form the first line of defense against virus-infected and tumor cells, and can initiate target cell death via death receptor ligation or the granule exocytosis pathway [3]. In the latter pathway, cytotoxic lymphocytes deliver a set of structurally homologous serine proteases known as granzymes into the target cell, where they can activate intracellular cell death pathways [8]. Human granzyme M (hGrM) efficiently induces apoptosis in a wide variety of human tumor cells [30-32, 41]. Recently, this induction of cell death has been shown to occur via hGrM-mediated cleavage of Fas-Associated protein with Death Domain (FADD) at Met^{196}, resulting in FADD self-association and initiation of the caspase cascade [32]. Replacement of FADD with a non-cleavable FADD mutant makes human tumor cells more resistant to hGrM-induced cell death, underlining the importance of this pathway [32]. Mice express the hGrM orthologue mouse GrM (mGrM). In mouse models, conflicting results have been obtained regarding the role of mGrM in tumor clearance. On the one hand, Pao et al. [62] found no effect of mGrM-deficiency on in vivo rejection of various tumor types, whilst Pegram et al. [63] noted that mGrM-deficient natural killer cells are significantly impaired in their ability to inhibit tumor growth. Interestingly, we have recently found that hGrM and mGrM exhibit only partially overlapping substrate specificities, and that both can efficiently induce apoptosis in human tumor cells, but not in various mouse tumor cells [30]. This suggests that key GrM substrates in human tumor cells are absent or cannot be cleaved in mouse tumor cells.

In order to explain this apparent difference in GrM cytotoxicity towards human and mouse tumor cells, we investigated whether the recently unraveled pathway of hGrM-mediated cell death induction—via FADD cleavage—is intact in murine tumor cells. Although human FADD (hFADD) and mouse FADD (mFADD) display almost 70 % sequence homology, the GrM cleavage site at Met^{196} (P1 residue) in hFADD is not conserved in mFADD, which harbors a Val at this position (Fig. 1a). This suggests that GrM cannot cleave and activate FADD in a murine setting. In order to test this hypothesis, hGrM was incubated with lysates of the human HeLa cervix carcinoma and mouse C2C12 myoblast cell lines (Fig. 1b). We confirmed that GrM cleaves hFADD [32]. In mouse C2C12 lysate, however, no cleavage of mFADD could be observed (Fig. 1b), even though GrM was active in this lysate (data not shown). Similar results were obtained when isolated recombinant hFADD and mFADD were incubated with hGrM or mGrM (Fig. 1c). Whereas recombinant hFADD was efficiently processed by both hGrM and mGrM, mFADD was not cleaved by either (Fig. 1c).

To restore GrM-mediated cleavage of mFADD, residues Val^{193} and Leu^{194} in mFADD were 'humanized' by substitution with the corresponding GrM cleavage site residues (P1 and P1') of hFADD, i.e. Met^{196} and Ser^{197}, respectively (Fig. 1c). In contrast to wild-type mFADD, this mFADD P1P1' mutant was cleaved by both mGrM and hGrM (Fig. 1c). Interestingly, hFADD seemed to be cleaved more efficiently by mGrM, which may be due to the presence of a Met at the P1 position, for which

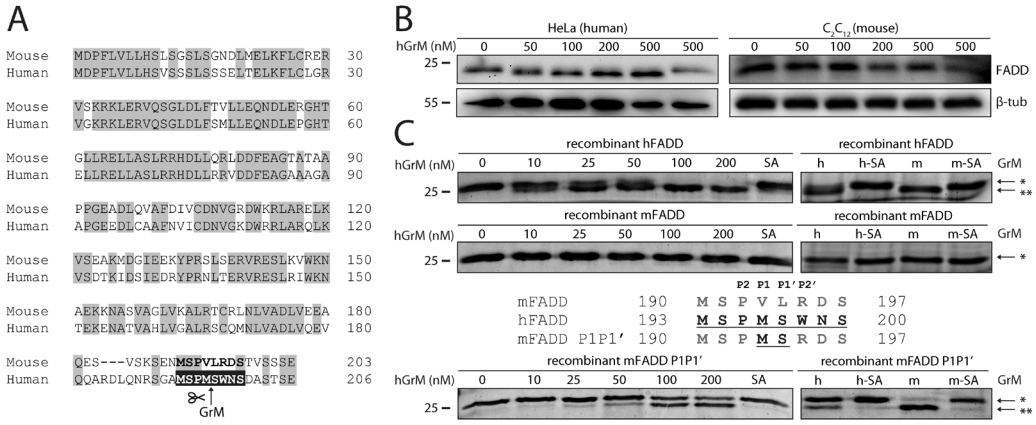

Figure 1. Human and mouse GrM cannot cleave mouse FADD due to a species-specific difference in the GrM cleavage site. (A) Alignment of the primary sequences of hFADD and mFADD. Residues boxed in grey are amino acids shared by hFADD and mFADD. The P4-P4' GrM cleavage site in hFADD (with Met[196] at P1) is bolded and boxed in black. The corresponding residues in mFADD are also bolded. (B) Cell lysates derived from human HeLa or mouse C2C12 cells were incubated at 37°C with different concentrations of hGrM for 4 h, or with 500 nM of the catalytically inactive hGrM-SA mutant, in which the Ser of the catalytic triad has been mutated into an Ala. Samples were immunoblotted, using antibodies against hFADD, mFADD, or β-tubulin (β-tub; loading control). (C) Isolated recombinant hFADD and mFADD were incubated for 4 h at 37°C with the indicated concentrations of hGrM or with 200 nM of inactive hGrM-SA. Recombinant hFADD and mFADD were also treated for 4 h at 37°C with 100 nM hGrM (h), hGrM-SA (h-SA), mGrM (m) or mGrM-SA (m-SA). Site-directed mutagenesis was used to replace the P1 and P1' residues of mFADD (Val[193] and Leu[194]) with the corresponding residues in hFADD (Met[196] and Ser[197]). This mFADD P1P1' mutant was treated for 4 h with the indicated concentrations of hGrM, hGrM-SA, mGrM or mGrM-SA. All reactions were separated by SDS-PAGE and proteins were visualized by Instant Blue staining. *Full-length (intact) FADD. **Cleaved FADD. Experiments were performed at least 3 times, representative images are shown.

mGrM has a stronger preference [30].

Taken together, these data show that GrM cannot cleave FADD in mice because of a species-specific difference at the GrM cleavage site. This may explain why mGrM is not cytotoxic in mice [30, 62], and underlines that caution is essential when using mouse models to elucidate the anti-tumor functions of GrM.

Acknowledgments

This study was supported by the Netherlands Organization for Scientific Research (NWO) (Grant 916.66.044) and the Dutch Cancer Society (UU-2009-4302) (to NB).

Chapter 5

Granzyme M targets topoisomerase II alpha to trigger cell cycle arrest and caspase-dependent apoptosis

Stefanie A.H. de Poot[1], Ka Wai Lai[1], Lennart van der Wal[1], Kim Plasman[2,3], Petra Van Damme[2,3], Andrew C. Porter[4], Kris Gevaert[2,3], Niels Bovenschen[1]

1. Department of Pathology, University Medical Center Utrecht, Utrecht, the Netherlands
2. Department of Medical Protein Research, VIB, B-9000 Ghent, Belgium
3. Department of Biochemistry, Ghent University, B-9000 Ghent, Belgium
4. Centre for Haematology, Faculty of Medicine, Imperial College London, London, UK

Cell Death Differ. doi: 10.1038/cdd.2013.155

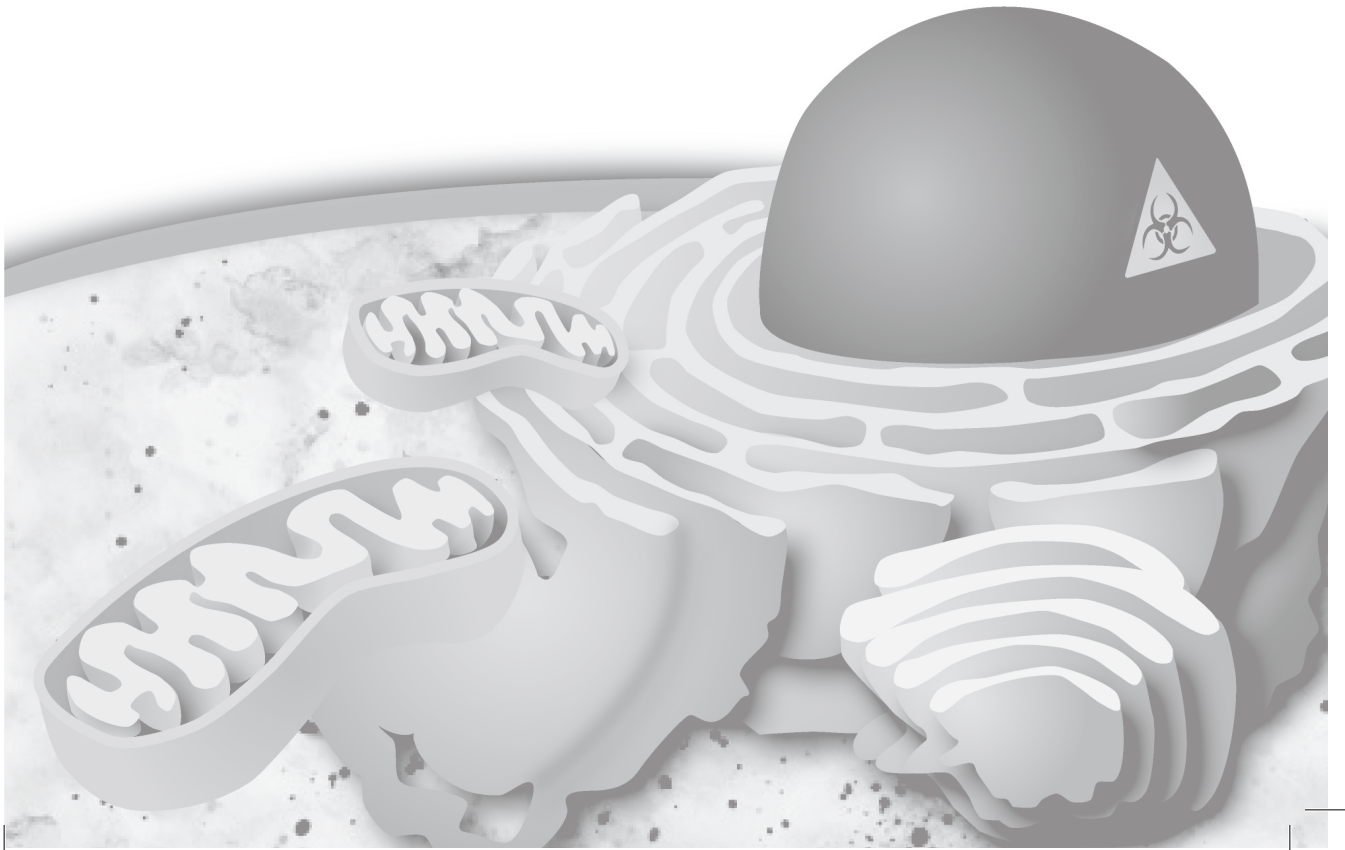

Abstract
Cytotoxic lymphocyte protease granzyme M (GrM) is a potent inducer of tumor cell death. The apoptotic phenotype and mechanism by which it induces cell death, however, remain poorly understood and controversial. Here, we show that GrM-induced cell death was largely caspase-dependent with various hallmarks of classical apoptosis, coinciding with caspase-independent G2/M cell cycle arrest. Using positional proteomics in human tumor cells, we identified the nuclear enzyme topoisomerase II alpha (topoIIα) as a physiological substrate of GrM. Cleavage of topoIIα by GrM at Leu^{1280} separated topoIIα functional domains from the nuclear localization signals, leading to nuclear exit of topoIIα catalytic activity, thereby rendering it nonfunctional. Similar to the apoptotic phenotype of GrM, topoIIα depletion in tumor cells led to cell cycle arrest in G2/M, mitochondrial perturbations, caspase activation, and apoptosis. We conclude that cytotoxic lymphocyte protease GrM targets topoIIα to trigger cell cycle arrest and caspase-dependent apoptosis.

Abbreviations: AnnV, AnnexinV-fluos; casp8$^{-/-}$, caspase-8 deficient, CI, cell index; COFRADIC, combined fractional diagonal chromatography; dox, doxycycline; FADD, Fas-associated protein with death domain; FCS, fetal calf serum; GrB, granzyme B; GrM, granzyme M; GrM-SA, inactive GrM mutant in which the catalytic site Ser residue has been mutated to an Ala residue; LC-MS/MS, liquid chromatography-MS/MS; NK cells, natural killer cells; NLS, nuclear localization signal; NPM, nucleophosmin; MS, mass spectrometry; PI, propidium iodide; ROS, reactive oxygen species; SILAC, stable isotope labeling by amino acids in cell culture; SLO, streptolysin O; TCEP, Tris carboxyethyl phosphine; topoIIα, topoisomerase II alpha; TUNEL, TdT dUTP nick-end labeling; wt, wild-type.

Keywords: granzyme M, cell cycle arrest, topoisomerase II alpha, protease, apoptosis

Introduction

Cytotoxic T lymphocytes and natural killer (NK) cells form the first line of defense against virus-infected and tumor cells. [3] Upon target cell recognition, these cytotoxic lymphocytes can initiate target cell death via the death receptor or the granule exocytosis pathway. [2] In the latter, cytotoxic lymphocytes release the pore-forming protein perforin and a set of structurally homologous serine proteases known as granzymes. Perforin facilitates entry of granzymes into the target cell, where they can cleave intracellular substrates to induce cell death. In humans, five granzymes have been identified. [3, 6, 8, 69]

Human granzyme M (GrM)[9] is expressed in NK, γδ-T, NKT, and CD8+ T cells. [11, 37, 38] GrM is unique in that it preferably cleaves after a Leu or Met residue. [29, 30] GrM efficiently kills tumor cell lines such as HeLa, Jurkat, HL60, and K562 cells. [31, 32, 41, 45, 204] In addition, a GrM-anti CD64 fusion protein has recently been shown to induce cell death in human primary leukemic cells *in vitro*. [204] The *in vivo* importance of GrM is still unclear. In one study, GrM knockout mice clear tumors just as efficiently as wild-type mice. [62] However, in another study, GrM is important in the anti-tumor effect mediated by adoptively transferred NK cells. [63] The lack of a clear-cut phenotype in GrM knockout mice may be due to the redundancy of the murine granzymes or to species-specific differences between the human and mouse GrM orthologues. [30, 33]

The apoptotic phenotype and molecular mechanism of GrM-mediated cell death in human tumor cells are still unclear and remain controversial in the literature. Several studies have shown that GrM triggers cell death in a caspase-independent fashion, without fragmentation of DNA or perturbation of the mitochondria. [31, 41] In contrast, other studies reported that GrM-mediated cell death occurs in the presence of caspase-3 activation, DNA fragmentation, ROS generation, and cytochrome *c* release from the mitochondria. [32, 42-44] Over the years, several GrM substrates have been identified. [30-32, 42-45, 47] Of these, only Fas-Associated protein with Death Domain (FADD) was univocally proven to play an important role in GrM-mediated apoptosis. [32] Cleavage of human FADD by GrM promotes procaspase-8 recruitment and activation, and subsequent initiation of the caspase cascade. [32, 33] However, FADD-deficient cancer cells are only partially resistant to GrM, [32] indicating that there is at least one other important mediator via which GrM induces apoptosis.

In the present study, we comprehensively characterized the phenotype of GrM-induced cell death. GrM treatment resulted in largely caspase-dependent cell death exhibiting classical hallmarks of apoptosis. Furthermore, we showed for the first time that GrM triggered G2/M cell cycle arrest. In the absence of caspase-8 –and thus the GrM-FADD-caspase-8 pathway [32]– both cell cycle arrest and caspase activation still occurred. To understand these caspase-8/FADD-independent GrM functions, we used positional proteomics in HeLa tumor cells to identify DNA topoisomerase II alpha (topoIIα) as a novel GrM substrate. We conclude that, next to FADD-cleavage mediated caspase activation, cytotoxic lymphocyte protease GrM

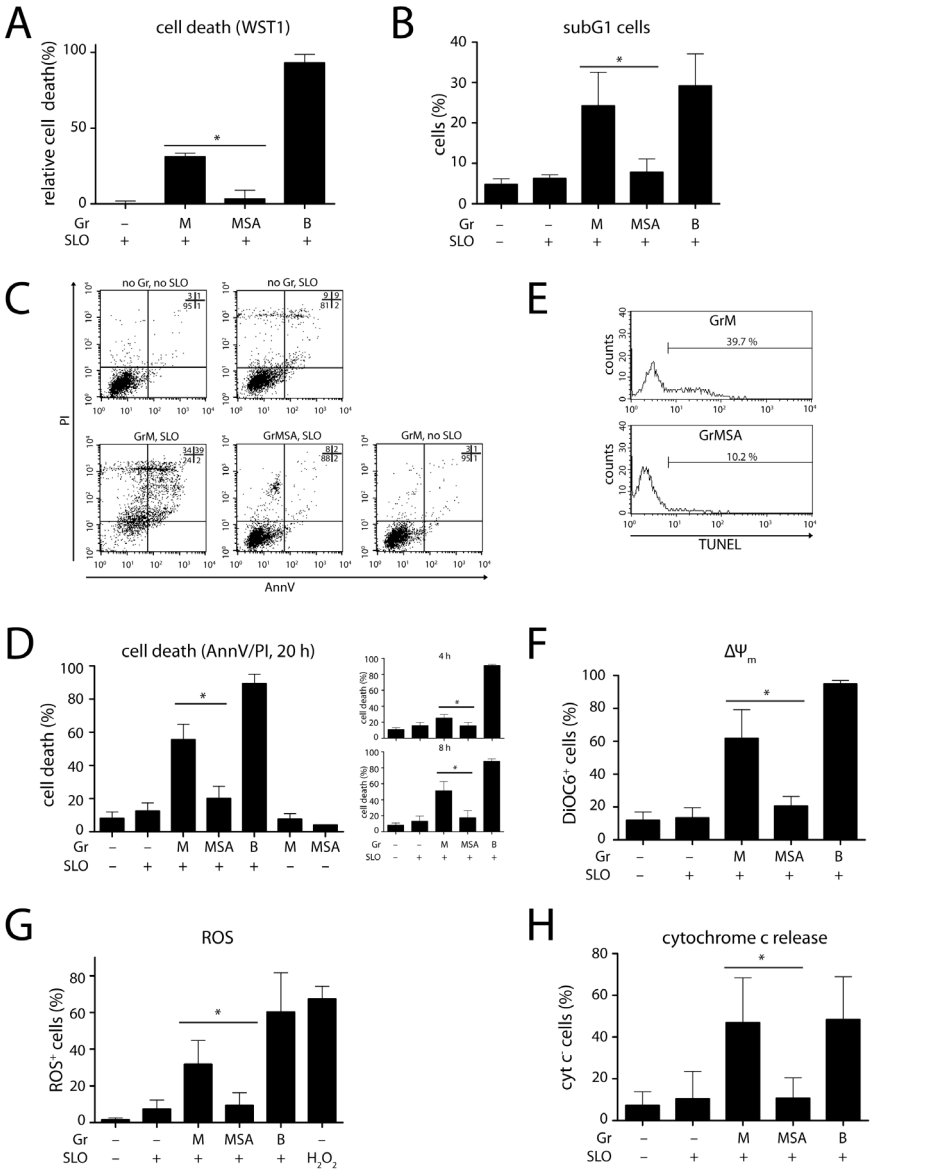

Figure 1. Cell death induced by GrM is characterized by apoptotic hallmarks. **(a)** HeLa cells were treated with 1 µM GrM (M), 1 µM GrM-SA (MSA; control inactive GrM mutant in which the catalytic Ser has been replaced with Ala), or 100 nM GrB, and 0.5 µg/ml SLO or no SLO for 20 h at 37°C. Metabolically active cells were quantified using the WST-1 assay, and the relative loss of viability compared to untreated (SLO-negative) cells was calculated. **(b)** Jurkat cells were treated with 1 µM GrM (M), 1 µM GrM-SA (MSA), or 100 nM GrB in the absence or presence of 0.1 µg/ml SLO for 16 h. DNA fragmentation was determined by PI-staining and flow cytometry to assess the percentage of subG1 cells. **(c)** HeLa cells were treated as in (a), and tested for induction of apoptosis with AnnV/PI flow cytometry. Results are representative of at least 3 experiments. **(d)** HeLa cells were treated as in (a) for 4, 8 or 20 h, and tested for induction of apoptosis with AnnV/PI flow cytometry. AnnV and/or PI positive cells are plotted on y-axis. **(e-h)** HeLa cells were treated as in (a), and tested for **(e)** DNA fragmentation with TUNEL (results are representative of at least 3 experiments), **(f)** loss of mitochondrial membrane potential ($\Delta\Psi_m$) with DiOC6, **(g)** generation of reactive oxygen species with CM-H_2DCFDA, and **(h)** release of cytochrome c using flow cytometry. Bar graphs depict the mean +/- SD, with * representing p values < 0.05.

targets topoIIα to trigger cell cycle arrest and caspase-dependent apoptosis.

Results

GrM triggers classical hallmarks of apoptosis.

The phenotype of GrM-mediated cell death remains controversial in the literature. Therefore, we comprehensively characterized apoptotic hallmarks in GrM-treated human tumor cells. Recombinant human GrM or catalytically inactive mutant GrM-SA were delivered into cells with the perforin-analogue streptolysin O (SLO). GrM triggered cell death in HeLa cells as measured by a WST-1 cell viability assay, reflecting the number of metabolically active, adherent cells (Figure 1a). Similarly, when Jurkat cells were treated with GrM, an increase in cells with fragmented DNA (subG1) was observed (Figure 1b). To further characterize the type of cell death induced by GrM, HeLa cells were stained with AnnV and PI, and analyzed by flow cytometry (Figures 1c and d) or fluorescence microscopy (Supplemental Figure 1a). GrM-treated cells first became AnnV positive, and later AnnV/PI double-positive, suggesting death via classical apoptosis. Similar results were obtained for Jurkat cells treated with GrM delivered by SLO (data not shown) and perforin (Supplemental Figure 1b). Typically, upon induction of classical apoptosis, DNases are activated, leading to DNA fragmentation. Indeed, in GrM-treated cells, an increase in TdT dUTP nick-end labeling (TUNEL)-positive cells was observed (Figure 1e), indicative of DNA fragmentation. In addition, loss of mitochondrial membrane potential –as measured with the fluorescent dye DiOC6– accompanied by an increase in reactive oxygen species (ROS) and the release of cytochrome *c* were observed (Figures 1f-h). Interestingly, treatment with GrM resulted in rapid changes in cellular morphology (Supplemental Figure 1c). Already 2 h after treatment –before AnnV/PI positivity– HeLa cells displayed long, thick protrusions, and irregularly shaped nuclei. These changes in morphology were also verified in FSC/SSC plots: GrM-treated cells were reduced in size (FSC), but displayed increased granularity (SCC) (Supplemental Figure 1d). Using time-lapse microscopy, we tracked these morphological alterations over an 8 h time-course (Supplemental Figure 1e, Supplemental Movie 1). The rapid changes in morphology preceded apoptotic blebbing. Finally, no upregulation of the stress-inducible protein CHOP [205] and no accumulation of ubiquitylated proteins were detected (Supplemental Figure 1f), indicating that GrM-mediated apoptosis is not accompanied by endoplasmic reticulum stress.

GrM indirectly activates caspases.

It remains unclear whether or not caspase activation is involved in GrM-mediated cell death. [31, 32, 41, 42, 44] Therefore, cell-free protein extracts from HeLa cells were incubated for 4 h with increasing concentrations of GrM, in the presence or absence of the pan-caspase inhibitor zVAD-fmk. Caspase activation of a subset of the caspase family was monitored using immunoblot (Figure 2a). Whereas GrB cleaved caspase-3, -8, and -9 in lysate (and indirectly activated caspase-6) [135], GrM treatment did not lead to any detectable caspase activation in lysate. However,

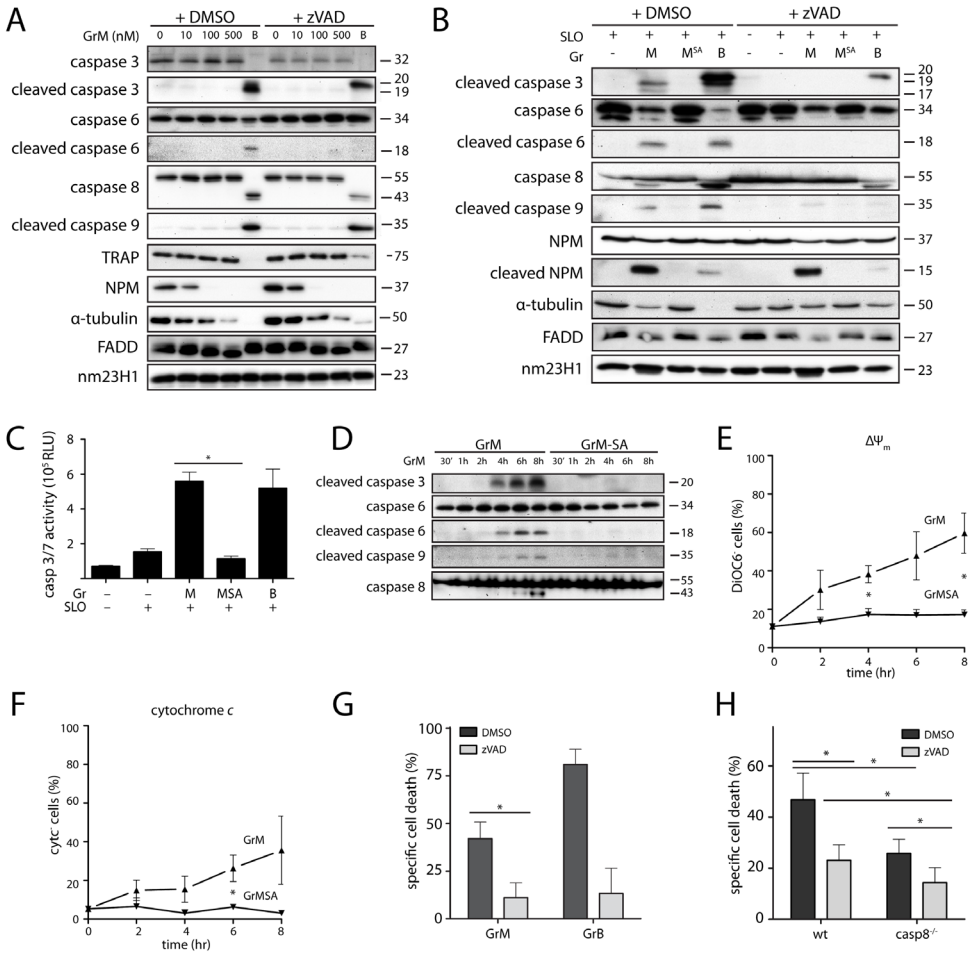

Figure 2. GrM indirectly activates caspases-3, -6, -8, and -9, and induces caspase-8 dependent and independent cell death. **(a)** 5 µg of HeLa cell lysate was incubated with the indicated concentrations of GrM (0-500 nM) or 500 nM GrB for 2 h at 37°C in the absence (DMSO) or presence of 100 µM z-VAD-fmk, after which caspase activation was assessed using immunoblot. The effects of GrM on known substrates TRAP,[43] NPM,[31] α-tubulin,[45] and FADD[32] were also determined. Nm23H1 served as loading control. **(b)** HeLa cells were treated with 1 µM GrM (M), 1 µM GrM-SA (MSA), or 100 nM GrB (B), and 0.5 µg/ml SLO in the absence (DMSO) or presence of 100 µM z-VAD-fmk for 8 h at 37°C. Caspase activation and substrate cleavage were visualized using immunoblot with nm23H1 serving as the loading control. Known GrM substrates (NPM, α-tubulin, and FADD) were used as positive controls, of which α-tubulin cleavage was partially mediated by caspases. **(c)** Jurkat cells were treated for 6 h at 37°C with 1 µM GrM, 1 µM GrM-SA, or 50 nM GrB, and 0.1 µg/ml SLO. Caspase-3/-7 activation was detected using the CaspaseGlo assay. Relative light units (RLU) are depicted. **(d-f)** HeLa cells were treated with 1 µM GrM or 1 µM GrM-SA, and 0.5 µg/ml SLO. Caspase activation **(d)** was detected in time using immunoblot analysis, and the kinetics of $\Delta\Psi_m$ (DiOC6) loss **(e)** and cytochrome c release **(f)** were also determined at various time intervals (n=3, means +/- SEM). **(g)** HeLa cells were treated as in (b), and the effects of 100 µM zVAD on GrM-induced cell death were determined using AnnV/PI flow cytometry. **(h)** Wild-type (wt) and caspase-8 deficient (casp8$^{-/-}$) Jurkat cells were treated with 1 µM GrM and 0.1 µg/ml SLO in the absence (DMSO) or presence of 100 µM z-VAD-fmk. Cell death induction was assessed using AnnV/PI flow cytometry.

as a control, known GrM substrates nucleophosmin (NPM) [31], α-tubulin [45], and FADD [32] were cleaved by GrM in a caspase-independent manner (Figure 2a). Remarkably, GrM-mediated proteolysis of the previously reported GrM substrate

TRAP/Hsp75 [43] could not be verified. Similar results were obtained in Jurkat lysate (data not shown). These data indicate that GrM cannot directly activate caspases. Next, HeLa cells were treated with GrM in the presence or absence of zVAD-fmk, and again, caspase activation was monitored (Figure 2b). GrB served as a control for monitoring caspase activation and directly activated caspase-3 and -8, whereas caspase-6 and -9 activation was at least partially dependent on the activity of other caspases (Figure 2b). In contrast to cell-free tumor lysates, GrM was capable of activating caspase-3, -6, -8 and -9 in living cells. This activation was inhibited by zVAD-fmk, confirming that GrM did not directly proteolyze caspases. Similar results were obtained with Jurkat cells in which GrM was delivered with SLO (data not shown) and with perforin (Supplemental Figure 1g). Caspase-3/-7 activation in GrM-treated Jurkat cells was further validated using the Caspase-Glo activity assay (Figure 2c). To study the kinetics of caspase activation in HeLa cells, caspase activation was determined at various time points following GrM treatment (Figure 2d). At 4 h after treatment, activation of caspase-3, -6 and -9 could be detected; after 6 h, caspase-8 activation was also detected (Figure 2d). Loss of mitochondrial membrane potential and the release of cytochrome c were already observed after 2 h of GrM treatment (and thus before measurable caspase activation), suggesting that targeting of mitochondria occurs relatively early in GrM-mediated cell death (Figures 2d-f).

Consistent with the zVAD-sensitivity of GrM-mediated caspase activation (Figure 2b), zVAD-fmk treatment of HeLa cells almost completely inhibited GrM-induced apoptosis (Figure 2g). Recently, Wang *et al*. demonstrated that GrM activates caspase-8 via cleavage of FADD [32], resulting in mitochondrial damage and initiation of the caspase cascade. In caspase-8 deficient (casp-8$^{-/-}$) Jurkat cells (Supplemental Figure 2a), GrM-induced cell death was indeed reduced (~50%) as compared to wild-type Jurkat cells, but it was not completely inhibited (Figure 2h). This suggests that GrM activates an alternative cell death pathway that does not rely on FADD-cleavage/caspase-8 activation. zVAD-fmk even further inhibited GrM-induced apoptosis in casp-8$^{-/-}$ cells (Figure 2h), whereas Bcl-2 overexpression did not (Supplemental Figure 2b). This suggests that in casp-8$^{-/-}$ Jurkat cells, GrM-induced cell death is independent of caspase-8, but (at least partially) relies on the indirect activation of other caspases. zVAD-fmk did not affect GrM-mediated morphological changes (Supplemental Figure 2c) and mitochondrial perturbations (Supplemental Figure 2d). Taken together, these data indicate that GrM triggers cellular morphological changes, mitochondrial perturbations, and activation of the caspase cascade that is only partially dependent on caspase-8, leading to DNA fragmentation and apoptosis.

Proteomic identification of GrM substrates in living cancer cells.

To identify candidates via which GrM activates caspase-8-independent apoptosis, we compared the N-terminomes of control HeLa cells (SLO treated) to those of HeLa cells treated for 15 or 60 min with SLO and GrM (Figure 3a) to increase the

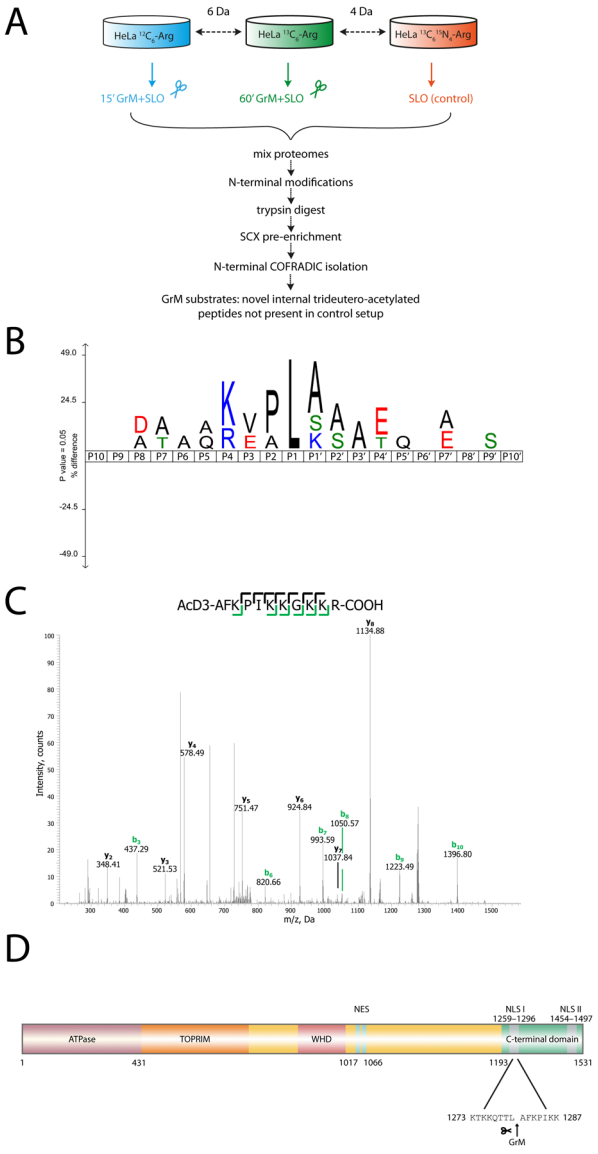

Figure 3. Positional proteomics-based identification of GrM-mediated topoIIα cleavage at Leu^{1280} in HeLa cells. **(a)** Schematic overview of the N-terminal positional proteomics strategy. L-Arg SILAC labeled HeLa cells were incubated with 1 µM GrM and 0.5 µg/ml SLO for either 15 ($^{12}C_6$) or 60 ($^{13}C_6$) min, or with 0.5 µg/ml SLO only for 60 min ($^{13}C_6$ $^{15}N_4$) at 37°C. N-terminal COFRADIC was used to identify *in vivo* GrM substrates. **(b)** IceLogo visualization of the 38 non-redundant P10-P10' GrM cleavage site motifs identified. Multiple sequence alignments {Colaert, 2009 #70} of peptide substrate motifs from P10 to P10' are given with cleavage of the substrate occurring between P1 and P1'. Statistically significant residues with a p-value threshold of ≤ 0.05 are plotted. The amino acid heights are indicative for their degree of conservation at the indicated position. The frequency of the amino acid occurrence at each position in the sequence set was compared with the human Swissprot 2011_11 database {Colaert, 2009 #70}. **(c)** MS/MS spectrum of the N-terminally trideutero-acetylated neo-N-terminus of topoIIα (^{1280}AFKPIKKGKKR, Swiss-Prot accession: P11388) with the observed b- and y-type fragment ions indicated. **(d)** Schematic domain representation of human topoIIα. Proteomics identified GrM cleavage of topoIIα at Leu^{1280} in the regulatory C-terminal domain, within the first nuclear localization signal (NLS). TOPRIM: topoisomerase-primase domain; WHD: winged-helix domain; NES: nuclear export signal.

overall possibility of identifying both early and late proteolytic events. In this way, 1,361 N-terminal peptides were identified, 597 potentially hinting to proteolytic neo-N-termini; *i.e.*, peptides that were N-terminally trideutero-acetylated and did not start at position 1 or 2. Of these, 38 neo-N-termini were uniquely identified in (one of) the GrM-treated setups and could thus be assigned to 34 (direct or indirect) GrM substrates (Supplemental Table 1). Amino acids surrounding the scissile bond are denoted as Pn-P2-P1↓P1'-P2'-Pn'.[27] Out of 38 GrM-generated neo-N-termini, 25 (65.8%) were cleaved after a P1 Leu or Met. A multiple sequence alignment of the 38 cleavage sites by iceLogo [198] (Figure 3b) clearly showed the P4-P1 sequence specificity profile [K/R][V/E][P/A]L↓, which closely matches

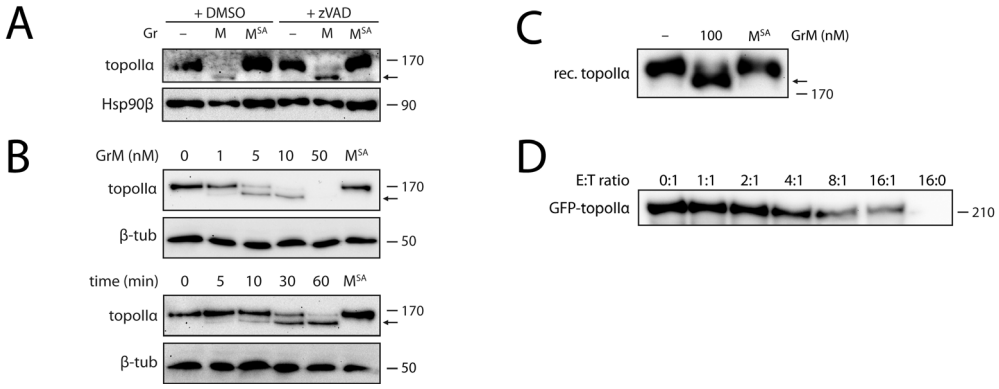

Figure 4. GrM efficiently and directly cleaves topoIIα. **(a)** HeLa cells were incubated with 1 μM GrM or 1 μM GrM-SA, and 0.5 μg/ml SLO in the absence (DMSO) or presence of 100 μM z-VAD-fmk for 6 h at 37°C. TopoIIα cleavage was determined using immunoblot analysis. Hsp90β was used as loading control. **(b)** 10 μg HeLa cell lysate was incubated at 37°C with indicated concentrations of GrM or 50 nM GrM-SA for 30 min, or with 5 nM GrM for indicated lengths of time or 60 min with 5 nM GrM-SA. TopoIIα cleavage was determined using immunoblot analysis. β-tubulin was used as a loading control. **(c)** 20 units of purified recombinant human topoIIα were incubated with 100 nM GrM or GrM-SA for 30 min at 37°C. Cleavage was determined using immunoblot. **(d)** Cos7 cells were transiently transfected with eGFP-topoIIα and co-cultured with increasing effector:target (E:T) ratio's of NK cells (KHYG1) for 4 h at 37°C. Cleavage of eGFP-topoIIα was determined using immunoblot for eGFP. An arrow is used to indicate the topoIIα cleavage fragment.

previously characterized GrM specificity profiles. [28-30] Topoisomerase II alpha (topoIIα) was amongst the 25 GrM substrates identified upon cleavage at a P1 Leu or Met (Figure 3c). TopoIIα is a nuclear enzyme that can alter DNA topology to resolve DNA overwinding, and is often highly expressed in cancers where it correlates with poor patient survival. The here identified GrM cleavage site in topoIIα, Leu^{1280}, resides inside the first nuclear localization signal (NLS) of the enzyme (Figure 3d).

GrM targets topoIIα.

To validate topoIIα as a GrM substrate, HeLa cells were treated with GrM in the presence or absence of zVAD-fmk. TopoIIα cleavage by GrM was confirmed by immunoblotting and was independent of caspase activation (Figure 4a). Full-length topoIIα (~170 kDa) disappeared and the expected N-terminal fragment (~140 kDa) was detected. In Jurkat cells treated with GrM and perforin, topoIIα was also efficiently cleaved (Supplemental Figure 1h). Expression levels of topoIIα, however, did not change in GrM-treated Jurkat cells (Supplemental Figure 2f). Similarly, in cell-free lysates, topoIIα was cleaved with high efficiency: already within 30 min, 10 nM of GrM had completely proteolyzed topoIIα (Figure 4b, upper panel). GrM cleaved purified recombinant topoIIα, validating topoIIα as a direct GrM substrate (Figure 4c). Finally, Cos7 cells were transfected with eGFP-linked topoIIα and co-cultured with increasing effector:target (E:T) ratios of KHYG1 NK cells, [206] which are known to express GrM. [207] Using immunoblotting with an anti-eGFP antibody, cleavage of eGFP-topoIIα inside target cells was observed (Figure 4d), indicating that topoIIα is a physiological substrate during NK-cell mediated tumor cell killing. No cleavage fragment was detected, which may be due to further processing and

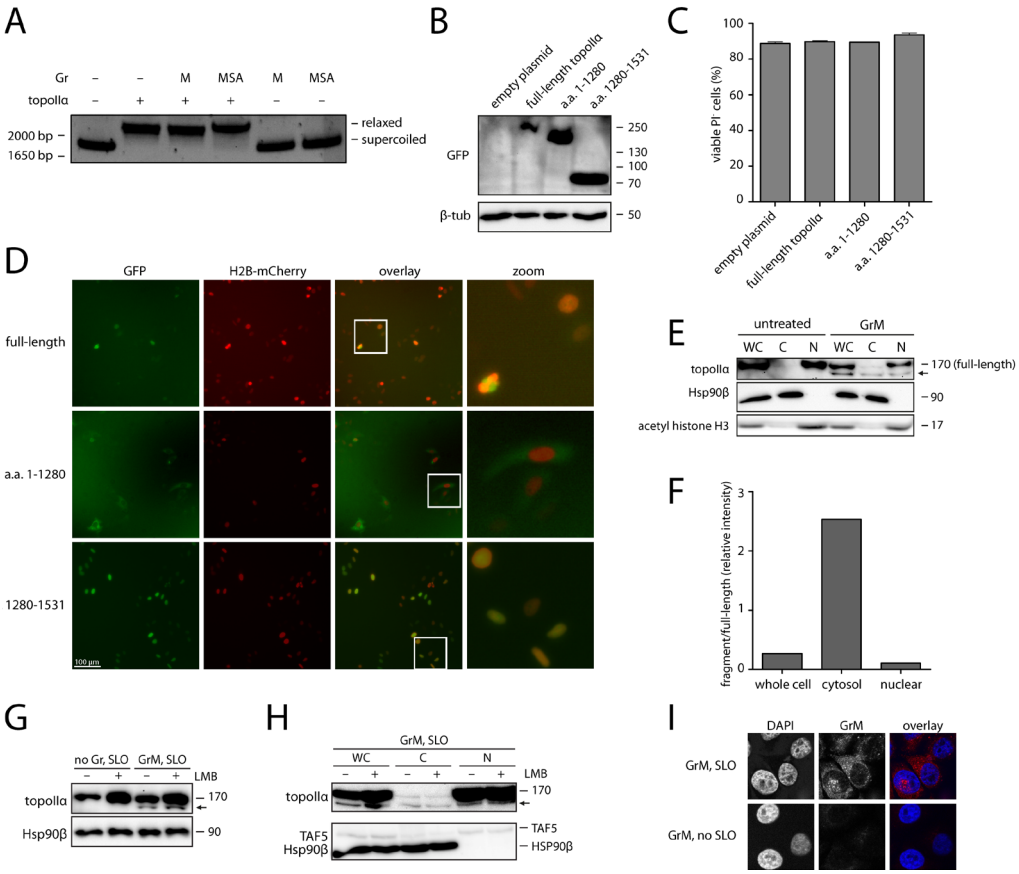

Figure 5. GrM disrupts topoIIα nuclear localization. **(a)** 20 units of recombinant topoIIα were treated with 100 nM GrM or GrM-SA for 30 min at 37°C (also see Figure 4c.) These samples were incubated with 500 ng of supercoiled pUC18 plasmid for 30 min at 37°C. pUC18 DNA relaxation was assessed on a 0.7% agarose gel. Supercoiled and relaxed pUC18 are indicated. **(b)** HeLa cells were transfected with full-length eGFP-topoIIα or topoIIα fragments that mimic GrM cleavage: *i.e.* the N-terminal eGFP-topoIIα 1-1280 and C-terminal eGFP-topoIIα 1280-1531 fragments. Expression of the fragments was verified by immunoblotting for GFP. β-tubulin was used as a loading control. **(c)** Cells were transfected as in (b), and cell viability was determined using PI staining. **(d)** Cells were transfected as in (b), and H2B-mCherry was co-transfected to stain nuclei. Localization was determined by fluorescent microscopy. **(e)** HeLa cells were incubated with 1 μM GrM and 0.5 μg/ml SLO for 30 min or mock treated, after which they were fractionated. Whole cell (WC) lysate, cytosolic (C) and nuclear (N) fractions were immunoblotted for topoIIα. An arrow is used to indicate the topoIIα cleavage fragment. **(f)** Semi-quantitative analysis was performed on the immunoblot of (e), and ratios of fragment/full-length topoIIα are plotted for WC, C, and N fractions. (**g-h**) HeLa cells were pre-treated with 12 nM LMB for 2 hours, after which they were treated with 0.5 μg/ml SLO in the absence or presence of 1 μM GrM. After a 30-minute incubation, samples were immunoblotted for topoIIα (g). In addition, GrM-treated samples were fractionated and immunoblotted for topoIIα, and for TAF5 and Hsp90β (as controls for the nuclear and cytosolic fractions, respectively) (h). (**i**) HeLa cells were treated with 1 μM GrM in the presence or absence of 0.5 μg/ml SLO, followed by a 30-minute incubation. Cells were then washed, fixed, stained, and GrM localization was visualized using confocal microscopy. DAPI was used to stain the nuclei.

degradation of cleaved topoIIα during NK-cell mediated cytotoxicity.

GrM disrupts topoIIα nuclear localization.

GrM cleaved topoIIα at Leu^{1280}, which is located in its C-terminal regulatory domain

within the first nuclear localization signal (NLS) (Figure 3d). Previous studies have shown that the N-terminal domain of topoIIα can function *in vitro* without its C-terminal regulatory domain, [208, 209] suggesting that topoIIα functionality should not necessarily be affected by GrM cleavage. Human DNA topoIIα regulates DNA topology and can relax supercoiled DNA. An *in vitro* DNA relaxation assay was performed to study the effect of GrM cleavage on topoIIα functioning. Recombinant topoIIα was first cleaved by GrM (Figure 4c), after which supercoiled pUC18 DNA was added. As expected, topoIIα fragments rendered by GrM cleavage were still capable of relaxing supercoiled DNA (Figure 5a), suggesting that the catalytic topoIIα domains remain active following GrM cleavage.

Although GrM cleavage did not affect topoIIα functionality *in vitro*, the generated fragments could be proapoptotic in living cells. Full-length eGFP-linked topoIIα was expressed in HeLa cells, as well as the N- and C-terminal topoIIα fragments that mimic GrM cleavage (eGFP-topoIIα 1-1280 and eGFP-topoIIα 1280-1531, respectively). Expression of the fragments (Figure 5b) did not affect cell viability (Figure 5c). However, whereas full-length topoIIα and the C-terminal fragment containing the NLS clearly localized to the nuclei of transfected cells, the N-terminal fragment bearing the topoIIα catalytic domains and nuclear export signals [210] localized to the cytoplasm (Figure 5d). Expression of protein lacking a nuclear localization signal is not identical to the removal of a localization signal of a nuclear protein. Therefore, the effects of GrM-mediated cleavage of endogenous nuclear topoIIα were investigated. HeLa cells were treated with GrM, fractionated, and topoIIα localization was monitored (Figures 5e and f). As expected, full-length topoIIα in untreated control cells was only present in the nuclear fraction. In GrM-treated cells, however, the N-terminal topoIIα fragment relocalized to the cytoplasmic fraction, indicative of a cleavage-induced nuclear exit of this fragment. Pre-treatment of cells with the nuclear export inhibitor leptomycin B (LMB) (Suppl. Figure 2e) which prevents topoIIα nuclear/cytoplasmic shuttling, [210] did not prevent GrM-mediated cleavage of topoIIα, nor did it prevent the nuclear exit of the cleavage fragment (Figures 5g and 5h). This suggests that the cleavage fragment may exit the nucleus via alternative mechanisms, *e.g.* as the result of nuclear disintegration. For GrA and GrB, nuclear localization has been described previously. [211-215] For GrM, however, nuclear localization remains unknown. To test this, GrM localization was determined after intracellular delivery using immunofluorescence and confocal microscopy (Figure 5i). GrM entered the nucleus, already within 30 minutes after GrM delivery. Combined, these data indicate that GrM enters the nucleus where it cleaves topoIIα, resulting in nuclear exit of the N-terminal fragment, impairing topoIIα function.

TopoIIα depletion phenotypically resembles GrM-induced apoptosis.
Since GrM abolishes nuclear topoIIα function, the effects of genetic topoIIα depletion were compared with GrM-mediated cell death. TopoIIα was conditionally

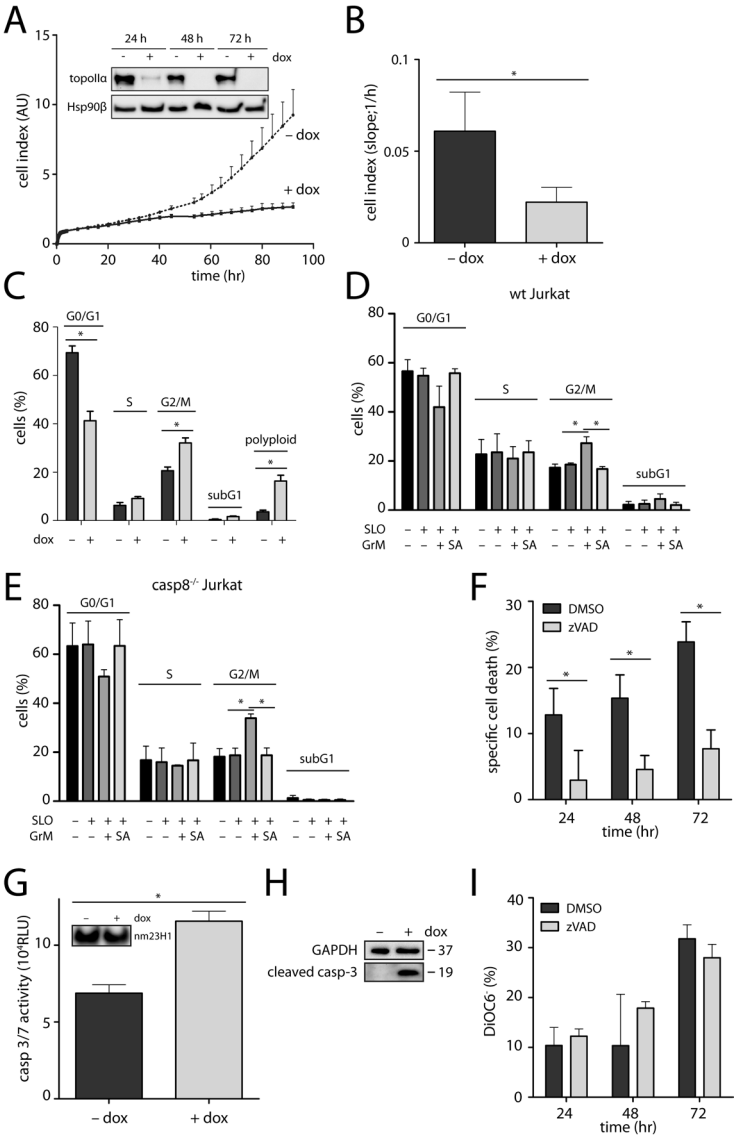

Figure 6. TopoIIα depletion phenotypically resembles GrM-induced apoptosis. **(a)** Treatment with 1 µg/ml doxycycline (dox) for 48 h depleted topoIIα in HTETOP cells as determined using immunoblot (*inset*). Hsp90β was used as loading control. HTETOP cells depleted of topoIIα for 48 h were seeded in the xCELLigence system, and cell index (CI) was monitored in time (every 30 min for 96 h). Medium was refreshed after 48 h. Graph depicts *n*=4 with mean +/- SD of a single experiment that is representative of 3 independent experiments. **(b)** The increase in CI (slope) between 12 and 96 h after seeding was determined for 3 independent xCELLigence experiments. **(c)** The cell cycle profile of HTETOP cells that had been depleted of topoIIα was determined 5 days after the seeding of the cells using PI-cell cycle flow cytometry. **(d-e)** Both wt and casp8$^{-/-}$ Jurkat cells were treated in the presence of z-VAD-fmk with 1 µM GrM or GrM-SA and 0.1 µg/ml SLO for 24 h, after which cell cycle distributions were determined using PI-cell cycle flow cytometry. **(f)** Cell death of topoIIα-depleted HTETOPs grown in the absence (DMSO) or presence of 100 µM z-VAD-fmk was determined at different time points after seeding using AnnV/PI flow cytometry. **(g)** Caspase-3/-7 activity was assessed in topoIIα-depleted HTETOPs at 48 h after seeding using the CaspaseGlo assay. Nm23H1 served as a loading control. **(h)** Cells were seeded as in (g), and caspase-3 activation was detected using immunoblot. GAPDH was used as a loading control. In all experiments, medium (supplemented with dox) was refreshed every 48 h. **(i)** Loss of mitochondrial membrane potential was measured at different time-points after seeding of topoIIα-depleted HTETOPs grown in the absence (DMSO) or presence of 100 µM z-VAD-fmk.

depleted from HTETOP cells by adding doxycycline (dox). [216] At 48 h after administration of dox, topoIIα levels were reduced to undetectable levels (Figure 6a, *inset*; Supplemental Figure 2g). To examine general cell behavior, topoIIα-depleted cells were monitored real-time by xCELLigence over a period of 96 h (Figures 6a and b). Whereas the cell index (CI) in control (–dox) cells increased over time due to cell proliferation, topoIIα-depleted cells (+dox) were markedly impaired. Decreased CI values correlated with lower numbers of adherent topoIIα-depleted HTETOP cells as visualized by light microscopy (Supplemental Figure 2h). This decrease in adherent cells could be due to decreased proliferation, increased apoptosis, or a combination. TopoIIα-depletion is known to result in G2/M arrest and increased polyploidy, [216] which was confirmed using cell cycle analysis (Figure 6c). G2/M arrest was also observed within 3 days after topoIIα depletion (data not shown). If topoIIα function is impaired by GrM, one would expect that GrM also triggers a G2/M arrest in tumor cells. Indeed, the topoIIα-depleted cell cycle profile was remarkably similar to that of GrM-treated Jurkat cells, which also arrested in G2/M (Figure 6d). Likewise, G2/M arrest was also seen in GrM-treated casp8$^{-/-}$ Jurkat cells, indicating that this arrest is independent of caspase-8 activation upon FADD cleavage (Figure 6e). In addition, topoIIα-depleted cells also displayed increased rates of caspase-dependent apoptosis (Figure 6f). Caspase-3/-7 was activated in topoIIα-depleted cells (Figure 6g), and activation of caspase-3 was further confirmed by immunoblotting (Figure 6h). Finally, caspase-independent perturbation of the mitochondrial membrane potential was observed in topoIIα-depleted cells (Figure 6i), suggesting that this contributes to the induction of apoptosis. Thus, topoIIα depletion in tumor cells phenotypically resembles GrM-induced apoptosis, including G2/M cell cycle arrest, mitochondrial perturbations, and caspase activation.

Discussion

Granzymes are important effector molecules in the cellular immune response against tumor and virus-infected cells. While the literature clearly describes GrM as a significant inducer of cell death, the general characteristics of cell death induction remain controversial and unclear. We have therefore comprehensively characterized the GrM-mediated apoptotic phenotype (Figures 1-2). GrM triggered classical hallmarks of apoptosis, including the initial appearance of AnnV-single positive (early apoptotic) cells, followed by the appearance of AnnV/PI double positive (late apoptotic/necrotic) cells. This is in agreement with some studies, [42, 44] but in contradiction with other studies that describe only the formation of AnnV and PI double positive cells. [31, 41] Kelly *et al*. find no evidence of DNA fragmentation after GrM treatment, [41] whereas Lu *et al*. do. [44] In our study, GrM also induced DNA fragmentation. Similarly, Kelly *et al.* do not detect any changes in mitochondrial membrane potential or release of cytochrome c, [41] whilst GrM is found to disturb the mitochondria in studies by Hua *et al.*, Wang *et al*., and in the present study. [32, 43] Furthermore, we confirmed that

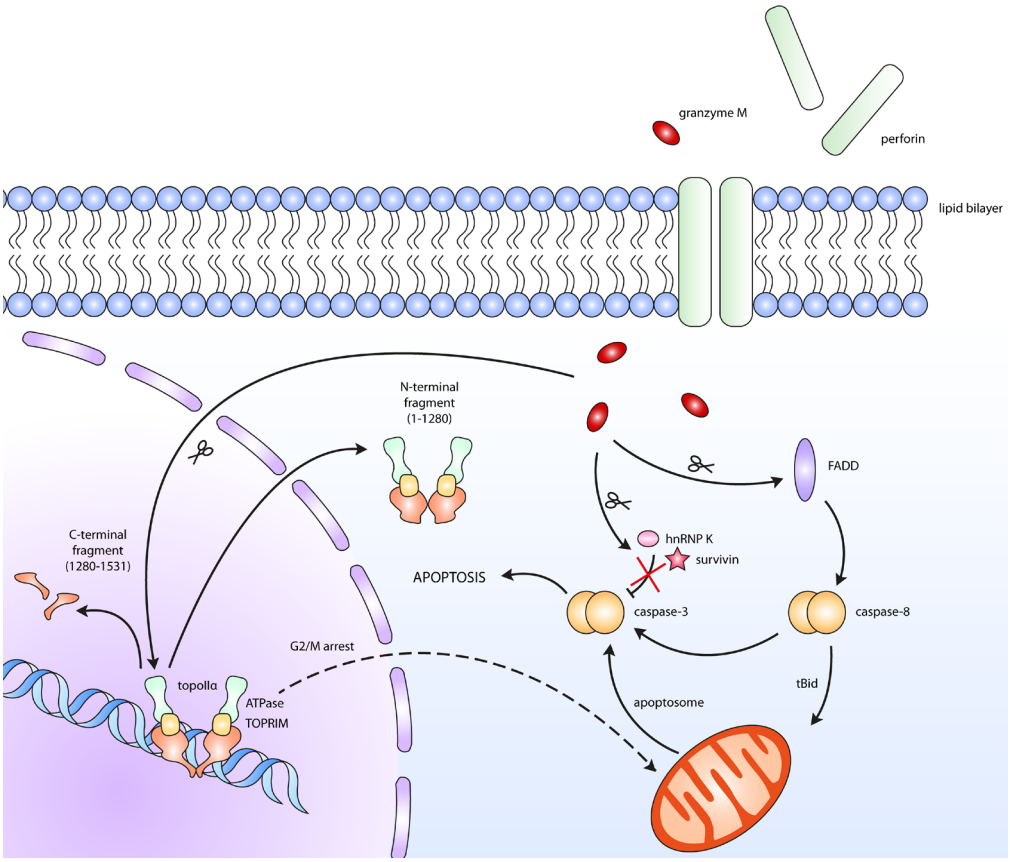

Figure 7. Schematic model of GrM-induced cell death. Perforin facilitates entry of GrM into the target cell via pore formation. Upon entry, GrM can cleave FADD,[32] resulting in the recruitment and auto-processing of caspase-8, and subsequently activation of caspase-3 – either directly, or via Bid-mediated targeting of the mitochondria and apoptosome formation. In addition, GrM can cleave nuclear topoIIα, resulting in the formation of a C-terminal fragment that bears the NLS and remains in the nucleus, and an N-terminal fragment, which bears the catalytic domains, and translocates to the cytosol. The depletion of functional topoIIα in the nucleus results in G2/M cell cycle arrest, which also leads to mitochondrial perturbations and caspase-dependent cell death, via a yet to be identified mechanism. Furthermore, GrM can also cleave and inactivate survivin[42] and hnRNP K,[47] resulting in a decrease in the levels of caspase inhibitors, thereby facilitating caspase-induced apoptosis.

GrM treatment results in ROS generation, as first described by Hua *et al*. [43] Discrepancies have also been found concerning the activation of caspases upon GrM treatment. Lu *et al*. describe that GrM can directly cleave pro-caspase-3 in lysates; [44] this has however been refuted by studies done by Kelly *et al*., Cullen *et al*., Bovenschen *et al*., and the present study. [31, 41, 45] Whilst we did not find caspase activation by GrM in lysates, we did find caspase activation in living cells. This observation is in agreement with studies by Hu *et al*. and Wang *et al*., [32, 42] but in disagreement with studies by Kelly *et al*. and Cullen *et al*. [31, 41] However, in the latter study, caspase activation has been monitored in the presence of zVAD-fmk, which means that indirect activation of the caspases by GrM would not have been detected, as shown here to be the case in zVAD-fmk pretreated cells (Figure 2b). [31] The presence or absence of (indirect) caspase activation is likely

an important determinant of the GrM cell death phenotype: caspases are known to activate DNases, which leads to positive TUNEL-staining, and are also known to lead to cytochrome c release and AnnV-positivity. Therefore, the inconsistency in caspase activation between studies may lie at the base of all other discrepancies. Participation of caspases in GrM-mediated tumor cell death is further supported by the findings that GrM targets hnRNP K [47] and survivin [42] which stabilize the caspase-inhibitor XIAP. [42, 217] This suggests that GrM coordinates induction of the caspase cascade by both inducing caspase activation and reducing caspase inhibition. Next to the general apoptotic hallmarks described above, we showed for the first time that GrM rapidly triggered G2/M cell cycle arrest in tumor cells (Figure 6). Thus, we propose that GrM triggers classical hallmarks of apoptosis with mitochondrial damage, caspase activation, and cell cycle arrest.

To date, FADD is the only univocally proven GrM substrate that plays a direct role in GrM-mediated cell death. [32] Cleavage of human FADD by GrM promotes procaspase-8 recruitment and activation, and subsequent initiation of the caspase cascade. [32] FADD-deficient tumor cells, however, are still partially sensitive to GrM. [32] Consistently, we showed that GrM still induced caspase-dependent apoptosis in casp8$^{-/-}$ cells (Figure 2h). Interestingly, neither caspase-8-deficiency, nor chemical caspase-inhibition blocked GrM-induced G2/M cell cycle arrest, which may precede apoptosis. [218] Thus, these data indicate that GrM triggers caspase-dependent cell death via at least one other mechanism that is independent of FADD/caspase-8, likely involving G2/M cell cycle arrest. To elucidate this pathway, we employed positional proteomics in HeLa cells and identified DNA topoIIα as a novel GrM substrate, a nuclear enzyme essential in proliferating cells where it assists in chromosome condensation, segregation, and replication. [219] Overexpression of topoIIα correlates with poor prognosis in breast, ovarian and peritoneum cancer, and oligodendrogliomas. [220-222] TopoIIα is a current anti-cancer target for chemotherapeutics such as etoposide and doxorubicin [223] and depletion of topoIIα leads to G2/M cell cycle arrest and apoptosis [216] (Figure 6). GrM cleaved topoIIα after Leu^{1280} (Supplemental Table 1), thereby separating the topoIIα functional domains from its nuclear localization signals. Indeed, GrM cleavage led to nuclear exit of the N-terminal fragment of topoIIα that harbors the catalytic domains (Figure 5), thereby rendering the protein nonfunctional. Interestingly, the GrM apoptotic phenotype, including G2/M arrest, mitochondrial perturbation, and caspase activation (Figures 1 and 2), resembled the phenotype of topoIIα depletion (Figure 6). Although the relative importance of this pathway remains to be investigated, these data suggest that inactivation of topoIIα by GrM contributes to G2/M arrest and caspase-dependent apoptosis (Figure 7).

Although previous work has hinted towards a role of GrB in targeting mitosis-regulating kinases, [224, 225] we present -to our knowledge- the first evidence of cell cycle arrest induction by a granzyme. GrM-induced cell cycle arrest occurred independently of caspases (Figure 6). This raises the interesting possibility that if the immune system cannot kill a tumor cell –*e.g.* because it expresses certain

inhibitors of apoptosis [226], such as Bcl2, XIAP [227], or the GrB inhibitor SERPINB9 [50-53]– GrM can still trigger apoptosis or cell cycle arrest to reduce tumor growth. Alternatively, GrM-induced effects on DNA topology may also contribute to help dispose of the cell corpse and facilitate DNA degradation post-mortem.

TopoIIα belongs to a general family of isomerases that act on the topology of DNA, *e.g.* during DNA replication and cell division. [219] This family also includes topoisomerases I and IIβ. Interestingly, proteolytic targeting of topoisomerases during apoptosis has been observed previously. GrB cleaves topoisomerase I, which is involved in breaking and rejoining of DNA single strands [228], and caspases can cleave topoisomerases I, IIα and IIβ [229-231] at multiple sites. [229] Finally, we have preliminary data showing that, in tumor cell lysate, GrA and GrB can also cleave topoIIα in close proximity to the GrM cleavage site (data not shown). These findings suggest that targeting of topoisomerases is a common phenomenon during apoptosis, although the effects of these cleavage events on cell cycle progression remain unknown. In this context, we and others have previously established that GrM and GrB can cleave α-tubulin, resulting in the stabilization of microtubule polymers [45, 232, 233] in a manner that resembles the effects of the anti-cancer drug paclitaxel (Taxol). Paclitaxel is known to induce G2/M arrest, and granzyme-mediated cleavage of α-tubulin may therefore also contribute to the induction of a G2/M arrest in GrM-treated cells. The relative contribution of these substrates and potentially other pathways to the induction of granzyme-induced cell cycle arrest and cytotoxicity remains to be elucidated. Whether granzymes other than GrM also induce cell cycle arrest remains an interesting question that deserves further study.

Materials and methods

Cells. HeLa and Cos7 cells were grown in DMEM supplemented with 10% fetal calf serum (FCS), 100 units/ml penicillin and 100 µg/ml streptomycin (pen/strep; Invitrogen). HTETOP cells [216] were grown in the same medium, with L-glutamine (2 mM) and non-essential amino acids (20 ml/500 ml; Gibco). To deplete topoIIα in HTETOP cells, medium was supplemented with 1 µg/ml doxycycline (dox) and refreshed every 2-3 days. Jurkat and caspase-8-deficient Jurkat cells (clone I 9.2, ATCC) were maintained in RPMI-1640 medium with 10% FCS, pen/strep, and 2 g/L sodium bicarbonate. The natural killer cell line KHYG1 (Japan Health Sciences Foundation, JCRB0156) was maintained in the same medium with 50 ng/ml recombinant human interleukin-2 (Tebu-Bio). Cells were transfected using polyethylenimine (Polysciences). For COFRADIC, HeLa cells were grown in Glutamax-containing SILAC DMEM (Invitrogen) with 10% dialyzed FCS (Invitrogen) and pen/strep, containing natural, $^{13}C_6$- or $^{13}C_6{}^{15}N_4$-labeled L-arginine (Cambridge Isotope Laboratories) (80 µM). Cells were cultured for 6 population doublings (8 days) for complete incorporation of labeled arginine. For leptomycin B (LMB) pretreatment, cells were incubated with 12 nM LMB (Sigma-Aldrich) for 2 h. For caspase inhibition,

100 µM zVAD-fmk (Bio-Connect) was used. Cells were fractionated as described. [234]

Proteins. Granzyme production and granzyme treatment with streptolysin O (SLO; Aalto) and human perforin (Enzo Life Sciences) were performed as described previously. [30, 45] Briefly, human GrB, GrM, and its catalytically inactive mutant GrM-SA, in which the Ser^{195} residue has been replaced with Ala, were produced in *Pichia pastoris* and purified using cation-exchange chromatography. Catalytic activity was verified using synthetic chromogenic substrates.

Antibodies and cloning. Antibodies were anti-acetyl-histone-H3 (06-599; Upstate), anti-α-tubulin (B-5-1-2; Sigma), anti-β-tubulin (Tub2.1; Sigma), anti-caspase 3 (H-277, Santa-Cruz), anti-Asp175 cleaved caspase 3 (Cell Signaling Technologies), anti-caspase 6 (3E8; MBL International Corporation), anti-caspase 8 (5F7; MBL International Corporation), anti-Asp315 cleaved caspase 9 (Cell Signaling Technologies), anti-CHOP (L63F7; Cell Signaling Technologies), anti-Erk-2 (C14, Santa-Cruz), anti-GAPDH (6C5, Abcam), anti-GFP (clones 7.1 and 13.1, Roche), anti-GrM (4B2G4) [38], anti-Hsp90β (K3701; Enzo Life Sciences), anti-nm23H1 (C-20; Santa Cruz), anti-nucleophosmin (FC-61991; Invitrogen), anti-topoIIα (Ki-S1, DAKO), anti-TRAP (TR-1A, Abcam), and HRP-conjugated anti-ubiquitin (Enzo Life Sciences, PA, USA). Fragments of topoIIα cDNA were cloned in pCDNA3.1+ (Invitrogen) using pBL-eGFP-topoIIα [216] as a template.

Viability assays and flow cytometry. WST-1 assays were performed as described by the manufacturer (Roche). For AnnexinV-fluos (AnnV; Invitrogen) and propidium iodide (PI; Sigma) analysis, cells were stained for 15 min in 140 mM NaCl, 4 mM KCl, 0.75 mM $MgCl_2$, 1.5 mM $CaCl_2$, and 10 mM HEPES pH 7.4. Flow cytometry was performed on a FACSCalibur with CellQuest Pro software (BD Biosciences). AnnV- and PI-negative cells were considered viable. Cells were stained with 20 nM DiOC6 (Tebu-Bio) for 15 min at 37°C. TUNEL (Merck Millipore), CM-H_2DCFDA (Life Technologies), and cytochrome c (VWR Omnilabo) staining was performed according to manufacturers' protocols. For cell cycle analysis, cells were washed in PBS and fixed in 70% ice-cold ethanol for >15 min at 4°C. Cells were washed with 0.1% Triton-X100 in PBS, and stained in 0.1% Triton-X100, 15 µg/ml RNase A, and 100 µg/ml PI in PBS for 2 h. Cells were plotted on FL2-A and FL2-W to discriminate between individual cells and aggregates.

Fluorescence microscopy. Untransfected cells (living, or stained with Giemsa) and cells transfected with fluorescently-tagged constructs (H2B-mCherry and eGFP-topoIIα variants) were directly imaged by inverted fluorescence microscopy (Leica DMI4000b, Leica DFC300 FX camera). Confocal microscopy was performed on a Leica LSM700.

xCELLigence. The xCELLigence system (Roche) measures electrical impedance (represented in the cell index [CI]) across micro-electrodes integrated on the bottom of 16-well plates, which provides quantitative information about the overall status of cells (cell number, viability, adherence, morphology). Untreated or topoIIα-depleted HTETOP cells were seeded at 1,250 cells/well. Doxycycline was refreshed after 48 h. CI values were measured every 30 min for 96 h.

***In vitro* topoIIα activity assay.** Recombinant topoIIα (Affymetrix/USB) (20 units) was incubated with 100 nM GrM or GrM-SA for 30 min at 37°C. Subsequently, 500 ng of supercoiled plasmid pUC18 was added for 30 min at 37°C, electrophorized using a 0.7% agarose gel, and stained with Midori Green Advance DNA stain (Biolegio).

N-terminal COFRADIC analysis. L-arginine labeled HeLa cells were treated with SLO for 60 min (control setup; $^{13}C_6{}^{15}N_4$-Arg), or with SLO and 1 µM GrM for 15 min ($^{12}C_6$-Arg) or 60 min ($^{13}C_6$-Arg) (Figure 3A). Cells were lysed on ice for 5 min in lysis buffer containing 100 mM NaCl, 1% CHAPS, 0.5 mM EDTA and 50 mM sodium phosphate buffer (pH 7.5) and freshly added protease inhibitor cocktail, EDTA-free. Cellular debris was spun down for 1 min at 18,000 *g*. Protein concentration in the supernatant was determined by Bradford assay. Guanidinium hydrochloride was added to a final concentration of 4 M to inactivate GrM and denature all proteins. Before mixing equal amounts of samples proteins were reduced and alkylated using TCEP.HCl (1 mM) and iodoacetamide (2 mM) respectively, for 1 h at 30°C. N-terminal COFRADIC was performed as described previously. [235] The protein mixture was digested overnight at 37°C with sequencing-grade, modified trypsin (Promega) (enzyme/substrate of 1/100, w/w). LC-MS/MS analysis and data processing was performed as described previously[236] (Supplemental Materials and Methods).

Statistical analysis. Unless otherwise indicated, data are depicted as mean ± SD of at least three independent experiments. Statistical analyses were performed using independent samples t-test. $P<0.05$ was considered statistically significant (*).

Acknowledgements
Authors are supported by the Dutch Cancer Society (UU-2009-4302 to NB), the Dutch Organization for Scientific Research (NWO) [grant number 916.66.044 (to NB)], PRIME-XS (grant agreement number 262067, funded by the European Union 7th Framework Program). KP is supported by a PhD grant from the Institute for the Promotion of Innovation through Science and Technology in Flanders (IWT-Vlaanderen). PVD is a Postdoctoral Fellow of the Research Foundation-Flanders (FWO-Vlaanderen). The MS proteomics data have been deposited to the ProteomeXchange Consortium (http://proteomecentral.proteomexchange.org) via the PRIDE partner repository [237] with the dataset identifier PXD000252 and DOI

10.6019/PXD000252. Confocal microscopy was performed at the Cell Microscopy Center at the University Medical Center Utrecht.

Authorship contributions
SdP participated in the design of the study, performed experiments, analyzed and interpreted the data, and wrote the paper. KWL and LvdW performed experiments. KP and PVD participated in the design of the study, performed experiments, analyzed and interpreted the data. KG participated in the design of the study, and analyzed and interpreted the data. AP analyzed and interpreted the data, and provided vital unique reagents. NB participated in the design of the study, analyzed and interpreted the data, and wrote the paper.

Disclosure of conflicts of interest
None of the authors declare any competing financial interests.

Supplemental material and methods

Immunofluorescence microscopy. Cells were washed three times with PBS, and then fixed in 4% PFA at room temperature for 10 minutes. Cells were permeabilized with 0.25% TritonX100 in PBS for 10 minutes at room temperature, washed once with PBS, and blocked for 1 hour with 5% BSA in PBS-Tween (0.1%). Cells were then incubated for 1 hour with primary mouse anti-topoIIα, anti-GrM, or anti-Erk-2 antibody, after which they were washed three times with PBS-Tween. Cells were incubated in the dark for 1 hour with the secondary antibody in 5%BSA/PBS-Tween (goat anti-mouse-Alexa Fluor 488 or 595; 1:500), after which they were washed twice with PBS-Tween and once with PBS. Nuclear staining was done with 200 ng/ml DAPI (#10236276001, Roche) for 5 minutes in PBS, after which the cells were washed three times with PBS before microscopic visualization. Confocal microscopy was performed with a Leica LSM700 confocal microscope and Zen software. Time-lapse imaging was performed in a 37°C chamber with 5% CO_2 using an identical camera, a Leica DM-IL microscope and Leica Application Suite software V.3.5.0. Images were taken every 30 min for 8 h.

Lentiviral transductions. A pLV-Bcl2 construct was made by subcloning Bcl2 from pSG5-Bcl2 (a kind gift from Prof. P.J. Coffer, UMC Utrecht) into the pLV plasmid using SalI and XbaI restriction sites. Casp8-/- Jurkats were lentivirally transduced as described previously. [238] Briefly, COS7 cells were transfected with third-generation lentivirus packaging plasmids and the pLV-Bcl2 or empty pLV constructs to produce lentiviral particles. On 48 hours post transfection, supernatant was harvested and filtered (0.45 µm). Casp8-/- Jurkat cells were spinoculated in the presence of 8 µg/ml polybrene at 1300 rpm for 1.5 hours, followed by overnight incubation with the virus.

LC-MS/MS analysis and data processing. The obtained peptide fractions were introduced into an LC-MS/MS system, the Ultimate 3000 nano (Dionex, Amsterdam, The Netherlands) in-line connected to an LTQ Orbitrap XL (Thermo Fisher Scientific, Bremen, Germany). The sample mixture was loaded on a trapping column (made in-house, 100 µm I.D. x 20 mm, 5 µm beads C18 Reprosil-HD, Dr. Maisch). After back-flushing from the trapping column, the sample was loaded on a reverse-phase column (made in-house, 75 µm I.D. x 150 mm, 5 µm beads C18 Reprosil-HD, Dr. Maisch). Peptides were loaded in 0.1% trifluoroacetic acid and 2% acetonitrile, and were separated with a linear gradient from 2% solvent A (0.05% formic acid) to 50% solvent B (0.05% formic acid and 80% acetonitrile) at a flow rate of 300 nl/min followed by a wash reaching 100% solvent B. The mass spectrometer was operated in data dependent mode, automatically switching between MS and MS/MS acquisition for the five most abundant peaks in a given MS spectrum. Full scan MS spectra were acquired in the Orbitrap at a target value of 1E6 with a resolution of 60,000. The five most intense ions were then isolated for fragmentation in the linear ion trap, with a dynamic exclusion of 60 seconds. Peptides were fragmented after filling the ion trap at a target value of 1E4 ion counts. From the MS/MS data in each LC run, Mascot Generic Files were created using Distiller software (version 2.3.2.0, Matrix Science, www.matrixscience.com/Distiller). While generating these peak lists, grouping of spectra was allowed in distiller with a maximum intermediate retention time of 30 seconds and a maximum intermediate scan count of 5 was used where possible. Grouping was done with 0.005 Da precursor tolerance. A peak list was only generated when the MS/MS spectrum contained more than 10 peaks. There was no de-isotoping and the relative signal to noise limit was set at 2. These peak lists were then searched with Mascot search engine (MatrixScience, www.matrixscience.com) [239] using the Mascot Daemon interface (version 2.3, Matrix Science). Spectra were searched against the human SwissProt database (version 2011_11 of UniProtKB/Swiss-Prot protein database containing 20,251 sequence entries). Variable modifications were set to pyro-glutamate formation of N-terminal glutamine and acetylation or trideutero-acetylation of the N-terminus. Fixed modifications were set as trideutero-acetylation of lysine, carbamidomethylation of cysteine and methionine oxidation. Mass tolerance on precursor ions was set to 10 ppm (with Mascot's C13 option set to 1) and on fragment ions to 0.5 Da. The peptide charge was set to 1+,2+,3+ and instrument setting was put on ESI-TRAP. Enzyme was set to semi Arg-C/P, allowing for 1 missed cleavage, also cleavage was allowed when arginine was followed by proline. Only peptides that were ranked one and scored above the threshold score, set at 99% confidence, were withheld. The estimated false discovery rate by searching decoy databases was typically found to lie between 2 and 4% on the spectrum level. [153] Identified peptides were quantified using Mascot Distiller Toolbox version 2.3.2.0 (MatrixScience) in the precursor mode. The software tries to fit an ideal isotopic distribution on the experimental data based on the peptide average amino acid composition. This is followed by extraction of the XIC signal of both peptide components (light and heavy) from the

raw data. Ratios are calculated from the area below the light and heavy isotopic envelope of the corresponding peptide (integration method 'trapezium', integration source 'survey'). To calculate this ratio value, a least squares fit to the component intensities from the different scans in the XIC peak was created. MS scans used for this ratio calculation are situated in the elution peak of the precursor determined by the Distiller software (XIC threshold 0.3, XIC smooth 1, Max XIC width 250). To validate the calculated ratio, the standard error on the least square fit has to be below 0.16 and correlation coefficient of the isotopic envelope should be above 0.97. All data management was done by ms_lims. [240] Of note, cleavage events solely identified in one of both GrM incubated proteomes were only considered to be genuine GrM-generated neo-N-termini if the corresponding protein N-termini were identified in all 3 proteomes analyzed.

Q-PCR analysis. RNA was extracted from 300,000 treated Jurkat cells using the Arcturus PicoPure RNA isolation Kit (Applied Biosystems). The SuperScript III First-Strand Synthesis System for RT-PCR (Life Technologies) was used to synthesize the cDNA. Subsequently, amplification of the cDNA was performed using Taqman gene expression assays for GAPDH (hs99999905_m1, Life Technologies) and topoIIα (Hs01032137_m1, Life Technologies) on the LightCycler 480 II (Roche). Expression levels of the household gene GAPDH did not change upon GrM treatment. Relative expression levels were determined as the ratios of topoIIα/GAPDH Cq-values.

Supplemental table and figure legends

Supplemental Table 1. List of trideutero-acetylated, internal peptides generated upon *in vivo* delivery of GrM to human tumor cells. All unique neo N-termini (#38) exclusively present in the proteome(s) of SLO and GrM treated HeLa cells, their corresponding protein accession (SwissProt and Uniprot), protein description, preceding P4 to P1 sequence, the observed P1 protein position and corresponding P1 amino acid, peptide sequence (i.e. sequence of the identified neo-N-terminus as well as P10-P10' sequence), matching SwissProt protein isoforms (if any), maximum Mascot ion score and minimum identity threshold (and their calculated difference), spectral count number as well as their identification after 15 min and/or 60 min GrM incubation together with the observed ratio (if any)(i.e. 15 min hGrM/60 min hGrM ratio). Furthermore, additional information whether these neo N-termini were previously identified as *in vitro* human granzyme M specific neo-N or matching neo-C-termini [30]are indicated. N-termini are ranked alphabetically according to their protein description and cleavage site location. Of note, in nascent polypeptide-associated complex subunit alpha and in the 60S ribosomal protein L24, downstream proteolytic activity is evident by the identification of multiple neo-N-termini downstream of the initial GrM cleavages matching the preferred P1 substrate specificity of GrM. Suppl. Table 1 can be viewed at: https://docs.google.com/file/d/0B17lRh8XPFn6VjloUmRLUWRra0k/edit?usp=sharing.

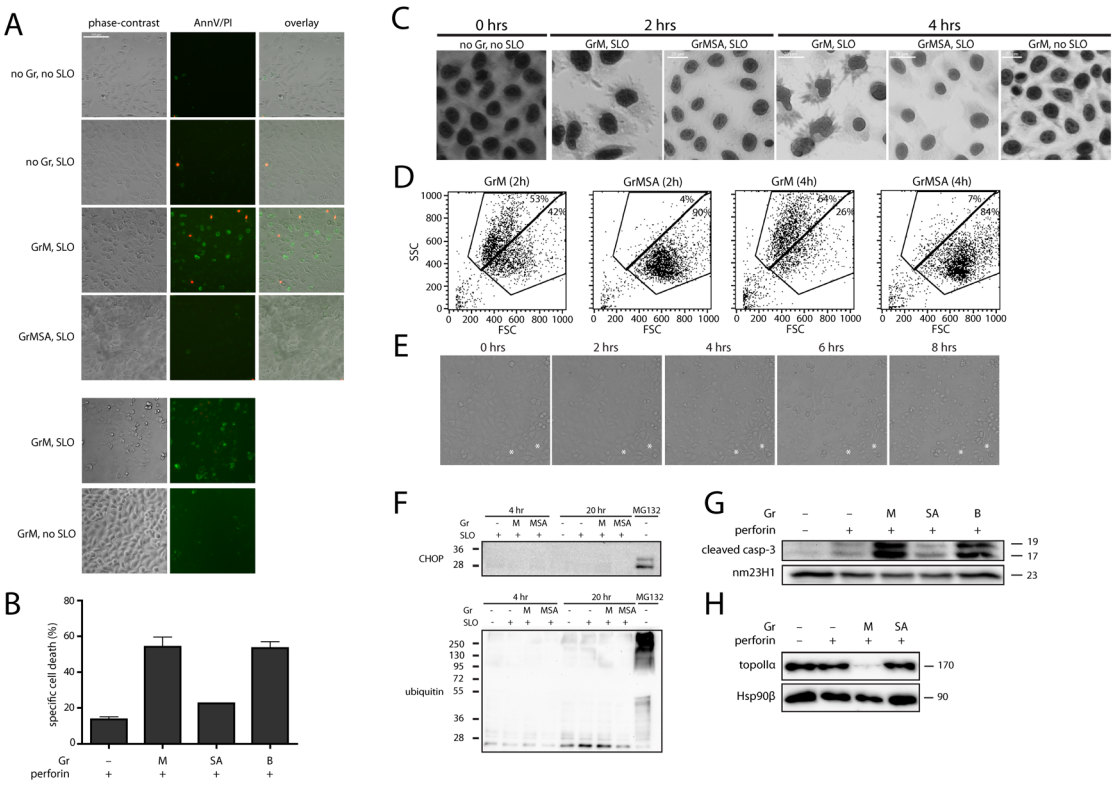

Supplemental Figure 1. GrM delivery in cells results in AnnV-positive cells and gross morphological changes. (a) HeLa cells were treated with 1 µM GrM or GrM-SA and/or 0.5 µg/ml SLO, and were subsequently incubated for 6 hours, after which they were stained with AnnV/PI and visualized using fluorescence microscopy. (b) Jurkat cells were treated with 2 µM GrM or GrM-SA and 0.95 permeabilizing units of perforin for 6 hours, after which viability was assessed using AnnV/PI flow cytometry. (c-e) HeLa cells were treated as in (a), but for indicated lengths of time. Giemsa staining was performed and morphological changes were detected using light microscopy (c), flow cytometry (d) or time-lapse imaging (e). (f) Jurkat cells were treated with 1 µM GrM and/or 100 ng/ml SLO for 2 or 6 hours, after which expression of topoIIα was determined using Q-PCR analysis. Expression of the household gene GAPDH was used as a control. Neither topoIIα, nor GAPDH expression was affected by GrM treatment. Ratios of topoIIα/GAPDH expression are shown. (g) HeLa cells treated with 1 µM GrM or GrM-SA for either 4 or 20 hours were blotted for ER-stress protein CHOP or ubiquitin. MG132-treated cells were used as a positive control. (h-i) Jurkat cells were treated as in (b), and after 6 hours whole cell lysates were prepared for immunoblot for cleaved caspase-3 (g) and topoIIα (h).

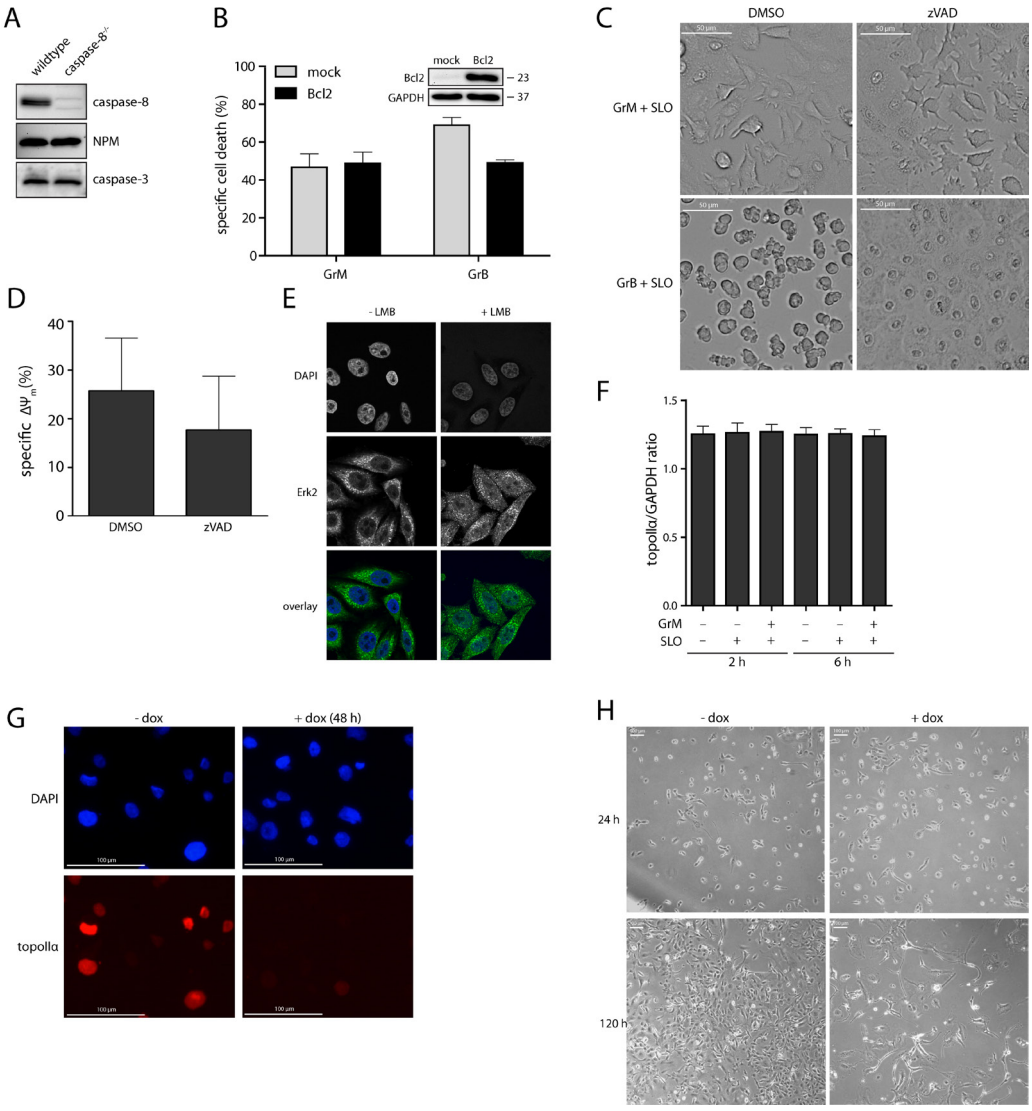

Supplemental Figure 2. (a) 10 µg of wildtype (wt) and caspase-8 deficient (casp8$^{-/-}$) Jurkat cell lysate was probed for the presence of caspase-8, nucleophosmin and caspase-3. (b) Casp8$^{-/-}$ Jurkat cells were lentivirally transduced with a plasmid encoding Bcl-2 or an empty (mock) plasmid. Bcl-2 overexpression was verified by immunoblotting for Bcl-2 (inset). Cells were treated with 1 µM GrM, GrM-SA or 100 nM GrB and 100 ng/ml SLO, after which their viability was assessed using AnnV/PI flow cytometry. (c) The morphological changes observed upon GrM treatment are caspase-independent. HeLa cells treated for 4 hours with 1 µM GrM and 0.5 µg/ml SLO display similar morphological changes in the presence of 100 µM zVAD-fmk. The morphological changes induced by GrB could be (partially) inhibited by zVAD. (d) Loss of mitochondrial membrane potential (corrected for the percentage of DiOC6- cells after 1 µM GrM-SA treatment) is independent of caspase activation in HeLa cells treated for 8 hours with 1 µM GrM in the presence of 100 µM zVAD-fmk. (e) HeLa cells were treated with 12 nM LMB for 2 hours, after which Erk-2 localization was determined using confocal microscopy. DAPI was used to stain the nuclei.(f) HTETOP cells were grown in the absence or presence of 1 µg/ml dox for 48 hours, after which they were stained with anti-topoIIα and DAPI. (g) HTETOP cells that had been cultured either in the presence or absence of 1 µg/ml dox for 48 hours were counted and 30.000 cells were seeded in a 6-well plate. 24 hours and 120 hours later, they were observed using light microscopy.

Chapter 6

Intracellular Serine Protease Inhibitor SERPINB4 Inhibits Granzyme M-Induced Cell Death

Pieter J. A. de Koning*, J. Alain Kummer*, Stefanie A. H. de Poot*, Razi Quadir*, Roel Broekhuizen*, Anne F. McGettrick†, Wayne J. Higgins†, Bart Devreese‡, D. Margaret Worrall†, and Niels Bovenschen*.

*Department of Pathology, University Medical Center Utrecht, Utrecht, The Netherlands
†School of Biomolecular and Biochemical Science, University College Dublin
‡ Laboratory for Protein Biochemistry and Biomolecular Engineering, Department of Biochemistry and Microbiology, Ghent University, Ghent, Belgium

PLoS One. 2011;6(8):e22645.

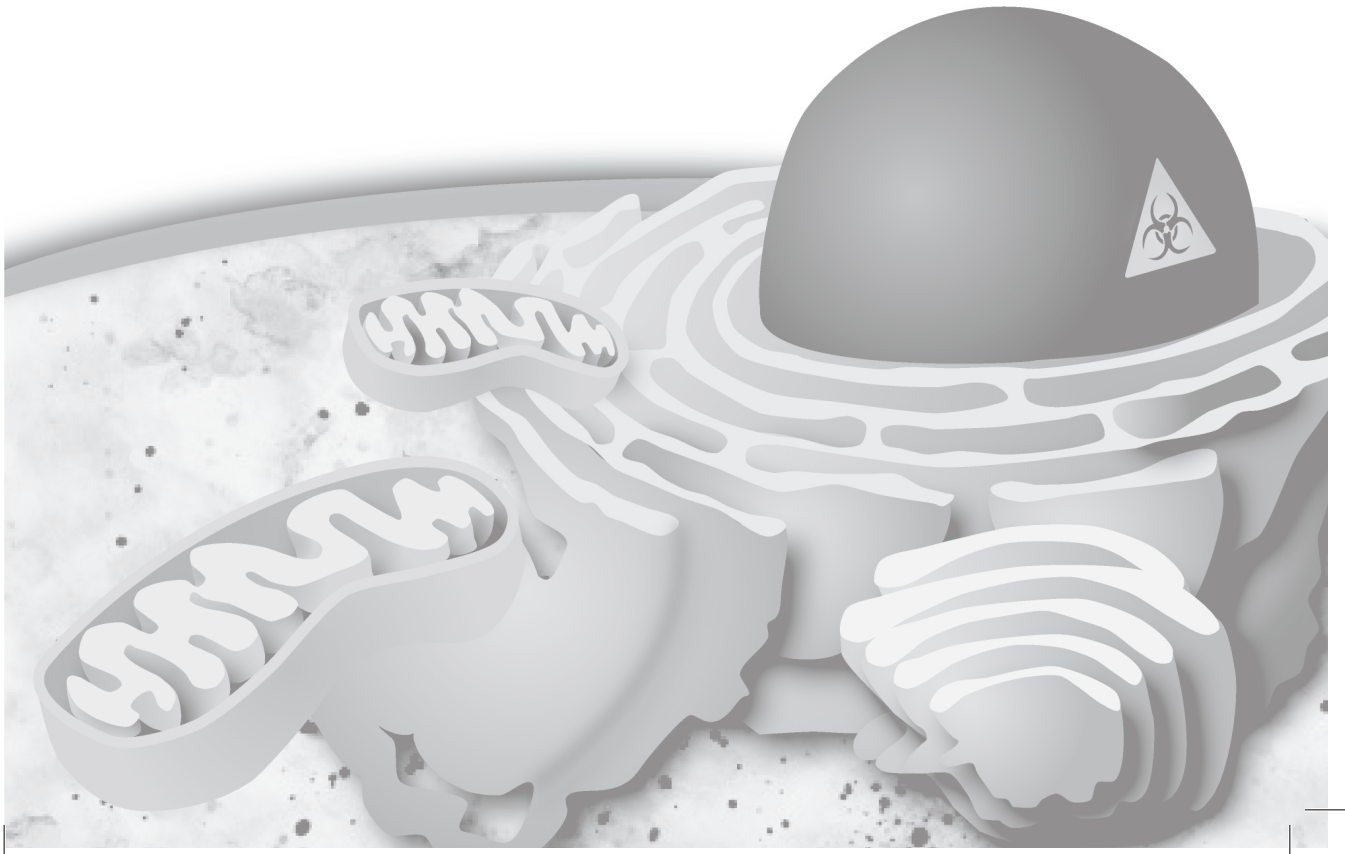

Abstract

Granzyme-mediated cell death is the major pathway for cytotoxic lymphocytes to kill virus-infected and tumor cells. In humans, five different granzymes (*i.e.* GrA, GrB, GrH, GrK, and GrM) are known that all induce cell death. Expression of intracellular serine protease inhibitors (serpins) is one of the mechanisms by which tumor cells evade cytotoxic lymphocyte-mediated killing. Intracellular expression of SERPINB9 by tumor cells renders them resistant to GrB-induced apoptosis. In contrast to GrB, however, no physiological intracellular inhibitors are known for the other four human granzymes. In the present study, we show that SERPINB4 formed a typical serpin-protease SDS-stable complex with both recombinant and native human GrM. Mutation of the P2-P1-P1′ triplet in the SERPINB4 reactive center loop completely abolished complex formation with GrM and N-terminal sequencing revealed that GrM cleaves SERPINB4 after P1-Leu. SERPINB4 inhibited GrM activity with a stoichiometry of inhibition of 1.6 and an apparent second order rate constant of 1.3×10^4 $M^{-1}s^{-1}$. SERPINB4 abolished cleavage of the macromolecular GrM substrates α-tubulin and nucleophosmin. Overexpression of SERPINB4 in tumor cells inhibited recombinant GrM-induced as well as NK cell-mediated cell death and this inhibition depended on the reactive center loop of the serpin. As SERPINB4 is highly expressed by squamous cell carcinomas, our results may represent a novel mechanism by which these tumor cells evade cytotoxic lymphocyte-induced GrM-mediated cell death.

Introduction

Cytotoxic T lymphocytes (CTLs) and natural killer (NK) cells (*i.e.* cytotoxic lymphocytes) play a pivotal role in the effector arm of the immune response that eliminate virus-infected cells and tumor cells [113]. Cytotoxic lymphocytes predominantly destroy their target cells by releasing the content of their cytolytic granules. These granules contain perforin and a family of unique structurally homologous serine proteases known as granzymes [241]. While perforin facilitates the entry of granzymes into the target cell, the latter induce cell death by cleaving critical intracellular substrates [242].

In humans, five different granzymes (GrA, GrB, GrH, GrK, and GrM) are known that differ on the basis of their substrate specificity [114]. All granzymes induce cell death with partially overlapping morphological hallmarks [114]. While GrA and GrB have been extensively studied, far less is known about the molecular cell death mechanisms of the other human granzymes [8]. Recently, it has been demonstrated that GrM, which is highly expressed by NK cells, NKT cells, γδ-T cells, and $CD8^+$ effector T cells [35, 37, 38], mediates a major and novel perforin-dependent cell death pathway that plays a significant role in cytotoxic lymphocyte induced death [41]. In tumor cell lines, GrM directly and efficiently cleaves a diverse set of substrates, *i.e.* ICAD, PARP, HSP75, ezrin, α-tubulin, PAK 2, survivin, and nucleophosmin [31, 42-45].

Tumor cells can escape from cytotoxic lymphocyte-induced killing by expression of cell death inhibitors in their cytoplasm, like the caspase-inhibitors XIAP and FLIP [243, 244], and the GrB-inhibitor SERPINB9 (PI9) [50]. SERPINB9 is the only known intracellular human granzyme inhibitor and protects against GrB-induced apoptosis [50, 245]. Expression of SERPINB9 is associated with a poor clinical outcome in various types of tumors (*e.g.* lymphomas and melanomas) [52, 53, 246]. SERPINB9 belongs to the intracellular (B-clade) sub-family of human serine protease inhibitors (serpins). Serpins share a unique inhibitory mechanism. Upon cleavage by a specific target protease in their reactive center loop (RCL), serpins undergo a conformational change after which the serpin and the target protease are covalently bound, leaving the latter kinetically inactive [247].

In contrast to GrB, no physiological intracellular inhibitors are known for the other four human granzymes [248]. Since GrM is a very potent specialized inducer of tumor cell death [8, 9] and plays an important role in anti-tumor function *in vivo* [63], we aimed to identify an intracellular inhibitor of human GrM. In the present study, we demonstrate that SERPINB4 [also called squamous cell carcinoma antigen 2 (SCCA-2) or leupin] directly inhibits human GrM proteolytic activity and that overexpression of SERPINB4 in HeLa cells inhibits recombinant GrM-induced as well as NK cell-mediated cell death. This may represents a novel mechanism by which tumor cells evade GrM-mediated killing by cytotoxic lymphocytes.

Materials and Methods

Recombinant proteins

Expression and purification of recombinant human GrM and the catalytically inactive GrM-SA variant was performed as described previously [45]. Briefly, cDNA encoding mature human GrM (residues Ile^{26}-Ala^{257}) was cloned into the yeast expression vector pPIC9 (Invitrogen, Paisley, UK). Catalytically inactive GrM-SA, in which the Ser^{195} residue in the catalytic center is replaced by Ala, was generated by site-directed mutagenesis (Stratagene, Cedar Creek, TX). Plasmids were transformed into the GS115 strain of *P. pastoris* (Invitrogen) and granzymes were expressed in conditioned media for 72 h. Recombinant GrM and GrM-SA were purified to homogeneity by cation-exchange chromatography (GE Healthcare, Diegem, Belgium) and dialyzed against 50 mM Tris (pH 7.4) and 150 mM NaCl. Recombinant GrM, but not GrM-SA, was active as determined by a synthetic chromogenic leucine substrate (Bachem, Weil am Rhein, Germany).

Expression and purification of recombinant SERPINB4 wild type and SERPINB4 RCL-mutant was performed using the expression vector pRSETC (Invitrogen) as described previously [249]. SERPINB4, coding an N-terminal His_6-tagged fusion protein, and SERPINB4 RCL-mutant, in which the P2-Glu^{353}, P1-Leu^{354}, P1'-Ser^{355} amino acids were mutated into P2-Gln^{353}, P1-Gly^{354}, P1'-Ala^{355}, were expressed in E.coli BL21 (DE3) using Overnight Express auto inducing medium (Merck, Nottingham, UK) containing 100 µg/ml ampicillin. Following growth at 37°C for 24 h, cells were harvested by centrifugation at 15,000 g for 30 minutes and lysed using Bugbuster (Merck) lysis reagent. Soluble material was clarified by centrifugation of the lysate at 21,000 g for 30 minutes at 4°C. The recombinant serpin was purified using a His-Bind Purification kit (Merck). Pooled imidazole eluted fractions were buffer exchanged into 50 mM Tris pH 8.0 and recombinant protein was stored at −80°C until required. Concentrations of the purified proteins were measured according to the procedure of Bradford (Bio-Rad, Hercules, CA).

Generation of a novel mAb against human GrM

Mice were immunized with purified recombinant human GrM. Obtained hybridomas were screened for antibodies that reacted with GrM in different applications as previously described [250]. Anti-GrM mAb 3D4D7 (IgG1 isotype) was highly sensitive against Western-blotted recombinant GrM as well as native GrM from NK cell lysates (Fig. 1). Cross-reactivity of mAb 3D4D7 against recombinant human GrB and GrK was excluded (data not shown).

Cell culture and transfection

293T and Jurkat cells were maintained in DMEM and RPMI-1640 medium (Invitrogen), respectively, supplemented with 10% (v/v) heat-inactivated fetal bovine serum (Sigma), 100 U/ml penicillin, and 100 µg/ml streptomycin (Invitrogen). The human NK cell line KHYG-1 [206] was purchased from the Health Science Research Resources

Bank (JCRB0156) of the Japan Health Sciences Foundation and cultured similarly to Jurkat cells, with the addition of 50 ng/ml recombinant human interleukin 2 (Wako, Osaka, Japan). The previously described HeLa cell lines, stably transfected with pcDNA3 SERPINB4, pcDNA3 SERPINB4 RCL-mutant, or pcDNA3 vector only [249], were cultured similarly to 293T cells, with the addition of G418 (0.5 mg/ml). The plasmid pEGFP-N1 containing C-terminal green fluorescent protein (GFP)-tagged SERPINB4 (kindly provided by Dr. Wun-Shaing W. Chang, National Institute of Cancer Research, National Health Research Institutes, Taiwan, ROC) or mock control vector were transiently transfected into 293T cells using linear polyethylenimine (PEI) (Polysciences, Warrington, PA), according to the manufacturer's instructions. Cell lysates were prepared by three freezing-thawing cycles in liquid nitrogen of cells resuspended in a buffer containing 20 mM Tris (pH 7.4) and 150 mM NaCl. Protein concentrations of the supernatants were measured according to the procedure of Bradford.

Analysis of complex formation by SDS-PAGE and immunoblotting

Indicated amounts of purified recombinant SERPINB4 and GrM proteins were incubated in 20 mM Tris (pH 7.4) and 150 mM NaCl for 1 h at 37°C. When noted, Jurkat or KHYG-1 cell lysate was incubated with the recombinant protein(s) for the indicated times at 37°C. Samples containing recombinant proteins only were additionally treated with PNGase F (New England BioLabs, Ipswich, MA), according to the manufacturer's instructions. Subsequently, samples were separated on 10% SDS-PAGE gels under reducing conditions. For SDS-PAGE analysis, gels were stained with SimplyBlue (Invitrogen), according to the manufacturer's instructions. For immunoblot analysis, proteins were transferred onto immobilon–P membranes (Millipore, Billerica, MA). After blocking with 5% (w/v) Marvel dried skimmed milk (Premier International Foods, Coolock, UK) in TBS-T (10 mM Tris-HCl, pH 8.0, 150 mM NaCl, 0.1% Tween-20), membranes were incubated for two hours at RT with our novel mouse anti-human GrM mAb (clone 3D4D7; 1.0 µg/ml), mouse anti-human α-tubulin mAb (clone B-5-1-2; 0.4 µg/ml) (Sigma), mouse anti-human nucleophosmin (clone FC-61991; 2.0 µg/ml) (Invitrogen), rabbit anti-human nm23H-1 (clone C-20:sc-343; 1.0 µg/ml) (Santa Cruz Biotechnology, Santa Cruz, CA), or mouse anti-human β-actin mAb (clone 2A2.1) (US Biological, Swampscott, MA). Goat anti-mouse IgG+IgM HRP (Biosource, Camarillo, CA) conjugate was used as secondary antibody. Bound antibodies were visualized using 3,3'-diaminobenzidine (DAB) (0.6 mg/ml) or enhanced chemiluminescence substrate (ECL) (GE Healthcare).

Immunoprecipitation

Cell lysates of mock and GFP-tagged SERPINB4 transfected 293T cells were incubated with 10 µg/ml anti-GFP mAb (Roche, Mannheim, Germany) and protein A/G plus-agarose (Santa Cruz Biotechnology), and rotated end-over-end in non-sticky microfuge tubes (Ambion, Austin, TX) for 16 h at 4°C. Precipitates were washed three times with 50 mM Tris (pH 7.4), 150 mM NaCl and incubated with 2.3

μM rh-GrM for 1 h at 37°C. Next, the samples were washed twice more and finally boiled in reducing Laemmli sample buffer. Immunoblotted samples were stained by Coomassie Brilliant Blue (BioRad) and the cleavage-product of interest was excised and identified by Edman degradation, using a 476A protein sequencer (Applied Biosystems, Foster City, CA).

Stoichiometry of inhibition
Increasing concentrations (0–3 μM) of recombinant SERPINB4 was incubated with a constant amount of recombinant human GrM (2 μM) in 50 mM Tris (pH 7.4) and 150 mM NaCl for 2 h at 37°C. Samples were diluted 10-fold in 100 mM Tris (pH 7.4), 200 mM NaCl, and 0.01% Tween containing 1 mM synthetic chromogenic leucine substrate (AAPL-pNA) (Bachem) to terminate the inhibition reactions and transferred to a microplate (Greiner, Kremsmunster, Austria) to assay residual GrM activity. The velocity of substrate hydrolysis by residual active GrM was measured at A_{405} using a microtiter plate reader (Anthos, Cambridge, UK). The fractional activity (velocity of GrM with a serpin/velocity of GrM only) was plotted against the ratio of $[serpin]_0/[GrM]_0$. Linear regression analysis was used to determine the x-axis intercept as a value for the stoichiometry of inhibition.

Apparent second order rate constant
The interaction of SERPINB4 with GrM was determined under second order conditions [251]. Recombinant GrM was incubated with recombinant SERPINB4 at equimolar concentrations. Samples of this reaction were taken after 30, 60, 120, 180, 240 and 360 seconds and directly diluted 20-fold in 100 mM Tris (pH 7.4), 200 mM NaCl, and 0.01% Tween containing 1 mM of the chromogenic substrate AAPL-pNA. The rate of substrate hydrolysis by GrM was measured in time at A_{405} using a microtiter plate reader (Anthos). Since serpin-serine protease interactions are irreversible, velocities of the substrate hydrolysis were converted to residual active GrM concentrations using a GrM concentration standard curve incubated without SERPINB4. The rate of change in the amount of residual active GrM over time is described in equation (1), where the slope of the plot of reciprocal residual active GrM over time yields the apparent second order rate constant (k_{inh}).

(1) $1/[\text{residual active GrM}] = k_{inh} \times t + 1 / [GrM]_0$

RT-PCR and immunoblot analysis for SERPINB4 expression
RNA was isolated from (stably transfected) HeLa cells using RNA isolator™ (Genosys). RNA (1–5 μg) was reverse transcribed using MMLV-reverse transcriptase, and the resulting cDNA was used for RT-PCR amplification. The following primers were used: GAPDH-sense 5′-TGAAGGT-CGGAGTCAACG-3′, GAPDH-antisense 5′-CATGTGGGCCATGAGGTC-3′, SERPINB4-sense 5′-GGGGGATCCATATGAATTCACTCAGTGAAG-3′, and SERPINB4-

antisense 5′-CCCCCGGGTACCTACGGGGATGAGAATCTG-3′. Immunoblot analysis for SERPINB4 protein expression by (stably transfected) HeLa cells was performed as previously described [249].

Granzyme M killing assays
HeLa cells stably transfected with SERPINB4 or SERPINB4 RCL-mutant were grown to confluence in a 96-well tissue-culture plate. Cells were washed twice in serum-free DMEM, after which they were incubated at 37°C with a sublytic dose of streptolysin O (SLO) (0.5 µg/ml) (Sigma) and indicated concentrations of granzyme in serum-free DMEM for 30 min. Cells were washed twice with supplemented DMEM, after which cells were incubated for indicated periods of time at 37°C. For the methylene blue assay, cells were carefully washed with PBS and remaining adherent cells were fixed with methanol for 30 min at room temperature. After drying, cells were stained with 0.05% (w/v) methylene blue dye (Merck) in borate-buffered saline (pH 8.4) for 15 min, washed 3 times with water, and air dried. Bound dye was dissolved in 0.1 N HCl (100 µl/well) and measured photospectrometrically at 630 nm. To assess cell viability by flow cytometry, cells were stained with AnnexinV-fluos (Invitrogen) and propidium iodide (PI) for 15 min in a buffer containing 140 mM NaCl, 4 mM KCl, 0.75 mM $MgCl_2$, 1.5 mM $CaCl_2$, and 10 mM HEPES (pH 7.4). Flow cytometry was performed on a FACSCalibur (BD Biosciences) and data was analyzed using CellQuest Pro software (BD Biosciences).

NK-cell mediated cytotoxicity assay
HeLa cells stably transfected with SERPINB4 or SERPINB4 RCL-mutant were grown to confluence in a 96-well tissue-culture plate and loaded for 10 min with 10 µM of the fluorescent cell staining dye carboxyfluorescein diacetate succinimidyl ester (CFDA-SE). These HeLa cells were co-cultured with KHYG-1 NK cells in varying E:T ratio's for 16 h at 37°C. Cells were stained with PI and analyzed by flow cytometry. During data analysis, a gate on CFDA-SE positive cells was used to distinguish between KHYG-1 and HeLa cells. The percentage of living untreated HeLa cells was set at 100% and the percentages of treated cells were matched correspondingly, after which the percentage of specific cytotoxicity was calculated.

Statistical analysis
All statistical analyses were performed using the Student's t-test.

Results

SERPINB4 forms a typical serpin-protease SDS-stable complex with human GrM
Upon cleavage by a specific target protease, most serpins form SDS-stable covalent-bound complexes with that protease, in which the latter one becomes inactive [247]. Since human GrM displays a restricted cleavage site specificity in that it predominantly cleaves after P1-Leu [28, 31, 42, 45] and that SERPINB4 is

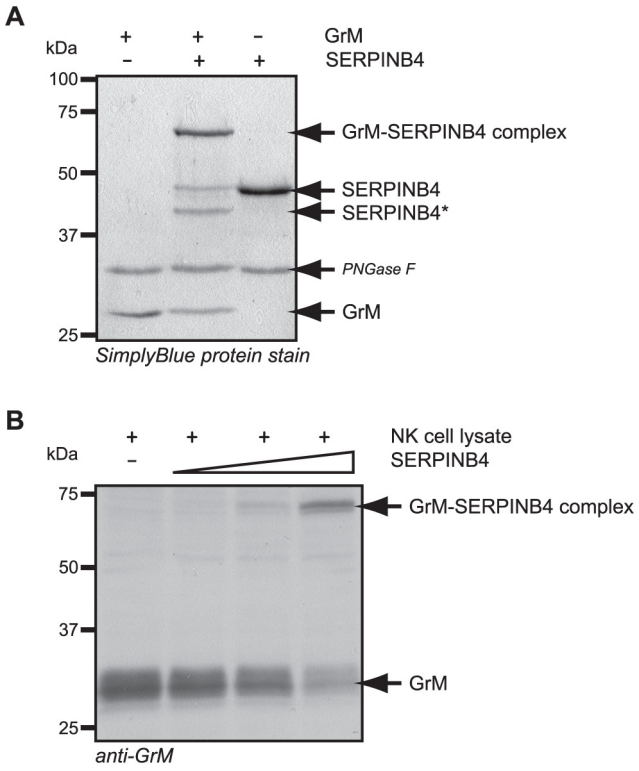

Figure 1. SERPINB4 forms a typical serpin-protease SDS-stable complex with recombinant and native human GrM. (A) Purified recombinant GrM (1.8 µM) and SERPINB4 (1.8 µM) were incubated for 1 h at 37°C. All samples were treated with PNGase F, separated by SDS-PAGE, and analyzed by SimplyBlue staining. (B) Cell lysate of the NK cell line KHYG-1 (33 µg) was incubated with recombinant SERPINB4 (0, 50, 150, and 450 ng) for 2 h at 37°C. Subsequently, samples were immunoblotted for native GrM. GrM, SERPINB4, GrM-SERPINB4 complexes, and cleaved SERPINB4 (SERPINB4*) are indicated.

the only human intracellular B-clade serpin that harbours a Leu at the putative P1-position in its RCL [252, 253], we investigated complex formation of SERPINB4 with GrM by SDS-PAGE analysis using purified recombinant proteins (Fig. 1A). Purified recombinant GrM and SERPINB4 migrated with a molecular mass of 28 and 44 kDa, respectively (Fig. 1A, left and right lane). Incubation of GrM with SERPINB4 revealed an SDS-stable complex band with the expected molecular mass of around 70 kDa (Fig. 1A, middle lane). The majority of SERPINB4 molecules formed a complex with GrM, whereas a small fraction of SERPINB4 was cleaved by GrM without trapping this protease. Next, we studied whether SERPINB4 could also bind to and form an SDS-stable complex with native human GrM (Fig. 1B). The human NK cell line KHYG-1 was used as a source for native GrM. Incubation of a KHYG-1 cell lysate with recombinant SERPINB4 and subsequent immunoblotting for the protease revealed the formation of a complex between native GrM and recombinant SERPINB4 in a concentration-dependent manner (Fig. 1B). These data demonstrate that SERPINB4 forms a classical SDS-stable serpin-protease complex with both recombinant and native human GrM.

GrM cleaves SERPINB4 in its RCL after P1-Leu

To investigate if complex formation of SERPINB4 with GrM depends on the RCL and corresponding conformational change of the serpin, a RCL-mutant of SERPINB4 was employed in which the amino acids at the putative P2(Glu^{353})-P1(Leu^{354})-P1′(Ser^{355}) positions were mutated into P2(Gln^{353})-P1(Gly^{354})-P1′(Ala^{355}). Western blot analysis for GrM revealed a complex with a molecular mass of about 70 kDa when the purified recombinant wild type proteins of GrM and SERPINB4 were incubated (Fig. 2A). In contrast, no complex formation was detected upon incubation of SERPINB4 RCL-mutant with GrM. Furthermore, a mutated catalytically inactive counterpart of GrM was included (GrM-SA). As expected, this GrM-SA was not able to form a complex with SERPINB4 (Fig. 2A). Thus, complex formation of SERPINB4 with GrM appears to depend on the RCL of the serpin and the catalytic triad of the protease.

Next, the cleavage site of GrM in the RCL of SERPINB4 was determined. Therefore, cell lysates of 293T cells expressing either C-terminal GFP-tagged full length SERPINB4 or an empty vector were incubated with GrM. Immunoblotting for GFP showed a C-terminal cleavage product of SERPINB4 (SERPINB4*-GFP) with the expected molecular mass of about 29 kDa (Fig. 2B), as the RCL of SERPINB4 is near its C-terminus and the molecular mass of the linked GFP is about 25 kDa.

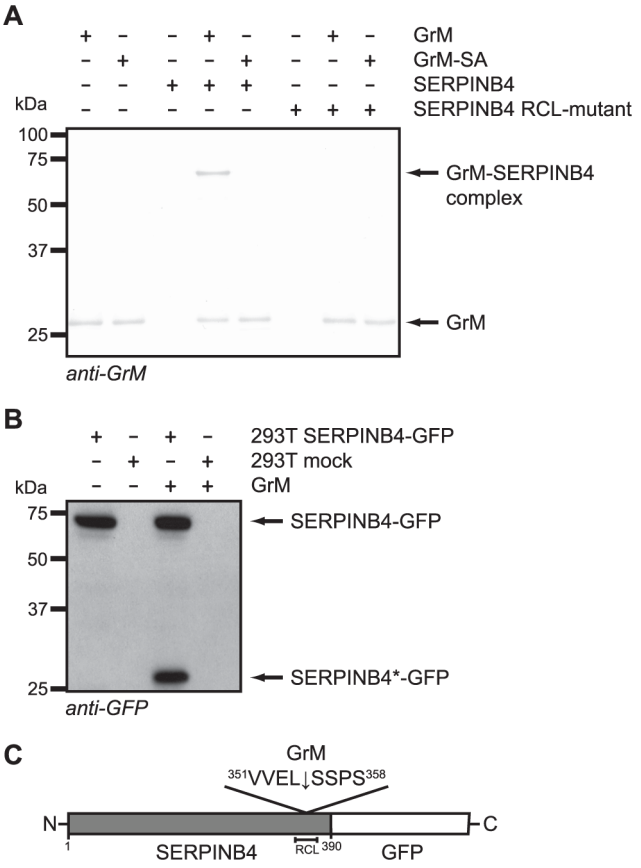

Figure 2. Mutation of the SERPINB4 RCL at the P2-P1-P1′ positions completely abolishes complex formation with human GrM. (**A**) A RCL-mutant of SERPINB4 was employed in which the amino acids at the putative P2(Glu^{353})-P1(Leu^{354})-P1′(Ser^{355}) positions were mutated into P2(Gln^{353})-P1(Gly^{354})-P1′(Ala^{355}). Purified recombinant GrM (0.9 µM), GrM-SA (0.9 µM), SERPINB4 (0.9 µM), and SERPINB4 RCL-mutant (0.9 µM) were incubated for 1 h at 37°C. All samples were treated with PNGase F, separated by SDS-PAGE, and immunoblotted for GrM. Bound antibodies were visualized using DAB. (**B**) Cell lysates of 293T cells transfected with C-terminal GFP-conjugated SERPINB4 or an empty vector (mock) were incubated with recombinant GrM (0.5 µM) for 1 h at 37°C. Subsequently, samples were immunoblotted for GFP. SERPINB4-GFP represents the full length protein, whereas SERPINB4*-GFP depicts the C-terminal cleavage product. (**C**) Schematic representation of C-terminal GFP-conjugated SERPINB4, including the GrM cleavage site after Leu^{354} at the P1-position in the RCL.

Immunoprecipitation of GFP-conjugated SERPINB4 from 293T cell lysate and N-terminal sequencing of the subsequent GrM-induced C-terminal cleavage fragment revealed that GrM indeed cleaves SERPINB4 in its RCL, at least after the amino acid Leu[354] at the P1-position in the sequence [351]VVEL↓SSPS[358] (Fig. 2C).

Stoichiometry of inhibition of GrM and SERPINB4

The interaction of a serpin with its physiological target protease usually results in complex formation with a stoichiometry of inhibition (SI) value close to 1. The SI value indicates how many serpin-molecules are needed to inhibited one molecule of target protease. If a serpin is also a substrate in parallel to an inhibitor of its target protease, this is reflected by a SI value greater than 1. The SI value for inhibition of GrM by SERPINB4 was determined by measurement of residual GrM activity at increasing $[SERPINB4]_0/[GrM]_0$ ratios (Fig. 3A). Complete inhibition of GrM activity was obtained at a $[SERPINB4]_0/[GrM]_0$ ratio of 1.6±0.07 (mean ± SD of 4 independent experiments) (Fig. 3A). This indicates that about three molecules of SERPINB4 are needed to inhibit two GrM molecules.

Kinetic analysis of the inhibition of GrM activity by SERPINB4

To determine the rate of complex formation between GrM and SERPINB4, the

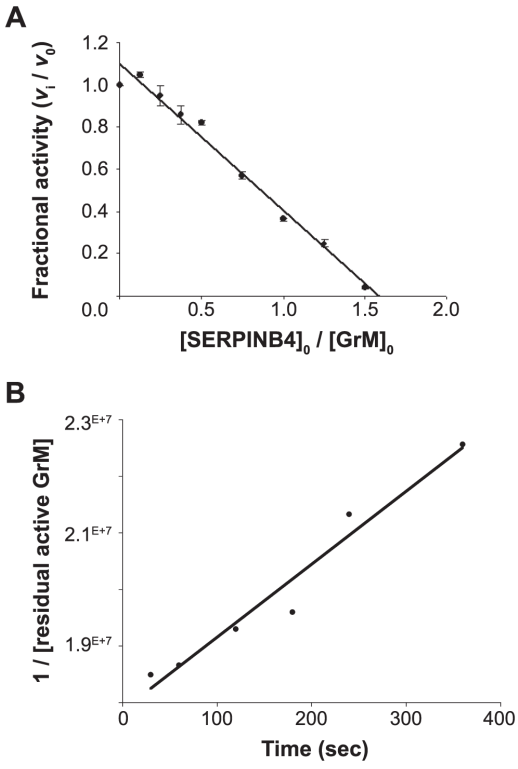

Figure 3. Kinetic analyses of GrM-inhibition by SERPINB4. (**A**) Purified recombinant human GrM (2 μM) was incubated with different concentrations of recombinant SERPINB4 (0–3 μM) for 2 h at 37°C. Residual GrM activity was monitored by addition of a synthetic chromogenic leucine substrate (1 mM) and measuring A_{405} in time. The fractional activity (velocity of substrate hydrolysis by GrM in the presence of SERPINB4/velocity of substrate hydrolysis by GrM without SERPINB4) was plotted against the ratio of $[SERPINB4]_0/[GrM]_0$. Linear regression analysis was used to calculate the x-intercept as a value for the SI and determined to be 1.6±0.07 (mean ± SD of 4 independent experiments). (**B**) The apparent second order rate constant (k_{inh}) of the inhibition of GrM by SERPINB4 was determined under second order conditions. Equimolar concentrations of recombinant human GrM and SERPINB4 were incubated. Aliquots were removed at different time points and the reaction was directly stopped by 20-fold dilution with buffer containing a synthetic chromogenic leucine substrate (1 mM). Residual GrM activity was determined by measuring the velocity of substrate hydrolysis in time at A_{405}. These velocities were converted to residual active GrM concentrations using a GrM concentration standard curve. The apparent second order rate constant (k_{inh}) was calculated from the slope of the plot of reciprocal residual active GrM over time and determined to be 1.3×10^4 $M^{-1}s^{-1}$ (graph indicates one representative example of three independent experiments with similar results).

apparent second order rate constant (k_{inh}) was measured under second order conditions. Upon incubation of recombinant GrM with equimolar concentrations of SERPINB4 samples were taken in time to measure the residual GrM-activity. Addition of a synthetic chromogenic leucine substrate to these aliquots revealed that the concentration of active GrM decreased linear in time (Fig. 3B). The apparent second order rate constant (k_{inh}) was calculated from the slope of the plot of reciprocal residual active GrM over time and was determined to be 1.3 (±0.05)×10^4 $M^{-1}s^{-1}$(mean ± SD of 3 independent experiments). This k_{inh} was not affected by inclusion of the glycosaminoglycan heparin in these experiments, which is a known co-factor of several serpins that enhances the k_{inh} towards their target proteases [254] (data not shown).

SERPINB4 inhibits cleavage of natural macromolecular substrates by GrM

The inhibitory effect of SERPINB4 on the activity of human GrM was further investigated using natural macromolecular substrates of GrM. GrM and SERPINB4 were incubated at various concentration-ratios and GrM-activity towards two known direct GrM-substrates [31, 45] in a Jurkat tumor cell lysate was determined by immunoblotting (Fig. 4). As expected, in the absence of SERPINB4, human recombinant GrM efficiently cleaved the 55 kDa α-tubulin subunit as well as the 37 kDa nucleolar phosphoprotein nucleophosmin. Recombinant SERPINB4 impaired cleavage of both α-tubulin and nucleophosmin by GrM in a concentration-dependent manner (Fig. 4). Excessive concentrations of SERPINB4 over GrM completely inhibited GrM activity towards α-tubulin, whereas some nucleophosmin cleavage was still observed, suggesting that nucleophosmin is a more efficient GrM-substrate than α-tubulin. β-actin served as a loading control (Fig. 4). In conclusion, SERPINB4 inhibits GrM-mediated cleavage of the natural macromolecular substrates α-tubulin and nucleophosmin in a tumor cell lysate.

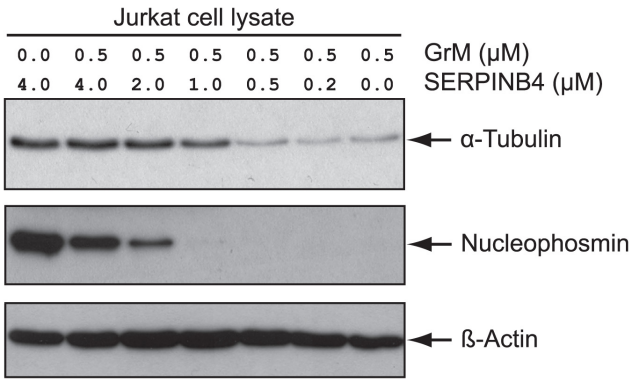

Figure 4. SERPINB4 inhibits GrM-mediated cleavage of macromolecular substrates. Indicated concentrations of recombinant GrM and SERPINB4 were incubated for 2 h at 37°C. Jurkat tumor cell lysate (2 μg) was added to the samples and incubated for another 4 h at 37°C to determine the residual GrM-activity towards macromolecular substrates. Finally, all samples were immunoblotted for α-tubulin, nucleophosmin, and β-actin.

Overexpression of SERPINB4 inhibits recombinant GrM-induced as well as NK cell-mediated cell death

To examine whether SERPINB4 also inhibits the proteolytic activity of GrM in tumor cells, the effect of overexpression of SERPINB4 in HeLa cells on GrM-induced cell death was investigated. First, SERPINB4 RNA and protein expression by HeLa cells stable transfected with SERPINB4, SERPINB4 RCL-mutant, or an empty vector were determined. RT-PCR analysis revealed SERPINB4 RNA expression in both HeLa cells that overexpressed SERPINB4 and SERPINB4 RCL-mutant (Fig. 5A, upper panel). Mock-transfected HeLa cells and HeLa cells transfected with the empty vector

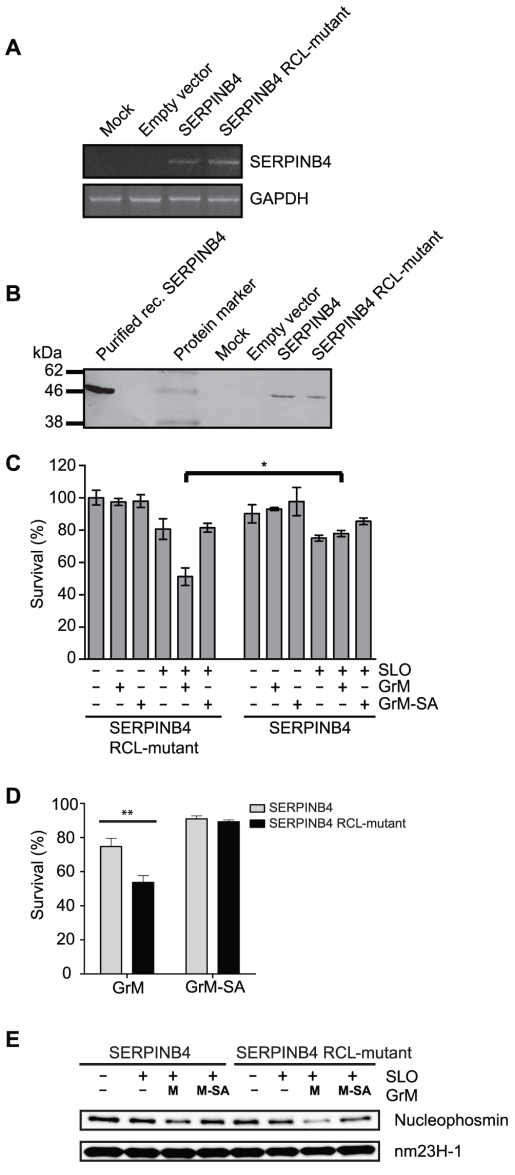

Figure 5. Overexpression of SERPINB4 in HeLa cells inhibits GrM-induced cell death. (**A**) RT-PCR analysis of stably transfected HeLa cells for SERPINB4 and GAPDH mRNA expression (upper and lower panel, respectively). (**B**) Immunoblot analysis of SERPINB4 protein expression by HeLa cells stably transfected with pcDNA3 SERPINB4, pcDNA3 SERPINB4 RCL-mutant or pcDNA3 empty vector. (**C**) HeLa cells stably transfected with SERPINB4 or SERPINB4 RCL-mutant were treated with the indicated combinations of a sublytic dose of SLO (500 ng/ml), recombinant GrM (0.5 μM), and/or recombinant GrM-SA (0.5 μM) for 16 h at 37°C. Viable cells were quantified using the methylene blue assay. Data represent the percentages of viable cells as compared to HeLa cells that overexpressed SERPINB4 RCL-mutant and were treated with buffer only, which was set as 100%. Figure represents the mean ± SD of 4 independent experiments; * $p<0.05$. (**D**) HeLa cells stably transfected with SERPINB4 or SERPINB4 RCL-mutant were treated with the indicated combinations of a sublytic dose of SLO (500 ng/ml), recombinant GrM (1 μM), and/or recombinant GrM-SA (1 μM) for 20 h at 37°C. Cell viability was determined using flow cytometry, with AnnexinV and PI negative cells considered viable (mean ± S.D., $n = 3$, ** $p<0.005$). (**E**) HeLa cells stably transfected with SERPINB4 or SERPINB4 RCL-mutant were treated with the indicated combinations of a sublytic dose of SLO (500 ng/ml), recombinant GrM (1 μM), and/or recombinant GrM-SA (1 μM) for 4 h at 37°C. Total cell lysates were immunoblotted using antibodies against nucleophosmin and nm23H-1 (which served as a loading control).

did not express SERPINB4 RNA. GAPDH RNA expression served as a control for RNA/cDNA input (Fig. 5A, lower panel). In accordance with the RNA expression, immunoblot analysis revealed SERPINB4 protein expression by both HeLa cells stable transfected with SERPINB4 and SERPINB4 RCL-mutant, and not by mock-transfected HeLa cells or HeLa cells transfected with the empty vector (Fig. 5B). Second, a GrM cell death assay was employed in which the pore-forming protein SLO was used to deliver recombinant GrM into HeLa cells that overexpressed either SERPINB4 or SERPINB4 RCL-mutant. As a control, we included the catalytically inactive GrM mutant (*i.e.* GrM-SA). The methylene blue assay revealed that treatment of the cells with only a sublytic dose of SLO resulted in about 20% reduction of viable cells. As expected, the percentage of viable HeLa cells that overexpressed inactive SERPINB4 RCL-mutant significantly decreased upon treatment with SLO and recombinant GrM, but not with recombinant GrM only, SLO only, or the SLO/GrM-SA combination (Fig. 5C, left panel). In contrast, GrM-induced cell death of HeLa cells was fully rescued by overexpression of SERPINB4 (Fig. 5C, right panel). Similar results were obtained on a single cell level by staining with Annexin V and PI and subsequently FACS analysis. Again, GrM-induced cell death was inhibited by overexpression of SERPINB4 (Fig. 5D).

To further determine whether GrM is inactivated by SERPINB4 after intercellular delivery, cleavage of the preferred GrM-substrate nucleophosmin was investigated. As expected, nucleophosmin was cleaved upon SLO-mediated delivery of GrM, and not GrM-SA, into HeLa cells overexpressing SERPINB4 RCL mutant (Fig. 5D, right lanes). In contrast, GrM-mediated intracellular cleavage of nucleophosmin was inhibited by overexpression of SERPINB4 (Fig. 5D, left lanes), indicating that GrM is inactivated by SERPINB4 upon intracellular delivery.

In addition to exogenous recombinant GrM-induced cell death, we also investigated whether SERPINB4 inhibits endogenous native GrM-induced cell death. The NK cell line KHYG-1, which is known to express large amounts of GrM and hardly,

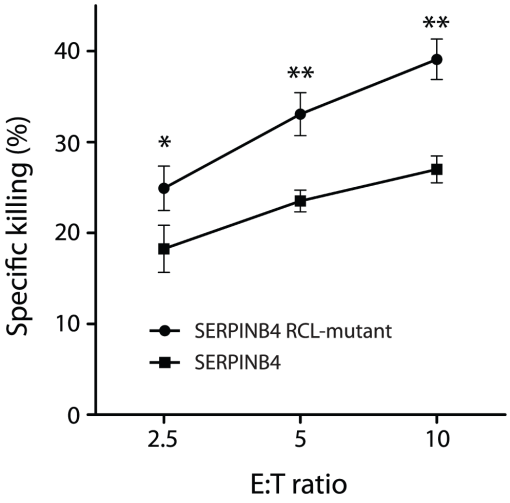

Figure 6. Overexpression of SERPINB4 in HeLa cells inhibits NK cell-mediated cell death. HeLa cells stably transfected with SERPINB4 or SERPINB4 RCL-mutant were loaded with the fluorescent cell staining dye CFDA-SE and co-cultured with KHYG-1 NK cells in varying E:T ratio's for 16 h at 37°C. Cells were stained with PI and analyzed by flow cytometry. HeLa cells were separated from KHYG-1 cells by gating for CFDA-SE positive cells. Depicted is the percentage of specific cytotoxicity (mean ± SD, $n = 3$, *$p<0.05$, ** $p<0.005$).

if any, GrA and GrB [207], was co-cultured in various ratios with HeLa cells stably transfected with either SERPINB4 or SERPINB4 RCL mutant. HeLa cells were killed by KHYG-1 cells in a ratio dependent manner (Fig. 6). In contrast, overexpression of SERPINB4 significantly inhibited KHYG-1 mediated cell death as compared to HeLa cells stably transfected with SERPINB4 RCL mutant. These results indicate that cellular overexpression of SERPINB4 inhibits recombinant GrM-induced as well as NK cell-mediated cell death and that this inhibition is dependent on the RCL of the serpin.

Discussion

The granule-exocytosis pathway is the major mechanism for cytotoxic lymphocytes to kill tumor and virus-infected cells [113, 114, 241, 242]. Tumor cells can evade GrB-mediated cell death by expression of the intracellular serine protease inhibitor SERPINB9 [50, 245]. However, such physiological intracellular inhibitors are unknown for the other four human granzymes. In mice, GrM is inhibited by the murine serpin SPI-CI, which protects cells from GrM-mediated cell death [36]. SPI-CI is unique for mice and no human orthologue is known. In the present study, we show for the first time that human GrM also has an endogenous intracellular inhibitor that protects cells from GrM-mediated killing. We have demonstrated that GrM cleaves SERPINB4 in its RCL after P1-Leu, resulting in the formation of a typical serpin-protease SDS-stable complex (Figs. 1, 2, 3). Furthermore, SERPINB4 inhibited the proteolytic activity of GrM towards natural macromolecular substrates (Fig. 4 and 5E) and overexpression of SERPINB4 in HeLa cells inhibited recombinant GrM-induced as well as NK-cell mediated cell death (Fig. 5 and 6).

Our findings are consistent with the facts that GrM preferably cleaves after a P1-Leu and, to a lesser extent, after P1-Met [20, 28], and that SERPINB4 harbours a Leu at the P1-position in its RCL [253, 255]. Indeed, mutation of the P2-P1-P1' triplet in the SERPINB4 RCL completely abolished complex formation with GrM (Fig. 2A) and N-terminal sequencing revealed that GrM cleaved SERPINB4 at least after the Leu residue at the RCL P1-position (Fig. 2C). In addition, protection of HeLa cells against both recombinant GrM-induced and NK cell-mediated cell death by cellular overexpression of SERPINB4 also depended on the RCL of the serpin (Fig. 5 and 6). Although SERPINB4 is the only intracellular serpin that meets the primary specificity of human GrM in that it harbours a Leu or Met amino acid at the putative P1-position in its RCL [93, 252], we cannot fully exclude that other intracellular serpins than SERPINB4 inhibit human GrM. Few serpins are known to use more than one RCL P1-residue to inhibit different target proteases, thereby broadening their inhibitory profile [93]. Interestingly, the GrB-inhibitor SERPINB9 harbours a Met residue at the putative P3' position in its RCL. Indeed, GrM cleaves SERPINB9, however, an SI value of 59 points to a substrate rather than an inhibitor [28]. Therefore, it has been proposed that cleavage and inactivation of SERPINB9 by GrM clears the way for GrB-induced target cell killing [28]. Whether intracellular serpins other than SERPINB4 exist that inhibit human GrM activity remains an open question.

Whether SERPINB4 is a physiologic inhibitor of GrM remains to be investigated. We showed that SERPINB4 forms a typical serpin-protease SDS-stable complex with both recombinant and native human GrM (Fig. 1). Kinetic analysis of GrM-inhibition by SERPINB4 revealed a SI of 1.6 (Fig. 3A), indicating that about two-third of the SERPINB4 molecules forms a covalent complex with GrM and inhibits its activity, whereas about one-third of the SERPINB4 molecules is a substrate of GrM without trapping the protease. This corresponds with the relative intensity of the bands in Fig. 1A representing complexed and cleaved SERPINB4. The SI for SERPINB4 and GrM is in the similar range as the physiological interaction between SERPINB9 and caspase-1 (SI~1.7) [256] and somewhat higher as compared to SERPINB9 and GrB (SI~1.0) [95]. The inhibitory potency of SERPINB4 towards GrM seems different for a small molecular substrate (SI = 1.6; Fig. 3A) as compared to macromolecular substrates (SI>1.6; Fig. 4). The reason for this discrepancy remains unclear, but might be due to our recombinant proteins. It could be that a tiny fraction (<1%) of our recombinant GrM is not properly inhibited by SERPINB4 due to abnormal folding or glycosylation by P. pastoris, but retains its proteolytic activity. If so, this will not influence the determined SI-value significantly (Fig. 3A). However, cleavage of nucleophosmin by GrM is very efficient and occurs already at nanomolar concentrations of GrM [31], therefore a tiny fraction of non-inhibited GrM can be demonstrated by Western blot analysis (Fig. 4). The determined k_{inh} of 1.3×10^4 $M^{-1}s^{-1}$ for the rate of GrM inhibition by SERPINB4 (Fig. 3B) was into a similar range as compared with other SERPINB4-protease interactions. Previously, SERPINB4 has been demonstrated to inhibit cathepsin G and chymase with k_{inh}-values of 1.0×10^5 $M^{-1}s^{-1}$ and 2.8×10^4 $M^{-1}s^{-1}$, respectively [92]. The k_{inh}-value for SERPINB4 and GrM is lower as compared to SERPINB9 and GrB ($1.7\times10^6M^{-1}s^{-1}$) [95]. However, a physiological inhibitory role has been proposed for serpins with a relative low k_{inh}-value [252], for instance inhibition of TNF-mediated apoptosis by SERPINB4 via cathepsin G (k_{inh} 1.0×10^5 $M^{-1}s^{-1}$) [249], endogenous anti-inflammatory action of SERPINB9 via inhibition of caspase 1 (k_{inh} 7×10^2 $M^{-1}s^{-1}$) [256], activated protein C inhibition by Protein C inhibitor (SERPINA5) (k_{inh} 2.5×10^4 $M^{-1}s^{-1}$) during anti-coagulation [257], and complement C1 and kallikrein inhibition by C1-inhibitor (SERPING1) (k_{inh} 2.8×10^3–1.7×10^4 $M^{-1}s^{-1}$) [258]. In this context, it should also be mentioned that, like for other serpins [259], the inhibitory capacity of SERPINB4 towards GrM or other serine proteases could potentially be further enhanced by serpin cofactors, although here we excluded a role for heparin (data not shown). We provide *in vitro* evidence that overexpression of SERPINB4 inhibits both GrM-induced and NK cell-mediated cell death in tumor cells (Fig. 5 and 6). Whether SERPINB4 indeed is a physiological GrM-inhibitor in humans is ultimately determined by local concentrations of GrM and SERPINB4 *in vivo*.

In normal tissue, SERPINB4 is mainly expressed by stratified squamous epithelium of both the upper gastrointestinal tract and the female genitourinary system, and by pseudo-stratified columnar epithelium of the conducting airways [97]. Interestingly, tumors originating from these epithelial tissues also

express SERPINB4, *i.e.* squamous cell carcinomas of the cervix [260], head and neck, and lung [97]. Moreover, elevated SERPINB4 levels in patients with squamous cell carcinomas are associated with an advanced stage of tumor progression and poor disease-free survival [96, 261]. This indicates that expression of SERPINB4 is beneficial for tumor cells. Indeed, SERPINB4 inhibits both radiation- and TNF-induced apoptosis in transfected cell lines, probably by inhibition of the p38 MAPK pathway and the proteolytic activity of endogenous cathepsin G, respectively [249, 262]. Our current findings that SERPINB4 binds to human GrM and that cellular overexpression of SERPINB4 inhibits GrM-induced cell death suggest a novel function for SERPINB4, *i.e.* enhancement of tumor progression through interference with the granule-exocytosis cell death pathway of cytotoxic lymphocytes. This intriguing concept has been well studied for SERPINB9-expressing tumor cells that efficiently inhibit GrB-induced cell death [50]. SERPINB9 expression in several types of tumors is associated with a poor clinical outcome of patients [53, 246]. In analogy with SERPINB9, SERPINB4 expression may constitute a novel mechanism by which human squamous cell carcinoma tumor cells evade GrM-mediated cytotoxic lymphocyte-induced cell death.

Acknowledgments
We greatly thank Selçuk Çolak, Ka Wai Lai, and Isabel Vandenberghe for excellent technical assistance.

Author Contributions
Conceived and designed the experiments: PJAdK JAK DMW NB. Performed the experiments: PJAdK SAHdP RQ RB AFM WJH BD. Analyzed the data: PJAdK SAHdP JAK BD DMW NB. Contributed reagents/materials/analysis tools: DMW BD. Wrote the paper: PJAdK NB.

Chapter 7

Granzyme M targets host cell hnRNP K that is essential for human cytomegalovirus replication

R. van Domselaar[1], S.A.H. de Poot[1], E.B.M. Remmerswaal[2,3], K.W. Lai[1], I.J.M. ten Berge[3] and N. Bovenschen[1]

[1]Department of Pathology, University Medical Center Utrecht, Utrecht, The Netherlands
[2]Department of Experimental Immunology, Academic Medical Center, Amsterdam, The Netherlands
[3]Renal Transplant Unit, Department of Internal Medicine, Academic Medical Center, Amsterdam, The Netherlands

Cell Death Differ. 2013;20(3):419-29.

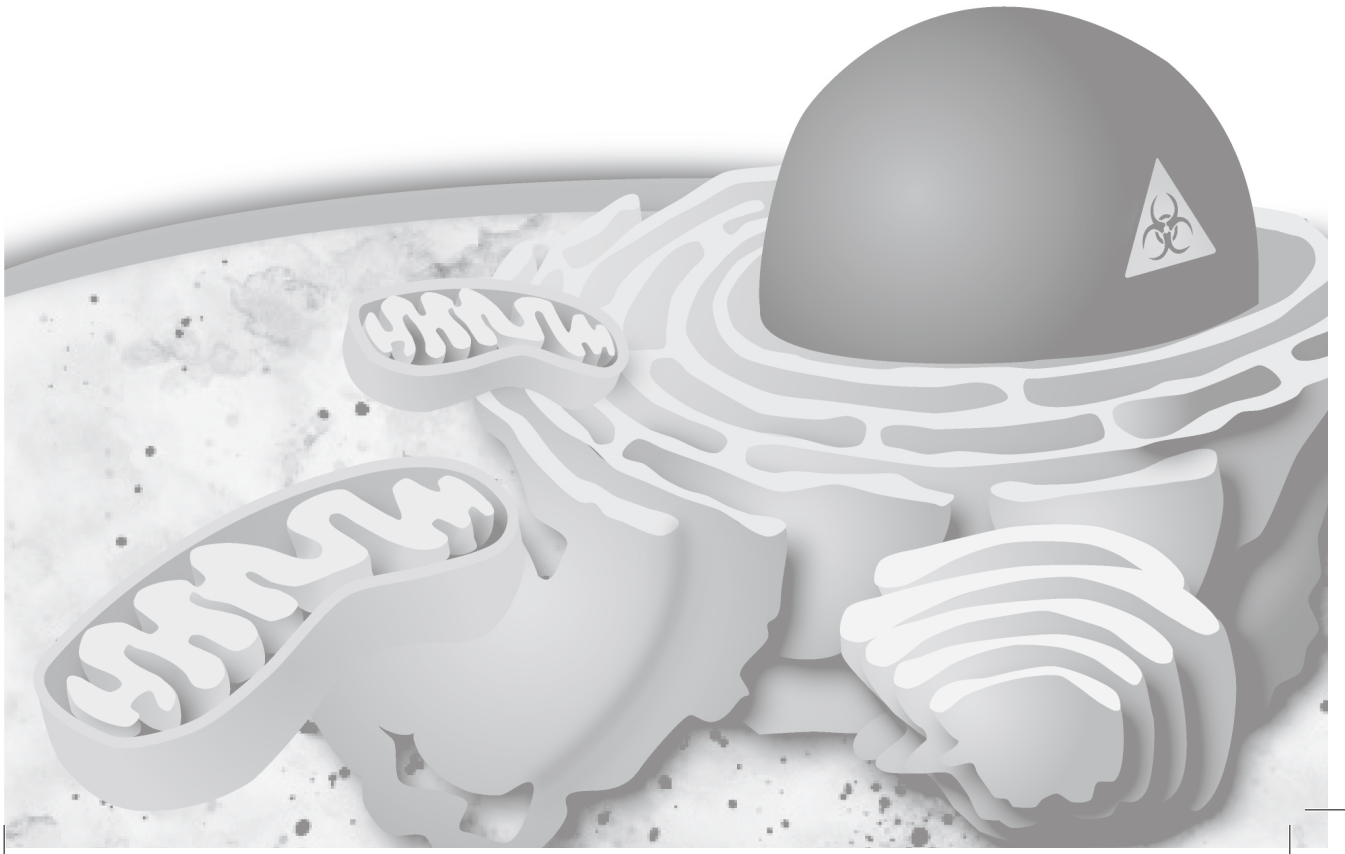

Abstract
Human cytomegalovirus (HCMV) is the most frequent viral cause of congenital defects and HCMV infection in immunocompromised patients may trigger devastating disease. Cytotoxic lymphocytes control HCMV by releasing granzymes towards virus-infected cells. In mice, granzyme M (GrM) plays a physiological role in controlling murine CMV infection. However, the underlying mechanism remains poorly understood. In the present study, we showed that human GrM was expressed by HCMV-specific $CD8^+$ T cells both in latently-infected healthy individuals and in transplant patients during primary HCMV infection. We identified host cell heterogeneous nuclear ribonucleoprotein K (hnRNP K) as a physiological GrM substrate. GrM most efficiently cleaved hnRNP K in the presence of RNA at multiple sites, thereby likely destroying hnRNP K function. Host cell hnRNP K was essential for HCMV replication not only by promoting viability of HCMV-infected cells but predominantly by regulating viral immediate-early 2 (IE2) protein levels. Furthermore, hnRNP K interacted with IE2 mRNA. Finally, GrM decreased IE2 protein expression in HCMV-infected cells. Our data suggest that targeting of hnRNP K by GrM contributes to the mechanism by which cytotoxic lymphocytes inhibit HCMV replication. This is the first evidence that cytotoxic lymphocytes target host cell proteins to control HCMV infections.

Keywords (3-6): cytomegalovirus, cytotoxic lymphocyte, granzyme M, hnRNP K, transplantation

Abbreviations: BSA, bovine serum albumin; GAPDH, glyceraldehyde 3-phosphate dehydrogenase; Gr, granzyme; HCMV, human cytomegalovirus; hnRNP K; heterogeneous nuclear ribonucleoprotein K; HFF, human foreskin fibroblast; HSV-1, herpes simplex virus-1; IE1, immediate-early 1; IE2, immediate-early 2; LAK, lymphokine-activated killer; MCMV, murine cytomegalovirus; MIEP, major immediate-early promotor; PBMCs, peripheral blood mononuclear cells; PBS, phosphate buffered saline; PI, propidium iodide; pp71, phosphoprotein 71; SLO, streptolysin O.

Introduction

Human cytomegalovirus (HCMV) is a widespread β-herpesvirus that infects the majority of the population. [263, 264] It is the most frequent viral cause of congenital defects. [263, 264] Primary HCMV infection induces a life-long latent infection in cells of the myeloid lineage with asymptomatic episodes of viral replication, which is controlled by a vigorous immune response. In the absence of an adequate immune response, however, HCMV can cause invasive disease with end-organ failure, morbidity, and mortality, *e.g.* after allogeneic stem cell or solid organ transplantation, or in HIV-infected patients. [263, 264] Treatment of HCMV infection is an urgent clinical problem. Vaccines against HCMV are not available and treatment by antiviral drugs has not definitively proven efficient to improve overall survival due to toxicity of antiviral agents and continual appearance of drug-resistant viruses. [263] Cellular anti-HCMV immunotherapy is now emerging as a promising alternative approach. [265] Understanding the mechanism by which our immune system counteracts HCMV infections could provide new possibilities for the development of novel (immuno)therapeutic antiviral strategies.

HCMV is the largest and most complex member of the human herpesvirus family. Activation of the HCMV major immediate-early promotor (MIEP) is central in controlling the latent state and essential for HCMV reactivation. During productive infection, the HCMV genome is expressed in a temporally coordinated cascade of transcriptional events that leads to expression of immediate-early, early, and late viral proteins. [266]

HCMV infection is controlled by cytotoxic lymphocytes, *i.e.* antigen-specific $CD8^+$ and $CD4^+$ αβT cells, γδT cells, and NK cells. [263, 267, 268] Cytotoxic lymphocytes produce interferon-γ to block HCMV replication, but most importantly release cytotoxic granules towards infected host cells. [8, 113, 114, 269] These granules contain the pore-forming protein perforin and a family of structurally homologous serine proteases called granzymes. While perforin facilitates entry of granzymes into infected cells, granzymes are believed to be the death executors during the antiviral immune response. In humans, five granzymes exist (GrA, GrB, GrH, GrK, GrM) that display distinct proteolytic substrate specificities. [29] Although all five human granzymes are able to induce cell death, evidence is emerging that granzymes also use noncytotoxic strategies to control virus replication. [64-68, 70]

In mice, GrM has been shown to be important for murine cytomegalovirus (MCMV) clearance. [62] We have recently discovered that human GrM can efficiently inhibit HCMV replication *in vitro* in the absence of host cell death. [70] GrM efficiently cleaves HCMV phosphoprotein 71 (pp71) and completely abolishes its function to transactivate the MIEP, [70] which is indispensable for effective HCMV replication. [71] In the present study, we addressed the possibility that GrM targets host cell proteins that HCMV hijacks for its own replication. We demonstrate that human GrM cleaves host cell protein heterogeneous nuclear ribonucleoprotein K (hnRNP K) that is essential for immediate-early 2 (IE2) protein translation and HCMV replication. This may provide a novel mechanism by which cytotoxic lymphocytes

mediate direct anti-HCMV activity.

Results

GrM is expressed in HCMV-specific CD8$^+$ T cells

GrM knockout mice are more susceptible to MCMV infections, indicating a role of GrM in CMV clearance at least in mice. [62] If GrM plays a major role in controlling HCMV infections in humans, one would expect that GrM is present in HCMV-specific cytotoxic lymphocytes. Therefore, we analyzed GrM expression in CD8$^+$ T cells of healthy human HCMV-seropositive individuals as well as in seronegative renal transplant recipients receiving a kidney from a HCMV-seropositive donor, followed by primary HCMV infections. First, pp65- and IE1-tetramer specific CD8$^+$ T cells – comprising both CD27$^-$ effector and CD27$^+$CD45RA$^-$ memory phenotypes – of a healthy HCMV-seropositive individual were analyzed (Figure 1a). Both pp65- and IE1-tetramer specific CD8$^+$ T cells expressed increased levels of GrM as compared to naive CD8$^+$ T cells (Figure 1b). A similar increase of GrM levels was observed in pp65-specific CD8$^+$ T cells from a second HCMV-seropositive (latently-infected) healthy individual (Suppl. figure 1). Increased GrM protein levels were not restricted to HCMV-specific CD8$^+$ T cells, since EBV- and influenza-specific CD8$^+$ T cells also contained higher GrM protein levels (Suppl. figure 1). Second, GrM protein expression was analyzed longitudinally in HCMV-specific CD8$^+$ T cells from a HCMV-seronegative renal transplant recipient of a HCMV-seropositive donor, who experienced a primary HCMV infection (Figure 1c). IE1-specific effector CD8$^+$ T cells appeared around the peak of the viral load and expressed increased levels of GrM as compared to naive CD8$^+$ T cells. After cessation of the viral load, there was an increase in percentage of CD8$^+$CD27$^-$ T cells within the IE1-specific CD8$^+$ T cell compartment, which also coincided with an increase in GrM expression in these cells as compared to the naive CD8$^+$ T cell pool. The percentage of circulating GrM-expressing IE1-specific CD8$^+$CD27$^-$T cells reached a peak after one year post-transplantation and these cells were maintained for at least five years. Maintenance of CD8$^+$CD27$^-$ T cells, known as vigilant resting effector cells, is characteristic for latent HCMV infections. [268, 270] Identical results were obtained when pp65-specific CD8$^+$ T cells were analyzed longitudinally in a second renal transplant patient (Suppl. figure 2). Collectively, these data indicate for the first time that HCMV-reactive CD8$^+$ T cells not only express GrM but also show elevated levels of GrM as compared to naive CD8$^+$ T cells, both in HCMV-seropositive healthy individuals and in the peripheral blood of seronegative renal transplant recipients in response to primary HCMV infection. Furthermore, GrM-positive HCMV-reactive CD8$^+$ T cells are maintained in the blood during latency. This supports the concept of an active antiviral role of GrM in HCMV infection and HCMV reactivation in humans.

GrM targets host cell protein hnRNP K

To investigate the mechanism by which GrM inhibits HCMV replication, we addressed the possibility that GrM targets host cell proteins that are required for efficient HCMV

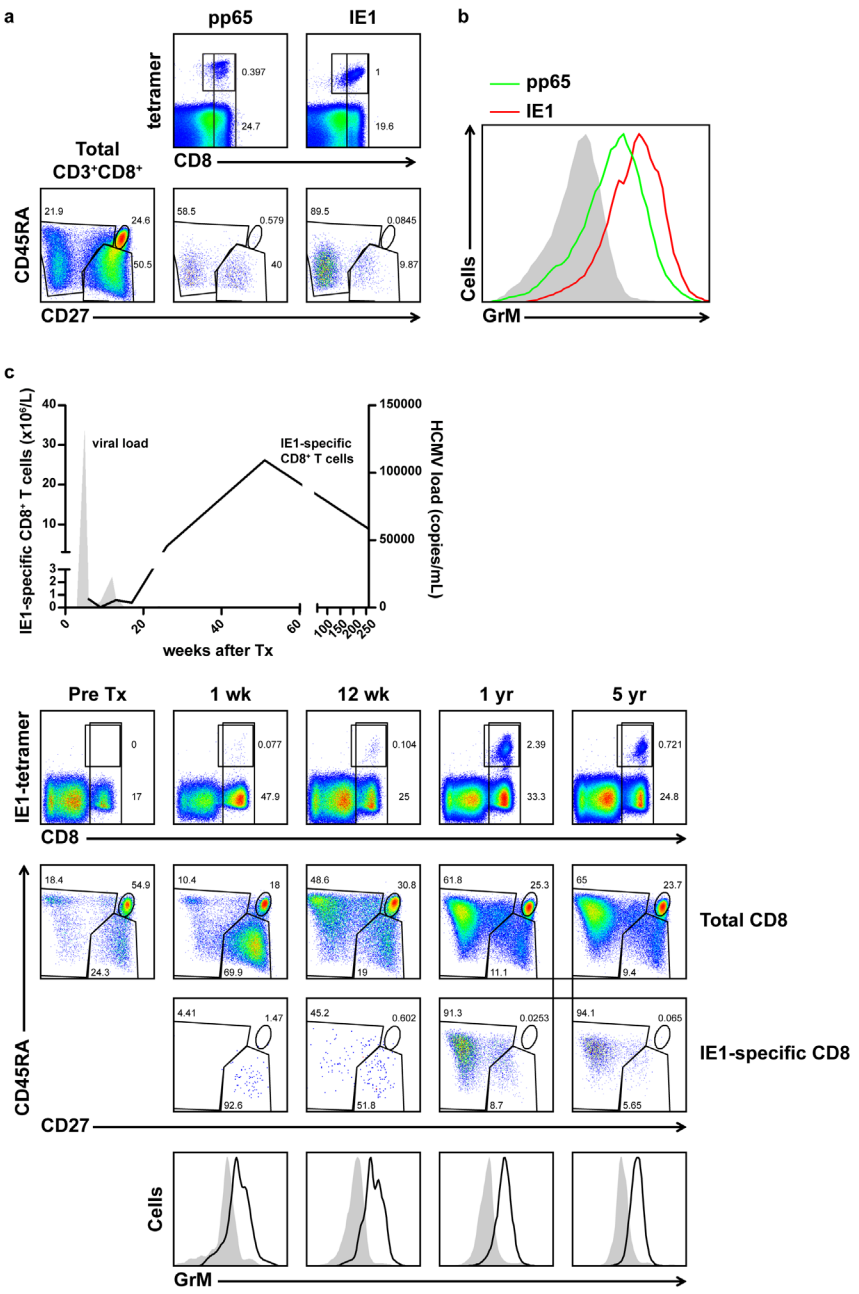

Figure 1. GrM is expressed in HCMV-specific CD8⁺ T cells. (a) FACS plots show the expression of CD8 and HCMV-specific pp65 and IE1 tetramers on CD3⁺ T cells (upper row) or the expression of CD27 and CD45RA (bottom row) on total CD3⁺CD8⁺ T cells (left) or HCMV-specific CD3⁺CD8⁺ T cells (middle, right). **(b)** FACS histogram visualizes the relative intracellular GrM protein levels in naive CD3⁺CD8⁺ T cells (filled gray) and HCMV-specific CD3⁺CD8⁺ T cells (lines). **(c)** PBMCs were isolated from a renal transplant patient pre- and post-transplantation. Graph depicts kinetically the absolute numbers of IE1-specific CD3⁺CD8⁺ cells (line) and HCMV viral load (filled gray). FACS plots show the expression of CD8 and IE1 tetramers on CD3⁺ T cells (upper row), and CD27 and CD45RA on total or IE1-specific CD3⁺CD8⁺ T cells (middle rows). Histograms (bottom row) visualize the relative intracellular GrM protein levels in naive CD3⁺CD8⁺ T cells (filled gray) and IE1-specific CD3⁺CD8⁺ T cells (line).

replication. Recently, we have employed multiple proteomic approaches to identify potential macromolecular cellular substrates of GrM.[30] Both gel-based (2D-DIGE) (Figure 2a) and complementary positional (cofradic) proteomics have identified heterogeneous ribonucleoprotein K (hnRNP K) as potential GrM substrate. [30]

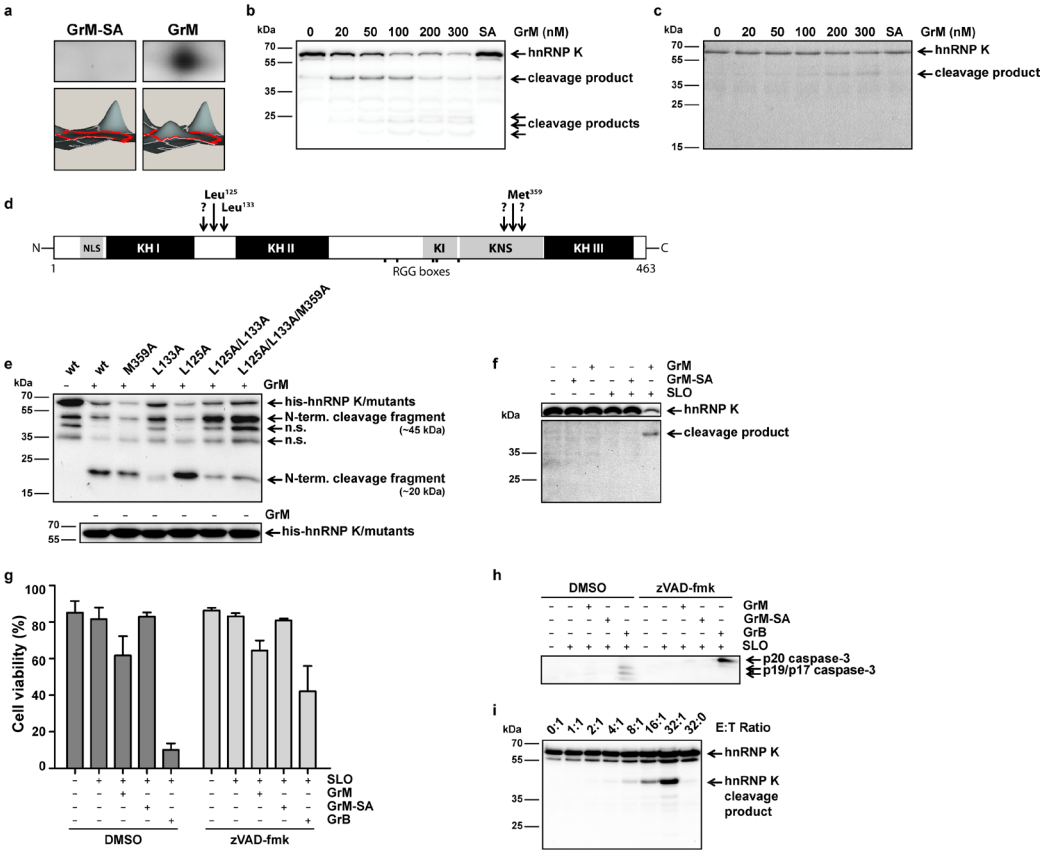

Figure 2. GrM cleaves host cell protein hnRNP K. (a) HeLa cell lysates were incubated with GrM (1 µM) or GrM-SA (1 µM) for 1 h at 37°C and then subjected to 2D-DIGE. A representative protein spot that is identified by MS as a cleavage fragment of hnRNP K is depicted. **(b)** Jurkat lysates (5 µg) were incubated with increasing concentrations of GrM or GrM-SA (300 nM) for 4 h at 37°C and immunoblotted for hnRNP K. **(c)** Purified His-hnRNP K (1.5 µg) was incubated with increasing concentrations of GrM or GrM-SA (300 nM) for 16 h at 37°C and subjected to SDS PAGE. Proteins were stained with InstantBlue. **(d)** Schematic overview of GrM cleavage sites within hnRNP K (NLS, nuclear localization signal; KH, K homology domain; KI, K interactive region; KNS, K nuclear shuttling signal; RGG, arginine-glycine-glycine). **(e)** HeLa cells were transfected with His-tagged hnRNP K wild-type (wt) or mutant expression plasmids and lysed two days post transfection. Expression of recombinant proteins was determined by subjecting untreated lysates to immunoblotting using anti-6xHis antibody (bottom panel). Lysates were incubated with 300 nM GrM or left untreated for 4 h at 37°C and immunoblotted using anti-6xHis antibody (upper panel). (n.s., non-specific). **(f)** HFFs were incubated with GrM (2.8 µM) or GrM-SA (2.8 µM) in the presence or absence of SLO (2 µg/mL) for 16 h at 37°C. Lysates were immunoblotted for hnRNP K. **(g)** HFFs were incubated with GrM (1 µM), GrM-SA (1 µM), GrB (100 nM), or left untreated in the presence or absence of SLO (1 µg/mL) with or without zVAD-fmk (100 µM) for 16 h at 37°C**.** Cell viability was assessed by staining cells with annexin-V-FLUOS and PI followed by flow cytometry analysis. Annexin-V and PI double negative cells were considered to be viable. Bars represent the mean ± SD of three independent experiments. **(h)** HFFs were incubated with GrM (1 µM), GrM-SA (1 µM), GrB (100 nM), or left untreated in the presence or absence of SLO (1 µg/mL) with or without zVAD-fmk (100 µM) for 16 h at 37°C**.** Cells were lysed and immunoblotted using antibodies against active caspase-3 (D175). **(i)** HFFs were challenged with increasing effector:target (E:T) ratios of LAK cells for 4 h at 37°C. Lysates were subjected to immunoblotting using hnRNP K antibodies. Data depicted are representative for at least two independent experiments.

We focused on hnRNP K because it has been shown to play a role in Herpes Simplex Virus-1 (HSV-1) and Hepatitis B Virus replication. [271, 272] To validate hnRNP K cleavage by GrM, cell lysates were incubated with increasing concentrations of GrM or catalytically inactive control GrM-SA. Cleavage of hnRNP K by GrM was apparent with a decrease of full-length hnRNP K (~62 kDa) and the appearance of a clear ~45 kDa cleavage product and several smaller cleavage fragments, using an antibody directed against the mid-region of hnRNP K (Figure 2b). GrM also cleaved purified recombinant His-hnRNP K with the appearance of the ~45 kDa fragment (Figure 2c), indicating that GrM directly cleaves hnRNP K. Using complementary positional proteomics, we identified at least three GrM cleavage sites in hnRNP K, *i.e.* Leu^{125}, Leu^{133}, and Met^{359} (Figure 2d). [30] We mutated Leu^{125}, Leu^{133}, Met^{359}, or combinations into Ala and we evaluated these mutants in cellular lysates for GrM cleavage using immunoblotting with an anti-His antibody to detect the hnRNP K N-terminus (Figure 2e). Cleavage of wild-type hnRNP K resulted in a decrease of full-length hnRNP K and the appearance of a ~20 kDa N-terminal cleavage fragment. The hnRNP K^{L133A} single mutant, hnRNP $K^{L125A/L133A}$ double mutant, and hnRNP $K^{L125A/L133A/M359A}$ triple mutant showed no ~20 kDa cleavage fragment, but did show an N-terminal ~45 kDa cleavage fragment upon GrM treatment. This indicates that Leu^{133} is an important GrM cleavage site in hnRNP K. However, GrM was still able to cleave all hnRNP K mutants, indicating that other GrM cleavage sites exist in hnRNP K other than Leu^{125}, Leu^{133}, and Met^{359}. First, GrM cleavage of hnRNP K^{L133A}, hnRNP $K^{L125A/L133A}$, and hnRNP $K^{L125A/L133A/M359A}$ mutants showed a cleavage fragment that migrated 1-2 kDa below the ~20 kDa band (Figure 2e), indicating at least one additional GrM cleavage site N-terminal of Leu^{125} (Figure 2d). Second, the hnRNP $K^{L125A/L133A/M359A}$ triple mutant still showed accumulation of the N-terminal ~45 kDa cleavage fragment, indicating at least one additional GrM cleavage site in close proximity to Met^{359} (Figure 2e). Thus, hnRNP K proteolysis by GrM is complex in that GrM cleaves hnRNP K after at least five independent sites that are clustered in two apparent proteolysis-sensitive hot spots (Figure 2d). Next, human foreskin fibroblasts (HFFs) were incubated with purified GrM or GrM-SA in the presence or absence of perforin-analog streptolysin O (SLO). Whereas hnRNP K remained unaffected in all control settings, it was cleaved when cells were incubated with both GrM and SLO with the concomitant appearance of at least the ~45 kDa hnRNP K cleavage fragment (Figure 2f). GrM induced minor cell death in HFFs (Figure 2g), which was not affected by the pan-caspase inhibitor zVAD-fmk and virtually no pro-caspase 3 activation was observed (Figure 2g,h). GrB did trigger efficient cell death in HFFs with pro-caspase-3 activation (Figure 2g,h). HnRNP K cleavage was also observed when living HFFs were challenged with living lymphokine-activated killer (LAK) cells (Figure 2i). No decrease in full-length hnRNP K was observed due to the presence of endogenous hnRNP K in LAK cells that were present in analyzed cellular lysates. Taken together, these data indicate that hnRNP K is directly cleaved by GrM and targeted during cytotoxic lymphocyte-mediated attack.

RNA promotes GrM-mediated cleavage of hnRNP K

Cleavage of hnRNP K by GrM was more efficient in cell lysates (Figure 2b) as compared to recombinant purified hnRNP K (Figure 2d), suggesting that cellular factors contribute to this proteolysis. Because hnRNP K is an RNA-interacting protein, [273, 274] the effects of RNA on GrM-mediated hnRNP K cleavage were examined. Cell lysates were pre-incubated with or without RNase followed by GrM treatment. Immunoblot analysis showed that hnRNP K was less efficiently cleaved by GrM when lysates were pre-incubated with RNase, whereas RNase had no effect on the cleavage of GrM substrate α-tubulin (Figure 3a). RNase did not affect the proteolytic activity of GrM itself as determined by the small synthetic chromogenic substrate AAPL-pNA (data not shown). Consistent with this finding, purified His-hnRNP K was more efficiently cleaved by GrM when pre-incubated with RNA (Figure 3b). These data suggest that GrM cleaves hnRNP K more efficiently in its functional RNA-bound conformation.

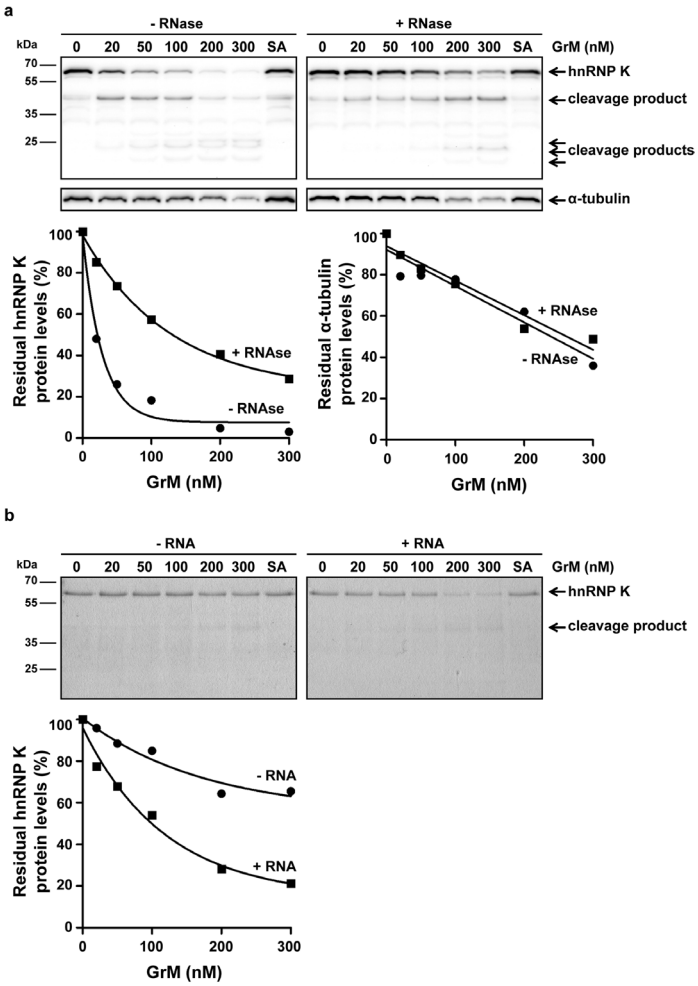

Figure 3. GrM cleaves hnRNP K more efficiently in the presence of RNA. (a) Jurkat cell lysates were pre-treated with RNase (100 µg/mL) or left untreated for 30 min at 37°C followed by incubations with increasing concentrations of GrM or GrM-SA (300 nM) for 4 h at 37°C and immunoblotted for hnRNP K or α-tubulin (upper panel). Band intensities were quantified and depicted in graphs (lower panel). **(b)** Purified His-hnRNP K (1.5 µg) was pre-treated with RNA (100 ng) or left untreated followed by incubations with increasing concentrations of GrM or GrM-SA (300 nM) for 16 h at 37°C. Samples were subjected to SDS PAGE and gels were stained with InstantBlue (upper panel). Band intensities were quantified and depicted in graphs (lower panel). Data depicted are representative for at least two independent experiments.

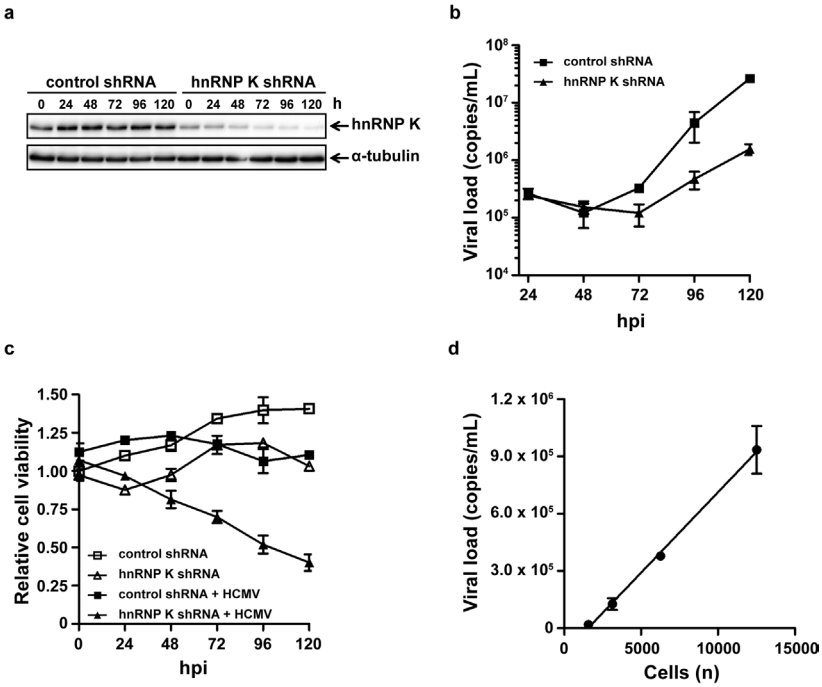

Figure 4. HnRNP K is essential for HCMV replication. (a) HFFs were transduced with hnRNP K-specific or control shRNA and lysed at different time points. Lysates were subjected to immunoblotting using antibodies against hnRNP K or α-tubulin (loading control). **(b)** HnRNP K-deficient and control HFFs were infected with HCMV and viral load in supernatants at different time points was assessed by quantitative PCR. **(c)** Cell viability of uninfected or HCMV-infected transduced HFFs was determined by WST-1 assay and relative cell viability of uninfected control shRNA-treated cells at 0 hpi was set to 1. **(d)** HFFs were seeded at different cell densities and infected with HCMV at a multiplicity of 1.0 plaque-forming unit per cell. Viral load in supernatants at 96 hpi was assessed by quantitative PCR and a linear regression curve was plotted. Data depicted represent the mean ± SD of triplicates.

HnRNP K is required for efficient HCMV replication

The role of hnRNP K during HCMV replication is unknown. To investigate this, we downregulated hnRNP K protein levels in HFFs (Figure 4a), infected these cells with HCMV, and viral replication was kinetically determined by quantifying HCMV viral load in supernatants. The viral load was 10-17 fold decreased in hnRNP K-deficient HFFs as compared to control HFFs (Figure 4b), indicating that hnRNP K is required for efficient HCMV replication. This dramatic decrease in viral load in hnRNP K-deficient HFFs was accompanied with a slow decrease in cell viability (up to 2-3 fold) (Figure 4c). Quite remarkable is the observation that cell viability is only decreased in HCMV-infected cells but not in uninfected hnRNP K-deficient cells, suggesting that hnRNP K is important in coping with cell survival after stress induced by HCMV infection. Since there is a linear correlation between the number of cells and viral load (Figure 4d), the observed 2-3 fold decrease in cell viability does not explain the major decrease in viral load (10-17 fold) when hnRNP K protein levels are downregulated. These data indicate that hnRNP K is required for efficient HCMV replication, predominantly in a host cell death-independent manner.

HnRNP K regulates IE2 translation

The temporally controlled expression of HCMV proteins during viral replication allows us to determine at which stage of the HCMV viral life cycle hnRNP K is involved. Lysates of HCMV-infected hnRNP K-deficient and control HFFs were immunoblotted for several HCMV proteins. Interestingly, the 86 kDa IE2 but not the 72 kDa immediate-early 1 (IE1) protein level was dramatically reduced in HCMV-infected HFFs when hnRNP K was downregulated (Figure 5a). Furthermore, a slight if any reduction in early HCMV proteins pp65 and pp71 as well as a dramatic reduction of the late HCMV protein pp28 were observed in hnRNP K-deficient HFFs. However, these latter effects likely are the functional consequence of decreased IE2 protein levels. These data indicate that hnRNP K plays a dominant role during the initial immediate-early phase of HCMV replication by regulating IE2 but not IE1 protein expression.

In view of the importance of IE2 as an absolutely indispensable protein in HCMV replication, [275, 276] we further examined the mechanism by which hnRNP K regulates IE2 protein levels. First, we investigated the transcriptional activity of hnRNP K towards the MIEP, which regulates IE2 gene (*UL122*) expression. In contrast to control pp71, no transcriptional activity of hnRNP K towards the MIEP was detected in a luciferase MIEP reporter assay (Figure 5b). In line with this observation, IE2 mRNA levels were similar between hnRNP K-deficient and control HFFs after HCMV infection at 8 hpi (Figure 5c), 24 hpi and 72 hpi (data not shown). These data indicate that hnRNP K does not regulate IE2 protein levels via transcription of the *UL122* gene or promoting IE2 mRNA stability. Second, besides the 86 kDa IE2 protein, there are two alternatively unspliced IE2 variants of 60 and 40 kDa, each regulated by its own promoter. [277, 278] Protein levels of all three IE2 protein variants were decreased when hnRNP K was downregulated (Figure 5d), further suggesting that hnRNP K regulates IE2 protein levels at the post-transcriptional level. Third, we investigated whether hnRNP K is required for IE2 protein stability by using the chemical compound MG132, a proteasome inhibitor that does not affect IE gene expression. [279] MG132 failed to restore IE2 protein levels in HCMV-infected hnRNP K-deficient HFFs (Figure 5e), indicating that hnRNP K does not protect IE2 protein from proteasomal degradation. Finally, since hnRNP K is an RNA-binding protein, we addressed the possibility that hnRNP K interacts with IE2 mRNA. Purified His-tagged hnRNP K or unrelated control His-β-tubulin was incubated with lysates of HCMV-infected HFFs followed by pull-down of His-tagged proteins (inset of Figure 5f). Interestingly, hnRNP K pull-down resulted in a clear enrichment of IE2 mRNA whereas no enrichment was observed for viral mRNAs IE1 and UL54 and host cell mRNA GAPDH, or when His-β-tubulin was used (Figure 5f). These data suggest that hnRNP K specifically binds to IE2 mRNA, pointing to a role of hnRNP K during IE2 translation.

GrM reduces IE2 protein expression during HCMV infection

The diverse functions of hnRNP K require both nuclear and cytoplasmic localization

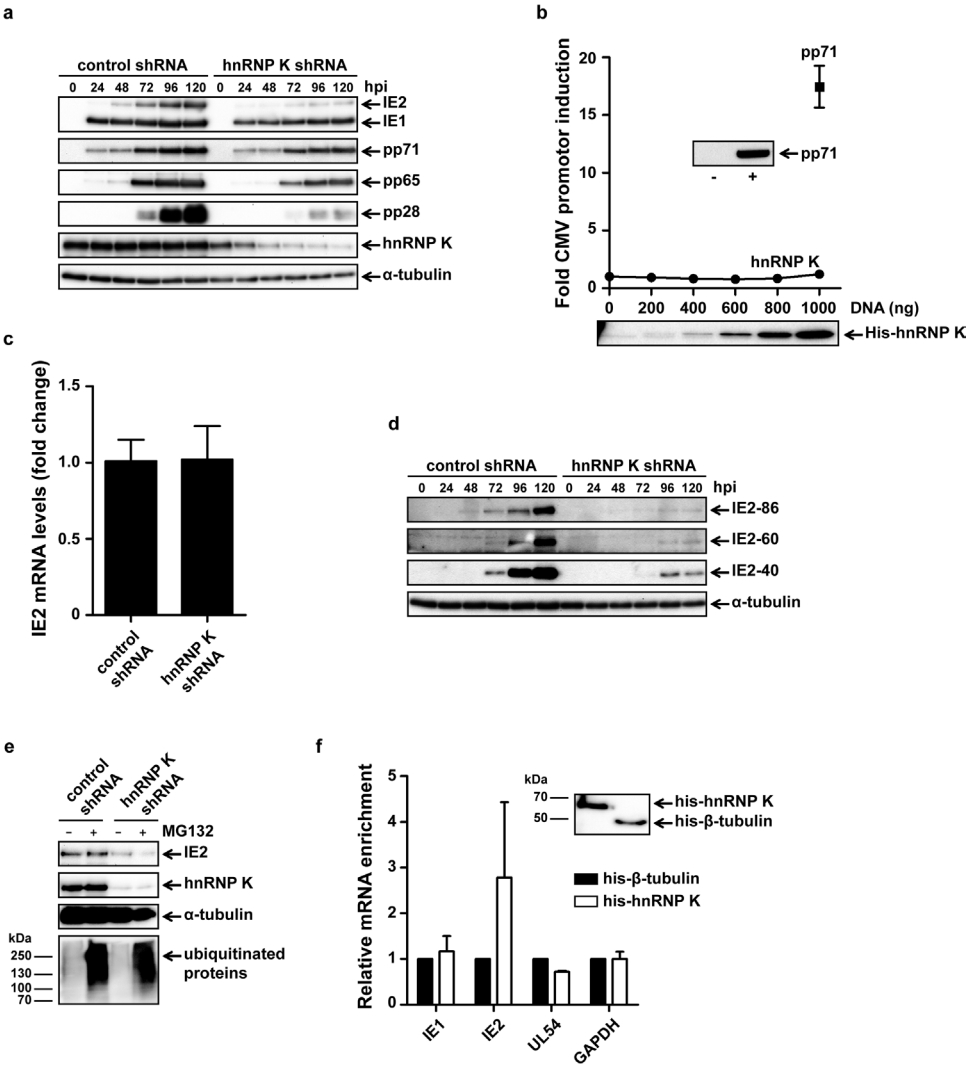

Figure 5. **HnRNP K regulates IE2 protein expression. (a)** HFFs were transduced with hnRNP K-specific or control shRNA, infected with HCMV, and lysed at different time points. Lysates were subjected to immunoblotting using antibodies against IE1/2, pp71, pp65, pp28, hnRNP K, and α-tubulin. **(b)** HeLa cells were co-transfected with pGL3-SV40 (50 ng), pRL-CMV (10 ng), complemented with pCGN-71 vector (1 µg) or pSG5-His-hnRNP K and pcDNA3.1^{+} vector (1 µg total DNA). Cells were lysed 48 h post-transfection, and luciferase activity was assessed. Relative luciferase activity is represented as fold CMV promoter (MIEP) induction. Lysates used in the luciferase reporter assay were subjected to immunoblotting using an anti-pp71 or anti-6xHis antibody. **(c)** HCMV-infected hnRNP K-deficient and control HFFs were lysed 8 hpi and mRNA was isolated and subjected to reverse transcriptase PCR and quantitative PCR using IE2- and GAPDH-specific primers and probes. Relative IE2 mRNA levels were normalized for GAPDH mRNA levels and the mean from control cells was set at 1. **(d)** HCMV-infected transduced HFFs were lysed at different time points and immunoblotted for the C-terminus of IE2 or α-tubulin. **(e)** HCMV-infected hnRNP K-deficient and control HFFs were treated with MG132 (250 nM) or left untreated at 48 hpi and lysed at 72 hpi. Lysates were subjected to immunoblotting using antibodies against IE2, hnRNP K, α-tubulin, and ubiquitin. Data depicted are representative for triplicate experiments. **(f)** HCMV-infected HFFs were lysed 72 hpi and incubated with His-hnRNP K or His-β-tubulin as a negative control for 16 h at 4°C. Immunoprecipitation of His-tagged proteins was followed by isolation of mRNA, reverse transcriptase PCR, and quantitative PCR using specific primers and probes against *UL123* (IE1), *UL122* (IE2), *UL54*, and *GAPDH*. The mean mRNA levels from His-β-tubulin control samples for each mRNA were set to 1 and all samples were normalized for GAPDH mRNA levels. Bars represent the mean ± SD of triplicates. *Inset*, samples after immunoprecipitation were subjected to immunoblotting using anti-6xHis antibody..

and bidirectional shuttling. Viruses can enrich hnRNP K in a specific subcellular compartment in favor of the replication of the virus. [272, 280] In uninfected HFFs, hnRNP K was predominantly localized in the cytoplasm (Figure 6a, upper panels). After infection with HCMV, HFFs showed typical rounded morphology and hnRNP K predominantly remained cytoplasmic (Figure 6a, bottom panels). Thus, during HCMV infection hnRNP K is located at the site where IE2 mRNA translation occurs. Previously, we demonstrated that GrM can inhibit HCMV replication independent of host cell death. [70] Our findings that GrM cleaved hnRNP K (Figure 2), that hnRNP K interacted with IE2 mRNA (Figure 5g), and that hnRNP K downregulation dramatically reduced IE2 protein expression during HCMV infection (Figure 5a), prompted us to investigate whether GrM-treatment of HCMV-infected fibroblasts affects IE2 protein expression. Indeed, immunoblot analysis showed a clear decrease in IE2 protein levels when HCMV-infected fibroblasts were treated with GrM/SLO as compared to control GrM-SA/SLO treatment (Figure 6b). The decrease in IE2 protein levels correlated with decreased viral loads (Figure 6c) and little cell death (Figure 6d) in GrM-treated HCMV-infected fibroblasts. These data indicate that GrM reduces IE2 protein expression to inhibit HCMV replication.

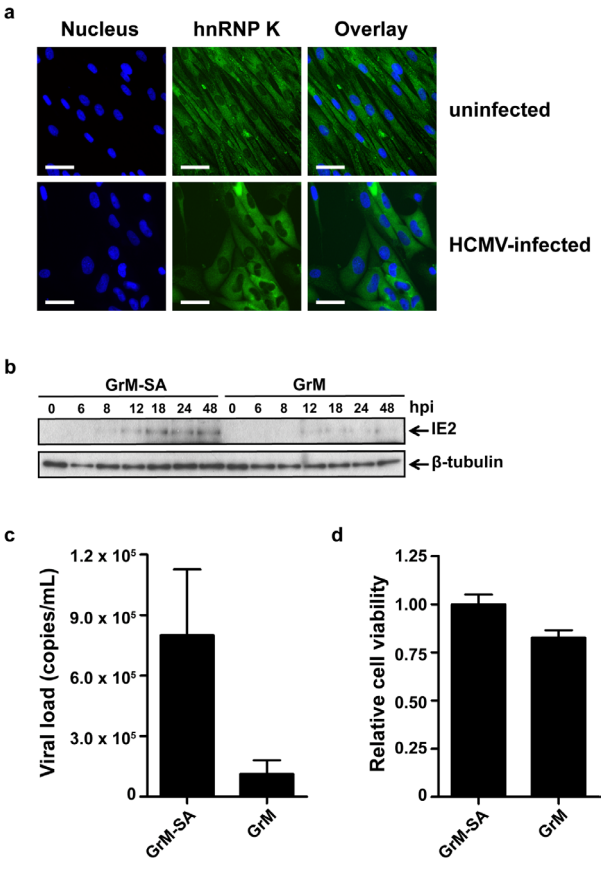

Figure 6. HnRNP K localization and GrM-mediated decrease of IE2 protein expression. (a) Immunofluoresence images of uninfected (upper panel) and HCMV-infected (lower panel) HFFs at 72 hpi. Nuclei are stained blue and hnRNP K is visualized in green. Bars, 50 µm. **(b)** HCMV-infected fibroblasts were treated with GrM-SA (500 nM) or GrM (500 nM) in the presence of SLO (1 µg/mL) at 2 hpi and cells were lysed at indicated time points. Lysates were subjected to immunoblotting using antibodies against IE2 or β-tubulin. Data depicted are representative of at least two independent experiments performed in triplicates. **(c)** HCMV-infected fibroblasts were incubated with GrM (500 nM) or GrM-SA (500 nM) in the presence of SLO (1 µg/mL) at 2 hpi. HCMV viral load in supernatants at 72 hpi was assessed by quantitative PCR. Bars represent the mean ± SD of triplicates. **(d)** HCMV-infected fibroblasts were incubated with GrM (500 nM) or GrM-SA (500 nM) in the presence of SLO (1 µg/mL) at 2 hpi. Relative cell viability at 24 hpi was assessed by WST-1 assay. Bars represent the mean ± SD of triplicates.

Discussion

The granule exocytosis pathway is a crucial mechanism that cytotoxic lymphocytes use to control virus infections. The physiological importance of GrM as an antiviral mediator has been demonstrated in GrM-deficient mice, which are more susceptible to MCMV infections. [62] However, both murine GrM and MCMV have been largely diverged from their human counterparts, [30, 264] emphasizing that caution is essential when extrapolating data from mice to humans. In the present study, we demonstrated for the first time that human GrM is expressed in HCMV-specific $CD8^+$ T cells after primary infection and during latency (Figure 1). HCMV-specific $CD8^+CD27^-$ T cells, so called vigilant resting effector T cells, are proposed to act in response to reactivation and to maintain HCMV latency. [268, 270] Interestingly, accumulation of these vigilant resting effector cells after primary HCMV infection coincided with increased GrM protein expression in these HCMV-specific $CD8^+$ T cells (Figure 1). This supports a model in which GrM actively mediates an antiviral function in HCMV infections *in vivo*. In this study, we demonstrated that GrM cleaved hnRNP K and that hnRNP K was required for efficient HCMV replication by promoting cell viability in virus-infected cells and more importantly by regulating IE2 protein expression (Figures 2-5). This provides the first evidence that GrM targets a host cell protein that is hijacked by HCMV and that is critical for its replication. Apart from HCMV, GrM protein levels were also elevated in EBV- and influenza-specific $CD8^+$ T cells (Suppl. figure 1), pointing to an antiviral role of GrM in a broad range of viral infections.

A previous study has shown that hnRNP K is important for the egress of HSV-1. [272] In HCMV infection, however, hnRNP K appears to play a different role. Knockdown of hnRNP K not only limited HCMV replication but also decreased cell viability in HCMV-infected but not in uninfected fibroblasts (Figure 4). The latter finding suggests that hnRNP K is required for cell survival only following HCMV infection. However, host cell death only partly explains the dramatic reduction in HCMV replication in hnRNP K-deficient fibroblasts. More importantly, decreased viral load was accompanied with markedly reduced IE2 but not IE1 protein levels in hnRNP K-deficient HCMV-infected fibroblasts (Figure 5). IE2 is absolutely indispensable for HCMV replication. [275, 276] Therefore, we explored how hnRNP K regulates IE2 protein levels. As a multifunctional protein, hnRNP K is involved in many biological processes, including transcription, mRNA splicing, translation, and protein signaling. [273] The decrease of IE2 protein levels in hnRNP K-deficient fibroblasts is most likely the result of decreased IE2 mRNA translation, because hnRNP K did not affect transcription of the IE2 gene nor IE2 mRNA and protein stability, but rather bound IE2 mRNA (Figure 5). This is compatible with the previous observation that hnRNP K binds to and thereby regulates translation of the mRNA of cytoskeleton genes and myelin basic protein. [281, 282]

Binding of hnRNP K to RNA is mediated by three KH domains within hnRNP K that act synergistically to provide both high affinity binding and specificity (Figure 2). [273, 274] Hence, loss of only a single KH domain dramatically reduces the RNA binding

capacity of hnRNP K. [274] GrM cleaved hnRNP K at least at five independent sites, including.Leu^{125}, Leu^{133}, and Met^{359}, that are located in two apparent proteolysis-sensitive hot spots, thereby dissecting the functional KH domains (Figure 2). This strongly suggests that GrM abrogates the ability of hnRNP K to bind to IE2 mRNA, resulting in reduced IE2 protein expression and reduced HCMV replication. It should be mentioned that hnRNP K was more efficiently cleaved by GrM in the presence of RNA (Figure 3). This suggests that the conformational change of hnRNP K after binding to RNA allows for efficient proteolysis by GrM or that RNA facilitates the interaction between hnRNP K and GrM. In this model, the functional interaction between hnRNP K protein and IE2 mRNA promotes the antiviral activity of GrM to cleave hnRNP K.

Previously, we have demonstrated that GrM cleaves and inactivates the HCMV tegument protein pp71, [70] which is essential for IE protein expression and effective HCMV replication. [71] In the present study, we demonstrated that GrM also targets a host cell substrate (hnRNP K) that plays a major role in HCMV replication and is necessary for efficient IE2 protein expression (Figures 5-6). Apparently, cytotoxic lymphocytes and GrM target the initial IE machinery that HCMV requires for both lytic replication and reactivation from latency. Since viruses highly depend on the transcription/translation machinery of the host cell, it could be possible that other hnRNPs also play a role in viral infections and are also cleaved by GrM. Indeed, several proteomic screens have identified hnRNP A1, A2/B1, C1/C2, E1, M, and U as potential GrM substrates. [30, 45] Interestingly, many members of the hnRNP protein family have also been identified as potential substrates of other granzymes than GrM. [124, 138, 196, 283] Further studies are needed to validate these findings in the context of an antiviral immune response.

It remains an intriguing question why GrM targets viral pp71 [70] and host cell hnRNP K to attack the initial immediate-early events of HCMV replication rather than just killing HCMV-infected cells. Consistent with our findings, IE1- and pp65-specific CD4$^+$ T cells and CD8$^+$ T cells can recognize and kill IE1 and pp65 peptide-loaded target cells but fail to induce cell death in HCMV-infected target cells after recognition and degranulation, whereas HCMV replication is efficiently inhibited [284, 285] (Personal communication: Dr. M.R. Wills, Dept. of Medicine, University of Cambridge, United Kingdom). This apparently noncytotoxic mechanism to block HCMV replication might be an important pathway to prevent HCMV reactivation from latency and to preserve latently infected CD34$^+$ hematopoietic progenitor cells. This model is compatible with the recent finding that antigen-specific CD8$^+$ T cells recognize HSV-1 latently-infected ganglion cells, release GrB towards these cells, and inhibit HSV-1 reactivation without inducing cell death. [65]

Materials and Methods

Subjects

Two healthy HCMV-seropositive volunteers (HLA-B7$^+$, HLA-B8$^+$ and/or HLA-A2$^+$) and two HCMV-seronegative renal transplant recipients who received a kidney from a

HCMV-seropositive donor (HLA-B8$^+$ and HLA-A2$^+$) were included in this study. Both patients received immunosuppressive therapy (consisting of CD25mAb induction therapy followed by prednisolone, mycophenolate mofetil, and tacrolimus), experienced primary HCMV infection, and had no acute cellular rejection episodes. Patients gave written informed consent, and the study was approved by the medical ethics committee of the Academic Medical Center (Amsterdam, The Netherlands). Peripheral blood mononuclear cells (PBMCs) were isolated from heparinized blood and subsequently cryopreserved until flow cytometry analysis. HCMV viral load was determined in EDTA-treated blood by quantitative PCR.

Flow cytometry stainings

PBMCs were washed in phosphate buffered saline (PBS) containing 0.01% NaN_3 and 0.5% bovine serum albumin (BSA). PBMCs (2 x 10^6) were incubated with an appropriate concentration of APC-conjugated tetrameric complexes for 30 min at 4°C. For analysis of surface marker expression, cells were incubated with fluorescence-labeled monoclonal antibodies for 30 min at 4°C at concentrations according to the manufacturer's instructions. After tetramer and surface marker stainings, cells were fixed (FACS Lysing Solution, BD Biosciences) and permeabilized (FACS Permeabilizing Solution 2, BD Biosciences) followed by incubation with Alexa Fluor 488-conjugated anti-GrM (1.2 µg/mL) for 30 min at 4°C to stain intracellular GrM. Live/Dead Fixable Red Dead Cell Stain Kit (Invitrogen) was used to exclude dead cells from all analysis. Cells were measured on a LSR-Fortessa flow cytometer (BD Biosciences) and analyzed with FlowJo software (FlowJo). APC-conjugated tetrameric complexes were obtained from Sanquin: HLA-B0702 tetramer loaded with the HCMV pp65-derived TPRVTGGGAM peptide, HLA-B0801 tetramer loaded with the HCMV IE1-derived QIKVRVDMV peptide, HLA-B0801 tetramer loaded with the HCMV IE-1 derived ELRRKMMYM peptide, HLA-A0201 tetramer loaded with the HCMV pp65-derived NLVPMVATV peptide, HLA-B0801 tetramer loaded with the EBV EBNA3A-derived FLRGRAYGL peptide, HLA-B0801 tetramer loaded with the EBV BZLF1-derived RAKFKQLL peptide, and HLA-A0201 tetramer loaded with the influenza matrix protein (FLU MP)-derived GILGFVFTL peptide. The following antibodies were obtained from commercial sources: CD3-V500, and CD8-V450, (BD Biosciences); CD45RA eFluor 605NC (eBioscience Inc.); and CD27 APC-Alexa Fluor 750 (Invitrogen). Alexa Fluor 488-conjugated anti-GrM (clone 4B2G4) was generated as described previously.[38]

Cell culture and cell-free protein lysates

Cells were cultured in a 5% CO_2 atmosphere at 37°C. Human foreskin fibroblasts (HFFs), HEK293T and HeLa cells were maintained in Dulbecco's modified Eagle medium (DMEM, Gibco) supplemented with 10% fetal calf serum, 100 units/mL penicillin and 100 µg/mL streptomycin (Invitrogen). Jurkat cells were maintained in RPMI 1640 medium supplemented with 10% fetal calf serum, sodium bicarbonate (Gibco), 100 units/mL penicillin and 100 µg/mL streptomycin (Invitrogen). Cell-free

protein lysates were generated by washing cells three times in PBS and subsequent lysis by three cycles of freeze-thawing in PBS. Samples were centrifuged at 18,000 x g for 10 min at 4°C and protein concentration was determined by the method of Bradford (Biorad).

Antibodies and reagents

Human cytomegalovirus (HCMV) purified virus, strain AD169, was purchased from Advanced Biotechnologies Inc. Primary antibodies to the following proteins were obtained from commercial sources: cleaved caspase-3 (D175, rabbit polycolonal, Cell Signaling), hnRNP K (rabbit polyclonal, ab18195; Abcam), IE1/2 (mouse monoclonal; Argene), IE2 (mouse monoclonal, 5A8.2; Chemicon), α-tubulin (mouse monoclonal, B-5-1-2; Sigma), β-tubulin (mouse monoclonal, TUB 2.1; Sigma), pp28 (mouse monoclonal, 5C3; Santa Cruz), pp65 (mouse monoclonal, 1-L-11; Santa Cruz), pp71 (goat polyclonal, vC-20; Santa Cruz), HRP-conjugated 6xHis (mouse monoclonal; BD Biosciences), and HRP-conjugated anti-ubiquitin (mouse monoclonal; Enzo Life Sciences). Mouse monoclonal antibodies against pp71 (2H10-9 and 10G11) were kindly provided by Dr. T. Shenk (Princeton University, Princeton, NJ, USA). Secondary HRP-conjugated goat anti-mouse and goat anti-rabbit antibodies were purchased from Jackson ImmunoResearch Laboratories. HRP-conjugated rabbit anti-goat was obtained from Dako. Alexa Fluor 488-conjugated goat anti-rabbit and DAPI were purchased from Invitrogen and Roche, respectively. Immunoblotted proteins were detected using the Enhanced Chemiluminescence detection system (Amersham) and ChemiDoc XRS+ (Bio-Rad). InstantBlue stain was purchased from Expedeon and MG132 was obtained from Sigma. Pan-caspase inhibtor zVAD-fmk was obtained from Enzo Life Sciences. RNase A was purchased from Roche and dissolved in granzyme activity buffer (20 mM Tris pH 7.4, 150 mM NaCl). Total RNA was isolated using Trizol according to manufacturers' protocol (Invitrogen).

HnRNP K mutagenesis

The hnRNP K mutants (L125A, L133A, M359A, L125A/L133A, and L125A/L133A/M359A) were generated using the QuikChange Site-Directed Mutagenesis (Stratagene) using the pSG5-His-hnRNP K expression plasmid (a kind gift from Dr. Antje Ostareck-Lederer, Martin Luther University Halle-Wittenberg, Germany) as template. DNA sequences of all constructs were verified by sequencing.

Purified recombinant proteins

The cDNA encoding mature human GrM was amplified and cloned into yeast expression vector pPIC9 (Invitrogen). Using the QuikChange Site-Directed Mutagenesis Kit (Stratagene), the Ser^{195} residue in the catalytic center of GrM was replaced by an Ala residue, resulting in the catalytically inactive GrM variant (GrM-SA) that we have used as a control in this study. GrM and GrM-SA proteins were expressed and purified as described previously.[45] Briefly, *Pichia pastoris* GS115 cells were transformed with the pPIC9-granzyme expression plasmids and granzymes

were expressed for 72 h in conditioned media, according to the manufacturers' protocol (Invitrogen). GrM and GrM-SA were purified to homogeneity using an SP-Sepharose column (GE Healthcare) with 1 M NaCl for elution. GrM protein fractions were dialyzed against 50 mM Tris pH 7.4 and 150 mM NaCl, and stored at -80°C. Recombinant GrM and GrM-SA proteins were pure (>98%) as determined by SDS-PAGE and active as measured by hydrolysis of synthetic chromogenic leucine substrates Suc-AAPL-pNA (Bachem) and Suc-KVPL-pNA (GL Biochem), and known macromolecular substrates (data not shown).

BL21-CodonPlus competent *Escherichia coli* cells (Stratagene) were transformed with the pET16-b-His-hnRNP K expression plasmid (a kind gift from Dr. Antje Ostareck-Lederer, Martin Luther University Halle-Wittenberg, Germany) or pQE-80L-His-β-tubulin and cultured in LB medium. At an OD_{600} between 0.4 and 1.0, cells were stimulated with 0.4 mM IPTG and incubated for 3 h at 37°C at 225 rpm. Cells were harvested and lysed by sonification. N-terminal His-tagged hnRNP K and β-tubulin were purified to homogeneity using Talon metal ion chelate affinity chromatography (Clontech) with 125 mM imidazole in PBS for elution and stored at 4°C.

2D-DIGE

2D-DIGE was performed as described previously. [30] Briefly, cell-free protein extracts of HeLa cells (100 µg) were incubated with 1 µM GrM or GrM-SA for 1 h at 37°C. Samples were precipitated, solubilized, labeled, rehydrated into immobilized pH gradient strips and isoelectrically focused. Strips were reduced and overlaid on a 12% SDS PAGE gel. Images were acquired on a Typhoon 9410 scanner (GE Healthcare). Each condition was performed at least five times and a dye swab was included to exclude preferentially labeled proteins from the analysis. Relative quantification of matched gel features was performed using Decyder DIA and BVA software (GE Healthcare). For inter-gel analyses, the internal standard method was used.

GrM cleavage assay in living HFFs

HFFs (2×10^4) were seeded in 96-wells plates, washed twice with serum free DMEM, and incubated with the perforin-analog streptolysin O (SLO, Aalto) and purified granzyme in a final volume of 30 µL for 30 min at 37°C. Then, supernatant was removed and cells were cultured in 100 µL DMEM containing 10% fetal calf serum for 16 h. For analyzing caspase activation and cell death, HFFs were treated with zVAD-fmk (100 µM) or vehicle only (DMSO) for 30 min at 37°C prior to granzyme treatment, and zVAD-fmk (100 µM) or DMSO was added after granzyme treatment. Cells were washed two times with PBS and directly lysed in reducing sample buffer (50 µL) prior to immunoblotting. To measure GrM-mediated cell death, cells were trypsinized, harvested and washed twice with PBS. Cells were pelleted and stained with annexin-V-FLUOS (Roche) and propidium iodide (PI) in 100 µL annexin-V binding buffer (140 mM NaCl, 4 mM KCl, 0.75 mM $MgCl_2$, and 10 mM $CaCl_2$) for 15

min at room temperature after which 500 µL annexin-V binding buffer was added. Fluorescence was measured by FACS on a FACS Calibur (BD Biosciences) and data was analyzed with CellQuest Pro Software (BD Biosciences).

shRNA-mediated knockdown of hnRNP K protein expression
Lentiviral particles were produced using third generation lentivirus vectors. HEK293T cells were transfected with pCMV-VSV-G, pMDLg-RRE, pRSV-REV (kind gifts from Prof. dr. E.J.H.J. Wiertz, University Medical Center Utrecht, The Netherlands) and hnRNP K shRNA plasmid (sc-38282-SH, Santa Cruz) or control shRNA plasmid (sc-108060, Santa Cruz) using polyethylenimine (PEI, Polysciences Inc) in a 3:1 ratio with total DNA. Supernatant with viral particles was harvested at 48 and 72 hpi, filtered (0.45 µm), and stored at -80°C. HFFs were pre-treated with polybrene (10 µg/mL) for 20 min and transduced 4 times for 2 hours.

HCMV infection model
HFFs (2 x 10^4) were seeded in 96-wells plates and infected with purified HCMV at a multiplicity of 1.0 plaque-forming unit per cell for 2 h at 37°C. Cells were washed three times and cultured in 100 µL medium. For analysis of protein levels, cells were washed two times with PBS and directly lysed in reducing sample buffer prior to immunoblotting. To measure viral load by quantitative PCR, supernatant was collected at the indicated time points and HCMV was inactivated for 30 min at 60°C. Cell viability was measured using a WST-1 assay (Roche) according to the manufacturers' protocol.

mRNA isolation, reverse transcriptase PCR, and quantitative PCR
For direct mRNA isolation, cells were lysed (100 mM Tris pH 7.5, 500 mM LiCl, 10 mM EDTA, 5 mM EDTA, 1% SDS) and treated with proteinase K for 1h at 56°C. For mRNA isolation after hnRNP K immunoprecipitation, cells were lysed (100 mM Tris pH 7.5, 500 mM LiCl, 10 mM EDTA, 5 mM EDTA, 1% Triton X-100, supplemented with a protease cocktail inhibitor from Roche) and incubated with purified His-tagged hnRNP K or His-tagged β-tubulin overnight at 4°C. His-tagged proteins were immunoprecipitated using Talon metal ion chelate affinity chromatography (Clontech) and beads were washed 5 times followed by proteinase K treatment for 1h at 56°C. To isolate mRNA, samples were incubated with Oligo(dT) Dynabeads (Invitrogen) for 10 min and beads were washed twice with 10 mM Tris pH 7.5, 150 mM LiCl, 1 mM EDTA, 0.1% SDS, and twice with 10 mM Tris pH 7.5, 150 mM LiCl, 1 mM EDTA. The mRNA was eluted in Milli-Q water by incubating 2 min at 80°C and used as a template for reverse transcriptase PCR with SuperScript III First-Strand Synthesis System for RT PCR (Invitrogen). Amplification of cDNA was performed using quantitative PCR (LightCycler 480 II, Roche). Primers and probes against *UL123* (IE1), *UL122* (IE2), and *UL54* are listed in Table 1. Taqman gene expression assay for glyceraldehyde 3-phosphate dehydrogenase (*GAPDH*) was purchased from Applied Biosystems.

To measure viral replication, supernatants from HCMV-infected HFFs or samples for the standard curve were diluted 50-fold in water and amplification of HCMV DNA was performed using quantitative PCR (ABI Prism 7900 HT, Applied Biosystem). Primers and probes were located in the HCMV DNA polymerase gene *UL54* (Table 1). The viral load of supernatants was determined by plotting Cq-values on the standard curve.

Immunofluoresence
HFFs were grown in white 96-wells flat bottom plates. Cells were infected with purified HCMV at a multiplicity of 2.0 plaque-forming units per cell for 2 h at 37°C. Cells were washed three times and cultured in 100 µL medium. At different time points, cells were fixed in 100 µL 4% paraformaldehyde for 30 min at 37°C, washed three times with PBS, and stored in PBS at 4°C. For protein detection, fixed cells were incubated with anti-hnRNP K for 1 h followed by Alexa Fluor 488-conjugated secondary antibody for 1 h. DAPI was used for nuclear counterstaining and fluorescence was analyzed using a Leica DMI4000 B.

Dual luciferase reporter assay
HeLa cells were seeded in 12-wells plates and transfected with 50 ng of pGL3-SV40 (Invitrogen), 10 ng of pRL-CMV (Invitrogen), complemented with pCGN-71, pSG5-His-hnRNP K or pcDNA3.1+ to a total of 1 µg DNA. The pp71 protein activates the CMV promoter (MIEP) but does not activate the SV40 promotor and is used as a positive control. [286] SV40-firefly was used as a correction for transfection efficiency to allow adequate comparison between samples. After 48 h, cells were washed twice with PBS, freeze-thawed once at -80°C, and lysed with 200 µL passive lysis buffer (Promega, Madison, WI). Supernatant was collected and used for immunoblot analysis with an anti-6xHis or anti-pp71 antibody and to determine both renilla and firefly luciferase activities using the Dual-GLO Luciferase Assay System (Promega) in a Veritas Microplate Luminometer (Turner Biosystems, Sunnyvale, CA) according to the manufacturers' protocol (Promega). Both luciferase activities were normalized for background values. Then, changes in CMV-renilla luciferase activities relative to SV40-firefly luciferase activities (*i.e.*, renilla luciferase/firefly luciferase ratio) were determined. The mean renilla luciferase activity from control (pcDNA 3.1+)-transfected cells was set at 1.

Acknowledgements
We thank Dr. R.A. van Lier (Sanquin, Amsterdam, The Netherlands) for critical reading of the manuscript. This work was supported by The Netherlands Organization for Scientific Research (Grant 916.66.044) and the Dutch Cancer Society (UU-2009-4302) (to NB).

Table 1. Quantitative PCR primers and probes

Gene	Forward primer	Reverse primer	Probe
UL123 (IE1)	5'-CAA GTG ACC GAG GAT TGC AA-3'	5'-CAC CAT GTC CAC TCG AAC CTT-3'	5'-FAM-TCC TGG CAG AAC TCG TCA AAC AGA-TAMRA-3'
UL122 (IE2)	5'-TGA CCG AGG ATT GCA ACG A-3'	5'-CGG CAT GAT TGA CAG CCT G-3'	5'-FAM-TGG CAG AAC TCG GTG ACA TCC TCG CC-TAMRA-3'
UL54	5'-GCC GAT CGT AAA GAG ATG AAG AC-3'	5'-CTC GTG CGT GTG CTA CGA GA-3'	5'-FAM-AGT GCA GCC CCG ACC ATC GTT C-TAMRA-3'

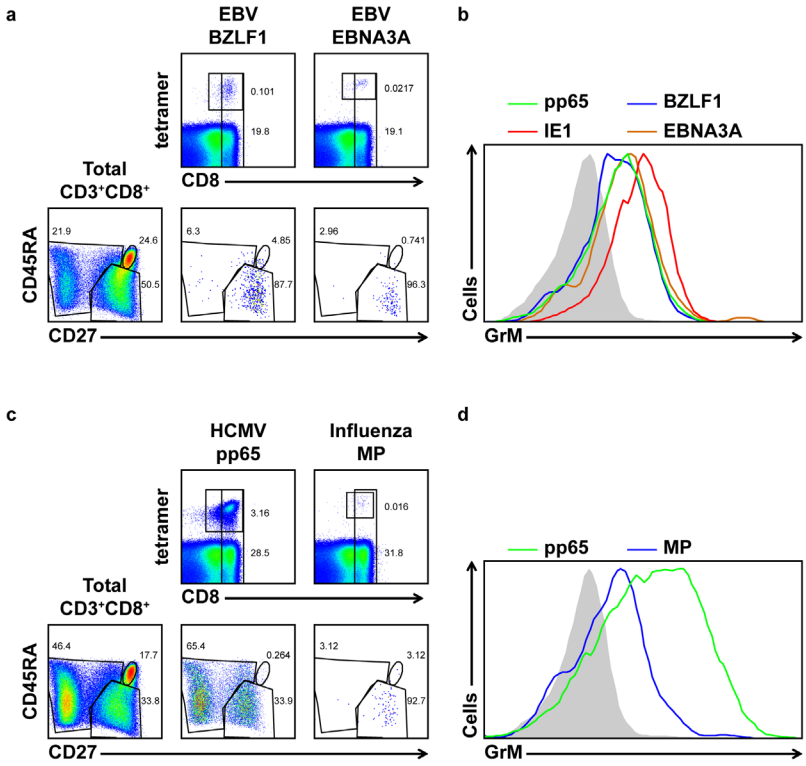

Supplementary figure 1. GrM is expressed in virus-specific CD8⁺ T cells of healthy individuals. (a) PBMCs were isolated from a EBV-seropositive healthy-individual (same donor as in Figure 1). FACS plots show the expression of CD8 and EBV-specific BZLF1 and EBNA3A tetramers on $CD3^+$ T cells (upper row) or the expression of CD27 and CD45RA (bottom row) on total $CD3^+CD8^+$ T cells (left) or EBV-specific $CD3^+CD8^+$ T cells (middle, right). **(b)** FACS histogram visualizes the relative intracellular GrM protein levels in naive $CD3^+CD8^+$ T cells (filled gray), and EBV- and HCMV-specific $CD3^+CD8^+$ T cells (lines). **(c)** PBMCs were isolated from a second HCMV-seropositive healthy-individual. FACS plots show the expression of CD8 and HCMV-specific pp65 or influenza-specific MP tetramers on $CD3^+$ T cells (upper row) or the expression of CD27 and CD45RA (bottom row) on total $CD3^+CD8^+$ T cells (left), HCMV-specific (middle) or influenza-specific $CD3^+CD8^+$ T cells (right). **(d)** FACS histogram visualizes the relative intracellular GrM protein levels in naive $CD3^+CD8^+$ T cells (filled gray), and HCMV- and influenza-specific $CD3^+CD8^+$ T cells (lines).

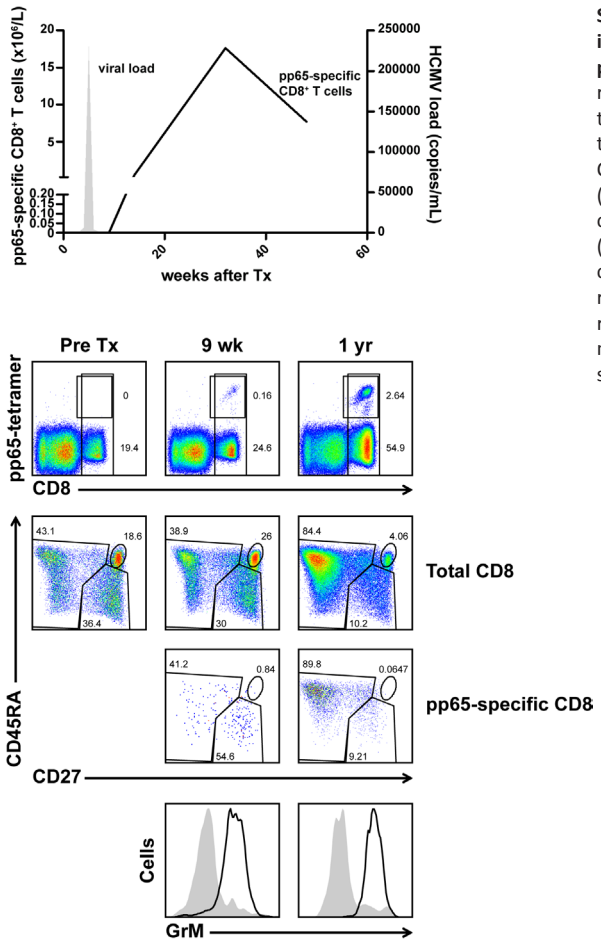

Supplementary figure 2. GrM is expressed in HCMV-specific CD8⁺ T cells of a SCT patient. PBMCs were isolated from a second renal transplant patient pre- and post-transplantation. Graph depicts kinetically the absolute numbers of pp65-specific $CD3^+CD8^+$ cells (line) and HCMV viral load (filled gray). FACS plots show the expression of CD3 and pp65 tetramers on $CD3^+$ T cells (upper row), and CD27 and CD45RA on total or pp65-specific $CD3^+CD8^+$ T cells (middle rows). Histograms (bottom row) visualize the relative intracellular GrM protein levels in naive $CD3^+CD8^+$ T cells (filled gray) and pp65-specific $CD3^+CD8^+$ T cells (line).

Chapter 8

Intracellular granzyme activity profiling using bioluminescent probes

S.A.H. de Poot, M.C. Olthof, E.A. van Erp, E.M. Steeghs, and N. Bovenschen

Department of Pathology, University Medical Center Utrecht, Utrecht, the Netherlands

Manuscript in preparation.

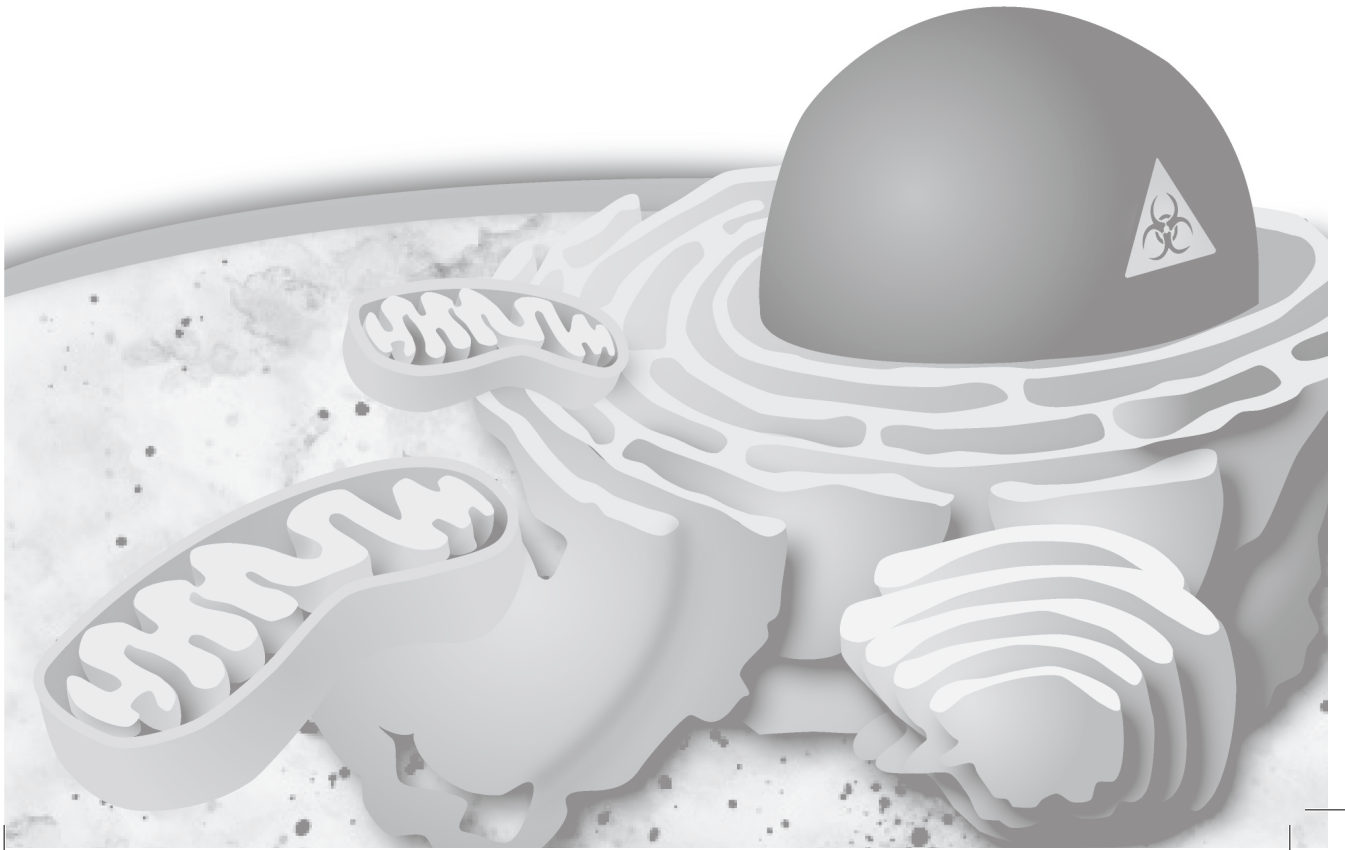

Abstract

In the effector arm of the immune system, cytotoxic lymphocytes release pre-stored granules that contain the pore-forming protein perforin and five serine proteases called granzymes. Perforin facilitates the entry of granzymes into target cells, allowing granzymes to cleave intracellular substrates during tumor clearance, inflammation, and anti-viral immunity. It is still unclear which granzymes are functionally delivered into which types of target cells. Here, as a proof-of-concept, we have developed an intracellular granzyme M (GrM)-specific gain-of-function bioluminescent sensor based on circularly permuted firefly luciferase. Upon GrM-mediated cleavage of a peptide linker, the luciferase folds into an active conformation. The GrM sensor was specifically activated by GrM, but not by the other human granzymes or by caspases. GrM treatment of human tumor cells resulted in sensor activation, as did co-culture of these target cells with cytotoxic effector cells. Thus, we have developed a bioluminescent sensor that specifically reports GrM proteolytic activity in the course of GrM-induced cell death *in vitro*, providing a promising tool to monitor and distinguish granzyme entry and functional activity in target cells *in vivo*.

Introduction

Cytotoxic lymphocytes, comprising natural killer (NK) cells and cytotoxic T lymphocytes, employ two molecular mechanisms to kill transformed or virus-infected cells: the death-receptor pathway [287] and the granule-exocytosis pathway [2-4, 8]. In the latter pathway, effector cells release perforin and a set of homologous serine proteases known as granzymes into the immunological synapse. Perforin forms pores in the target cell plasma membrane, which facilitates granzyme entry. Humans express five granzymes - (Gr)A, GrB, GrH, GrK, and GrM - that display diverging substrate specificities. GrA and GrB have been studied extensively [114], but much less is known about GrH, GrK, and GrM [8]. Granzymes play roles in tumor clearance by inducing apoptosis [69, 242, 288], inflammation [69, 80], and anti-viral immunity, through cleavage of intracellular substrates [64, 289]. It is, however, unclear which granzymes are functionally delivered into which types of target cells.

Here, as a proof-of-concept, we have developed an intracellular GrM-specific gain-of-function biosensor based on circularly permuted firefly luciferase (at residue 233) [290, 291], which is locked in an inactive state by a short peptide-linker. Upon GrM-mediated cleavage of this peptide linker, the luciferase subunits fold back into an active conformation. We show that the GrM sensor was specifically activated by GrM, but not by the other human granzymes or by caspases. GrM treatment of human tumor cells expressing the GrM sensor led to sensor activation, as did co-culture of these target cells with GrM-expressing effector cells. Thus, this biosensor specifically reports the proteolytic activity of GrM in the course of GrM-induced cell death *in vitro* and provides a promising tool to monitor granzyme entry and functional activity in target cells *in vivo*.

Materials & Methods

Cell lines and antibodies.

Human HeLa cervix carcinoma cells and OPM-2 multiple myeloma cells were grown in DMEM and RPMI medium, respectively, supplemented with 10% fetal calf serum, 100 units/ml penicillin and 100 µg/ml streptomycin (Invitrogen). The human NK cell line KHYG-1 [206] was grown in RPMI 1640 medium, supplemented with 10% fetal calf serum, 100 units/ml penicillin, 100 µg/ml streptomycin, 7.5% sodium bicarbonate and 100 units/ml IL-2. Lymphokine activated killer (LAK) cells were generated by culturing peripheral blood-derived mononuclear cells from healthy adult blood donors for 4 days in RPMI medium supplemented with 5% human AB serum and 1000 units/ml IL-2. Freeze-thaw lysates were prepared by washing subconfluent cells twice with ice-cold PBS, followed by three cycles of rapid freeze-thawing. Cell debris was removed by centrifugation at 13,000 g for 10 min at 4˚C, and supernatant protein concentration was determined using the Bradford method. Antibodies used were anti-α-tubulin (#T5168, Sigma), anti-cleaved caspase 3 (Asp175, Cell Signaling Technology), anti-GAPDH (6C5, Abcam), mouse anti-human GrM (clone 4A8E11[38]), and anti-luciferase (Luci17, Santa-Cruz).

Recombinant proteins.
Human GrA, GrB, GrH, GrK, GrM, and the catalytically inactive mutant GrM-SA – in which the Ser^{195} residue has been replaced with Ala – were produced in *Pichia pastoris* and purified using cation-exchange chromatography as described previously [45]. Granzyme activity was verified using chromogenic synthetic substrates as described previously [30, 45, 124].

Construction and production of the GrM sensor in vitro.
The GrM sensor was developed with the cleavage recognition site AKMPL↓AAEEE, based on the human GrM consensus cleavage site previously identified with complementary positional proteomics [30]. In the GrM mock sensor, the P1 Leu of the cleavage recognition sequence has been mutated to an Ala (AKMPA-AAEEE). The pProteaseGlo sensor plasmids were constructed (Protease-Glo™ Assay, Promega) and produced *in vitro* in a cell-free transcription/translation system (TNT Sp6 High-Yield Wheat Germ Master Mix, Promega) according to the manufacturer's protocol. For fluorescent labeling of the sensors, 0.5 µl FluoroTect Green Lys (Promega) was added to the transcription mix. The recombinant sensors were incubated for 15' at 37°C with the indicated concentrations of purified recombinant granzyme in 50 mM Tris, 150 mM NaCl, pH 7.4. Activation of the sensors was assessed with the Veritas Microplate Luminometer (Promega). Samples labeled with fluorescent green lysine were separated on a SDS-PAGE gel and scanned on a Typhoon 9410 scanner (GE Healthcare).

Cellular expression of the GrM sensor.
The GrM sensors were cloned into a pCDNA3.1+ plasmid (Invitrogen) and a lentiviral pLV plasmid. In addition, a pLV-Renilla luciferase (pLV-RLuc) plasmid was constructed. HeLa cells were transfected with the pCDNA3.1+ sensor constructs using polyethylenimine (PEI, Polysciences, Warrington, PA, USA) in a 3:1 ratio with DNA. Lentiviral transductions were performed as described previously [238]. Briefly, COS7 cells were transfected with third-generation lentivirus packaging plasmids and the pLV-mCherry, pLV-RLuc, or pLV-sensor constructs to produce lentiviral particles. On 48 hours post transfection, supernatant was harvested and filtered (0.45 µm). OPM-2 cells were spinoculated in the presence of 8 µg/ml polybrene at 1300 rpm for 1.5 hours, followed by overnight incubation with the virus. HeLa cells were transduced overnight in the presence of 8 µg/ml polybrene. Expression of the sensors was confirmed using Western blot and flow cytometry.

Flow cytometry.
Intracellular flow cytometry was used to verify expression of the biosensors in HeLa and OPM-2 cells. Briefly, cells were washed twice with PBS containing 0.5% BSA and 0.1% sodium azide (PBA), after which they were permeabilized at RT for 10 minutes in permeabilization/lysis buffer [1x permeabilizing solution 2 (BD Biosciences) and 1x FACS lysing solution (BD Biosciences) in water]. Cells were then again washed

with PBA, after which they were stained for 1 hour at 4°C with 1:50 mouse anti-luciferase. After two washes with PBA, cells were stained for 20 minutes at 4°C, with 1:100 goat-anti-mouse-Alexa Fluor 488, followed by another two washes in PBA. Flow cytometry was performed on a FACSCalibur with CellQuest Pro software (BD Biosciences).

Granzyme treatment and killing assays.
Cells were washed twice with serum free DMEM and treated with purified granzyme (1μM) and streptolysin O (SLO, 500 ng/ml, Aalto Bio Reagents) as described previously [30] in the presence of 300 μg/ml D-luciferin (BioSynth). Luminescence was measured directly. For co-culture experiments with KHYG-1 and LAK cells, 300 μg/ml D-luciferin was added simultaneously with the effector cells.

Statistical analysis.
Unless otherwise indicated, data are depicted as mean ± SD. Statistical analyses were performed using independent samples t-test. $P<0.05$ was considered statistically significant.

Results

GrM specifically activates the GrM sensor.
Using a circularly permuted firefly luciferase, which is normally locked in an inactive state by a short peptide-linker [290], we developed a GrM-specific bioluminescent sensor by inserting a peptide-linker with the GrM consensus cleavage motif. Cleavage of the peptide-linker results in a conformational change that leads to activation of the luciferase (Fig. 1A). We have previously characterized the extended substrate specificity of human GrM using complementary positional proteomics [30], identifying AKMPL↓AAEEE as an optimal cleavage recognition sequence. Based on this sequence, we developed a GrM-specific bioluminescent sensor and a corresponding mock sensor, in which the P1 Leu residue was substituted with an Ala (*i.e.* AKMPA-AAEEE). The sensors were synthesized *in vitro* using cell-free transcription/translation, and subsequently treated with purified recombinant GrM or catalytically inactive GrM-SA (Fig. 1B and C). With increasing concentrations of GrM, increasing activation of the GrM sensor was detected, whereas catalytically inactive GrM-SA did not result in sensor activation (Fig. 1B). While the GrM sensor was strongly activated by GrM, the GrM mock sensor was not (Fig. 1C), indicating that activation of the sensor was dependent on GrM-mediated cleavage after the P1 Leu residue within the peptide recognition sequence. Consistent with these data, visualization of the fluorescently-labeled sensors by SDS-PAGE showed that the full-length GrM sensor (~61 kDa) was cleaved by increasing concentrations of GrM, but not GrM-SA, resulting in the formation of the expected two separate subunits (~36 and ~25 kDa) (Fig. 1D). To determine the specificity of the GrM sensor, it was incubated with all purified human granzymes: GrA, GrB, GrH, GrK,

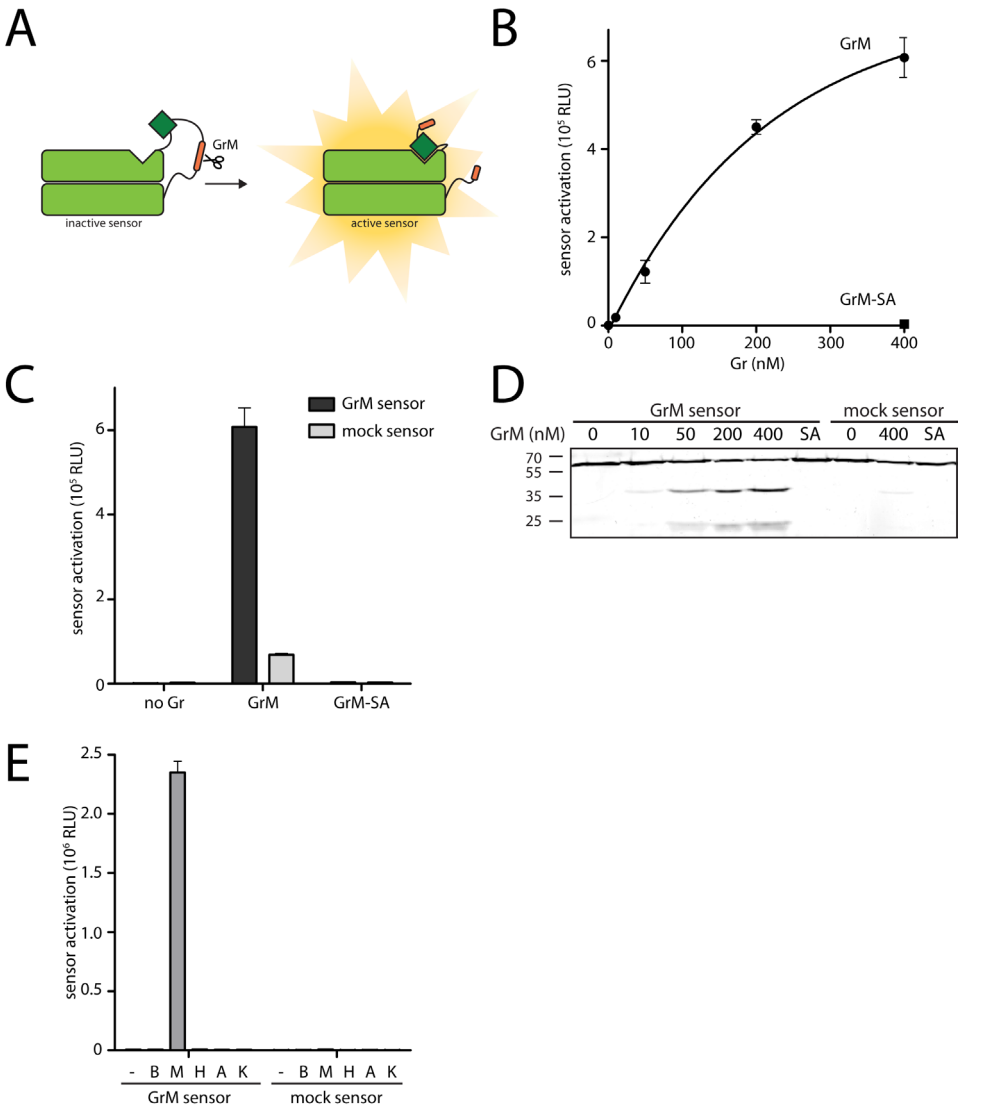

Figure 1. The GrM sensor is specifically activated by GrM in a concentration-dependent manner. (A) Schematic overview of the GrM sensor. The circularly permuted firefly luciferase molecule is locked in an inactive conformation by a short peptide-linker containing a GrM-specific recognition sequence. Upon cleavage of the linker by GrM, the luciferase subunits undergo a conformational change, resulting in the formation of an active luciferase molecule. **(B)** The GrM sensor was produced *in vitro* using a cell-free transcription/translation system, and subsequently incubated at 37°C for 30 min with increasing concentrations of GrM, or 400 nM GrM-SA. Resulting relative luminescence units (RLU) are plotted on the y-axis. GrM induced a statistically significantly higher GrM sensor signal than GrM-SA at 400 nM ($p \leq 0.05$). **(C)** The GrM and mock sensors were produced as in (b), and incubated at 37°C for 30 min with 400 nM GrM or GrM-SA. The GrM-induced signal of the GrM sensor was statistically significantly higher than all other conditions ($p \leq 0.05$). **(D)** The GrM and mock sensors were labeled with FluoroTect green lysines during the *in vitro* transcription/translation, incubated at 37°C for 30 min with indicated concentrations of GrM or 400 nM GrM-SA, and separated on SDS-PAGE. Full-length sensor (~61 kDa) and cleavage fragments (~36 and 25 kDa) are visible. **(E)** The GrM and mock sensors were produced as in (c), and incubated at 37°C for 30 min with 50 nM of recombinant GrA, GrB, GrH, GrK, or GrM. The GrM-induced signal of the GrM sensor versus other conditions was statistically significant ($p \leq 0.05$).

and GrM (Fig. 1E). Of these, only GrM led to robust activation of the GrM sensor. None of the granzymes could activate the GrM mock sensor. Taken together, we have successfully constructed a specific GrM bioluminescent sensor.

Intracellular GrM sensor activation.

To monitor GrM activity inside living cells, the GrM sensor was cloned into expression plasmids to allow sensor expression in human HeLa cervix carcinoma and OPM-2 multiple myeloma cells. To verify intracellular sensor expression, expression of firefly luciferase in HeLa and OPM-2 was determined using flow cytometry (Fig. 2A). Both the mock sensor and the GrM sensor were expressed in the majority (~50-60%) of sensor-transduced cells. In addition, cell-free lysates of sensor-transduced HeLa and OPM-2 cells were immunoblotted for firefly luciferase expression, which confirmed sensor expression (Fig. 2B). The functionality of the GrM sensor in cells was determined in cell-free lysates by adding recombinant GrM. Consistent with the *in vitro*-translated sensor data (Fig. 1), GrM cleaved and activated the GrM sensor in lysates of both HeLa and OPM-2 cells in a concentration-dependent manner (Fig. 2C). This correlated with GrM sensor cleavage as determined by immunoblot (Fig. 2D). Treatment GrM-SA did not lead to GrM sensor activation, and the GrM mock sensor could not be activated by GrM or GrM-SA (Fig. 2E). Neither the GrM sensor, nor the GrM mock sensor, could be activated by the addition of GrB to the lysate (Fig. 2E). Caspase-3, a known substrate of GrB [292], however, was cleaved and activated under these conditions (Fig. 2D), providing further evidence that the GrM sensor is not activated by GrB or GrB-activated caspases. To test whether activation of the GrM sensor in lysate correlated with the cleavage of macromolecular GrM substrates, lysate of GrM sensor-transduced HeLa cells was incubated with increasing concentrations of GrM, and then immunoblotted for α-tubulin, a known substrate of GrM [45] (Fig. 2F). In addition, sensor activation was assessed by luminescence. Luminescence of the GrM sensor correlated with increased cleavage of α-tubulin (R^2=0.9283), indicating that the activation of the GrM sensor correlated with cleavage of macromolecular GrM substrates.

Next, we delivered purified GrM inside living GrM sensor-transduced HeLa cells (via perforin-analog SLO), after which sensor activation was monitored using bioluminescence (Fig. 3A). GrM sensor activation was detected only in cells treated with both SLO and GrM, and not in cells treated with GrM alone, the GrM-SA/SLO combination, or GrB and SLO. GrM is known to indirectly activate caspases in living target cells [32](Chapter 5). To further exclude the involvement of caspases in sensor activation, the caspase cascade was activated in transduced HeLa cells by the addition of the kinase inhibitor staurosporine (STS) [293]. Addition of STS did not result in GrM (mock) sensor activation (Fig. 3A). These data indicate that intracellular delivery of purified GrM inside living tumor cells activates the GrM sensor in a caspase-independent manner.

To determine whether GrM activity can be profiled inside tumor cells that are attacked by cytotoxic lymphocytes, we co-cultured GrM sensor-transduced

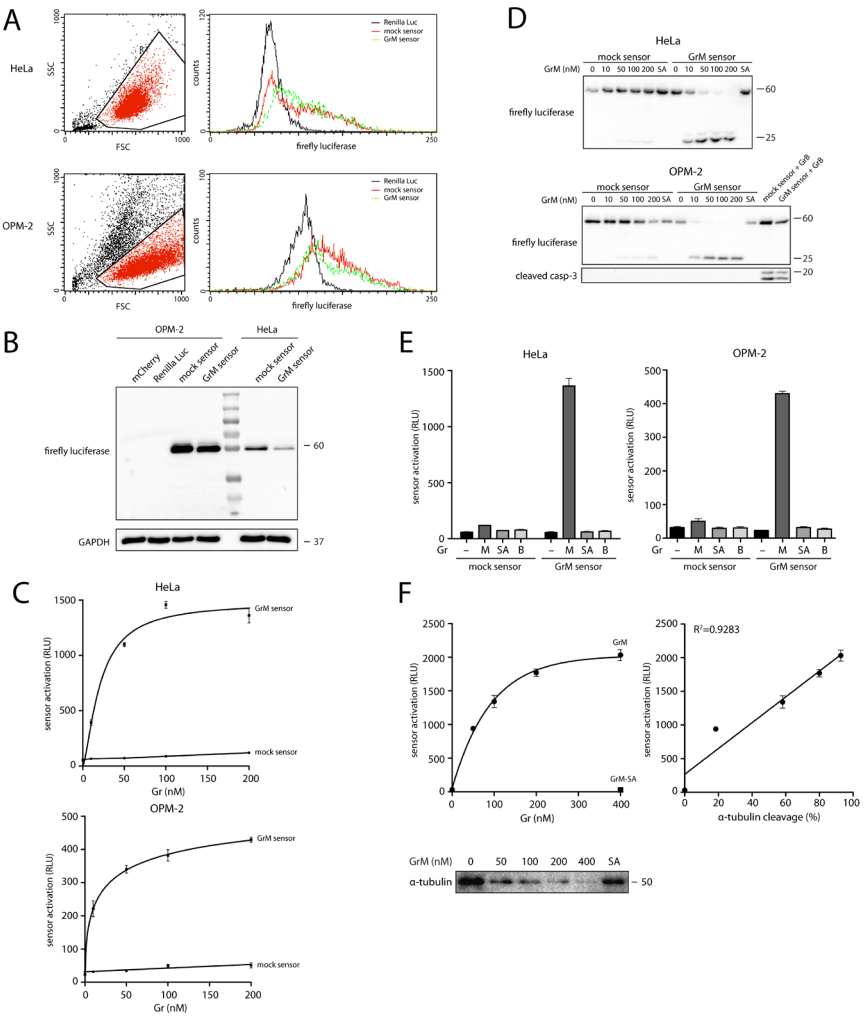

Figure 2. The GrM sensor is specifically activated by GrM in cell-free protein extracts of transfected cells. HeLa and OPM-2 cells were transfected with the GrM sensor or the mock sensor. **(A)** Expression of the sensors was verified using anti-firefly luciferase flow cytometry. Living cells were gated based on FSC/SSC plots, after which sensor expression was compared to untransfected cells (not shown) and cells transduced with Renilla Luc. **(B)** Freeze-thaw lysates of transfected cells were prepared, protein was quantified, and 15 µg was immunoblotted for firefly-luciferase or GAPDH (loading control). **(C)** Freeze-thaw lysates (10 µg) of HeLa cells were treated with indicated concentrations of GrM for 1 h at 37°C, after which Bright-Glo reagent was added and luminescence was measured. Already at 10 nM, GrM had induced significantly more activation of the GrM sensor than the mock sensor ($p \leq 0.05$). **(D)** Freeze-thaw lysates (10 µg) of OPM-2 cells were treated with indicated concentrations of GrM, 200 nM GrM-SA or 200 nM GrB for 1 h at 37°C, after which samples were immunoblotted for firefly luciferase or cleaved caspase-3. Already at 10 nM, GrM had induced significantly more activation of the GrM sensor than the mock sensor ($p \leq 0.05$). **(E)** Freeze-thaw lysates were treated as in (c), after which Bright-Glo reagent was added and luminescence was measured. The GrM-induced signal of the GrM sensor was significantly higher than all other conditions ($p \leq 0.05$). **(F)** Freeze-thaw lysates (10 µg) of HeLa cells were treated with increasing concentrations of GrM or 400 nM GrM-SA at 37°C for 30 min. To half of the samples, Bright-Glo was then added and luminescence was determined. GrM induced significantly more GrM sensor activation than GrM-SA at 400 nM ($p \leq 0.05$). For the other half of the samples, cleavage of known GrM substrate α-tubulin [45] was determined using immunoblot, and semi-quantified by determining band intensity of full-length α-tubulin. Activation of the GrM sensor was then correlated ($R^2=0.9283$) with α-tubulin cleavage.

HeLa cells with NK KHYG-1 cells or lymphokine activated killer (LAK) cells. We confirmed that both KHYG-1 and LAK cells express GrM protein (Fig. 3B). Increasing effector:target ratios of both KHYG-1 (Fig. 3C) and LAK cells (Fig. 3D) resulted in increased activation of the GrM sensor. Collectively, these data indicate that this biosensor specifically reports the proteolytic activity of GrM in the course of GrM-induced cell death *in vitro* and provides a promising tool to monitor granzyme entry and functional activity in target cells *in vivo*.

Discussion

Various anti-viral, anti-tumor, and pro-inflammatory activities have been ascribed to granzymes [64, 69, 289]. However, it is unclear which granzymes are actively delivered into which target cells. Up until now, entry and activity of granzymes in target cells *in vitro* has been analyzed via immunoblotting for known substrates. This is a time consuming approach, rather unspecific, and not suitable for *in vivo* analysis. In order to robustly profile and to distinguish intracellular granzyme activity *in vitro*

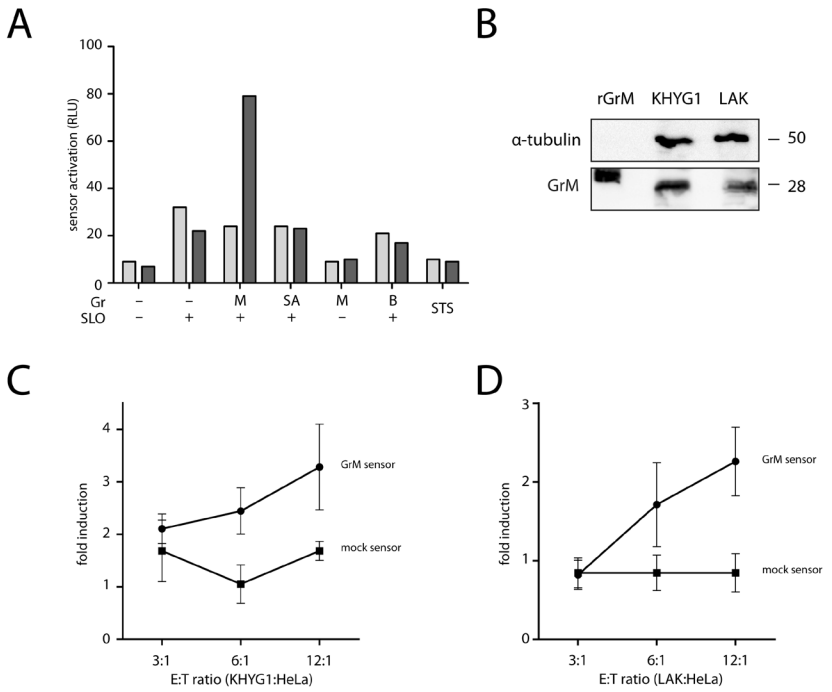

Figure 3. Intracellular activation of the GrM sensor by recombinant GrM and cytotoxic lymphocyte-mediated attack. (A) Living HeLa cells transfected with the GrM sensor (dark grey) or the mock sensor (light grey) were treated with 500 ng/ml SLO and/or 1 µM GrM, GrM-SA or GrB in medium containing 300 µg/ml D-luciferin. Sensor activation was monitored immediately. Caspase activation was induced by the addition of 2 µM staurosporine (STS) for 3 hours. (*n=1*) **(B)** 30 µg cell-free protein extract of KHYG-1 and LAK cells, and 50 ng recombinant GrM were loaded on SDS-PAGE and immunoblotted for GrM. Recombinant GrM (rGrM) runs slightly higher due to different glycosylation. α-tubulin was used as a loading control. **(C-D)** HeLa cells transduced with the GrM or mock sensor were cocultured with KHYG-1 cells (C) or LAK cells (D) for 2 h in varying effector:target ratios in the presence of 300 µg/ml D-luciferin. At E:T ratios larger than 6:1, the GrM sensor had a significantly higher signal than the mock sensor ($p \leq 0.05$).

and *in vivo*, the development of specific intracellular granzyme sensors is required. Here, we describe the first use of a gain-of-function bioluminescent sensor to detect intracellular granzyme activity. The GrM sensor was specifically activated by GrM *in vitro* following cleavage at P1 Leu within the linker peptide, but not by the other granzymes or caspases. Activation of the GrM sensor by GrM in cell lysates of tumor cells expressing the sensor correlated with macromolecular substrate cleavage. Intracellular delivery of GrM inside living GrM sensor-expressing tumor cells by the perforin-analogue SLO led to caspase-independent intracellular activation of the sensor. Finally, cytotoxic lymphocyte-mediated attack activated the GrM sensor in tumor cells within 2 hours, which is compatible with the kinetics of intracellular GrB delivery [294]. Our data pave the way towards the specific monitoring of granzyme entry and functional activity *in vivo.*

To our knowledge, this is the first time the intracellular use of a bioluminescent granzyme biosensor has been described. Previously, cell-permeable or retrovirally transduced fluorescence resonance energy transfer (FRET) probes have been developed for GrB (cleavage recognition site VGPD-FGR), which have been employed to detect GrB delivery by cytotoxic lymphocytes using low magnification time-lapse imaging [295] or flow cytometry [294]. However, FRET-based probes cannot easily be used to monitor granzyme activity *in vivo*, whereas bioluminescent sensors like our GrM probe are ideally suited for *in vivo* imaging. It should be mentioned, however, that the sensor signal that we obtained in living cells was rather low (Fig. 3), raising the possibility that the sensitivity of our sensor may not be sufficient to be detected *in vivo*. Recently, the use of a similar circularly permuted firefly luciferase sensor (at residue 358) has been described to detect intracellular caspase-3/-7 activity [296]. This sensor has also successfully been used in mouse models. Interestingly, the 358-circular permutation, in combination with a single Thr to Ile point mutation at amino acid 151, was found to lead to a better performing intracellular sensor. This suggests that our GrM biosensor may be enhanced further by changing its permutation and Thr151. As an alternative approach, a recently developed transgene-encoded bioluminescent sensor for protease activity based on Gaussia luciferase (GLuc) [297], could be adapted to detect GrM activity. iGLuc is a fusion protein of murine pro-interleukin 1 beta and GLuc, which forms protein aggregates that render GLuc enzymatically inactive. Upon protease-mediated cleavage of pro-interleukin 1 beta, the protein aggregates disassemble, leading to monomerization and activation of the sensor. This protease sensor has successfully been used to detect caspase-1 activity in mice in a specific manner, with high signal-to-background ratios.

Our GrM sensor provides an interesting tool to monitor and distinguish granzyme entry and intracellular activity during cancer development, inflammation, and virus infections *in vivo*. For this purpose, biosensors for the other human granzymes would also need to be developed. Granzyme delivery and activity in tumor clearance could be monitored in (humanized) mouse cancer models. When these mice are injected or (xeno)grafted with tumor cells expressing the granzyme sensor

together with constitutively active Renilla luciferase, granzyme entry and tumor growth/clearance can be monitored simultaneously. Alternatively, transgene mice expressing the sensor (under a tissue-specific promoter) could be used to monitor granzyme activity during inflammation or viral infections. As such, granzyme sensor activation is used to monitor the effector phase of the immune system, which will facilitate novel therapeutic advances.

Chapter 9

Summarizing discussion

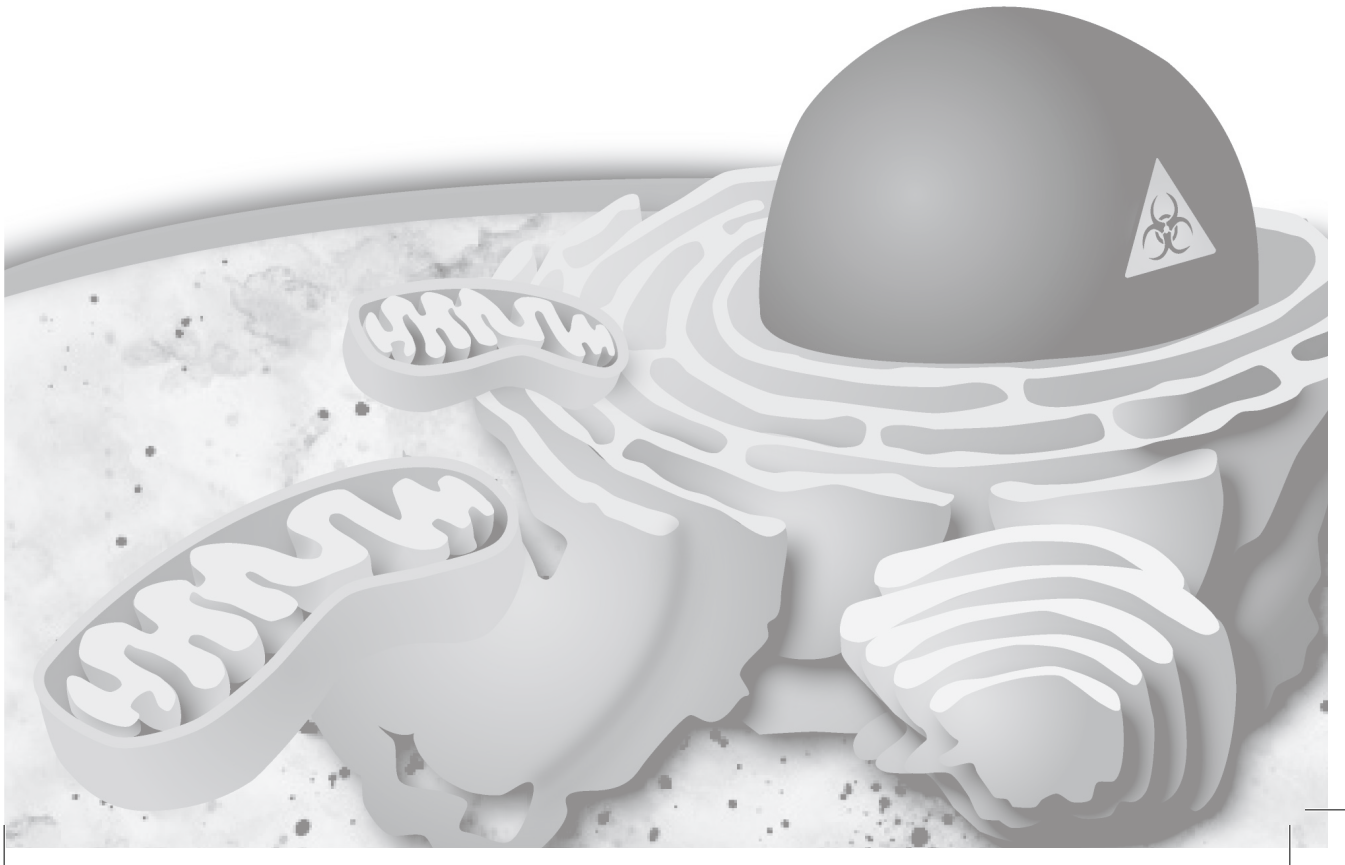

Summarizing discussion

The granule-exocytosis pathway is the main mechanism via which cytotoxic lymphocytes exert their anti-viral and anti-tumor functions. Upon recognition of a target cell, activated immune cells deliver a set of homologous serine proteases known as granzymes inside the target cell, where they can exert their intracellular functions.

Granzyme M (GrM) has been linked to the induction of cell death in tumor cells [31, 32, 41, 45] and the noncytotoxic inhibition of cytomegalovirus (CMV) replication [70]. In the present thesis, we have further elucidated the anti-cancer and anti-viral functions of GrM. Our findings have resulted in a better understanding of how immune cells fulfil their (non)cytotoxic functions, which may eventually lead to novel therapeutic approaches. The current findings as well as some future perspectives are discussed in this chapter.

Physiological relevance of GrM

The importance of the granule-exocytosis pathway in immunosurveillance against tumors becomes evident in human individuals bearing mutations in the perforin gene *PRF1*, which are more than 100 times more likely to develop haematological cancers [58]. Further evidence for the role of the granule-exocytosis pathway comes from perforin-deficient mouse models. These knockout mice are significantly impaired in their ability to clear transplanted and injected tumor cells, and spontaneously develop highly aggressive disseminated B-cell lymphomas [55-57]. Mice that are deficient in GrA and GrB, however, show no impaired tumor clearance [60]. Similarly, a GrM knockout mouse model showed no obvious phenotype regarding tumor clearance [62]. This may be due to several reasons. Firstly, the family of granzymes may be redundant in their functioning. For all human granzymes, roles in tumor cell killing have been suggested *in vitro* [288]. Secondly, there may be species-specific differences between human granzymes and their mouse orthologs. Human and mouse GrM are highly homologous (~70%), but the granzyme family is much more extensive in mice (10 granzymes) than in humans (5 granzymes), suggesting that granzyme specificities and functions may not have been conserved across species. Indeed, for GrA and GrB, species-specific differences have been identified between the human and mouse orthologs [121, 122, 154, 200]. GrB from both species cleaves pro-caspase 3, whereas only human GrB can cleave BID [121, 122, 154, 200]. In **Chapter 3**, we have characterized the primary and extended specificities of both human and mouse GrM. Profiling of the macromolecular substrate specificities of the two orthologs using both gel-based and MS-based proteomics approaches revealed that mouse and human GrM only shared a partially overlapping set of substrates. Furthermore, species-specific differences in substrate amino acid sequences also affected GrM cleavage: whilst both human and mouse GrM could efficiently proteolyze human NPM, neither ortholog could cleave mouse NPM. This was due to a difference in the prime site residues between human and mouse NPM: specific replacement of these residues with the amino acids present in human NPM

restored cleavage by GrM from both species (Chapter 3). This is the first time that prime site residues have been shown to be important for substrate recognition by GrM. Importantly, several mouse tumor cell lines resisted both human and mouse GrM-induced cell death, whereas all human tumor cell lines tested were sensitive to GrM from both species (Chapter 3). This corresponds to the absence of a phenotype on tumor clearance in GrM knockout mice. The lack of GrM-mediated cytotoxicity could be due to the presence of a GrM-specific serpin in mouse tumor cells (*e.g.* SPI-CI [36]), or due to species-specific differences in GrM substrates. In **Chapter 4**, we have identified at least one possible mechanism via which mouse tumor cells may resist GrM-induced cell death: whilst GrM can efficiently cleave human FADD and induce caspase activation and subsequent apoptosis [32], mouse FADD cannot be cleaved by GrM. Together, these results stress that caution is absolutely essential when interpreting data on GrM obtained in mouse models.

To study the physiological relevance of GrM in tumor cell clearance, a humanized mouse cancer model should be used. This mouse model should be completely immunodeficient (*e.g.* RAG2$^{-/-}$γc$^{-/-}$ mice), and should be xenografted or injected with luciferase-transduced human cancer cells. After the tumor has grown, human cytotoxic lymphocytes should be injected, and their ability to clear tumor should be observed over time using bioluminescence. To determine the physiological relevance of each granzyme, the cytotoxic lymphocytes could be transduced with (inducible) knockdown constructs targeting a specific granzyme. In **Chapter 9**, we have developed biosensors that could also be used in such a humanized mouse model to monitor granzyme activity inside the targeted tumor cells.

Mechanism of GrM-induced tumor cell killing

In **Chapter 5**, we first comprehensively characterized GrM-induced cell death. GrM perturbed the mitochondria and induced caspase-dependent cell death that bore various hallmarks of classical apoptosis. Over the years, a number of substrates have been identified that are cleaved by GrM during apoptosis: FADD [94], hnRNP K [47], survivin [42], NPM [31], α-tubulin [45], Hsp75 [43], ICAD and PARP [44]. Of these substrates, only FADD has unequivocally been shown to be required for GrM-induced cytotoxicity [94]. In Chapter 5, however, we demonstrate that cells lacking a downstream effector of FADD (caspase-8) are not completely resistant to GrM. Moreover, these cells go into G2/M cell cycle arrest after GrM treatment. In order to identify via which substrate GrM induces cell cycle arrest, we performed positional complementary proteomics on human tumor cells treated with GrM (Chapter 5). GrM cleaved the nuclear enzyme DNA topoisomerase II alpha (topoIIα), which is essential for chromosome condensation, segregation, and replication in proliferating cells [219]. Cleavage by GrM led to the nuclear exit of the topoIIα functional domains, and loss of topoIIα resulted in G2/M cell cycle arrest and caspase-dependent apoptosis, which phenocopied GrM-induced apoptosis (Chapter 5). This is the first time that a granzyme has been demonstrated to induce cell cycle arrest. The cell cycle arrest induced by GrM is caspase-independent, which makes it

tempting to speculate that if a tumor cell can resist cytotoxic lymphocyte-induced apoptosis, for instance by overexpressing inhibitors of apoptosis [226], it would still be sensitive to GrM-induced cell cycle arrest. This could fit into the equilibrium phase of the current cancer immunoediting model of the 'three E's' (elimination, equilibrium and escape) [298-300] in the sense that the immune system could maintain an equilibrium not only by killing tumor cells, but also by arresting tumor growth.

Interestingly, topoIIα is not the only topoisomerase that can be proteolytically cleaved during apoptosis: topoisomerase I, which breaks and rejoins single-stranded DNA in transcription, DNA recombination and DNA replication, is cleaved by GrB [228], and topoisomerases I, IIα and IIβ are cleaved by caspases during apoptosis [229-231, 301]. The effects of these cleavages are unknown, but suggest that the targeting of topoisomerases is a general phenomenon during apoptosis. A shared GrB/GrM substrate that could also contribute to cell cycle arrest induction is α-tubulin, the cleavage of which results in the stabilization of microtubule polymers [45, 232, 233] in a manner that resembles the effects of the G2/M cell cycle arrest-inducing anti-cancer drug paclitaxel (Taxol). Whether granzymes other than GrM also induce cell cycle arrest remains an interesting question that deserved further study.

TopoIIα is a current anti-cancer target for chemotherapeutics such as etoposide and doxorubicin [223]. It would be interesting to see how GrM and chemotherapeutics would function together. On the one hand, one might envision a synergistic role: cells that over-express topoIIα and are hence less sensitive to GrM, may be killed by topoIIα poisons such as etoposide, whereas cells that down-regulate their topoIIα levels to avoid chemotherapeutic killing, would be more sensitive to GrM. On the other hand, one could also imagine that GrM-mediated nuclear exit of topoIIα would lead to decreased sensitivity to topoIIα poisons. Such an effect has been described for a truncated topoIIα variant, which – as a result of a heterozygous gene deletion – lacks the C-terminal domain containing the NLS [302]. As a result, topoIIα no longer localizes to the nucleus, and the non-small-cell lung carcinoma cells expressing this variant are therefore less sensitive to etoposide-mediated killing [302]. Perhaps the cytoplasmic pool of topoIIα somehow competes with the nuclear topoIIα/DNA cleavage complexes for etoposide binding, resulting in less 'poisoned' nuclear topoIIα, and hence a decreased sensitivity. It would therefore be interesting to see how GrM and topoIIα poisons would act simultaneously.

Synergy between GrM and GrB

Another role that GrM may play in tumor cell killing, is as a synergistic effector to GrB. GrB can cleave Bid and procaspase-3 to efficiently induce apoptosis (reviewed in [48, 49]). By expressing the serine protease inhibitor (serpin) B9 (or PI-9), however, tumor cells can avoid GrB-mediated cytotoxicity [50-53]. PI-9 can be inactivated by GrM-mediated cleavage *in vitro* [28](Figure 1A), and GrM may therefore aid GrB-

functioning in PI-9 expressing tumor cells [28]. The physiological relevance of the GrB/GrM interplay deserves further study, since inhibition of GrB by PI-9 occurred at faster kinetics than GrM-mediated inactivation of PI-9 [28]. To study this, we have first identified the cleavage site of GrM in PI-9 (Figure 1C) (de Poot *et al*., unpublished). Using site-directed mutagenesis, we have developed several mutants of PI-9 in which we have replaced the P1', P2' and/or P3' amino acids with Ala residues (Figure 1B) (de Poot *et al.*, unpublished). GrM-mediated cleavage of the PI-9 P1' mutant was strongly decreased as compared to wild-type, whereas it could still form an SDS-stable serpin/protease complex with GrB (Figure 1C) (de Poot *et al.*, unpublished). The same was true for the PI-9 P2' mutant, but not for the P3' mutant. While GrM-mediated cleavage of the PI-9 P1' and the PI-9 P2' mutants was strongly decreased, it could still be cleaved. In order to completely abolish GrM-mediated cleavage, a PI-9 P1'/P2' double mutant was made. While this mutant could still form a complex with GrB, its cleavage by GrM was completely abrogated (de Poot *et al*., unpublished). We therefore conclude that GrM cleaves PI-9 at Cys^{341} and Cys^{342}. This uncleavable mutant of PI-9 can be used in future studies aimed at elucidating a possible synergistic role between GrB and GrM. Furthermore, PI-9 is known to protect dendritic cells from GrB-mediated destruction, which means that overexpression of our GrM-resistant PI-9 mutant could be of particular value in immunotherapeutic strategies employing PI-9-overexpressing dendritic cells [303].

Inhibition of GrM by SerpinB4

Trafficking, storage, and activity of granzymes in cytotoxic lymphocytes is high regulated to prevent collateral damage [241]. Several fail-safe mechanisms are in place to prevent unwanted granzyme activity. First, granzymes are synthesized as pre-pro-proteases that are not yet catalytically active; removal of the pre- and the pro-sequences at the endoplasmic reticulum and in the lysosomes, respectively, leads to a conformational change that results in active site exposure [18, 21, 22]. Second, the low pH in the cytotoxic storage granules prevents granzyme activity (GrM is maximally active at a pH between 7.5-9 [24]). Furthermore, the highly basic granzymes also bind to proteoglycans (*e.g.* serglycin) in these secretory granules; which also serves to keep granzymes proteolytically inactive. Should active granzymes – in spite of the above mentioned mechanisms – leak from the cytotoxic granules into the cytoplasm, then cytotoxic effector cells have one more means to inhibit granzyme-induced damage. Intracellular serine protease inhibitors (serpins) then serve to protect cells by irreversibly inhibiting the active granzymes. PI-9 is a suicide inhibitor that can prevent GrB-induced cell death [95]. Interestingly, PI-9 is also found in tumor cells, where it correlates with poor prognosis and increased resistance to GrB [50-53]. In **Chapter 6**, we have identified SerpinB4 as a novel intracellular serine protease inhibitor of human GrM. SerpinB4 is the first intracellular inhibitor known for human GrM and is highly expressed by squamous cell carcinomas, where its levels are associated with tumor progression [261]. Its expression may constitute a novel mechanism by which cancer cells can

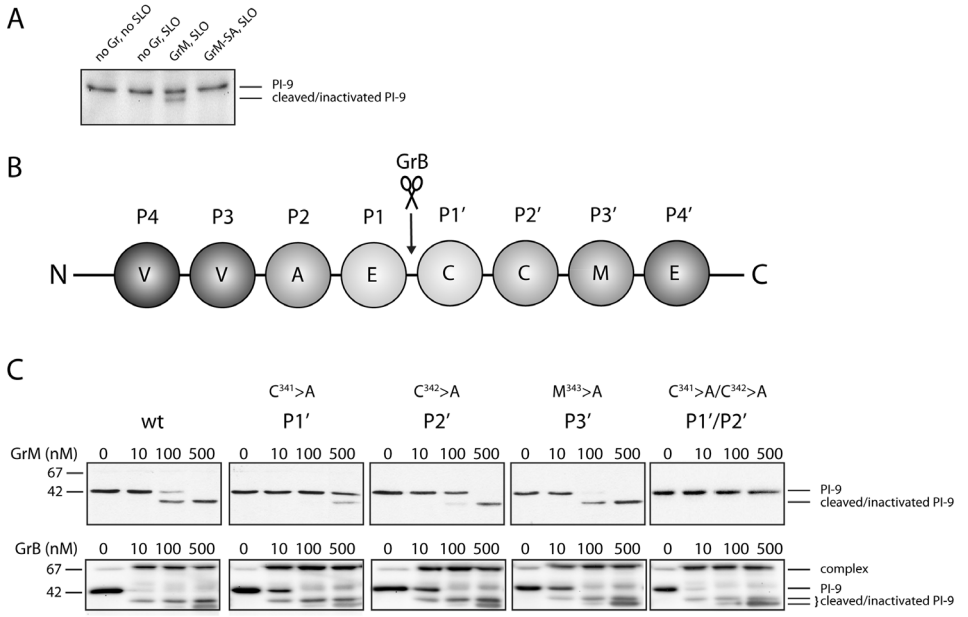

Figure 1. GrM cleaves PI-9 at Cys^{341} and Cys^{342}. (a) HeLa cells transfected with wildtype PI-9 were treated with GrM and the perforin-analogue SLO. Whole cell lysates were then prepared, and immunoblotted for PI-9. **(b)** Schematic overview of the GrB-cleavage site in PI-9, and the surrounding prime (P') and non-prime (P) residues. **(c)** Various mutants of PI-9, in which the P1', P2', P3', or the P1' and P2' residues had been replaced with Ala, were expressed in HeLa cells. Cell-free extracts of these transfected cells were then incubated with increasing concentrations of GrM (upper panels) or GrB (lower panels). Samples were then immunoblotted for PI-9. The classical SDS-stable serpin/protease complex could be seen for GrB/PI-9, as well as the cleavage product of PI-9 produced by GrM (de Poot *et al*., unpublished).

evade cytotoxic lymphocyte-induced GrM-mediated cell death. Overexpression of recombinant SerpinB4 in tumor cells render them less sensitive to GrM-induced cell death and to NK-mediated cytotoxicity (Chapter 6). The physiological relevance of this hypothesis merits further investigation. If SerpinB4 indeed constitutes an evasion mechanism employed by tumor cells to avoid GrM-mediated cytotoxicity, then this has several therapeutic implications. SerpinB4 is already widely used as a prognostic marker for squamous cell carcinomas [96]. In line with our findings, patients with squamous cell carcinomas overexpressing SerpinB4 may benefit less from cellular immunotherapy with for instance NK cells - which contain high levels of GrM - than patients with tumors that do not express SerpinB4. Perhaps SerpinB4 expression can be decreased by clinical intervention to render tumors more sensitive to GrM-induced cytotoxicity, leading to an improved clinical outcome. On the other hand, upregulation of GrM in cytotoxic lymphocytes may also prove to be beneficial in immunotherapy. It is still unknown whether SerpinB4 – like PI-9 – can prevent collateral damage in cytotoxic lymphocytes caused by misdirected granzymes. SerpinB4 protein and RNA expression was absent in hematopoietic cells of the bone marrow and in a variety of lymphoid cells [97]. This would contradict a role for SerpinB4 in the protection of cytotoxic lymphocytes against endogenous GrM. Other (non-)serpin inhibitors, however, could also act as a protection

mechanism against endogenous GrM. Interestingly, SerpinB1, which has originally been identified as a serpin of GrH, also shows some reactivity towards GrM [94]. SerpinB1 is expressed in all human bone marrow leukocytes [304], suggesting that it may function as a GrH/GrM inhibitor in cytotoxic lymphocytes.

GrM as an inhibitor of viral replication

CMV can be controlled by cytotoxic lymphocytes in immunocompetent individuals, but immunocompromised patients – including HIV patients and (stem cell) transplantation recipients – it can cause severe disease. A GrM knockout mouse model underlines the importance of mouse GrM in the control of CMV infection: GrM-deficient mice are more sensitive to mouse CMV than their wild-type counterparts [62]. Interestingly, GrM can cleave the human CMV tegument protein pp71, which is essential for viral replication, and GrM inhibits human CMV replication independently of cell death [70]. In **Chapter 7**, we show that GrM can also inhibit human CMV viral replication via cleavage of the host protein hnRNP K. HnRNP K regulates expression of the immediate-early 2 (IE2) protein, which is required for human CMV replication. Indeed, GrM can reduce IE2 protein levels in human CMV-infected fibroblasts. Importantly, we found for the first time that human CMV-specific CD8+ T cells express GrM. In human CMV-specific effector memory CD8+ T lymphocytes, GrM protein levels were elevated compared to naïve and effector CD8+ T lymphocytes (Chapter 7). These effector memory CD8+ T cells are thought to play an important role in the control of human CMV latency [270]. Interestingly, a number of other known hGrM substrates play roles in viral replication: α-tubulin [45] is involved in viral intracellular transport [72], NPM can be used by viral proteins for nuclear entry [73, 74], and a role for topoIIα has been suggested in the replication of HIV-1 [75, 76], HSV-1 [77], vaccinia virus [78], and Epstein-Barr virus [79]. It is therefore tempting to speculate that cleavage of these host proteins by GrM may also contribute to the anti-viral functions of GrM.

These findings have several therapeutic implications. Viral GrM substrates that are essential for viral replication, for instance, are interesting therapeutic targets. In addition, anti-viral immunotherapy with donor-derived virus-specific cytotoxic lymphocytes may be further boosted by upregulation of GrM in these cells – either via interleukin-stimulation or via genetic manipulation – to inhibit viral replication with increased efficiency. A proof-of-concept study for such a strategy has recently been performed in chronically hepatitis B virus-infected mice: adoptive transfer of GrH-overexpressing NK cells efficiently cleared the hepatitis B virus [68].

Conclusions

This thesis provides a better understanding of the anti-cancer and anti-viral functions of GrM. Novel substrates and an intracellular inhibitor of human GrM have been identified. This knowledge may result in the application of these proteins as novel diagnostic and/or prognostic markers in cancer. Furthermore, modulation of the protease-inhibitor balance between a granzyme and its corresponding serpin

might be a future therapeutic strategy to treat cancers or viral infections. Increased expression of granzymes by cytotoxic lymphocytes and/or down-regulation of serpins in target cells may result in increased intracellular granzyme activity and hence more efficient viral inhibition or tumor cell death.

Addendum

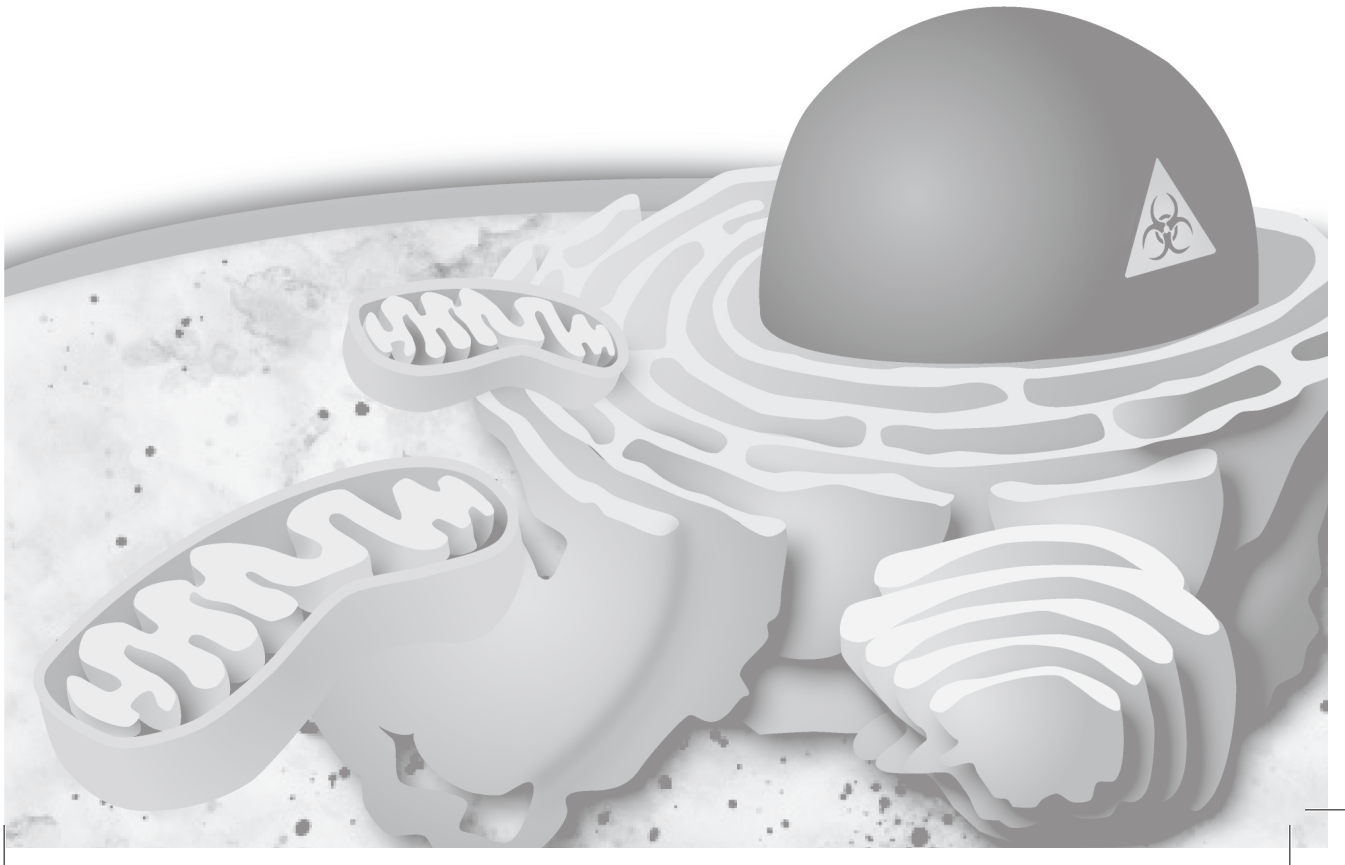

References

1 Walczak, H. and Krammer, P. H. (2000) The CD95 (APO-1/Fas) and the TRAIL (APO-2L) apoptosis systems. Experimental cell research **256**, 58-66

2 Cullen, S. P., Brunet, M. and Martin, S. J. (2010) Granzymes in cancer and immunity. Cell death and differentiation **17**, 616-623

3 Lieberman, J. (2010) Anatomy of a murder: how cytotoxic T cells and NK cells are activated, develop, and eliminate their targets. Immunol Rev **235**, 5-9

4 Russell, J. H. and Ley, T. J. (2002) Lymphocyte-mediated cytotoxicity. Annu Rev Immunol **20**, 323-370

5 Voskoboinik, I., Dunstone, M. A., Baran, K., Whisstock, J. C. and Trapani, J. A. (2010) Perforin: structure, function, and role in human immunopathology. Immunol Rev **235**, 35-54

6 Grossman, W. J., Revell, P. A., Lu, Z. H., Johnson, H., Bredemeyer, A. J. and Ley, T. J. (2003) The orphan granzymes of humans and mice. Current opinion in immunology **15**, 544-552

7 Sattar, R., Ali, S. A. and Abbasi, A. (2003) Bioinformatics of granzymes: sequence comparison and structural studies on granzyme family by homology modeling. Biochem Biophys Res Commun **308**, 726-735

8 Bovenschen, N. and Kummer, J. A. (2010) Orphan granzymes find a home. Immunol Rev **235**, 117-127

9 de Koning, P. J., Kummer, J. A. and Bovenschen, N. (2009) Biology of granzyme M: a serine protease with unique features. Crit Rev Immunol **29**, 307-315

10 Smyth, M. J., Wiltrout, T., Trapani, J. A., Ottaway, K. S., Sowder, R., Henderson, L. E., Kam, C. M., Powers, J. C., Young, H. A. and Sayers, T. J. (1992) Purification and cloning of a novel serine protease, RNK-Met-1, from the granules of a rat natural killer cell leukemia. J Biol Chem **267**, 24418-24425

11 Smyth, M. J., Sayers, T. J., Wiltrout, T., Powers, J. C. and Trapani, J. A. (1993) Met-ase: cloning and distinct chromosomal location of a serine protease preferentially expressed in human natural killer cells. J Immunol **151**, 6195-6205

12 Kelly, J. M., O'Connor, M. D., Hulett, M. D., Thia, K. Y. and Smyth, M. J. (1996) Cloning and expression of the recombinant mouse natural killer cell granzyme Met-ase-1. Immunogenetics **44**, 340-350

13 Baker, E., Sutherland, G. R. and Smyth, M. J. (1994) The gene encoding a human natural killer cell granule serine protease, Met-ase 1, maps to chromosome 19p13.3. Immunogenetics **39**, 294-295

14 Pilat, D., Fink, T., Obermaier-Skrobanek, B., Zimmer, M., Wekerle, H., Lichter, P. and Jenne, D. E. (1994) The human Met-ase gene (GZMM): structure, sequence, and close physical linkage to the serine protease gene cluster on 19p13.3. Genomics **24**, 445-450

15 Thia, K. Y., Jenkins, N. A., Gilbert, D. J., Copeland, N. G. and Smyth, M. J. (1995) The natural killer cell serine protease gene Lmet1 maps to mouse chromosome 10. Immunogenetics **41**, 47-49

16 Zimmer, M., Medcalf, R. L., Fink, T. M., Mattmann, C., Lichter, P. and Jenne, D. E. (1992) Three human elastase-like genes coordinately expressed in the myelomonocyte lineage are organized as a single genetic locus on 19pter. Proc Natl Acad Sci U S A **89**, 8215-8219

17 Smyth, M. J., Hulett, M. D., Thia, K. Y., Young, H. A., Sayers, T. J., Carter, C. R. and Trapani, J. A. (1995) Cloning and characterization of a novel NK cell-specific serine protease gene and its functional 5'-flanking sequences. Immunogenetics **42**, 101-111

18 McGuire, M. J., Lipsky, P. E. and Thiele, D. L. (1993) Generation of active myeloid and lymphoid granule serine proteases requires processing by the granule thiol protease dipeptidyl peptidase I. J Biol Chem **268**, 2458-2467

19 Smyth, M. J., O'Connor, M. D. and Trapani, J. A. (1996) Granzymes: a variety of serine

protease specificities encoded by genetically distinct subfamilies. J Leukoc Biol **60**, 555-562
20 Smyth, M. J., O'Connor, M. D., Trapani, J. A., Kershaw, M. H. and Brinkworth, R. I. (1996) A novel substrate-binding pocket interaction restricts the specificity of the human NK cell-specific serine protease, Met-ase-1. J Immunol **156**, 4174-4181
21 Pham, C. T. and Ley, T. J. (1999) Dipeptidyl peptidase I is required for the processing and activation of granzymes A and B in vivo. Proc Natl Acad Sci U S A **96**, 8627-8632
22 Kummer, J. A., Kamp, A. M., Citarella, F., Horrevoets, A. J. and Hack, C. E. (1996) Expression of human recombinant granzyme A zymogen and its activation by the cysteine proteinase cathepsin C. J Biol Chem **271**, 9281-9286
23 Rukamp, B. J., Kam, C. M., Natarajan, S., Bolton, B. W., Smyth, M. J., Kelly, J. M. and Powers, J. C. (2004) Subsite specificities of granzyme M: a study of inhibitors and newly synthesized thiobenzyl ester substrates. Archives of biochemistry and biophysics **422**, 9-22
24 Wu, L., Wang, L., Hua, G., Liu, K., Yang, X., Zhai, Y., Bartlam, M., Sun, F. and Fan, Z. (2009) Structural basis for proteolytic specificity of the human apoptosis-inducing granzyme M. J Immunol **183**, 421-429
25 Smyth, M. J., O'Connor, M. D., Kelly, J. M., Ganesvaran, P., Thia, K. Y. and Trapani, J. A. (1995) Expression of recombinant human Met-ase-1: a NK cell-specific granzyme. Biochem Biophys Res Commun **217**, 675-683
26 Khurshid, R., Saleem, M., Akhtar, M. S. and Salim, A. (2011) Granzyme M: characterization with sites of post-translational modification and specific sites of interaction with substrates and inhibitors. Mol Biol Rep **38**, 2953-2960
27 Schechter, I. and Berger, A. (1967) On the size of the active site in proteases. I. Papain. Biochem Biophys Res Commun **27**, 157-162
28 Mahrus, S., Kisiel, W. and Craik, C. S. (2004) Granzyme M is a regulatory protease that inactivates proteinase inhibitor 9, an endogenous inhibitor of granzyme B. J Biol Chem **279**, 54275-54282
29 Mahrus, S. and Craik, C. S. (2005) Selective chemical functional probes of granzymes A and B reveal granzyme B is a major effector of natural killer cell-mediated lysis of target cells. Chem Biol **12**, 567-577
30 de Poot, S. A., Westgeest, M., Hostetter, D. R., Van Damme, P., Plasman, K., Demeyer, K., Broekhuizen, R., Gevaert, K., Craik, C. S. and Bovenschen, N. (2011) Human and mouse granzyme M display divergent and species-specific substrate specificities. Biochem J **437**, 431-442
31 Cullen, S. P., Afonina, I. S., Donadini, R., Luthi, A. U., Medema, J. P., Bird, P. I. and Martin, S. J. (2009) Nucleophosmin is cleaved and inactivated by the cytotoxic granule protease granzyme M during natural killer cell-mediated killing. J Biol Chem **284**, 5137-5147
32 Wang, S., Xia, P., Shi, L. and Fan, Z. (2012) FADD cleavage by NK cell granzyme M enhances its self-association to facilitate procaspase-8 recruitment for auto-processing leading to caspase cascade. Cell death and differentiation **19**, 605-615
33 de Poot, S. A., Lai, K. W., Hovingh, E. S. and Bovenschen, N. (2013) Granzyme M cannot induce cell death via cleavage of mouse FADD. Apoptosis **18**, 533-534
34 Smyth, M. J., Browne, K. A., Kinnear, B. F., Trapani, J. A. and Warren, H. S. (1995) Distinct granzyme expression in human CD3- CD56+ large granular- and CD3- CD56+ small high density-lymphocytes displaying non-MHC-restricted cytolytic activity. J Leukoc Biol **57**, 88-93
35 Sayers, T. J., Brooks, A. D., Ward, J. M., Hoshino, T., Bere, W. E., Wiegand, G. W., Kelly, J. M. and Smyth, M. J. (2001) The restricted expression of granzyme M in human lymphocytes. J Immunol **166**, 765-771
36 Bots, M., Kolfschoten, I. G., Bres, S. A., Rademaker, M. T., de Roo, G. M., Kruse, M., Franken, K. L., Hahne, M., Froelich, C. J., Melief, C. J., Offringa, R. and Medema, J. P. (2005) SPI-CI and SPI-6 cooperate in the protection from effector cell-mediated cytotoxicity. Blood **105**, 1153-1161

37 Bade, B., Boettcher, H. E., Lohrmann, J., Hink-Schauer, C., Bratke, K., Jenne, D. E., Virchow, J. C., Jr. and Luttmann, W. (2005) Differential expression of the granzymes A, K and M and perforin in human peripheral blood lymphocytes. Int Immunol **17**, 1419-1428

38 de Koning, P. J., Tesselaar, K., Bovenschen, N., Colak, S., Quadir, R., Volman, T. J. and Kummer, J. A. (2010) The cytotoxic protease granzyme M is expressed by lymphocytes of both the innate and adaptive immune system. Mol Immunol **47**, 903-911

39 van Domselaar, R., de Poot, S. A., Remmerswaal, E. B., Lai, K. W., Ten Berge, I. J. and Bovenschen, N. (2013) Granzyme M targets host cell hnRNP K that is essential for human cytomegalovirus replication. Cell death and differentiation **20**, 419-429

40 Zhang, B., Zhang, J. and Tian, Z. (2008) Comparison in the effects of IL-2, IL-12, IL-15 and IFNalpha on gene regulation of granzymes of human NK cell line NK-92. Int Immunopharmacol **8**, 989-996

41 Kelly, J. M., Waterhouse, N. J., Cretney, E., Browne, K. A., Ellis, S., Trapani, J. A. and Smyth, M. J. (2004) Granzyme M mediates a novel form of perforin-dependent cell death. J Biol Chem **279**, 22236-22242

42 Hu, D., Liu, S., Shi, L., Li, C., Wu, L. and Fan, Z. (2010) Cleavage of survivin by Granzyme M triggers degradation of the survivin-X-linked inhibitor of apoptosis protein (XIAP) complex to free caspase activity leading to cytolysis of target tumor cells. J Biol Chem **285**, 18326-18335

43 Hua, G., Zhang, Q. and Fan, Z. (2007) Heat shock protein 75 (TRAP1) antagonizes reactive oxygen species generation and protects cells from granzyme M-mediated apoptosis. J Biol Chem **282**, 20553-20560

44 Lu, H., Hou, Q., Zhao, T., Zhang, H., Zhang, Q., Wu, L. and Fan, Z. (2006) Granzyme M directly cleaves inhibitor of caspase-activated DNase (CAD) to unleash CAD leading to DNA fragmentation. J Immunol **177**, 1171-1178

45 Bovenschen, N., de Koning, P. J., Quadir, R., Broekhuizen, R., Damen, J. M., Froelich, C. J., Slijper, M. and Kummer, J. A. (2008) NK cell protease granzyme M targets alpha-tubulin and disorganizes the microtubule network. J Immunol **180**, 8184-8191

46 Timmer, J. C. and Salvesen, G. S. (2007) Caspase substrates. Cell death and differentiation **14**, 66-72

47 van Domselaar, R., Quadir, R., van der Made, A. M., Broekhuizen, R. and Bovenschen, N. (2012) All human granzymes target hnRNP K that is essential for tumor cell viability. J Biol Chem **287**, 22854-22864

48 Lord, S. J., Rajotte, R. V., Korbutt, G. S. and Bleackley, R. C. (2003) Granzyme B: a natural born killer. Immunol Rev **193**, 31-38

49 Trapani, J. A. and Sutton, V. R. (2003) Granzyme B: pro-apoptotic, antiviral and antitumor functions. Current opinion in immunology **15**, 533-543

50 Bird, C. H., Sutton, V. R., Sun, J., Hirst, C. E., Novak, A., Kumar, S., Trapani, J. A. and Bird, P. I. (1998) Selective regulation of apoptosis: the cytotoxic lymphocyte serpin proteinase inhibitor 9 protects against granzyme B-mediated apoptosis without perturbing the Fas cell death pathway. Molecular and cellular biology **18**, 6387-6398

51 Medema, J. P., de Jong, J., Peltenburg, L. T., Verdegaal, E. M., Gorter, A., Bres, S. A., Franken, K. L., Hahne, M., Albar, J. P., Melief, C. J. and Offringa, R. (2001) Blockade of the granzyme B/perforin pathway through overexpression of the serine protease inhibitor PI-9/SPI-6 constitutes a mechanism for immune escape by tumors. Proc Natl Acad Sci U S A **98**, 11515-11520

52 Bladergroen, B. A., Meijer, C. J., ten Berge, R. L., Hack, C. E., Muris, J. J., Dukers, D. F., Chott, A., Kazama, Y., Oudejans, J. J., van Berkum, O. and Kummer, J. A. (2002) Expression of the granzyme B inhibitor, protease inhibitor 9, by tumor cells in patients with non-Hodgkin and Hodgkin lymphoma: a novel protective mechanism for tumor cells to circumvent the immune system? Blood **99**, 232-237

53 van Houdt, I. S., Oudejans, J. J., van den Eertwegh, A. J., Baars, A., Vos, W., Bladergroen,

B. A., Rimoldi, D., Muris, J. J., Hooijberg, E., Gundy, C. M., Meijer, C. J. and Kummer, J. A. (2005) Expression of the apoptosis inhibitor protease inhibitor 9 predicts clinical outcome in vaccinated patients with stage III and IV melanoma. Clin Cancer Res **11**, 6400-6407

54 Andrade, F., Fellows, E., Jenne, D. E., Rosen, A. and Young, C. S. (2007) Granzyme H destroys the function of critical adenoviral proteins required for viral DNA replication and granzyme B inhibition. Embo J **26**, 2148-2157

55 Kagi, D., Ledermann, B., Burki, K., Seiler, P., Odermatt, B., Olsen, K. J., Podack, E. R., Zinkernagel, R. M. and Hengartner, H. (1994) Cytotoxicity mediated by T cells and natural killer cells is greatly impaired in perforin-deficient mice. Nature **369**, 31-37

56 Lowin, B., Beermann, F., Schmidt, A. and Tschopp, J. (1994) A null mutation in the perforin gene impairs cytolytic T lymphocyte- and natural killer cell-mediated cytotoxicity. Proc Natl Acad Sci U S A **91**, 11571-11575

57 Smyth, M. J., Thia, K. Y., Street, S. E., MacGregor, D., Godfrey, D. I. and Trapani, J. A. (2000) Perforin-mediated cytotoxicity is critical for surveillance of spontaneous lymphoma. The Journal of experimental medicine **192**, 755-760

58 Chia, J., Yeo, K. P., Whisstock, J. C., Dunstone, M. A., Trapani, J. A. and Voskoboinik, I. (2009) Temperature sensitivity of human perforin mutants unmasks subtotal loss of cytotoxicity, delayed FHL, and a predisposition to cancer. Proc Natl Acad Sci U S A **106**, 9809-9814

59 Brennan, A. J., Chia, J., Trapani, J. A. and Voskoboinik, I. (2010) Perforin deficiency and susceptibility to cancer. Cell death and differentiation **17**, 607-615

60 Davis, J. E., Smyth, M. J. and Trapani, J. A. (2001) Granzyme A and B-deficient killer lymphocytes are defective in eliciting DNA fragmentation but retain potent in vivo anti-tumor capacity. Eur J Immunol **31**, 39-47

61 Smyth, M. J., Street, S. E. and Trapani, J. A. (2003) Cutting edge: granzymes A and B are not essential for perforin-mediated tumor rejection. J Immunol **171**, 515-518

62 Pao, L. I., Sumaria, N., Kelly, J. M., van Dommelen, S., Cretney, E., Wallace, M. E., Anthony, D. A., Uldrich, A. P., Godfrey, D. I., Papadimitriou, J. M., Mullbacher, A., Degli-Esposti, M. A. and Smyth, M. J. (2005) Functional analysis of granzyme M and its role in immunity to infection. J Immunol **175**, 3235-3243

63 Pegram, H. J., Haynes, N. M., Smyth, M. J., Kershaw, M. H. and Darcy, P. K. (2010) Characterizing the anti-tumor function of adoptively transferred NK cells in vivo. Cancer Immunol Immunother **59**, 1235-1246

64 van Domselaar, R. and Bovenschen, N. (2011) Cell death-independent functions of granzymes: hit viruses where it hurts. Rev Med Virol **21**, 301–314

65 Knickelbein, J. E., Khanna, K. M., Yee, M. B., Baty, C. J., Kinchington, P. R. and Hendricks, R. L. (2008) Noncytotoxic lytic granule-mediated CD8+ T cell inhibition of HSV-1 reactivation from neuronal latency. Science (New York, N.Y **322**, 268-271

66 Zhong, C., Li, C., Wang, X., Toyoda, T., Gao, G. and Fan, Z. (2012) Granzyme K inhibits replication of influenza virus through cleaving the nuclear transport complex importin alpha1/beta dimer of infected host cells. Cell death and differentiation **19**, 882-890

67 Romero, V., Fellows, E., Jenne, D. E. and Andrade, F. (2009) Cleavage of La protein by granzyme H induces cytoplasmic translocation and interferes with La-mediated HCV-IRES translational activity. Cell death and differentiation **16**, 340-348

68 Tang, H., Li, C., Wang, L., Zhang, H. and Fan, Z. (2012) Granzyme H of cytotoxic lymphocytes is required for clearance of the hepatitis B virus through cleavage of the hepatitis B virus X protein. J Immunol **188**, 824-831

69 Anthony, D. A., Andrews, D. M., Watt, S. V., Trapani, J. A. and Smyth, M. J. (2010) Functional dissection of the granzyme family: cell death and inflammation. Immunol Rev **235**, 73-92

70 van Domselaar, R., Philippen, L. E., Quadir, R., Wiertz, E. J., Kummer, J. A. and Bovenschen, N. (2010) Noncytotoxic inhibition of cytomegalovirus replication through NK cell protease granzyme M-mediated cleavage of viral phosphoprotein 71. J Immunol **185**, 7605-7613

71 Bresnahan, W. A. and Shenk, T. E. (2000) UL82 virion protein activates expression of

immediate early viral genes in human cytomegalovirus-infected cells. Proc Natl Acad Sci U S A **97**, 14506-14511

72 Dohner, K., Nagel, C. H. and Sodeik, B. (2005) Viral stop-and-go along microtubules: taking a ride with dynein and kinesins. Trends Microbiol **13**, 320-327

73 Mai, R. T., Yeh, T. S., Kao, C. F., Sun, S. K., Huang, H. H. and Wu Lee, Y. H. (2006) Hepatitis C virus core protein recruits nucleolar phosphoprotein B23 and coactivator p300 to relieve the repression effect of transcriptional factor YY1 on B23 gene expression. Oncogene **25**, 448-462

74 Huang, W. H., Yung, B. Y., Syu, W. J. and Lee, Y. H. (2001) The nucleolar phosphoprotein B23 interacts with hepatitis delta antigens and modulates the hepatitis delta virus RNA replication. J Biol Chem **276**, 25166-25175

75 Kondapi, A. K., Satyanarayana, N. and Saikrishna, A. D. (2006) A study of the topoisomerase II activity in HIV-1 replication using the ferrocene derivatives as probes. Archives of biochemistry and biophysics **450**, 123-132

76 Lokeswara Balakrishna, S., Satyanarayana, N. and Kondapi, A. K. (2013) Involvement of human topoisomerase II isoforms in HIV-1 reverse transcription. Archives of biochemistry and biophysics **532**, 91-102

77 Advani, S. J., Weichselbaum, R. R. and Roizman, B. (2003) Herpes simplex virus 1 activates cdc2 to recruit topoisomerase II alpha for post-DNA synthesis expression of late genes. Proc Natl Acad Sci U S A **100**, 4825-4830

78 Lin, Y. C., Li, J., Irwin, C. R., Jenkins, H., DeLange, L. and Evans, D. H. (2008) Vaccinia virus DNA ligase recruits cellular topoisomerase II to sites of viral replication and assembly. Journal of virology **82**, 5922-5932

79 Lee, C. P., Chen, J. Y., Wang, J. T., Kimura, K., Takemoto, A., Lu, C. C. and Chen, M. R. (2007) Epstein-Barr virus BGLF4 kinase induces premature chromosome condensation through activation of condensin and topoisomerase II. Journal of virology **81**, 5166-5180

80 Froelich, C. J., Pardo, J. and Simon, M. M. (2009) Granule-associated serine proteases: granzymes might not just be killer proteases. Trends Immunol **30**, 117-123

81 Romero, V. and Andrade, F. (2008) Non-apoptotic functions of granzymes. Tissue Antigens **71**, 409-416

82 Buzza, M. S., Zamurs, L., Sun, J., Bird, C. H., Smith, A. I., Trapani, J. A., Froelich, C. J., Nice, E. C. and Bird, P. I. (2005) Extracellular matrix remodeling by human granzyme B via cleavage of vitronectin, fibronectin, and laminin. J Biol Chem **280**, 23549-23558

83 Hiebert, P. R., Boivin, W. A., Abraham, T., Pazooki, S., Zhao, H. and Granville, D. J. (2011) Granzyme B contributes to extracellular matrix remodeling and skin aging in apolipoprotein E knockout mice. Exp Gerontol **46**, 489-499

84 Metkar, S. S., Menaa, C., Pardo, J., Wang, B., Wallich, R., Freudenberg, M., Kim, S., Raja, S. M., Shi, L., Simon, M. M. and Froelich, C. J. (2008) Human and mouse granzyme A induce a proinflammatory cytokine response. Immunity **29**, 720-733

85 Irmler, M., Hertig, S., MacDonald, H. R., Sadoul, R., Becherer, J. D., Proudfoot, A., Solari, R. and Tschopp, J. (1995) Granzyme A is an interleukin 1 beta-converting enzyme. The Journal of experimental medicine **181**, 1917-1922

86 Joeckel, L. T., Wallich, R., Martin, P., Sanchez-Martinez, D., Weber, F. C., Martin, S. F., Borner, C., Pardo, J., Froelich, C. and Simon, M. M. (2011) Mouse granzyme K has pro-inflammatory potential. Cell death and differentiation **18**, 1112-1119

87 Anthony, D. A., Andrews, D. M., Chow, M., Watt, S. V., House, C., Akira, S., Bird, P. I., Trapani, J. A. and Smyth, M. J. (2010) A Role for Granzyme M in TLR4-Driven Inflammation and Endotoxicosis. J Immunol **185**, 1794-1803

88 Hollestelle, M. J., Lai, K. W., van Deuren, M., Lenting, P. J., de Groot, P. G., Sprong, T. and Bovenschen, N. (2011) Cleavage of von Willebrand factor by granzyme M destroys its factor VIII binding capacity. PLoS One **6**, e24216

89 de Koning, P. J., Kummer, J. A., de Poot, S. A., Quadir, R., Broekhuizen, R., McGettrick, A. F.,

Higgins, W. J., Devreese, B., Worrall, D. M. and Bovenschen, N. (2011) Intracellular serine protease inhibitor SERPINB4 inhibits granzyme M-induced cell death. PLoS One **6**, e22645

90 Sun, J., Ooms, L., Bird, C. H., Sutton, V. R., Trapani, J. A. and Bird, P. I. (1997) A new family of 10 murine ovalbumin serpins includes two homologs of proteinase inhibitor 8 and two homologs of the granzyme B inhibitor (proteinase inhibitor 9). J Biol Chem **272**, 15434-15441

91 Bots, M., L, V. A. N. B., Rademaker, M. T., Offringa, R. and Medema, J. P. (2006) Serpins prevent granzyme-induced death in a species-specific manner. Immunol Cell Biol **84**, 79-86

92 Schick, C., Kamachi, Y., Bartuski, A. J., Cataltepe, S., Schechter, N. M., Pemberton, P. A. and Silverman, G. A. (1997) Squamous cell carcinoma antigen 2 is a novel serpin that inhibits the chymotrypsin-like proteinases cathepsin G and mast cell chymase. J Biol Chem **272**, 1849-1855

93 Silverman, G. A., Whisstock, J. C., Askew, D. J., Pak, S. C., Luke, C. J., Cataltepe, S., Irving, J. A. and Bird, P. I. (2004) Human clade B serpins (ov-serpins) belong to a cohort of evolutionarily dispersed intracellular proteinase inhibitor clades that protect cells from promiscuous proteolysis. Cell Mol Life Sci **61**, 301-325

94 Wang, L., Li, Q., Wu, L., Liu, S., Zhang, Y., Yang, X., Zhu, P., Zhang, H., Zhang, K., Lou, J., Liu, P., Tong, L., Sun, F. and Fan, Z. (2013) Identification of SERPINB1 as a physiological inhibitor of human granzyme H. J Immunol **190**, 1319-1330

95 Sun, J., Bird, C. H., Sutton, V., McDonald, L., Coughlin, P. B., De Jong, T. A., Trapani, J. A. and Bird, P. I. (1996) A cytosolic granzyme B inhibitor related to the viral apoptotic regulator cytokine response modifier A is present in cytotoxic lymphocytes. J Biol Chem **271**, 27802-27809

96 de Bruijn, H. W., Duk, J. M., van der Zee, A. G., Pras, E., Willemse, P. H., Boonstra, H., Hollema, H., Mourits, M. J., de Vries, E. G. and Aalders, J. G. (1998) The clinical value of squamous cell carcinoma antigen in cancer of the uterine cervix. Tumour Biol **19**, 505-516

97 Cataltepe, S., Gornstein, E. R., Schick, C., Kamachi, Y., Chatson, K., Fries, J., Silverman, G. A. and Upton, M. P. (2000) Co-expression of the squamous cell carcinoma antigens 1 and 2 in normal adult human tissues and squamous cell carcinomas. J Histochem Cytochem **48**, 113-122

98 Hsu, K. F., Huang, S. C., Shiau, A. L., Cheng, Y. M., Shen, M. R., Chen, Y. F., Lin, C. Y., Lee, B. H. and Chou, C. Y. (2007) Increased expression level of squamous cell carcinoma antigen 2 and 1 ratio is associated with poor prognosis in early-stage uterine cervical cancer. Int J Gynecol Cancer **17**, 174-181

99 Deng, Z., Hasegawa, M., Yamashita, Y., Matayoshi, S., Kiyuna, A., Agena, S., Uehara, T., Maeda, H. and Suzuki, M. (2012) Prognostic value of human papillomavirus and squamous cell carcinoma antigen in head and neck squamous cell carcinoma. Cancer Sci **103**, 2127-2134

100 van Domselaar, R., de Poot, S. A. and Bovenschen, N. (2010) Proteomic profiling of proteases: tools for granzyme degradomics. Expert Rev Proteomics **7**, 347-359

101 Lopez-Otin, C. and Overall, C. M. (2002) Protease degradomics: a new challenge for proteomics. Nat Rev Mol Cell Biol **3**, 509-519

102 Puente, X. S., Sanchez, L. M., Overall, C. M. and Lopez-Otin, C. (2003) Human and mouse proteases: a comparative genomic approach. Nat Rev Genet **4**, 544-558

103 Rawlings, N. D., Barrett, A. J. and Bateman, A. (2010) MEROPS: the peptidase database. Nucleic acids research **38**, D227-233

104 Khan, A. R. and James, M. N. (1998) Molecular mechanisms for the conversion of zymogens to active proteolytic enzymes. Protein Sci **7**, 815-836

105 Citron, M., Westaway, D., Xia, W., Carlson, G., Diehl, T., Levesque, G., Johnson-Wood, K., Lee, M., Seubert, P., Davis, A., Kholodenko, D., Motter, R., Sherrington, R., Perry, B., Yao, H., Strome, R., Lieberburg, I., Rommens, J., Kim, S., Schenk, D., Fraser, P., St George Hyslop, P. and Selkoe, D. J. (1997) Mutant presenilins of Alzheimer's disease increase production of

42-residue amyloid beta-protein in both transfected cells and transgenic mice. Nat Med **3**, 67-72

106 Bowen, D. J. (2002) Haemophilia A and haemophilia B: molecular insights. Mol Pathol **55**, 127-144

107 Gelb, B. D., Shi, G. P., Chapman, H. A. and Desnick, R. J. (1996) Pycnodysostosis, a lysosomal disease caused by cathepsin K deficiency. Science (New York, N.Y **273**, 1236-1238

108 Pham, C. T., Ivanovich, J. L., Raptis, S. Z., Zehnbauer, B. and Ley, T. J. (2004) Papillon-Lefevre syndrome: correlating the molecular, cellular, and clinical consequences of cathepsin C/ dipeptidyl peptidase I deficiency in humans. J Immunol **173**, 7277-7281

109 Wang, J., Zheng, L., Lobito, A., Chan, F. K., Dale, J., Sneller, M., Yao, X., Puck, J. M., Straus, S. E. and Lenardo, M. J. (1999) Inherited human Caspase 10 mutations underlie defective lymphocyte and dendritic cell apoptosis in autoimmune lymphoproliferative syndrome type II. Cell **98**, 47-58

110 Horikawa, Y., Oda, N., Cox, N. J., Li, X., Orho-Melander, M., Hara, M., Hinokio, Y., Lindner, T. H., Mashima, H., Schwarz, P. E., del Bosque-Plata, L., Horikawa, Y., Oda, Y., Yoshiuchi, I., Colilla, S., Polonsky, K. S., Wei, S., Concannon, P., Iwasaki, N., Schulze, J., Baier, L. J., Bogardus, C., Groop, L., Boerwinkle, E., Hanis, C. L. and Bell, G. I. (2000) Genetic variation in the gene encoding calpain-10 is associated with type 2 diabetes mellitus. Nature genetics **26**, 163-175

111 Van Eerdewegh, P., Little, R. D., Dupuis, J., Del Mastro, R. G., Falls, K., Simon, J., Torrey, D., Pandit, S., McKenny, J., Braunschweiger, K., Walsh, A., Liu, Z., Hayward, B., Folz, C., Manning, S. P., Bawa, A., Saracino, L., Thackston, M., Benchekroun, Y., Capparell, N., Wang, M., Adair, R., Feng, Y., Dubois, J., FitzGerald, M. G., Huang, H., Gibson, R., Allen, K. M., Pedan, A., Danzig, M. R., Umland, S. P., Egan, R. W., Cuss, F. M., Rorke, S., Clough, J. B., Holloway, J. W., Holgate, S. T. and Keith, T. P. (2002) Association of the ADAM33 gene with asthma and bronchial hyperresponsiveness. Nature **418**, 426-430

112 Lopez-Otin, C. and Matrisian, L. M. (2007) Emerging roles of proteases in tumour suppression. Nat Rev Cancer **7**, 800-808

113 Barry, M. and Bleackley, R. C. (2002) Cytotoxic T lymphocytes: all roads lead to death. Nat Rev Immunol **2**, 401-409

114 Chowdhury, D. and Lieberman, J. (2008) Death by a thousand cuts: granzyme pathways of programmed cell death. Annu Rev Immunol **26**, 389-420

115 Boivin, W. A., Cooper, D. M., Hiebert, P. R. and Granville, D. J. (2009) Intracellular versus extracellular granzyme B in immunity and disease: challenging the dogma. Lab Invest **89**, 1195-1220

116 Buzza, M. S. and Bird, P. I. (2006) Extracellular granzymes: current perspectives. Biol Chem **387**, 827-837

117 Roos, A., Ramwadhdoebe, T. H., Nauta, A. J., Hack, C. E. and Daha, M. R. (2002) Therapeutic inhibition of the early phase of complement activation. Immunobiology **205**, 595-609

118 Thomas, H. E., Trapani, J. A. and Kay, T. W. (2009) The role of perforin and granzymes in diabetes. Cell death and differentiation **17**, 577-585

119 Turk, B. (2006) Targeting proteases: successes, failures and future prospects. Nat Rev Drug Discov **5**, 785-799

120 Matthews, D. J. and Wells, J. A. (1993) Substrate phage: selection of protease substrates by monovalent phage display. Science (New York, N.Y **260**, 1113-1117

121 Kaiserman, D., Bird, C. H., Sun, J., Matthews, A., Ung, K., Whisstock, J. C., Thompson, P. E., Trapani, J. A. and Bird, P. I. (2006) The major human and mouse granzymes are structurally and functionally divergent. J Cell Biol **175**, 619-630

122 Cullen, S. P., Adrain, C., Luthi, A. U., Duriez, P. J. and Martin, S. J. (2007) Human and murine granzyme B exhibit divergent substrate preferences. J Cell Biol **176**, 435-444

123 Boulware, K. T. and Daugherty, P. S. (2006) Protease specificity determination by using cellular libraries of peptide substrates (CLiPS). Proc Natl Acad Sci U S A **103**, 7583-7588

124 Bovenschen, N., Quadir, R., van den Berg, A. L., Brenkman, A. B., Vandenberghe, I., Devreese, B., Joore, J. and Kummer, J. A. (2009) Granzyme K displays highly restricted substrate specificity that only partially overlaps with granzyme A. J Biol Chem **284**, 3504-3512

125 Bell, J. K., Goetz, D. H., Mahrus, S., Harris, J. L., Fletterick, R. J. and Craik, C. S. (2003) The oligomeric structure of human granzyme A is a determinant of its extended substrate specificity. Nat Struct Biol **10**, 527-534

126 Fan, Z., Beresford, P. J., Zhang, D., Xu, Z., Novina, C. D., Yoshida, A., Pommier, Y. and Lieberman, J. (2003) Cleaving the oxidative repair protein Ape1 enhances cell death mediated by granzyme A. Nat Immunol **4**, 145-153

127 Schilling, O. and Overall, C. M. (2008) Proteome-derived, database-searchable peptide libraries for identifying protease cleavage sites. Nat Biotechnol **26**, 685-694

128 Backes, B. J., Harris, J. L., Leonetti, F., Craik, C. S. and Ellman, J. A. (2000) Synthesis of positional-scanning libraries of fluorogenic peptide substrates to define the extended substrate specificity of plasmin and thrombin. Nat Biotechnol **18**, 187-193

129 Pinilla, C., Appel, J. R., Blanc, P. and Houghten, R. A. (1992) Rapid identification of high affinity peptide ligands using positional scanning synthetic peptide combinatorial libraries. Biotechniques **13**, 901-905

130 Harris, J. L., Peterson, E. P., Hudig, D., Thornberry, N. A. and Craik, C. S. (1998) Definition and redesign of the extended substrate specificity of granzyme B. J Biol Chem **273**, 27364-27373

131 Thornberry, N. A., Rano, T. A., Peterson, E. P., Rasper, D. M., Timkey, T., Garcia-Calvo, M., Houtzager, V. M., Nordstrom, P. A., Roy, S., Vaillancourt, J. P., Chapman, K. T. and Nicholson, D. W. (1997) A combinatorial approach defines specificities of members of the caspase family and granzyme B. Functional relationships established for key mediators of apoptosis. J Biol Chem **272**, 17907-17911

132 Krishnaswamy, S. (2005) Exosite-driven substrate specificity and function in coagulation. J Thromb Haemost **3**, 54-67

133 Overall, C. M. (2001) Matrix metalloproteinase substrate binding domains, modules and exosites. Overview and experimental strategies. Methods Mol Biol **151**, 79-120

134 O'Farrell, P. H. (1975) High resolution two-dimensional electrophoresis of proteins. J Biol Chem **250**, 4007-4021

135 Adrain, C., Murphy, B. M. and Martin, S. J. (2005) Molecular ordering of the caspase activation cascade initiated by the cytotoxic T lymphocyte/natural killer (CTL/NK) protease granzyme B. J Biol Chem **280**, 4663-4673

136 Marouga, R., David, S. and Hawkins, E. (2005) The development of the DIGE system: 2D fluorescence difference gel analysis technology. Anal Bioanal Chem **382**, 669-678

137 Unlu, M., Morgan, M. E. and Minden, J. S. (1997) Difference gel electrophoresis: a single gel method for detecting changes in protein extracts. Electrophoresis **18**, 2071-2077

138 Bredemeyer, A. J., Lewis, R. M., Malone, J. P., Davis, A. E., Gross, J., Townsend, R. R. and Ley, T. J. (2004) A proteomic approach for the discovery of protease substrates. Proc Natl Acad Sci U S A **101**, 11785-11790

139 Dix, M. M., Simon, G. M. and Cravatt, B. F. (2008) Global mapping of the topography and magnitude of proteolytic events in apoptosis. Cell **134**, 679-691

140 Thiede, B., Treumann, A., Kretschmer, A., Sohlke, J. and Rudel, T. (2005) Shotgun proteome analysis of protein cleavage in apoptotic cells. Proteomics **5**, 2123-2130

141 Gygi, S. P., Rist, B., Gerber, S. A., Turecek, F., Gelb, M. H. and Aebersold, R. (1999) Quantitative analysis of complex protein mixtures using isotope-coded affinity tags. Nat Biotechnol **17**, 994-999

142 Zhang, R., Sioma, C. S., Wang, S. and Regnier, F. E. (2001) Fractionation of isotopically labeled peptides in quantitative proteomics. Anal Chem **73**, 5142-5149

143 Zhang, R. and Regnier, F. E. (2002) Minimizing resolution of isotopically coded peptides in

comparative proteomics. J Proteome Res **1**, 139-147
144 Zhou, H., Ranish, J. A., Watts, J. D. and Aebersold, R. (2002) Quantitative proteome analysis by solid-phase isotope tagging and mass spectrometry. Nat Biotechnol **20**, 512-515
145 Ross, P. L., Huang, Y. N., Marchese, J. N., Williamson, B., Parker, K., Hattan, S., Khainovski, N., Pillai, S., Dey, S., Daniels, S., Purkayastha, S., Juhasz, P., Martin, S., Bartlet-Jones, M., He, F., Jacobson, A. and Pappin, D. J. (2004) Multiplexed protein quantitation in Saccharomyces cerevisiae using amine-reactive isobaric tagging reagents. Mol Cell Proteomics **3**, 1154-1169
146 Ong, S. E., Blagoev, B., Kratchmarova, I., Kristensen, D. B., Steen, H., Pandey, A. and Mann, M. (2002) Stable isotope labeling by amino acids in cell culture, SILAC, as a simple and accurate approach to expression proteomics. Mol Cell Proteomics **1**, 376-386
147 Butler, G. S., Dean, R. A., Tam, E. M. and Overall, C. M. (2008) Pharmacoproteomics of a metalloproteinase hydroxamate inhibitor in breast cancer cells: dynamics of membrane type 1 matrix metalloproteinase-mediated membrane protein shedding. Molecular and cellular biology **28**, 4896-4914
148 Tam, E. M., Morrison, C. J., Wu, Y. I., Stack, M. S. and Overall, C. M. (2004) Membrane protease proteomics: Isotope-coded affinity tag MS identification of undescribed MT1-matrix metalloproteinase substrates. Proc Natl Acad Sci U S A **101**, 6917-6922
149 Dean, R. A. and Overall, C. M. (2007) Proteomics discovery of metalloproteinase substrates in the cellular context by iTRAQ labeling reveals a diverse MMP-2 substrate degradome. Mol Cell Proteomics **6**, 611-623
150 McDonald, L., Robertson, D. H., Hurst, J. L. and Beynon, R. J. (2005) Positional proteomics: selective recovery and analysis of N-terminal proteolytic peptides. Nat Methods **2**, 955-957
151 Brown, M. G., Dokun, A. O., Heusel, J. W., Smith, H. R., Beckman, D. L., Blattenberger, E. A., Dubbelde, C. E., Stone, L. R., Scalzo, A. A. and Yokoyama, W. M. (2001) Vital involvement of a natural killer cell activation receptor in resistance to viral infection. Science (New York, N.Y **292**, 934-937
152 Gevaert, K., Goethals, M., Martens, L., Van Damme, J., Staes, A., Thomas, G. R. and Vandekerckhove, J. (2003) Exploring proteomes and analyzing protein processing by mass spectrometric identification of sorted N-terminal peptides. Nat Biotechnol **21**, 566-569
153 Staes, A., Van Damme, P., Helsens, K., Demol, H., Vandekerckhove, J. and Gevaert, K. (2008) Improved recovery of proteome-informative, protein N-terminal peptides by combined fractional diagonal chromatography (COFRADIC). Proteomics **8**, 1362-1370
154 Van Damme, P., Maurer-Stroh, S., Plasman, K., Van Durme, J., Colaert, N., Timmerman, E., De Bock, P. J., Goethals, M., Rousseau, F., Schymkowitz, J., Vandekerckhove, J. and Gevaert, K. (2009) Analysis of protein processing by N-terminal proteomics reveals novel species-specific substrate determinants of granzyme B orthologs. Mol Cell Proteomics **8**, 258-272
155 Mirgorodskaya, O. A., Kozmin, Y. P., Titov, M. I., Korner, R., Sonksen, C. P. and Roepstorff, P. (2000) Quantitation of peptides and proteins by matrix-assisted laser desorption/ionization mass spectrometry using (18)O-labeled internal standards. Rapid Commun Mass Spectrom **14**, 1226-1232
156 Van Damme, P., Martens, L., Van Damme, J., Hugelier, K., Staes, A., Vandekerckhove, J. and Gevaert, K. (2005) Caspase-specific and nonspecific in vivo protein processing during Fas-induced apoptosis. Nat Methods **2**, 771-777
157 Kaiserman, D., Buckle, A. M., Van Damme, P., Irving, J. A., Law, R. H., Matthews, A. Y., Bashtannyk-Puhalovich, T., Langendorf, C., Thompson, P., Vandekerckhove, J., Gevaert, K., Whisstock, J. C. and Bird, P. I. (2009) Structure of granzyme C reveals an unusual mechanism of protease autoinhibition. Proc Natl Acad Sci U S A **106**, 5587-5592
158 McDonald, L. and Beynon, R. J. (2006) Positional proteomics: preparation of amino-terminal peptides as a strategy for proteome simplification and characterization. Nat Protoc **1**, 1790-1798
159 Doucet, A. and Overall, C. M. (2008) Protease proteomics: revealing protease in vivo

functions using systems biology approaches. Mol Aspects Med **29**, 339-358
160 Kleifeld, O., Doucet, A., auf dem Keller, U., Prudova, A., Schilling, O., Kainthan, R. K., Starr, A. E., Foster, L. J., Kizhakkedathu, J. N. and Overall, C. M. (2010) Isotopic labeling of terminal amines in complex samples identifies protein N-termini and protease cleavage products. Nat Biotechnol **28**, 281-288
161 Enoksson, M., Li, J., Ivancic, M. M., Timmer, J. C., Wildfang, E., Eroshkin, A., Salvesen, G. S. and Tao, W. A. (2007) Identification of proteolytic cleavage sites by quantitative proteomics. J Proteome Res **6**, 2850-2858
162 Timmer, J. C., Enoksson, M., Wildfang, E., Zhu, W., Igarashi, Y., Denault, J. B., Ma, Y., Dummitt, B., Chang, Y. H., Mast, A. E., Eroshkin, A., Smith, J. W., Tao, W. A. and Salvesen, G. S. (2007) Profiling constitutive proteolytic events in vivo. Biochem J **407**, 41-48
163 Chang, T. K., Jackson, D. Y., Burnier, J. P. and Wells, J. A. (1994) Subtiligase: a tool for semisynthesis of proteins. Proc Natl Acad Sci U S A **91**, 12544-12548
164 Mahrus, S., Trinidad, J. C., Barkan, D. T., Sali, A., Burlingame, A. L. and Wells, J. A. (2008) Global sequencing of proteolytic cleavage sites in apoptosis by specific labeling of protein N termini. Cell **134**, 866-876
165 Xu, G., Shin, S. B. and Jaffrey, S. R. (2009) Global profiling of protease cleavage sites by chemoselective labeling of protein N-termini. Proc Natl Acad Sci U S A **106**, 19310-19315
166 Jessani, N., Liu, Y., Humphrey, M. and Cravatt, B. F. (2002) Enzyme activity profiles of the secreted and membrane proteome that depict cancer cell invasiveness. Proc Natl Acad Sci U S A **99**, 10335-10340
167 Kidd, D., Liu, Y. and Cravatt, B. F. (2001) Profiling serine hydrolase activities in complex proteomes. Biochemistry **40**, 4005-4015
168 Liu, Y., Patricelli, M. P. and Cravatt, B. F. (1999) Activity-based protein profiling: the serine hydrolases. Proc Natl Acad Sci U S A **96**, 14694-14699
169 Patricelli, M. P., Giang, D. K., Stamp, L. M. and Burbaum, J. J. (2001) Direct visualization of serine hydrolase activities in complex proteomes using fluorescent active site-directed probes. Proteomics **1**, 1067-1071
170 Williams, E. B., Krishnaswamy, S. and Mann, K. G. (1989) Zymogen/enzyme discrimination using peptide chloromethyl ketones. J Biol Chem **264**, 7536-7545
171 Borodovsky, A., Ovaa, H., Kolli, N., Gan-Erdene, T., Wilkinson, K. D., Ploegh, H. L. and Kessler, B. M. (2002) Chemistry-based functional proteomics reveals novel members of the deubiquitinating enzyme family. Chem Biol **9**, 1149-1159
172 Faleiro, L., Kobayashi, R., Fearnhead, H. and Lazebnik, Y. (1997) Multiple species of CPP32 and Mch2 are the major active caspases present in apoptotic cells. Embo J **16**, 2271-2281
173 Greenbaum, D., Medzihradszky, K. F., Burlingame, A. and Bogyo, M. (2000) Epoxide electrophiles as activity-dependent cysteine protease profiling and discovery tools. Chem Biol **7**, 569-581
174 Kato, D., Boatright, K. M., Berger, A. B., Nazif, T., Blum, G., Ryan, C., Chehade, K. A., Salvesen, G. S. and Bogyo, M. (2005) Activity-based probes that target diverse cysteine protease families. Nat Chem Biol **1**, 33-38
175 Nicholson, D. W., Ali, A., Thornberry, N. A., Vaillancourt, J. P., Ding, C. K., Gallant, M., Gareau, Y., Griffin, P. R., Labelle, M., Lazebnik, Y. A. and et al. (1995) Identification and inhibition of the ICE/CED-3 protease necessary for mammalian apoptosis. Nature **376**, 37-43
176 Thornberry, N. A., Peterson, E. P., Zhao, J. J., Howard, A. D., Griffin, P. R. and Chapman, K. T. (1994) Inactivation of interleukin-1 beta converting enzyme by peptide (acyloxy)methyl ketones. Biochemistry **33**, 3934-3940
177 Bogyo, M., McMaster, J. S., Gaczynska, M., Tortorella, D., Goldberg, A. L. and Ploegh, H. (1997) Covalent modification of the active site threonine of proteasomal beta subunits and the Escherichia coli homolog HslV by a new class of inhibitors. Proc Natl Acad Sci U S A **94**, 6629-6634

178 Kessler, B. M., Tortorella, D., Altun, M., Kisselev, A. F., Fiebiger, E., Hekking, B. G., Ploegh, H. L. and Overkleeft, H. S. (2001) Extended peptide-based inhibitors efficiently target the proteasome and reveal overlapping specificities of the catalytic beta-subunits. Chem Biol **8**, 913-929

179 Chan, E. W., Chattopadhaya, S., Panicker, R. C., Huang, X. and Yao, S. Q. (2004) Developing photoactive affinity probes for proteomic profiling: hydroxamate-based probes for metalloproteases. J Am Chem Soc **126**, 14435-14446

180 Saghatelian, A., Jessani, N., Joseph, A., Humphrey, M. and Cravatt, B. F. (2004) Activity-based probes for the proteomic profiling of metalloproteases. Proc Natl Acad Sci U S A **101**, 10000-10005

181 Fonovic, M. and Bogyo, M. (2008) Activity-based probes as a tool for functional proteomic analysis of proteases. Expert Rev Proteomics **5**, 721-730

182 Winssinger, N., Ficarro, S., Schultz, P. G. and Harris, J. L. (2002) Profiling protein function with small molecule microarrays. Proc Natl Acad Sci U S A **99**, 11139-11144

183 Blum, G., von Degenfeld, G., Merchant, M. J., Blau, H. M. and Bogyo, M. (2007) Noninvasive optical imaging of cysteine protease activity using fluorescently quenched activity-based probes. Nat Chem Biol **3**, 668-677

184 Edgington, L. E., Berger, A. B., Blum, G., Albrow, V. E., Paulick, M. G., Lineberry, N. and Bogyo, M. (2009) Noninvasive optical imaging of apoptosis by caspase-targeted activity-based probes. Nat Med **15**, 967-973

185 Lange, V., Picotti, P., Domon, B. and Aebersold, R. (2008) Selected reaction monitoring for quantitative proteomics: a tutorial. Mol Syst Biol **4**, 222

186 Shields, D. J., Niessen, S., Murphy, E. A., Mielgo, A., Desgrosellier, J. S., Lau, S. K., Barnes, L. A., Lesperance, J., Bouvet, M., Tarin, D., Cravatt, B. F. and Cheresh, D. A. (2010) RBBP9: a tumor-associated serine hydrolase activity required for pancreatic neoplasia. Proc Natl Acad Sci U S A **107**, 2189-2194

187 Timmer, J. C., Zhu, W., Pop, C., Regan, T., Snipas, S. J., Eroshkin, A. M., Riedl, S. J. and Salvesen, G. S. (2009) Structural and kinetic determinants of protease substrates. Nat Struct Mol Biol **16**, 1101-1108

188 Vogtle, F. N., Wortelkamp, S., Zahedi, R. P., Becker, D., Leidhold, C., Gevaert, K., Kellermann, J., Voos, W., Sickmann, A., Pfanner, N. and Meisinger, C. (2009) Global analysis of the mitochondrial N-proteome identifies a processing peptidase critical for protein stability. Cell **139**, 428-439

189 Martens, L., Hermjakob, H., Jones, P., Adamski, M., Taylor, C., States, D., Gevaert, K., Vandekerckhove, J. and Apweiler, R. (2005) PRIDE: the proteomics identifications database. Proteomics **5**, 3537-3545

190 Dustin, M. L. and Long, E. O. (2010) Cytotoxic immunological synapses. Immunol Rev **235**, 24-34

191 Smyth, M. J. and Trapani, J. A. (1995) Granzymes: exogenous proteinases that induce target cell apoptosis. Immunology today **16**, 202-206

192 Arnold, K., Bordoli, L., Kopp, J. and Schwede, T. (2006) The SWISS-MODEL workspace: a web-based environment for protein structure homology modelling. Bioinformatics **22**, 195-201

193 Dauber, D. S., Ziermann, R., Parkin, N., Maly, D. J., Mahrus, S., Harris, J. L., Ellman, J. A., Petropoulos, C. and Craik, C. S. (2002) Altered substrate specificity of drug-resistant human immunodeficiency virus type 1 protease. Journal of virology **76**, 1359-1368

194 Harris, J. L., Backes, B. J., Leonetti, F., Mahrus, S., Ellman, J. A. and Craik, C. S. (2000) Rapid and general profiling of protease specificity by using combinatorial fluorogenic substrate libraries. Proc Natl Acad Sci U S A **97**, 7754-7759

195 Alban, A., David, S. O., Bjorkesten, L., Andersson, C., Sloge, E., Lewis, S. and Currie, I. (2003) A novel experimental design for comparative two-dimensional gel analysis: two-dimensional difference gel electrophoresis incorporating a pooled internal standard.

Proteomics **3**, 36-44
196 Van Damme, P., Staes, A., Bronsoms, S., Helsens, K., Colaert, N., Timmerman, E., Aviles, F. X., Vandekerckhove, J. and Gevaert, K. (2010) Complementary positional proteomics for screening substrates of endo- and exoproteases. Nat Methods **7**, 512-515
197 Ghesquiere, B., Colaert, N., Helsens, K., Dejager, L., Vanhaute, C., Verleysen, K., Kas, K., Timmerman, E., Goethals, M., Libert, C., Vandekerckhove, J. and Gevaert, K. (2009) In vitro and in vivo protein-bound tyrosine nitration characterized by diagonal chromatography. Mol Cell Proteomics **8**, 2642-2652
198 Colaert, N., Helsens, K., Martens, L., Vandekerckhove, J. and Gevaert, K. (2009) Improved visualization of protein consensus sequences by iceLogo. Nat Methods **6**, 786-787
199 Grisendi, S., Bernardi, R., Rossi, M., Cheng, K., Khandker, L., Manova, K. and Pandolfi, P. P. (2005) Role of nucleophosmin in embryonic development and tumorigenesis. Nature **437**, 147-153
200 Casciola-Rosen, L., Garcia-Calvo, M., Bull, H. G., Becker, J. W., Hines, T., Thornberry, N. A. and Rosen, A. (2007) Mouse and human granzyme B have distinct tetrapeptide specificities and abilities to recruit the bid pathway. J Biol Chem **282**, 4545-4552
201 Plasman, K., Van Damme, P., Kaiserman, D., Impens, F., Demeyer, K., Helsens, K., Goethals, M., Bird, P. I., Vandekerckhove, J. and Gevaert, K. (2011) Probing the efficiency of proteolytic events by positional proteomics. Mol Cell Proteomics **10**, M110 003301
202 Okuwaki, M., Iwamatsu, A., Tsujimoto, M. and Nagata, K. (2001) Identification of nucleophosmin/B23, an acidic nucleolar protein, as a stimulatory factor for in vitro replication of adenovirus DNA complexed with viral basic core proteins. Journal of molecular biology **311**, 41-55
203 Ulanet, D. B., Torbenson, M., Dang, C. V., Casciola-Rosen, L. and Rosen, A. (2003) Unique conformation of cancer autoantigen B23 in hepatoma: a mechanism for specificity in the autoimmune response. Proc Natl Acad Sci U S A **100**, 12361-12366
204 Schiffer, S., Letzian, S., Jost, E., Mladenov, R., Hristodorov, D., Huhn, M., Fischer, R., Barth, S. and Thepen, T. (2013) Granzyme M as a novel effector molecule for human cytolytic fusion proteins: CD64-specific cytotoxicity of Gm-H22(scFv) against leukemic cells. Cancer Lett
205 Oyadomari, S. and Mori, M. (2004) Roles of CHOP/GADD153 in endoplasmic reticulum stress. Cell death and differentiation **11**, 381-389
206 Yagita, M., Huang, C. L., Umehara, H., Matsuo, Y., Tabata, R., Miyake, M., Konaka, Y. and Takatsuki, K. (2000) A novel natural killer cell line (KHYG-1) from a patient with aggressive natural killer cell leukemia carrying a p53 point mutation. Leukemia **14**, 922-930
207 Suck, G., Branch, D. R., Smyth, M. J., Miller, R. G., Vergidis, J., Fahim, S. and Keating, A. (2005) KHYG-1, a model for the study of enhanced natural killer cell cytotoxicity. Exp Hematol **33**, 1160-1171
208 Dickey, J. S. and Osheroff, N. (2005) Impact of the C-terminal domain of topoisomerase IIalpha on the DNA cleavage activity of the human enzyme. Biochemistry **44**, 11546-11554
209 Jensen, S., Andersen, A. H., Kjeldsen, E., Biersack, H., Olsen, E. H., Andersen, T. B., Westergaard, O. and Jakobsen, B. K. (1996) Analysis of functional domain organization in DNA topoisomerase II from humans and Saccharomyces cerevisiae. Molecular and cellular biology **16**, 3866-3877
210 Turner, J. G., Engel, R., Derderian, J. A., Jove, R. and Sullivan, D. M. (2004) Human topoisomerase IIalpha nuclear export is mediated by two CRM-1-dependent nuclear export signals. J Cell Sci **117**, 3061-3071
211 Shi, L., Mai, S., Israels, S., Browne, K., Trapani, J. A. and Greenberg, A. H. (1997) Granzyme B (GraB) autonomously crosses the cell membrane and perforin initiates apoptosis and GraB nuclear localization. The Journal of experimental medicine **185**, 855-866
212 Trapani, J. A., Browne, K. A., Smyth, M. J. and Jans, D. A. (1996) Localization of granzyme B in the nucleus. A putative role in the mechanism of cytotoxic lymphocyte-mediated apoptosis. J Biol Chem **271**, 4127-4133

213 Jans, D. A., Jans, P., Briggs, L. J., Sutton, V. and Trapani, J. A. (1996) Nuclear transport of granzyme B (fragmentin-2). Dependence of perforin in vivo and cytosolic factors in vitro. J Biol Chem **271**, 30781-30789

214 Jans, D. A., Briggs, L. J., Jans, P., Froelich, C. J., Parasivam, G., Kumar, S., Sutton, V. R. and Trapani, J. A. (1998) Nuclear targeting of the serine protease granzyme A (fragmentin-1). J Cell Sci **111 (Pt 17)**, 2645-2654

215 Blink, E. J., Jiansheng, Z., Hu, W., Calanni, S. T., Trapani, J. A., Bird, P. I. and Jans, D. A. (2005) Interaction of the nuclear localizing cytolytic granule serine protease granzyme B with importin alpha or beta: modulation by the serpin inhibitor PI-9. J Cell Biochem **95**, 598-610

216 Carpenter, A. J. and Porter, A. C. (2004) Construction, characterization, and complementation of a conditional-lethal DNA topoisomerase IIalpha mutant human cell line. Mol Biol Cell **15**, 5700-5711

217 Xiao, Z., Ko, H. L., Goh, E. H., Wang, B. and Ren, E. C. (2013) hnRNP K suppresses apoptosis independent of p53 status by maintaining high levels of endogenous caspase inhibitors. Carcinogenesis

218 Andersen, J. L., DeHart, J. L., Zimmerman, E. S., Ardon, O., Kim, B., Jacquot, G., Benichou, S. and Planelles, V. (2006) HIV-1 Vpr-induced apoptosis is cell cycle dependent and requires Bax but not ANT. PLoS Pathog **2**, e127

219 Vos, S. M., Tretter, E. M., Schmidt, B. H. and Berger, J. M. (2011) All tangled up: how cells direct, manage and exploit topoisomerase function. Nat Rev Mol Cell Biol **12**, 827-841

220 Depowski, P. L., Rosenthal, S. I., Brien, T. P., Stylos, S., Johnson, R. L. and Ross, J. S. (2000) Topoisomerase IIalpha expression in breast cancer: correlation with outcome variables. Mod Pathol **13**, 542-547

221 Costa, M. J., Hansen, C. L., Holden, J. A. and Guinee, D., Jr. (2000) Topoisomerase II alpha: prognostic predictor and cell cycle marker in surface epithelial neoplasms of the ovary and peritoneum. Int J Gynecol Pathol **19**, 248-257

222 Miettinen, H. E., Jarvinen, T. A., Kellner, U., Kauraniemi, P., Parwaresch, R., Rantala, I., Kalimo, H., Paljarvi, L., Isola, J. and Haapasalo, H. (2000) High topoisomerase IIalpha expression associates with high proliferation rate and and poor prognosis in oligodendrogliomas. Neuropathol Appl Neurobiol **26**, 504-512

223 Nitiss, J. L. (2009) Targeting DNA topoisomerase II in cancer chemotherapy. Nat Rev Cancer **9**, 338-350

224 Chen, G., Shi, L., Litchfield, D. W. and Greenberg, A. H. (1995) Rescue from granzyme B-induced apoptosis by Wee1 kinase. The Journal of experimental medicine **181**, 2295-2300

225 Shi, L., Chen, G., He, D., Bosc, D. G., Litchfield, D. W. and Greenberg, A. H. (1996) Granzyme B induces apoptosis and cyclin A-associated cyclin-dependent kinase activity in all stages of the cell cycle. J Immunol **157**, 2381-2385

226 Altieri, D. C. (2011) Survivin and IAP proteins in cell-death mechanisms. Biochem J **430**, 199-205

227 Goping, I. S., Barry, M., Liston, P., Sawchuk, T., Constantinescu, G., Michalak, K. M., Shostak, I., Roberts, D. L., Hunter, A. M., Korneluk, R. and Bleackley, R. C. (2003) Granzyme B-induced apoptosis requires both direct caspase activation and relief of caspase inhibition. Immunity **18**, 355-365

228 Casciola-Rosen, L., Andrade, F., Ulanet, D., Wong, W. B. and Rosen, A. (1999) Cleavage by granzyme B is strongly predictive of autoantigen status: implications for initiation of autoimmunity. The Journal of experimental medicine **190**, 815-826

229 Casiano, C. A., Martin, S. J., Green, D. R. and Tan, E. M. (1996) Selective cleavage of nuclear autoantigens during CD95 (Fas/APO-1)-mediated T cell apoptosis. The Journal of experimental medicine **184**, 765-770

230 Casiano, C. A., Ochs, R. L. and Tan, E. M. (1998) Distinct cleavage products of nuclear proteins in apoptosis and necrosis revealed by autoantibody probes. Cell death and

differentiation **5**, 183-190
231 Fischer, U., Janicke, R. U. and Schulze-Osthoff, K. (2003) Many cuts to ruin: a comprehensive update of caspase substrates. Cell death and differentiation **10**, 76-100
232 Goping, I. S., Sawchuk, T., Underhill, D. A. and Bleackley, R. C. (2006) Identification of {alpha}-tubulin as a granzyme B substrate during CTL-mediated apoptosis. J Cell Sci **119**, 858-865
233 Adrain, C., Duriez, P. J., Brumatti, G., Delivani, P. and Martin, S. J. (2006) The cytotoxic lymphocyte protease, granzyme B, targets the cytoskeleton and perturbs microtubule polymerization dynamics. J Biol Chem **281**, 8118-8125
234 Suzuki, K., Bose, P., Leong-Quong, R. Y., Fujita, D. J. and Riabowol, K. (2010) REAP: A two minute cell fractionation method. BMC Res Notes **3**, 294
235 Staes, A., Impens, F., Van Damme, P., Ruttens, B., Goethals, M., Demol, H., Timmerman, E., Vandekerckhove, J. and Gevaert, K. (2011) Selecting protein N-terminal peptides by combined fractional diagonal chromatography. Nat Protoc **6**, 1130-1141
236 Van Damme, P., Hole, K., Pimenta-Marques, A., Helsens, K., Vandekerckhove, J., Martinho, R. G., Gevaert, K. and Arnesen, T. (2011) NatF contributes to an evolutionary shift in protein N-terminal acetylation and is important for normal chromosome segregation. PLoS Genet **7**, e1002169
237 Vizcaino, J. A., Cote, R. G., Csordas, A., Dianes, J. A., Fabregat, A., Foster, J. M., Griss, J., Alpi, E., Birim, M., Contell, J., O'Kelly, G., Schoenegger, A., Ovelleiro, D., Perez-Riverol, Y., Reisinger, F., Rios, D., Wang, R. and Hermjakob, H. (2013) The PRoteomics IDEntifications (PRIDE) database and associated tools: status in 2013. Nucleic acids research **41**, D1063-1069
238 Schackmann, R. C., van Amersfoort, M., Haarhuis, J. H., Vlug, E. J., Halim, V. A., Roodhart, J. M., Vermaat, J. S., Voest, E. E., van der Groep, P., van Diest, P. J., Jonkers, J. and Derksen, P. W. (2011) Cytosolic p120-catenin regulates growth of metastatic lobular carcinoma through Rock1-mediated anoikis resistance. J Clin Invest **121**, 3176-3188
239 Perkins, D. N., Pappin, D. J., Creasy, D. M. and Cottrell, J. S. (1999) Probability-based protein identification by searching sequence databases using mass spectrometry data. Electrophoresis **20**, 3551-3567
240 Helsens, K., Colaert, N., Barsnes, H., Muth, T., Flikka, K., Staes, A., Timmerman, E., Wortelkamp, S., Sickmann, A., Vandekerckhove, J., Gevaert, K. and Martens, L. (2010) ms_lims, a simple yet powerful open source laboratory information management system for MS-driven proteomics. Proteomics **10**, 1261-1264
241 Smyth, M. J., Kelly, J. M., Sutton, V. R., Davis, J. E., Browne, K. A., Sayers, T. J. and Trapani, J. A. (2001) Unlocking the secrets of cytotoxic granule proteins. J Leukoc Biol **70**, 18-29
242 Cullen, S. P. and Martin, S. J. (2008) Mechanisms of granule-dependent killing. Cell death and differentiation **15**, 251-262
243 Deveraux, Q. L., Takahashi, R., Salvesen, G. S. and Reed, J. C. (1997) X-linked IAP is a direct inhibitor of cell-death proteases. Nature **388**, 300-304
244 Irmler, M., Thome, M., Hahne, M., Schneider, P., Hofmann, K., Steiner, V., Bodmer, J. L., Schroter, M., Burns, K., Mattmann, C., Rimoldi, D., French, L. E. and Tschopp, J. (1997) Inhibition of death receptor signals by cellular FLIP. Nature **388**, 190-195
245 Zhang, M., Park, S. M., Wang, Y., Shah, R., Liu, N., Murmann, A. E., Wang, C. R., Peter, M. E. and Ashton-Rickardt, P. G. (2006) Serine protease inhibitor 6 protects cytotoxic T cells from self-inflicted injury by ensuring the integrity of cytotoxic granules. Immunity **24**, 451-461
246 ten Berge, R. L., Meijer, C. J., Dukers, D. F., Kummer, J. A., Bladergroen, B. A., Vos, W., Hack, C. E., Ossenkoppele, G. J. and Oudejans, J. J. (2002) Expression levels of apoptosis-related proteins predict clinical outcome in anaplastic large cell lymphoma. Blood **99**, 4540-4546
247 Huntington, J. A., Read, R. J. and Carrell, R. W. (2000) Structure of a serpin-protease complex shows inhibition by deformation. Nature **407**, 923-926
248 Kaiserman, D. and Bird, P. I. (2010) Control of granzymes by serpins. Cell death and

differentiation **17**, 586-595
249 McGettrick, A. F., Barnes, R. C. and Worrall, D. M. (2001) SCCA2 inhibits TNF-mediated apoptosis in transfected HeLa cells. The reactive centre loop sequence is essential for this function and TNF-induced cathepsin G is a candidate target. Eur J Biochem **268**, 5868-5875
250 Kummer, J. A., Kamp, A. M., van Katwijk, M., Brakenhoff, J. P., Radosevic, K., van Leeuwen, A. M., Borst, J., Verweij, C. L. and Hack, C. E. (1993) Production and characterization of monoclonal antibodies raised against recombinant human granzymes A and B and showing cross reactions with the natural proteins. J Immunol Methods **163**, 77-83
251 Schechter, N. M. and Plotnick, M. I. (2004) Measurement of the kinetic parameters mediating protease-serpin inhibition. Methods **32**, 159-168
252 Gettins, P. G. (2002) Serpin structure, mechanism, and function. Chem Rev **102**, 4751-4804
253 Schneider, S. S., Schick, C., Fish, K. E., Miller, E., Pena, J. C., Treter, S. D., Hui, S. M. and Silverman, G. A. (1995) A serine proteinase inhibitor locus at 18q21.3 contains a tandem duplication of the human squamous cell carcinoma antigen gene. Proc Natl Acad Sci U S A **92**, 3147-3151
254 Keijer, J., Linders, M., Wegman, J. J., Ehrlich, H. J., Mertens, K. and Pannekoek, H. (1991) On the target specificity of plasminogen activator inhibitor 1: the role of heparin, vitronectin, and the reactive site. Blood **78**, 1254-1261
255 Barnes, R. C. and Worrall, D. M. (1995) Identification of a novel human serpin gene; cloning sequencing and expression of leupin. FEBS Lett **373**, 61-65
256 Young, J. L., Sukhova, G. K., Foster, D., Kisiel, W., Libby, P. and Schonbeck, U. (2000) The serpin proteinase inhibitor 9 is an endogenous inhibitor of interleukin 1beta-converting enzyme (caspase-1) activity in human vascular smooth muscle cells. The Journal of experimental medicine **191**, 1535-1544
257 Espana, F., Gruber, A., Heeb, M. J., Hanson, S. R., Harker, L. A. and Griffin, J. H. (1991) In vivo and in vitro complexes of activated protein C with two inhibitors in baboons. Blood **77**, 1754-1760
258 Wachtfogel, Y. T., Harpel, P. C., Edmunds, L. H., Jr. and Colman, R. W. (1989) Formation of C1s-C1-inhibitor, kallikrein-C1-inhibitor, and plasmin-alpha 2-plasmin-inhibitor complexes during cardiopulmonary bypass. Blood **73**, 468-471
259 Patston, P. A., Church, F. C. and Olson, S. T. (2004) Serpin-ligand interactions. Methods **32**, 93-109
260 Kato, H., Suehiro, Y., Morioka, H., Torigoe, T., Myoga, A., Sekiguchi, K. and Ikeda, I. (1987) Heterogeneous distribution of acidic TA-4 in cervical squamous cell carcinoma: immunohistochemical demonstration with monoclonal antibodies. Jpn J Cancer Res **78**, 1246-1250
261 Kato, H., Miyauchi, F., Morioka, H., Fujino, T. and Torigoe, T. (1979) Tumor antigen of human cervical squamous cell carcinoma: correlation of circulating levels with disease progress. Cancer **43**, 585-590
262 Murakami, A., Suminami, Y., Hirakawa, H., Nawata, S., Numa, F. and Kato, H. (2001) Squamous cell carcinoma antigen suppresses radiation-induced cell death. Br J Cancer **84**, 851-858
263 Crough, T. and Khanna, R. (2009) Immunobiology of human cytomegalovirus: from bench to bedside. Clin Microbiol Rev **22**, 76-98, Table of Contents
264 Mocarski, E., Shenk, T. and Pass, R. (2007) Cytomegaloviruss. Lippincott Williams & Wilkins, Philadelphia, PA
265 Moss, P. and Rickinson, A. (2005) Cellular immunotherapy for viral infection after HSC transplantation. Nat Rev Immunol **5**, 9-20
266 Wathen, M. W. and Stinski, M. F. (1982) Temporal patterns of human cytomegalovirus transcription: mapping the viral RNAs synthesized at immediate early, early, and late times after infection. Journal of virology **41**, 462-477
267 Gamadia, L. E., Remmerswaal, E. B., Weel, J. F., Bemelman, F., van Lier, R. A. and Ten Berge,

I. J. (2003) Primary immune responses to human CMV: a critical role for IFN-gamma-producing CD4+ T cells in protection against CMV disease. Blood **101**, 2686-2692

268 van Leeuwen, E. M., de Bree, G. J., ten Berge, I. J. and van Lier, R. A. (2006) Human virus-specific CD8+ T cells: diversity specialists. Immunol Rev **211**, 225-235

269 Trapani, J. A. and Smyth, M. J. (2002) Functional significance of the perforin/granzyme cell death pathway. Nat Rev Immunol **2**, 735-747

270 van Leeuwen, E. M., ten Berge, I. J. and van Lier, R. A. (2007) Induction and maintenance of CD8+ T cells specific for persistent viruses. Adv Exp Med Biol **590**, 121-137

271 Ng, L. F., Chan, M., Chan, S. H., Cheng, P. C., Leung, E. H., Chen, W. N. and Ren, E. C. (2005) Host heterogeneous ribonucleoprotein K (hnRNP K) as a potential target to suppress hepatitis B virus replication. PLoS Med **2**, e163

272 Schmidt, T., Striebinger, H., Haas, J. and Bailer, S. M. (2010) The heterogeneous nuclear ribonucleoprotein K is important for Herpes simplex virus-1 propagation. FEBS Lett **584**, 4361-4365

273 Bomsztyk, K., Denisenko, O. and Ostrowski, J. (2004) hnRNP K: one protein multiple processes. Bioessays **26**, 629-638

274 Paziewska, A., Wyrwicz, L. S., Bujnicki, J. M., Bomsztyk, K. and Ostrowski, J. (2004) Cooperative binding of the hnRNP K three KH domains to mRNA targets. FEBS Lett **577**, 134-140

275 Heider, J. A., Bresnahan, W. A. and Shenk, T. E. (2002) Construction of a rationally designed human cytomegalovirus variant encoding a temperature-sensitive immediate-early 2 protein. Proc Natl Acad Sci U S A **99**, 3141-3146

276 White, E. A., Clark, C. L., Sanchez, V. and Spector, D. H. (2004) Small internal deletions in the human cytomegalovirus IE2 gene result in nonviable recombinant viruses with differential defects in viral gene expression. Journal of virology **78**, 1817-1830

277 Stenberg, R. M., Depto, A. S., Fortney, J. and Nelson, J. A. (1989) Regulated expression of early and late RNAs and proteins from the human cytomegalovirus immediate-early gene region. Journal of virology **63**, 2699-2708

278 White, E. A., Del Rosario, C. J., Sanders, R. L. and Spector, D. H. (2007) The IE2 60-kilodalton and 40-kilodalton proteins are dispensable for human cytomegalovirus replication but are required for efficient delayed early and late gene expression and production of infectious virus. Journal of virology **81**, 2573-2583

279 Kaspari, M., Tavalai, N., Stamminger, T., Zimmermann, A., Schilf, R. and Bogner, E. (2008) Proteasome inhibitor MG132 blocks viral DNA replication and assembly of human cytomegalovirus. FEBS Lett **582**, 666-672

280 Lin, J. Y., Li, M. L., Huang, P. N., Chien, K. Y., Horng, J. T. and Shih, S. R. (2008) Heterogeneous nuclear ribonuclear protein K interacts with the enterovirus 71 5' untranslated region and participates in virus replication. J Gen Virol **89**, 2540-2549

281 Laursen, L. S., Chan, C. W. and Ffrench-Constant, C. (2011) Translation of myelin basic protein mRNA in oligodendrocytes is regulated by integrin activation and hnRNP-K. J Cell Biol **192**, 797-811

282 Liu, Y. and Szaro, B. G. (2011) hnRNP K post-transcriptionally co-regulates multiple cytoskeletal genes needed for axonogenesis. Development **138**, 3079-3090

283 Van Damme, P., Maurer-Stroh, S., Hao, H., Colaert, N., Timmerman, E., Eisenhaber, F., Vandekerckhove, J. and Gevaert, K. (2010) The substrate specificity profile of human granzyme A. Biol Chem **391**, 983-997

284 Besold, K., Wills, M. and Plachter, B. (2009) Immune evasion proteins gpUS2 and gpUS11 of human cytomegalovirus incompletely protect infected cells from CD8 T cell recognition. Virology **391**, 5-19

285 Delmas, S., Brousset, P., Clement, D., Le Roy, E. and Davignon, J. L. (2007) Anti-IE1 CD4+ T-cell clones kill peptide-pulsed, but not human cytomegalovirus-infected, target cells. J Gen Virol **88**, 2441-2449

286 Shen, W., Westgard, E., Huang, L., Ward, M. D., Osborn, J. L., Chau, N. H., Collins, L., Marcum, B., Koach, M. A., Bibbs, J., Semmes, O. J. and Kerry, J. A. (2008) Nuclear trafficking of the human cytomegalovirus pp71 (ppUL82) tegument protein. Virology **376**, 42-52

287 Dickens, L. S., Powley, I. R., Hughes, M. A. and MacFarlane, M. (2012) The 'complexities' of life and death: death receptor signalling platforms. Experimental cell research **318**, 1269-1277

288 Ewen, C. L., Kane, K. P. and Bleackley, R. C. (2012) A quarter century of granzymes. Cell death and differentiation **19**, 28-35

289 Andrade, F. (2010) Non-cytotoxic antiviral activities of granzymes in the context of the immune antiviral state. Immunol Rev **235**, 128-146

290 Wigdal, S. S., Anderson, J. L., Vidugiris, G. J., Shultz, J., Wood, K. V. and Fan, F. (2008) A novel bioluminescent protease assay using engineered firefly luciferase. Curr Chem Genomics **2**, 16-28

291 Fan, F., Binkowski, B. F., Butler, B. L., Stecha, P. F., Lewis, M. K. and Wood, K. V. (2008) Novel genetically encoded biosensors using firefly luciferase. ACS Chem Biol **3**, 346-351

292 Atkinson, E. A., Barry, M., Darmon, A. J., Shostak, I., Turner, P. C., Moyer, R. W. and Bleackley, R. C. (1998) Cytotoxic T lymphocyte-assisted suicide. Caspase 3 activation is primarily the result of the direct action of granzyme B. J Biol Chem **273**, 21261-21266

293 Manns, J., Daubrawa, M., Driessen, S., Paasch, F., Hoffmann, N., Loffler, A., Lauber, K., Dieterle, A., Alers, S., Iftner, T., Schulze-Osthoff, K., Stork, B. and Wesselborg, S. (2011) Triggering of a novel intrinsic apoptosis pathway by the kinase inhibitor staurosporine: activation of caspase-9 in the absence of Apaf-1. Faseb J **25**, 3250-3261

294 Packard, B. Z., Telford, W. G., Komoriya, A. and Henkart, P. A. (2007) Granzyme B activity in target cells detects attack by cytotoxic lymphocytes. J Immunol **179**, 3812-3820

295 Choi, P. J. and Mitchison, T. J. (2013) Imaging burst kinetics and spatial coordination during serial killing by single natural killer cells. Proc Natl Acad Sci U S A **110**, 6488-6493

296 Galban, S., Jeon, Y. H., Bowman, B. M., Stevenson, J., Sebolt, K. A., Sharkey, L. M., Lafferty, M., Hoff, B. A., Butler, B. L., Wigdal, S. S., Binkowski, B. F., Otto, P., Zimmerman, K., Vidugiris, G., Encell, L. P., Fan, F., Wood, K. V., Galban, C. J., Ross, B. D. and Rehemtulla, A. (2013) Imaging proteolytic activity in live cells and animal models. PLoS One **8**, e66248

297 Bartok, E., Bauernfeind, F., Khaminets, M. G., Jakobs, C., Monks, B., Fitzgerald, K. A., Latz, E. and Hornung, V. (2013) iGLuc: a luciferase-based inflammasome and protease activity reporter. Nat Methods **10**, 147-154

298 Dunn, G. P., Bruce, A. T., Ikeda, H., Old, L. J. and Schreiber, R. D. (2002) Cancer immunoediting: from immunosurveillance to tumor escape. Nat Immunol **3**, 991-998

299 Dunn, G. P., Old, L. J. and Schreiber, R. D. (2004) The immunobiology of cancer immunosurveillance and immunoediting. Immunity **21**, 137-148

300 Kim, R., Emi, M. and Tanabe, K. (2007) Cancer immunoediting from immune surveillance to immune escape. Immunology **121**, 1-14

301 Samejima, K., Svingen, P. A., Basi, G. S., Kottke, T., Mesner, P. W., Jr., Stewart, L., Durrieu, F., Poirier, G. G., Alnemri, E. S., Champoux, J. J., Kaufmann, S. H. and Earnshaw, W. C. (1999) Caspase-mediated cleavage of DNA topoisomerase I at unconventional sites during apoptosis. J Biol Chem **274**, 4335-4340

302 de Lucio, B., Manuel, V. and Barrera-Rodriguez, R. (2005) Characterization of human NSCLC cell line with innate etoposide-resistance mediated by cytoplasmic localization of topoisomerase II alpha. Cancer Sci **96**, 774-783

303 Kim, T. W., Hung, C. F., Boyd, D. A., He, L., Lin, C. T., Kaiserman, D., Bird, P. I. and Wu, T. C. (2004) Enhancement of DNA vaccine potency by coadministration of a tumor antigen gene and DNA encoding serine protease inhibitor-6. Cancer Res **64**, 400-405

304 Benarafa, C., LeCuyer, T. E., Baumann, M., Stolley, J. M., Cremona, T. P. and Remold-O'Donnell, E. (2011) SerpinB1 protects the mature neutrophil reserve in the bone marrow. J Leukoc Biol **90**, 21-29

Nederlandse samenvatting

Inleiding

Ons lichaam wordt continu geconfronteerd met bedreigingen zoals virussen en kankercellen. Gelukkig is ons immuunsysteem vaak in staat om deze bedreigingen te herkennen en te elimineren. Dit wordt gedaan door een gespecialiseerde tak van het immuunsysteem, die bestaat uit verschillende types witte bloedcellen, waaronder de natural killer (NK) cellen en cytotoxische T cellen. Deze immuuncellen worden ook wel cytotoxische lymfocyten genoemd. Wanneer een cytotoxische lymfocyt een virus-geïnfecteerde- of kankercel herkent, wordt er een immunologische synaps gevormd en zal de cytotoxische lymfocyt proberen de cel te doden (Figuur 1). Dit kan via twee verschillende mechanismes. Allereerst kan de cytotoxische lymfocyt contact maken met een speciale dood-receptor op de buitenkant van de doelwitcel. Dit resulteert in de initiatie van een dood-signaleringsroute in de cel, die uiteindelijk leidt to de inductie van celdood. Echter, de belangrijkste manier van celdoding is de zogeheten granule-exocytose route. Hierin scheiden cytotoxische lymfocyten bepaalde eiwitten uit in de immunologische synaps. Een van deze eiwitten heet perforine, en dit eiwit kan poriën vormen in het membraan van de doelwitcel. De vorming van deze poriën zorgt ervoor dat de andere eiwitten die

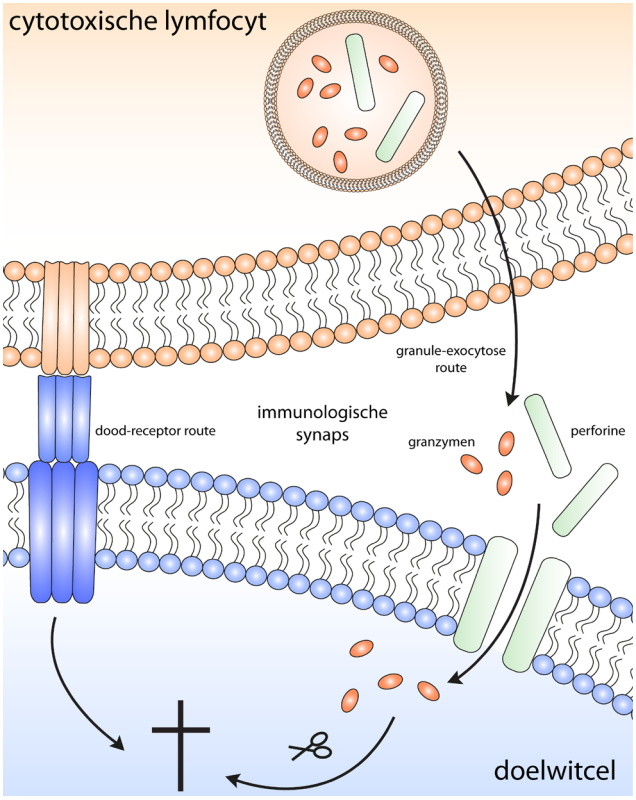

Figuur 1. Doelwitceldoding door een cytotoxische lymfocyt.
Cytotoxische lymfocyten kunnen op twee verschillende manieren doelwitcellen doden: via de dood-receptor route en de granule-exocytose route. In de dood-receptor route maakt een eiwit op het membraan van de cytotoxische lymfocyt contact met een dood-receptor op het membraan van de doelwitcel. Dit activeert een signaleringsroute in de doelwitcel, die leidt tot celdood. De granule-exocytose route is de belangrijkste manier van celdoding door cytotoxische lymfocyten. In deze route scheidt de cytotoxische lymfocyt verschillende eiwitten uit in de immunologische synaps. Een van deze eiwitten is het porie-vormende eiwit perforine, dat het celmembraan van de doelwitcel perforeert. Hierdoor kunnen andere uitgescheiden eiwitten – de granzymen – de doelwitcel binnen komen. Granzymen zijn proteases en kunnen dus andere eiwitten knippen, en op die manier deze eiwitten activeren of remmen. Zo kunnen granzymen ook dood-signaleringsroutes aanzetten, en celdood teweeg brengen.

worden uitgescheiden – granzymen – de cel binnen kunnen komen. Granzymen zijn proteases, wat betekent dat ze andere eiwitten (substraten) kunnen knippen en op die manier kunnen activeren of remmen. Dankzij perforine kunnen granzymen dus van binnenuit ('behind enemy lines') substraten van de doelwitcel knippen. In de mens zijn vijf verschillende granzymen geïdentificeerd: granzym A (GrA), GrB, GrH, GrK en GrM. Ieder granzym heeft een verschillende specificiteit, wat betekent dat elk granzym zijn eigen set substraten heeft. Op deze manier kunnen verschillende granzymen verschillende functies uitvoeren. Van alle granzymen is aangetoond dat ze doelwitcellen kunnen doden. Recentelijk is echter gebleken dat granzymen ook andere functies kunnen hebben, zoals het remmen van virusinfecties op een celdood-onafhankelijke manier.

Naar GrA en GrB is de afgelopen jaren diepgaand onderzoek gedaan, en we weten dan ook veel over hoe deze proteases functioneren. Over GrM is echter veel minder bekend. In dit proefschrift hebben we daarom de rol van GrM in virus- en kankerklaring onderzocht. In **hoofdstuk 1** van dit proefschrift worden de functies en substraten van GrM uitgebreid beschreven. Om nieuwe substraten van GrM te identificeren is het gebruik van hedendaagse proteomics technieken, die het mogelijk maken om alle eiwitten in een cel te bestuderen, van groot belang. **Hoofdstuk 2** geeft de laatste ontwikkelingen in dit veld weer, en concentreert zich vooral op het gebruik van deze technieken om granzym substraten en granzym specificiteit te bepalen.

Fysiologisch belang van GrM

Het belang van de granule-exocytose route in tumorklaring is duidelijk in muismodellen die het porie-vormende eiwit perforine missen. Deze muizen ontwikkelen spontaan tumoren en zijn minder goed in staat om kankercellen op te ruimen. Het belang van ieder granzym afzonderlijk is echter niet bekend. Om dit te bestuderen zijn muizen ontwikkeld die bepaalde granzymen missen, zogenoemde knockout-modellen. Deze knockout-modellen laten geen verminderd effect op tumorklaring zien. Muizen hebben echter tien granzymen, terwijl mensen er maar vijf hebben. Het zou dus kunnen dat als er één granzym niet meer werkt, dit geen effect heeft omdat de andere granzymen de functie van dit ene granzym kunnen overnemen (redundantie). Verder is aangetoond dat muis GrB verschilt van humaan GrB in specificiteit en functie. In **hoofdstuk 3** tonen wij aan dat ook muis GrM en humaan GrM soort-specifieke verschillen hebben. Dit bemoeilijkt het gebruik van muismodellen in het bestuderen van de fysiologische relevantie van GrM. In verschillende muizen tumorcellen kan GrM geen celdood veroorzaken, terwijl GrM wel efficiënt humane tumorcellen kan doden. Een mogelijke verklaring hiervoor beschrijven wij in **hoofdstuk 4**, waarin we laten zien dat een belangrijk humaan substraat van humaan GrM – het eiwit FADD – niet geknipt kan worden in muizencellen, omdat muizen FADD niet dezelfde knipplaats heeft als humaan FADD. Om de fysiologische relevantie van GrM aan te tonen is het dus van belang

om gehumaniseerde muismodellen te gebruiken, waarin humane kankercellen en humane lymfocyten kunnen worden bestudeerd. Om in deze modellen GrM activiteit te bestuderen hebben wij een sensor ontwikkeld die wordt geactiveerd door een knip van GrM. Deze sensor staat beschreven in **hoofdstuk 8**.

Antikanker functies van GrM

Het mechanisme dat GrM gebruikt om tumorcellen te doden is nog niet duidelijk. Er zijn enkele GrM substraten bekend, maar tot nu toe is slechts van één substraat – FADD – onomstotelijk bewezen dat het belangrijk is voor de inductie van celdood. Ook is niet bekend via welke routes de cellen nu precies dood gaan. In **hoofdstuk 5** tonen wij aan dat GrM kankercellen kan doden door andere proteases te activeren, de zogeheten caspases, die vervolgens essentiële onderdelen van de cel kapot knippen. Verder gebruiken we een proteomics techniek om nieuwe substraten van GrM te identificeren in tumorcellen. We laten zien dat GrM het kerneiwit topoisomerase II alfa knipt. Topoisomerase II alfa is een eiwit dat belangrijk is in de regulatie van de vorm (topologie) van het DNA. Dit is van cruciaal belang voor verschillende belangrijke processen, waaronder celdeling. Wanneer GrM topoisomerase II alfa knipt, verliest topoisomerase II alfa een signaleringskenmerk, waardoor het niet langer in de celkern – bij het DNA – zit, maar de kern uit gaat. Dit betekent dat topoisomerase II alfa niet meer kan functioneren in het reguleren van DNA topologie, waardoor de kankercel problemen krijgt bij celdeling. Dit resulteert in een stop in de celcyclus, en leidt uiteindelijk tot de inductie van celdood. Op deze manier kan GrM dus kankercel proliferatie remmen en kankercellen doden.

Kankercellen proberen vaak de aanval van granzymen af te weren door bepaalde remmers tot expressie te brengen. **Hoofdstuk 6** beschrijft de identificatie van een dergelijke remmer voor GrM: SerpinB4. SerpinB4 remt GrM op een onomkeerbare manier, en overexpressie van SerpinB4 in tumorcellen leidt tot een vermindering van GrM-geïnduceerde en cytotoxische lymfocyt-geïnduceerde celdood. SerpinB4 overexpressie wordt vaak gevonden in plaveiselcelcarcinomen. Deze tumoren zouden dus minder gevoelig kunnen zijn voor GrM.

Antivirale functies van GrM

Cytomegalovirus (CMV) is een herpesvirus dat leidt tot levenslange infectie, omdat het in staat is om eliminatie door het immuunsysteem te vermijden. Na infectie blijft het virus aanwezig in specifieke celsoorten, zonder tot symptomen te leiden (latentie). Wanneer iemand echter een verzwakt immuunsysteem heeft – bijvoorbeeld door ziektes of medicijnen – kan dit virus reactiveren en zo tot symptomen leiden. Nog niet zo lang geleden is voor het eerst aangetoond dat GrM belangrijk is voor het remmen van de replicatie van CMV doordat het pp71, een CMV-specifiek eiwit, kan knippen. In **hoofdstuk 7** wordt een tweede mechanisme beschreven dat GrM gebruikt om CMV replicatie te remmen. GrM kan namelijk het humane eiwit hnRNP K knippen. Het eiwit hnRNP K speelt voornamelijk een rol in

transcriptie van DNA en de synthese van eiwitten (transcriptie), en wordt misbruikt door CMV om virale eiwitten te maken. Doordat GrM hnRNP K knipt, kunnen belangrijke virale eiwitten dus minder goed gesynthetiseerd worden, wat resulteert in verminderde CMV replicatie.

Therapeutische toepassingen

Het in dit proefschrift beschreven onderzoek zal in de toekomst kunnen bijdragen aan de ontwikkeling van nieuwe en verbeterde klinische behandelingen van kanker en virusinfecties. Zo zou het kunnen resulteren in een verbeterde efficiëntie van immunotherapie. Bij immunotherapie wordt een patiënt behandeld met eigen bloedcellen, die buiten het lichaam zijn geëxpandeerd (en eventueel aangepast), en die bij het terugspuiten in de patiënt een verbeterde specificiteit hebben voor de tumor. Het verhogen van GrM expressie in deze lymfocyten zou kunnen bijdragen aan hogere antivirale en antikanker activiteit. Verder zou het verlagen van GrM-remmer (SerpinB4) expressie in tumorcellen ook kunnen leiden tot een verbetering van dergelijke therapieën, en zou het karakteriseren van SerpinB4 expressie in tumorcellen wellicht ook de kans op succes van immunotherapie kunnen voorspellen. De identificatie van GrM substraten die bijdragen aan virus- of kankerklaring levert ook nieuwe aangrijpingspunten op voor de ontwikkeling van nieuwe medicijnen.

Curriculum Vitae

Stefanie de Poot was born in 's-Hertogenbosch, the Netherlands, on August 23rd 1986. In 2004, she graduated *cum laude* from the d'Oultremontcollege in Drunen (VWO), after which she started her bachelor education at University College Utrecht. In 2006, she spent a semester abroad at University College Cork, Ireland. In 2007, she obtained her Bachelor of Science degree *summa cum laude*. In the same year, she began her master education in Biomolecular Sciences at the University of Utrecht.

During her master, she did a 9-month internship under the supervision of Dr. Raoul de Groot and Dr. Martijn Langereis at the department of Virology at the faculty of Veterinary Sciences at Utrecht University, where she studied the function of the hemagglutinin-esterase protein of human coronavirus OC43. After this internship, she worked for 6 months at the department of Pathology at Cambridge University in the UK, under supervision of Prof. Dr. Andrew Wyllie, where she tried to unravel the role of promyelocytic leukemia protein in the DNA damage response. Her master thesis was written under supervision of Dr. Bert van der Reijden and Dr. Sylvie Noordermeer from the department of Hematology at the Nijmegen Center for Molecular Life Sciences, and focused on the role of the ubiquitin-conjugating enzyme Ubc13 in the DNA damage response. During her master, Stefanie also participated in X-track, the two-year honours' programme of the Utrecht Graduate School of Life Sciences.

She graduated *cum laude* in 2009, and then began her PhD at the department of Pathology at the University Medical Center Utrecht in the group of Dr. Niels Bovenschen. The results obtained during her PhD are described in this thesis.

In 2014, she will start as a Post-Doc in the group of Professor Daniel Finley at Harvard Medical School in Boston, the US, to study the function and specificity of the deubiquitinase Usp14.

List of publications

Granzyme M targets topoisomerase II alpha to trigger cell cycle arrest and caspase-dependent apoptosis.
de Poot SAH, Lai KW, van der Wal L, Plasman K, Van Damme, P, Porter AC, Gevaert K, Bovenschen N.
Cell Death Differ. doi: 10.1038/cdd.2013.155

Granzyme M cannot induce cell death via cleavage of mouse FADD.
de Poot SAH, Lai KW, Hovingh ES, Bovenschen N.
Apoptosis. 2013;18(4):533-4.

Granzyme M targets host cell hnRNP K that is essential for human cytomegalovirus replication.
van Domselaar R, de Poot SAH, Remmerswaal EB, Lai KW, Ten Berge IJ, Bovenschen N.
Cell Death Differ. 2013;20(3):419-29.

Intracellular serine protease inhibitor SERPINB4 inhibits granzyme M-induced cell death.
de Koning PJ, Kummer JA, de Poot SAH, Quadir R, Broekhuizen R, McGettrick AF, Higgins WJ, Devreese B, Worrall DM, Bovenschen N.
PLoS One. 2011;6(8):e22645.

Human and mouse granzyme M display divergent and species-specific substrate specificities.
de Poot SAH, Westgeest M*, Hostetter DR, Van Damme P, Plasman K, Demeyer K, Broekhuizen R, Gevaert K, Craik CS, Bovenschen N.*
Biochem J. 2011;437(3):431-42.

Proteomic profiling of proteases: tools for granzyme degradomics.
de Poot SAH, van Domselaar R*, Bovenschen N.*
Expert Rev Proteomics. 2010;7(3):347-59.

Dankwoord

Na 4 jaar hard werken komt het einde van je PhD dan ineens toch heel snel in zicht. Ik zou hier echter niet zitten zonder de hulp en steun van vele anderen.

Dr. N. Bovenschen, beste Niels, mijn begeleider en co-promotor. Vier jaar geleden, bij mijn sollicitatiegesprek, wist ik al meteen dat ik me goed op mijn plek zou voelen in jouw granzymengroep. Je leerde me al snel af om je aan te spreken met 'U', en we praatten elkaar wekelijks bij op onze maandagbesprekingen. Eerst alleen jij en ik, later ook met Ka Wai en de al dan niet aanwezige studenten erbij. Je wist me regelmatig te overtuigen dat ik nog best wat extra studenten kon begeleiden, ook al had ik er dan al twee rondlopen, wat regelmatig resulteerde in overvolle (maar zeker niet minder gezellige) labruimtes en werkbesprekingen. Ik heb ontzettend genoten van onze samenwerking, het 'houden-van-de-focus' en hoe vaak wij op één lijn zaten. Ik denk dat we de laatste tijd misschien wel iets te veel aan elkaar gewend zijn geraakt – regelmatig weet ik al precies wat je gaat vragen nog voordat je het zegt. Het is dus misschien wel goed dat ik mijn PhD nu afrond, en het granzymenlab verlaat om de wijde wereld in te trekken. O, en natuurlijk nog bedankt voor het stimuleren van lentivirus-transducties!

Prof. P. van Diest, beste Paul, mijn promotor. Ondanks dat je niet direct betrokken was bij mijn onderzoek, ben ik je toch ontzettend dankbaar voor de mogelijkheid om bij de pathologie te promoveren. Verder is jouw enthousiasme voor het onderzoek inspirerend, en ik bewonder hoe je altijd overal tijd voor maakt en energie voor hebt.

Willy, het is bewonderingswaardig hoe jij altijd voor iedereen klaar staat. Bedankt voor al je hulp tijdens mijn promotietraject en bij het solliciteren voor een nieuwe baan! **Irma**, ook jij hebt me vaak geholpen met het regelen van congressen en vluchten, bedankt!

Leden van mijn leescommissie, **Susanne Lens, Leo Koenderman, Eric Hack** en **Roel Goldschmeding**, bedankt voor het lezen van mijn proefschrift en het opponeren tijdens mijn verdediging.

Mijn paranimfen en (ex-)collega's, **Jolien** en **Çiğdem**. Met jullie was het altijd een feest, en met jullie naast me kon ik zelfs de ergste aio-dip aan. Rooftop-BBQ's, salsa night, ladies night, 90's Now…. er was altijd wel iets leuks te doen. Ik wil nog altijd een keer terug naar Istanbul om die vieze taxi-chauffeur een lesje te leren (maar dan ga ik eerst wel wat groffe Turkse woorden leren bij Çiğdem). En ik heb ontzettend genoten van Çiğdems bruiloft in Ankara, ook al heb ik daarna nog twee weken lang met een 'poepvlek' op mijn hand rondgelopen. Jolien, we klikten al snel toen jij bij ons op het lab kwam, en ik ben erg blij dat ik over de dagelijkse ergernissen (en

positieve gebeurtenissen) met jou kon praten. Bedankt voor het altijd luisterende oor, de shoptripjes naar Antwerpen en Den Bosch, het spinnen bij Olympos, en natuurlijk ook voor de gezelligheid op het lab. Nog veel succes met het afronden van je PhD en met je muisjes. Misschien wil je in de toekomst toch een post-doc in Boston overwegen? Çiğdem, lief dat je altijd mijn haar wou vlechten als ik weer met Ron ging daten! Ik vond het heel erg leuk om jouw paranimf te zijn, en ben blij dat ik jou nu ook als mijn paranimf heb kunnen vragen. Ik wens je heel veel geluk toe voor de toekomst, of dat nu in Canada, Nederland, Duitsland, Turkije, of heel ergens anders is.

Ka Wai, jij kwam in mijn tweede jaar bij mij op het project, en hebt – op enkele korte onderbrekingen met CMV-werk na – hard gewerkt aan het GrM/tumorceldood onderzoek. Het was bijzonder fijn om met jou samen te werken. Zonder jou had dit boekje er bovendien heel anders uitgezien: veel minder blotjes en dus veel dunner. Bovendien zouden de blotjes lang niet zo mooi zijn. Maar ja, jij was dan ook niet voor niets de blotkoningin van ons lab. Het is jammer dat jij ook het lab hebt moeten verlaten. Ik hoop dat je snel een nieuwe baan vindt, waar jij je blot (en klonerings-) talenten weer kunt laten zien. Heel veel groetjes aan Mao Mao!

Natuurlijk wil ik ook graag de andere (ex-)leden van de granzymgroep bedanken. **Annette,** wat fijn dat je uiteindelijk toch op onze aio-kamer bent beland. Het werd er alleen maar gezelliger door, en het was fijn om granzym-zaken met je te kunnen bespreken en frustraties te delen. Nog heel veel succes met de laatste loodjes, ik weet zeker dat dat wel moet lukken. **Robert**, toen ik net begon heb je me ontzettend geholpen met van alles en nog wat. Bedankt voor de vaak oeverloze discussies, het ECDO congres in Gent, en het helpen doorspitten van de -80 vriezer op zoek naar mijn misplaatste KHYG1 cellen. Het is leuk dat je weer terug bent op de afdeling, bedankt voor de hulp met het CMV werk! **Roel Broekhuizen**, wat heb ik veel van jou geleerd. Nog steeds ga ik regelmatig naar je toe met vragen over microscopie, celkweek, Q-PCR-en of de xCELLigence. Fantastisch hoe jij altijd bereid bent om mensen te helpen. Bovendien ben ik blij dat ik op maandag 5 december 2011 ook nog eens je rijmkunsten heb mogen aanhoren. **Jan,** bedankt voor alle hulp met het kloneren en het altijd actief meedenken! Je zult gemist worden op de 3de. **Pieter**, leuk dat ik heb mogen meewerken aan het SerpinB4 artikel, en bedankt voor je voorwerk aan GrM. **Razi,** en studenten **Astrid, Karlijn, Vera, Job, Bernadette**, **Roderick** en **Robbert-Jan**, jullie waren gezellige toevoegingen aan de groep.

Mijn eigen studenten. **Marijn**, technisch gezien was jij natuurlijk helemaal niet ‘mijn’ student, maar die van Niels. Jij was er al toen ik begon, en hebt mij in die tijd veel geleerd. Ik herinner me nog liters gistkweken en een klagend PRL over de stankoverlast. Uiteindelijk was het wel voor een goed doel, want we hebben er een mooie publicatie mee gehaald. Veel succes met je studie geneeskunde. **Marjolein, Lieneke**, en **Liz**, jullie kennen elkaar niet, maar hebben allemaal aan

het GrM sensor project gewerkt, wat heeft geresulteerd in hoofdstuk 8. Marjolein, jij was een ontzettend gedreven student, en hebt het sensor-project als eerste opgezet. Lieneke, jij kon al enorm veel toen je bij ons op het lab kwam, en ik heb het als erg fijn ervaren om je te mogen begeleiden. Veel succes met je eigen PhD in Rotterdam! Liz, jij was mijn allerlaatste student, en bent nog nèt niet helemaal klaar met je stage. Je was een gezellige toevoeging aan onze groep, nog veel succes met je lab- en rugby-carrière, en veel succes in Missouri! **Michiel,** samen met Lieneke heb jij gewerkt aan lentivirale transducties van NK cellen, iets wat lastiger bleek dan verwacht. Toch is het uiteindelijk wel gelukt ze te transduceren, en ik heb later onze nieuwe transductie technieken nog voor veel andere proeven gebruikt. **Elise**, het was een en al gezelligheid met jou op het lab, en toch had je nog tijd genoeg om een hele hoop blotjes te draaien en een hoop FADD mutanten te maken. **Lennart**, jij hebt erg veel mogen FACSen en xCELLigencen… en dat heeft uiteindelijk toch maar mooi bijgedragen aan het topoIIα 'top' artikel. Verder wou ik ook **Philippine** en **Milou** bedanken die ik heb mogen begeleiden met hun bachelor stages. Ik vond het erg leuk om met jullie allemaal samen te werken, en ik wens jullie het beste voor de toekomst.

(Ex-)kamergenootjes **Laurien** (ik zal de wekelijkse voetbalupdates missen)**, Folkert** (altijd vrolijk, zelfs op maandagochtend)**, Ellen, Renée, Karijn, Rob, Jeroen** (jij wist ook echt altijd alles te vinden), **Wendy** (die CCKL accreditatie hebben we toch maar mooi gekregen), bedankt voor de gezelligheid op onze aio-kamer. En ook **Geert, Danielle, Jan-Willem, Amélie, Iordanka** (thanks for your help with the time-lapse imaging), **Pan, Yvonne, Stefan**, **Lucas, Aram, Tri, Dionne, Paulien, Cathy, Petra, Annelies, Nienke-Elske, Marise, Roel de Weger, Manon, Hisham, Johan**, en de rest van de afdeling pathologie **–** bedankt voor de fijne tijd. Ik heb het ontzettend leuk gehad met jullie op de labuitjes (voetballen op hoge hakken!), PRL borrels, aio/post-doc meetings, 90's Now avonden, de film/musical uitstapjes, Tour de Pathologie (the Rolling Clones en de Grammies waren topteams, tour-organisatie bedankt!) en de Efteling… De Derksen-groep: **Patrick**, **Milou, Eva, Miranda** en **Robert** (wat kun jij mijn huppeltje goed na doen…), fijn dat jullie nooit zeurden als ik weer eens langs jullie kamer kwam om Ron te zien. De ICT-ers die me hielpen als mijn computer weer eens niet mee werkte: **Nikolas, Kevin, Robbert-Jan,** en **Deepal**. **Jos** en **Gerrit** van het magazijn, die nooit moeilijk deden als ik na 12 uur weer eens iets kwam halen. **Kok** van de medische microbiologie, fijn dat ik zo vaak bij jullie kon FACSen. Uit het WKZ: **Sanne, Cordula, Wouter, Zsolt, Sabine, Samantha** and **Jürgen Kuball**, thanks for the OPM-2, Daudi, and gamma-delta-transduced alpha-beta T cells, helping me with the multi-colour FACS, and various other techniques.

UCU-docent **Fred Wiegant**. Fred, ik denk dat ik toch wel een recordaantal vakken bij jou heb gevolgd. Ik probeer zo af en toe nog steeds je 'helicopter-view' toe te passen. Grappig dat ik nu toch nog aan het ubiquitine-proteasoom systeem ga werken. Bedankt voor alle mogelijkheden die je me hebt gegeven.

Martijn en **Raoul**, mijn stage bij de virologie was erg geslaagd; niet alleen het labwerk was leuk, maar ook op sociaal vlak was het een erg fijne stage. Martijn, ik bewonder je doorzettingsvermogen en optimisme. Jij hebt me ontzettend veel geleerd en ik ben blij dat we nog steeds contact hebben. Ook van **Arno** en **Willem** heb ik veel mogen leren, en mede dankzij lab-maatje **Stephin** (HE-man) en mijn mede-studenten (o.a. **Rutger, Michiel, Indra, Bert, Olivier, Steph,** en **Ewoud**) was het altijd gezellig bij de vrijmibo's, die konden uitlopen tot 1 uur 's nachts. Als een toen-nog-erg-onschuldig meisje klapperden mijn oren regelmatig dankzij de wilde verhalen bij de borrels. Leuk dat we af en toe nog afspreken.

I would also like to thank **Professor Wyllie**, for his supervision during my second internship in Cambridge. I've thoroughly enjoyed working with you, and I've learned a lot during my stay. The rest of the roof-top lab in Cambridge: **Kahina, Jürgen, Suzie, Dave,** and **Mikhail,** thanks for showing me around the lab and around Cambridge. Mikhail, I still use your cell cycle FACS protocol. Suzie, Dave and Jürgen, I enjoyed the formal halls, Queen's day in London, and the after-work-drinks in the pub. I wish you all the best and hope to see you again one day!

Onze collaborators in Gent: **Kim, Petra** en **Kris**, bedankt voor jullie input en de fijne samenwerking. Er zijn twee mooie artikelen uit voort gekomen.

Middelbare school vrienden (en mede-roze-schapen) **Laurie, Yvonne, Jan, Martijn** en **Colinde**, jullie kennen me als geen ander en vrienden als jullie zijn onbetaalbaar. 'It is one of the blessings of old friends that you can afford to be stupid with them.' Ons high-tea schransfestijn moeten we snel nog een keer (dunnetjes) overdoen, en ik kijk nu al uit naar jullie gedichten bij de Sinterkerst surprise van dit jaar. Laurie, fijn dat je er altijd voor me bent - al 15 jaar 'officieel' beste vriendinnen! Ik ga je missen als ik in de VS zit.

UCU-vriendinnen ('mijn 3 vrienden') **Sanne, Xandra,** en **Frederieke**: leuk dat we nog steeds afspreken, wanneer mogelijk. Sanne, je zit nu al een tijdje in Engeland, en ondanks dat we elkaar niet heel regelmatig zien, is het toch altijd gezellig als je hier bent. Kromhout Unit 1 was de leukste unit van de hele campus. Xannie, ik ga onze eet/LOST/film avonden missen als ik in de VS zit. Via Skype maar af en toe samen een filmpje kijken dan? Fre, veel succes met jouw eigen promotie. Samen lunchen zal er wel niet meer in zitten… maar daar verzinnen we wel iets op.

Fellow-X-trackers, **Tessa, Xenia,** and **Janneke**: organizing the Boost Your Body symposium with you was a great experience. Wish you the best for the future!

Aad en **Tine**, ontzettend bedankt voor jullie zoon, ik ben heel erg blij en dankbaar dat ik Ron heb leren kennen. Tine, bijna ieder weekend kan ik bij Ron en Martin van een van uw recepten genieten, en ik heb nog nooit zulke lekkere appelmoes op

als die van u. Aad, gezellig dat u zo vaak bij Ron en Martin langs komt. We moeten snel weer eens eten bij Gauchos, het is hoog tijd dat ik eens een keer trakteer. **Opa** en **oma Schaap,** bedankt dat jullie mij zo warm welkom hebben geheten in jullie familie. Ik weet hoe fantastisch Ron is, dus ik zal zuinig op hem zijn. **Martin**, jij hebt er nooit moeilijk over gedaan dat ik bijna ieder weekend bij jullie over de vloer kwam en al jullie Snickers ijsjes op at. Ik ben blij dat Ron zo'n leuke broer heeft. Bedankt dat je me kennis hebt laten maken met Age of Mythology, AoEIII, Starcraft, Civ en Anno. Misschien besluit jij uiteindelijk om je post-doc ook in Boston te gaan doen? En anders kunnen we vast wel via het internet samen wat titans afmaken.

Lieve **papa en mama**, jullie staan altijd voor me klaar en hebben me altijd in iedere keuze gesteund. Niets was te veel – zelfs over 8 keer verhuizen in 9 jaar deden jullie niet moeilijk. Ik ben ontzettend dankbaar dat ik zulke begrijpende en liefhebbende ouders heb, en ik weet niet wat ik zonder jullie zou moeten. Ik vind het vervelend dat we elkaar minder zullen gaan zien als ik in Boston zit, maar we gaan veel bellen en mailen, en een potje bollen via Skype moet te regelen zijn. En als papa met pensioen is, kunnen jullie natuurlijk gewoon iedere maand op en neer vliegen om ons te bezoeken. In de omgeving van Boston is (vast) een erg mooi wandel- en fietsgebied te vinden! **Maarten**, broertje, opgroeien met jou was enorm fijn – wat zou het saai zijn geweest zonder jou. Jammer dat ik je nu veel minder vaak spreek, maar als we elkaar zien, dan is het weer als vroeger. Hyena's neerschieten met Call of Duty, een filmpje kijken, of een potje Age of Empires II(I)… het is altijd gezellig samen. Ik ben erg trots op je dat je zo snel na je afstuderen al zo fanatiek aan het werken bent. **Familie de Bonth** en **familie de Poot,** ooms en tantes, nichten en neven, bedankt voor de familiedagen (elk jaar weer een groot succes), surprise-avonden, kerstdiners en verjaardagen. Ik hoop dat jullie er 12 december allemaal bij kunnen zijn!

Lieve **Ron**, omdat ik weet hoe kostbaar (kotsbaar?) je dit vindt, heb ik voor jou een speciaal plekje helemaal onderaan mijn dankwoord gereserveerd. Halverwege mijn PhD traject leerden we elkaar kennen. Daar ben ik iedere dag nog steeds erg blij om, want mijn lentivirus transducties lopen nu als een trein. Heerlijk hoe je er altijd bent om me op te vrolijken, ik voel me echt nergens fijner dan bij jou en ben ontzettend dankbaar dat ik jou naast me heb. Ik kan me niet meer voorstellen hoe het zonder je zou zijn, dus ik ben erg blij dat we samen naar het buitenland gaan. Wanneer het geregel allemaal op zijn eind loopt, hoop ik dat we nog een beetje kunnen ontspannen voordat we weg gaan (zou het schaatsen er dan eindelijk een keer van komen?). Ik heb heel veel zin in ons post-doc avontuur! P.S. Natuurlijk ook bedankt voor alle plasmiden, cellijnen, en technische support. ♥